CU1148 Serial #16

Los Alamos Environmental Restoration Facility

15368

GJ-54

ER Record I.D.# 0015368

VADOSE ZONE CHARACTERIZATION OF TECHNICAL AREA 54, WASTE DISPOSAL AREAS G AND L, LOS ALAMOS NATIONAL LABORATORY, NEW MEXICO

REPORT 4: PRELIMINARY ASSESSMENT OF THE HYDROLOGIC SYSTEM THROUGH FISCAL YEAR 1986

By
Peter M. Kearl;
James J. Dexter;
Mark Kautsky

December 1986

10415

UNC Service Through Technology

UNC Technical Services, Inc.
Grand Junction, Colorado

GJ-54

VADOSE ZONE CHARACTERIZATION OF TECHNICAL AREA 54, WASTE DISPOSAL AREAS G AND L, LOS ALAMOS NATIONAL LABORATORY, NEW MEXICO

REPORT 4: PRELIMINARY ASSESSMENT OF THE HYDROLOGIC SYSTEM THROUGH FISCAL YEAR 1986

By
Peter M. Kearl;
James J. Dexter;
Mark Kautsky

December 1986

Work Performed Under Contract No. DE-AC07-86ID12584

Prepared for
U.S. Department of Energy
Assistant Secretary for Nuclear Energy
Los Alamos National Laboratory
Los Alamos, New Mexico
in Conjunction with
U.S. Department of Energy
Grand Junction Projects Office
Grand Junction, Colorado

Prepared by
UNC Technical Services, Inc.
Hazardous and Mixed Waste Program
Grand Junction, Colorado 81502

CONTENTS LISTING

		Page
FOREWORD		ix
EXECUTIVE SUMMARY		x
SECTION 1	INTRODUCTION	1
	1.1 Purpose and Scope	3
	1.2 Terminology and Units	4
	1.2.1 Terminology	4
	1.2.2 Units	5
	1.3 Previous Work	6
SECTION 2	GEOLOGIC CHARACTERIZATION OF THE STUDY AREA	7
	2.1 Regional and Site Geology	9
	2.2 Welding and Correlation of Ash-Flow Units at Mesita del Buey	14
	2.3 Petrographic Analyses	17
	2.4 Interpretation of Geophysical Logs	22
	2.4.1 Natural Gamma and Epithermal Neutron Moisture Logs	23
	2.4.2 Spectral Gamma Logs	23
	2.4.3 Magnetic Susceptibility and Gamma-Gamma Logs	26
	2.5 Fractures	32
	2.5.1 Subsurface Characteristics	32
	2.5.2 Surface Characteristics	33
SECTION 3	HYDROLOGIC CHARACTERIZATION OF THE VADOSE ZONE	35
	3.1 General Characteristics	37
	3.1.1 Gravimetric Moisture Content	37
	3.1.2 Porosity	45
	3.1.3 Moisture Characteristic Curves	47
	3.2 Permeability Determinations	50
	3.2.1 Borehole-Injection Tests	50
	3.2.2 Vacuum Tests	59
	3.2.3 Laboratory Measurements	63
	3.2.4 Hydraulic Conductivity as a Function of Moisture Content	68
	3.2.5 Permeability Summary	69
	3.3 Gradient Determinations	74
	3.3.1 Temperature and Water-Potential Measurements	74
	3.3.2 Atmospheric/Rock-Pore Pressure Monitoring System	90
SECTION 4	NEUTRON MOISTURE MEASUREMENTS	93
	4.1 Purpose and Scope	95
	4.2 Casing Installations	95
	4.3 Calibration of the Neutron Probe	97
	4.4 Monitoring Program	97

CONTENTS LISTING (continued)

		Page
SECTION 5	PORE-GAS SAMPLING SYSTEM.	99
	5.1 Purpose and Scope.	101
	5.2 Design	101
	5.3 Installation	101
SECTION 6	PETREX SURVEY	105
	6.1 Purpose and Scope.	107
	6.2 Sampling and Analysis.	107
	6.3 Results.	107
SECTION 7	CONCLUSIONS	115
SECTION 8	REFERENCES.	119

LIST OF APPENDICES

Appendix A.	Lithologic Logs and Instrument Completion Diagrams	A-1
Appendix B.	Petrographic Reports	B-1
Appendix C.	Moisture Characteristic Curves	C-1
Appendix D.	Effective Permeability as a Function of Saturation	D-1
Appendix E.	Listing of Fortran V Program for Converting Psychrometer Microvoltage Outputs to Water Potential.	E-1
Appendix F.	Geophysical Logs	F-1

LIST OF FIGURES

Figure 2-1.	Location of the Study Area and Regional Geologic Relationships	10
2-2.	Geologic Cross Section from the Jemez Mountains on the West, Through the Pajarito Plateau, to the Rio Grande River on the East.	11
2-3.	Locations of Drill Holes in Areas G and L, Technical Area 54, Los Alamos National Laboratory, New Mexico . . .	12
2-4.	Cross Section Showing Parts of the Tshirege Member of the Bandelier Tuff, Drawn Through Mesita del Buey and Technical Area 54	15
2-5.	Fence Diagram Through Waste Disposal Area L Showing Subsurface Stratigraphy of the Bandelier Tuff	19
2-6.	Epithermal Neutron, Natural Gamma, and Lithologic Logs for Hole LGC-85-10.	24
2-7.	Comparison of Moisture Curves for Hole LGM-85-06, Derived by Geophysical and Gravimetric Methods.	25
2-8.	Spectral Gamma and Lithologic Logs for Hole LGM-85-11 . .	27

LIST OF FIGURES (continued)

			Page
Figure	2-9.	Magnetic Susceptibility, Apparent Density, and Lithologic Logs for Hole LGC-85-10.	28
	2-10.	Magnetic Susceptibility, Apparent Density, and Lithologic Logs for Hole LLM-85-02.	30
	2-11.	Magnetic Susceptibility, Apparent Density, and Lithologic Logs for Hole LGM-85-11.	31
	2-12.	Rose Diagram of Joint Orientations of Exposed Fractures in Area L, Los Alamos National Laboratory	34
	3-1.	Plots of Volumetric Moisture Content as a Function of Depth for Drill Holes LLM-85-01, LLM-85-02, LLM-85-05, LGM-85-06, and LGM-85-11	40
	3-2.	Plots of Volumetric Moisture Content as a Function of Depth for Drill Holes LLC-86-19 and LLC-86-20	41
	3-3.	Plots of Volumetric Moisture Content as a Function of Depth for Drill Holes LLC-86-21 and LLC-86-22	42
	3-4.	Plots of Volumetric Moisture Content as a function of Depth for Drill Holes LLC-86-23 and LLC-86-24	43
	3-5.	Plots of Volumetric Moisture Content as a Function of Depth for Drill Hole LLC-86-25.	44
	3-6.	Porosity of Battleship Rock Ash-Flow Tuff, Valles Mountains, New Mexico	48
	3-7.	Air-Injection Apparatus Used for In-Situ Permeability Measurements.	53
	3-8.	Water-Injection Apparatus Used for In-Situ Permeability Measurements.	54
	3-9.	Vacuum-Testing Apparatus Used for In-Situ Permeability Measurements.	60
	3-10.	Unsaturated Hydraulic Conductivities as Functions of Moisture Content and Water Potential for Samples MCG-603 and MCG-604	70
	3-11.	Unsaturated Hydraulic Conductivities as Functions of Moisture Content and Water Potential for Samples MCG-607 and MCG-613	71
	3-12.	Unsaturated Hydraulic Conductivities as Functions of Moisture Content and Water Potential for Samples MCG-616 and MCG-617	72
	3-13.	Unsaturated Hydraulic Conductivities as Functions of Moisture Content and Water Potential for Sample MCG-620	73
	3-14.	Sketch of the Single-Junction Stainless Steel Screen-Shielded Thermocouple Psychrometer.	76
	3-15.	Sketch of the Stainless Steel Calibration Chamber Showing Seals and Screen-Shielded Thermocouple Psychrometer	78
	3-16.	Water Potential Versus Time for Selected Psychrometers in Hole LLP-85-03	81
	3-17.	Temperature Versus Time for Selected Psychrometers in Hole LLP-85-03	82
	3-18.	Water Potential Versus Time for Selected Psychrometers in Hole LGP-85-07	83

LIST OF FIGURES (continued)

			Page
Figure	3-19.	Temperature Versus Time for Selected Psychrometers in Hole LGP-85-07	84
	3-20.	Air Temperature Versus Time at Hole LLP-85-03	85
	3-21.	Water Potential Versus Depth for Hole LLP-85-03	86
	3-22.	Temperature Versus Depth for Hole LLP-85-03	87
	3-23.	Water Potential Versus Depth for Hole LGP-85-07	88
	3-24.	Temperature Versus Depth for Hole LGP-85-07	89
	3-25.	Results from the Pressure Transducers Installed in Hole LLP-85-03	92
	4-1.	Casing Installation and Depths of Neutron Probe Measurements in Hole LLN-85-04	96
	4-2.	Casing Installation and Depths of Neutron Probe Measurements in Hole LGN-85-08	98
	5-1.	Diagram of a Pore-Gas Sampling Port	102
	6-1.	Normalized Trichloroethylene Ion-Count Map, Waste Disposal Area L, Los Alamos National Laboratory, New Mexico	108
	6-2.	Normalized Tetrachloroethylene Ion-Count Map, Waste Disposal Area L, Los Alamos National Laboratory, New Mexico	109
	6-3.	Non-Normalized Benzene Ion-Count Map, Waste Disposal Area L, Los Alamos National Laboratory, New Mexico	110
	6-4.	Non-Normalized Toluene Ion-Count Map, Waste Disposal Area L, Los Alamos National Laboratory, New Mexico	111

LIST OF TABLES

			Page
Table	2-1.	Volume-Percent Quartz and Sanidine Determined from Point-Count Analysis of Thin Sections	21
	2-2.	Number of Fractures Logged in the Los Alamos Drill Holes	33
	3-1.	Results of Porosity Determinations Using the Helium-Injection Method and Boyle's Law	46
	3-2.	Hydraulic Conductivity Determined from Air-Injection Tests in Los Alamos Drill Holes	57
	3-3.	Hydraulic Conductivity Values Determined from Water-Injection Tests in Hole LLM-85-05	58
	3-4.	Comparison of Intrinsic Permeability Values Determined from Water-Injection and Air-Injection Tests in Hole LLM-85-05	59
	3-5.	Permeability Values Determined from Vacuum Tests in Los Alamos Drill Holes	64
	3-6.	Comparison of Intrinsic Permeability Values Determined from Air-Injection and Vacuum Tests in Los Alamos Drill Holes	65

LIST OF TABLES (continued)

			Page
Table	3-7.	Intrinsic Permeability Values Determined from Laboratory Analysis of Core Samples.	67
	3-8.	Comparison of Average Intrinsic Permeability Values for the Major Geologic Units of the Bandelier Tuff in the Study Area	74
	3-9.	Installation Depths and Calibration Coefficients for Psychrometers in Hole LLP-85-03	79
	3-10.	Installation Depths and Calibration Coefficients for Psychrometers in Hole LGP-85-07	80

ATTACHMENTS

The 1986 geophysical logs for the Los Alamos National Laboratory drill holes are contained in the envelope attached to this report.

FOREWORD

This study was initiated in response to a Compliance Order/Schedule (Docket Number 001007) issued by the State of New Mexico's Environmental Improvement Division under the authority of New Mexico's Hazardous Waste Management Act. The Order/Schedule, dated 7 May 1985, specifies a time line for obtaining certain geotechnical information regarding Waste Disposal Areas G and L in Technical Area 54, Los Alamos National Laboratory, New Mexico. This report addresses the informational requirements outlined in Paragraph 25, Tasks 1 through 5, of the Compliance Order/Schedule. Certain field investigations performed in the Summer and Fall 1986 were above and beyond the requirements of the Compliance/Order Schedule. The investigations on which this report are based were performed by personnel of Bendix Field Engineering Corporation (Bendix), the contractor for the U.S. Department of Energy Grand Junction Projects Office (DOE/GJPO) through 30 September 1986. This report was prepared by the same professionals, now employed by UNC Technical Services, Inc., the current contractor.

The tasks requested by the State of New Mexico in Paragraph 25 of the Compliance Order/Schedule are addressed in the following sections of this report:

Compliance Order Task and Brief Title	Section in Report
1: Permeability Determinations	3.2.1, 3.2.2, 3.2.3
2: Moisture Characteristic Curves	3.1.3
3: Unsaturated Hydraulic Conductivity	3.2.4
4: Infiltration and Redistribution of Water	3.1.1, 3.3.1, 4.0
5: Pore-Gas-Sampling Installations	5.0

The emphasis of the Compliance Order/Schedule is on the quantification of capillary or liquid-flow transport processes. However, moisture data presented by Purtymun and Kennedy (1971) and Abeele and others (1981), as well as the moisture data presented in this report, indicate that movement by vapor phase is the major transport mechanism in the Bandelier Tuff in the study area. Thus, while much of the capillary-related information is useful, it can draw attention away from vapor transport. The reader is therefore asked to focus on relating the information presented in this report to vapor-transport processes.

In addition to the authors cited on the title page, a number of other contractor technical professionals at the Grand Junction Projects Office contributed significantly to this study and to preparation of this report. These individuals and their respective contributions are listed below.

- Sue Rush served as Project Manager and assisted in the drilling and the pore-gas-sampler installations.
- Nic Korte served as Project Manager and assisted in the design and test of the pore-gas samplers.
- Steve Sturm assisted in the drilling and the logging of core.

- Jeff Price assisted in the hydrologic testing.
- Jack McCaslin assisted in the drilling procurement as well as the drilling and the pore-gas-sampler installations.
- Steve Donivan assisted in the design and test of the pore-gas samplers.
- Sandy Wagner performed the field chemical monitoring and set up the analytical subcontract.
- Sue Knutson, Dave Traub, and Joseph Krabacher performed the geophysical logging.
- Rich Zinkl provided the computer support.
- Bonnie Edwardson and Marilynne Gossett performed the editing and document coordination.
- Kenneth Karp assisted with calibration and installation of psychrometers.

The following personnel from Los Alamos National Laboratory also played a significant role in the completion of this study.

- Micheline Devaurs was the principal technical contact, assisted in the planning and conduct of field activities, and wrote Section 4 of this report.
- Dave McInroy assisted in several aspects of the field activities.
- Bill Purtymun recommended the drilling technique and provided much useful insight with respect to logging the Bandelier Tuff.

EXECUTIVE SUMMARY

The hydrologic characteristics of the vadose zone in Areas G and L, Technical Area 54, at Los Alamos National Laboratory were investigated in response to a Compliance Order/Schedule (Docket Number 001007) issued to the Laboratory by the State of New Mexico's Environmental Improvement Division under the authority of New Mexico's Hazardous Waste Management Act. This report summarizes an assessment of the hydrologic system, specifically in response to Tasks 1 through 5, Paragraph 25, of the Compliance Order/Schedule. Vadose zone characterization work completed above and beyond the requirements of the Compliance Order/Schedule is also discussed herein.

The most significant conclusion resulting from this investigation is that vapor-phase transport is the predominant mechanism controlling the potential subsurface movement of contaminants in the study area. Evidence for this conclusion includes the low moisture content of the underlying rock and the high moisture-retention values observed in the moisture characteristic curves (Task 2 of the Compliance Order/Schedule). These results indicate that there is no interconnection or movement of liquid water in the interval of Bandelier Tuff examined in this study.

Permeability measurements were required by Task 1 (field tests) and Task 3 (laboratory tests) of the Compliance Order/Schedule. Field measurements were made using a vacuum-test method and by means of borehole injection with both air and water. Laboratory determinations were made using both the Klinkenberg Correction and the Dynamic methods. Agreement among the various methods was generally good, yielding an intrinsic permeability for the Bandelier Tuff in the range 10^{-8} to 10^{-9} cm^2.

Determination of the water distribution in the tuff was required by Task 4. Gravimetric results indicate a moisture content of 2 to 4 percent for the center portion of the profile, with generally higher contents in the lower portion of Unit 1b. Preliminary data from the thermocouple psychrometers indicate that water potentials range from -1 to -15 bar, suggesting low moisture conditions in the tuff. Neutron-measurement tools used for acquiring moisture data were also installed in two holes in the study area. Although data acquired with the probe were not available at the time of this writing, it is feared that the tuff may be too dry for such measurements to be effective.

The various field and laboratory activities conducted during this study permit an evaluation of the effects of porosity, pumice content, and degree of welding on the unsaturated transport processes. As expected, porosity and pumice content are highly correlated. The high porosity demonstrates that the tuff acts like a sponge: A quantity of water equal to approximately one-quarter of the rock volume is required to satisfy the capillary forces and permit the movement of water in the liquid phase. Permeability, on the other hand, is inversely proportional to porosity due to the significant amount of dead-end pore space which occurs in pumice. Finally, a high degree of welding apparently reduces the average radii of pores, the result being an increase in the capillary forces and the residual moisture content.

In partial fulfillment of the requirements of Task 5, installations for sampling pore gas in discrete subsurface zones were completed in certain holes. The rationale behind each sampling-port location is described in this report. Quarterly monitoring of the pore-gas samplers is being conducted by employees of the Laboratory; data from the monitoring were not available for this report.

Another major objective of this study was to evaluate the role of fractures as avenues of transport in the Bandelier Tuff. Results obtained thus far, however, are inconclusive. Although predominant northeasterly trends were measured, a bias in the data resulted from sampling limitations imposed by available exposures. The permeability of fractured zones, where fractures are filled, is not significantly greater than that of the surrounding rock. Certain fractured zones exhibit a higher moisture content and may be indicative of relatively open fractures. Petrex survey results indicate that ion counts of volatile organic compounds are not distributed uniformly in a radial pattern around the source. Instead, the distribution of volatile organic compounds is spatially variable, as if venting occurs in discrete zones whose fracture apertures and/or intensities may be locally elevated. Transport of contaminants from the source probably follows tortuous routes determined by a combination of fracture orientations and degree of dialation, and interconnections of fractures related to the position of infill materials. It is anticipated that results of the pore-gas sampling and analysis will be of particular benefit to the definition of the role of fractures in the vadose zone. In addition, more extensive Petrex surveys just under the rim of Mesita del Buey and in Area L may also better define the role of fractures relative to contaminant transport.

Section 1

INTRODUCTION

1.1 PURPOSE AND SCOPE

This report summarizes work conducted for Los Alamos National Laboratory (LANL) to assess the hydrologic processes that could contribute to transport of hazardous waste buried in the Bandelier Tuff at the LANL facility in New Mexico. More specifically, the study area encompasses Waste Disposal Areas G and L in Technical Area 54. The study was initiated in response to a Compliance Order/Schedule issued by the Environmental Improvement Division of the State of New Mexico. Included in the Order was a directive to obtain certain geotechnical information regarding the above-mentioned waste-disposal areas.

Work conducted during FY-1986 for this project included drilling, logging, and installation of monitoring equipment in additional boreholes. Seven new holes were drilled and two existing holes (drilled during FY-1985) were deepened. Pore-gas samplers were installed in selected holes. Geophysical logs were run in the new holes and lithologic logs were prepared to show monitoring equipment installation points. A Petrex survey was conducted to measure relative ion counts of organic vapors in the soil.

The FY-1986 work was conducted primarily to support preliminary conclusions based on results of earlier work. Consequently, this report has been prepared by amending and supplementing an earlier report by Kearl and others (1986). New material in this report includes a section on the Petrex survey, expansion of a section on pore-gas sampling, additional lithologic and geophysical logs, petrographic reports on FY-1986 samples, and a fence diagram showing the subsurface stratigraphy of Waste Area L.

The report is organized into eight sections, followed by six appendices. The emphasis throughout is on the transport processes in the unsaturated zone that control potential contaminant migration in the Bandelier Tuff. Immediately following this Introduction, Section 2 defines the geologic framework through which these processes occur in the study area. Section 3 presents a characterization of the vadose zone in terms of the driving forces of transport, namely, gradients such as temperature and pressure. These evaluations require a considerable amount of data regarding the vadose zone, including permeability and such general parameters as moisture content and porosity. Thus, the early subsections of Section 3 describe the field and laboratory measurements conducted to acquire these data, together with the necessary calculations.

Sections 4 and 5 contain discussions of the neutron-moisture-measurement and pore-gas sampling-port installations, respectively; Section 6 describes results of the Petrex survey. A comprehensive summary of results and conclusions is presented in Section 7, followed by a list of the references (Section 8) cited throughout the text and appendices. Appendices A through F contain much of the data acquired throughout the course of this study, including lithologic logs, petrographic data, moisture characteristic and permeability curves, and geophysical logs.

For this study, several experimental techniques were used to drill test holes and to measure important unsaturated flow parameters. In those cases, descriptions of the equipment, procedures, and assumptions associated with a specific test are included in the appropriate discussion.

Analysis of the rock core was hampered by several problems. From the core obtained during drilling, representative samples of the Tshirege Member of the Bandelier Tuff were selected and sent to TerraTek Research Laboratory of Salt Lake City, Utah, for analysis. Approximately 75 percent of this core was either completely unconsolidated or so friable that special handling techniques and procedures had to be developed. Moreover, mercury injection was not feasible on the unconsolidated samples, requiring that alternative laboratory techniques be substituted for the measurement of capillary forces. As a result, it was not possible to quantify the pore-size distributions and the imbibition or wetting curves for the porous media in the study area.

1.2 TERMINOLOGY AND UNITS

1.2.1 TERMINOLOGY

The terms 'vadose zone' and 'unsaturated zone' are often used synonymously in the literature, even though there is a distinction between the two. The unsaturated zone is defined as a subsurface area above the water table in which the porous material contains both air and water, the latter under pressures that are less than those of the atmosphere. The vadose zone also refers to the subsurface area above the water table composed of partially saturated porous material. The distinction lies in the fact that the vadose zone can contain perched zones of water, and the water in these perched zones is under pressures greater than those of the atmosphere. For purposes of this study, the term vadose zone will be used when referring to the subsurface area above the water table, but the processes controlling contaminant migration in that zone will be referred to as the 'unsaturated transport processes.'

Other potentially confusing terms used throughout the report include permeability, coefficient of permeability, hydraulic conductivity, and intrinsic permeability. Distinctions between these terms are summarized below.

- Permeability, when used alone, refers to the movement of a fluid through the porous or fractured media. No quantification is intended to be associated with the term.

- Hydraulic conductivity is the term used to quantify the permeability of the medium. It is dependent on the porous medium and the fluid, and must therefore be expressed in such a way that the fluid represented by the term is specified. The dimensions for hydraulic conductivity are length per unit time (L/t). The term coefficient of permeability is synonymous with hydraulic conductivity.

- Intrinsic permeability is a function of only the medium and has dimensions of length squared (L^2). Expressing permeability in this way permits comparison of permeability values obtained through different techniques using different fluids. (The relationship between hydraulic conductivity and intrinsic permeability is defined in Section 3.2.1.4.)

Laboratory results express the hydraulic conductivity as a function of the moisture content (Section 3.2.4) in terms of effective permeability (in units of millidarcys). Permeability expressed in this manner is considered an

intrinsic permeability. For example, the effective permeability for water is a measurement of the intrinsic permeability of the void space occupied by water, so the value is expressed in terms which are independent of the fluid.

The terms capillary forces, capillary pressure, soil tension, and soil suction are used synonymously. For purposes of this report, capillary forces are quantified using the term water potential which is measured in pressure units of negative bars or negative pounds per square inch (psi).

The terms residual moisture content, residual saturation, and moisture retention are also used synonymously. These terms refer to the undrainable quantity of water which remains in the sample even at increasingly higher capillary pressures. At these pressures, the water exists in discontinuous pockets or as thin films throughout the porous matrix. Vapor transport is the dominant transport mechanism below this range of saturation.

One other term used throughout the report requires clarification. As used herein, lapilli is defined in a manner consistent with the definition presented by Ross and Smith (1961): Lapilli consist of either juvenile lava fragments, still plastic or liquid when ejected, or of broken rock of any sort from the walls of the vent, or from the bedrock (country rock); in other words, they may be essential, accessory, or accidental ejecta. These authors state, however, that the term lapilli should be restricted to describing fragments in the size range 4 to 32 millimeters (mm); fragments of pyroclastic material larger than 32 mm are called blocks, whereas fragments smaller than 4 mm are called coarse ash (Ross and Smith, 1961). For purposes of simplification in this report, the size restriction for lapilli was ignored. For example, the presence of 'accessory' or 'accidental' lithic fragments (e.g., basalt fragments) less than 4 mm in diameter is one of the distinguishing characteristics of Unit 1b; these fragments are referred to as lithic lapilli in this report. In addition, fragments of pyroclastic ejecta of pumice or rock in the size range 32 to 60 mm (the latter value being the approximate diameter of the rock core obtained during this study) are also referred to as lapilli in this report.

1.2.2 UNITS

Inconsistencies in the unit systems used to express measurements occur throughout the report. Unfortunately, this inconsistency is unavoidable for the following reason. Several different types of instrument were used in the study, some of which display data in metric units (mks or cgs systems), while others are based on the British engineering system (fps system).* Conversion from one set of units to another is often cumbersome. For example, an instrument which measures pressure in the range 0 to 60 pounds per square inch (psi), with 0.2-psi increments, is described efficiently in British-system units. Conversion to the metric system results in an awkward description [i.e., 0 to 413.47 kilonewtons per square meter (kN/m^2) with 1.38-kN/m^2 increments]. Thus, for purposes of this report, both systems of units are given only when appropriate, in which cases the value in metric units is cited

*For metric-system units, mks = meter-kilogram-second and cgs = centimeter-gram-second. For British-system units, fps = foot-pound-second.

first, followed in parentheses by the equivalent value in British-engineering-system units.

1.3 PREVIOUS WORK

This report draws heavily on three earlier reports prepared for Los Alamos National Laboratory by the GJPO contractor personnel based on work conducted prior to FY-1986. The first report (Rush and Dexter, 1985) describes and discusses drilling and logging activities performed during the Summer of 1985. The second report (Bendix Field Engineering Corporation, 1985b) describes the procedures used for operating monitoring instruments installed for assessment of the hydrogeologic conditions of Waste Disposal Areas G and L in Technical Area 54. The third report (Kearl and others, 1986) presents a preliminary assessment of the hydrologic system based on FY-1985 work.

Section 2

GEOLOGIC CHARACTERIZATION OF THE STUDY AREA

This description of the geologic characteristics of the Bandelier Tuff in the study area is divided into five subsections. The first describes regional and site geology, based on information contained in the literature and observations of core obtained from holes drilled at the site (Rush and Dexter, 1985). This is followed by a discussion of the degree of welding observed in the tuff and the correlation of ash-flow units across the study area. Results of petrographic analyses of core samples from the drill holes and interpretations of the geophysical logs from the holes are summarized in Sections 2.3 and 2.4, respectively. The final subsection describes fractures observed in the core, since the presence of fractures can affect the nature and direction of waste transport in the tuff.

2.1 REGIONAL AND SITE GEOLOGY

The study area is located just east of the southeastern boundary of the Colorado Plateau (see Figure 2-1), on the eastern flank of the Jemez Mountains, also known as the Pajarito Plateau. The Jemez Mountains lie at the intersection of the volcanically active Jemez Lineament and the tectonically active Rio Grande rift. The Jemez Lineament is an alignment of Late Cenozoic volcanic fields; volcanism along the lineament has been continuous since Pliocene time (Goff and Bolivar, 1983).

Waste Disposal Areas G and L, located within Technical Area 54 at Los Alamos National Laboratory, are situated on Mesita del Buey, which is part of the Pajarito Plateau (Figure 2-2). Mesita del Buey, a narrow, southeast-trending mesa approximately two miles long and one-quarter of a mile wide, is underlain by rhyolitic ash-flow and air-fall deposits of the Bandelier Tuff. The Bandelier Tuff is composed of two members: the lower Otowi Member, 1.4 million years old, and the upper Tshirege Member, 1.1 million years old (Bailey and others, 1969). The Otowi Member consists of basal, air-fall tuff overlain by nonwelded ash-flow deposits containing abundant lithic lapilli. The Tshirege Member, which overlies the Otowi, consists of basal, bedded, air-fall tuff overlain by nonwelded to welded ash-flow tuffs containing abundant pumice and lithic lapilli. The Otowi and Tshirege members are both over 100 feet (ft) thick under Mesita del Buey (Purtymun and Kennedy, 1971). All waste-disposal excavations in Technical Area 54 are located in the upper portion of the Tshirege Member of the Bandelier Tuff.

The Tshirege Member can be subdivided into three units, two of which occur at Mesita del Buey (Units 1 and 2); the third unit, a nonwelded to moderately welded pumiceous tuff, is absent in the study area (Purtymun and Kennedy, 1971). The first two units dip 2 to 3 degrees to the southeast and become thinner in the direction of dip, away from their source in the Valles Caldera. Each of the units consists of two subunits (a and b), which are described by Purtymun and Kennedy (1971). Their descriptions, together with characteristics observed in the field and in the core collected for this study, were used to distinguish between each of the subunits. Lithologic logs of Units 1a through 2b, derived from drill holes in the study area, are presented in Appendix A; drill-hole locations are shown in Figure 2-3.

The lowermost subunit of the Tshirege Member encountered during this study was Unit 1a, a slightly welded to nonwelded, light-orange to light-brown,

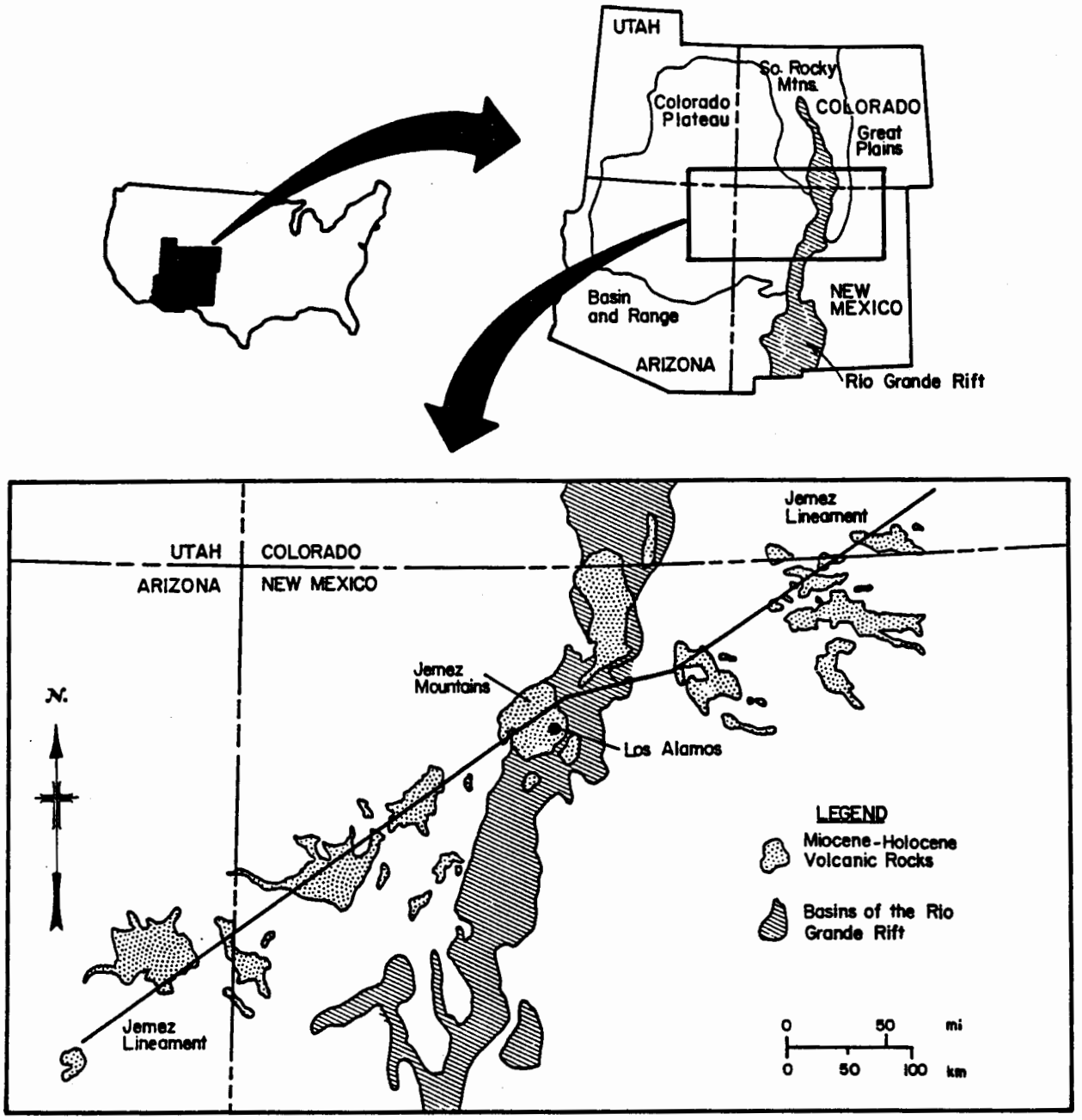

Figure 2-1. Location of the Study Area and Regional Geologic Relationships (modified from Goff and Bolivar, 1983)

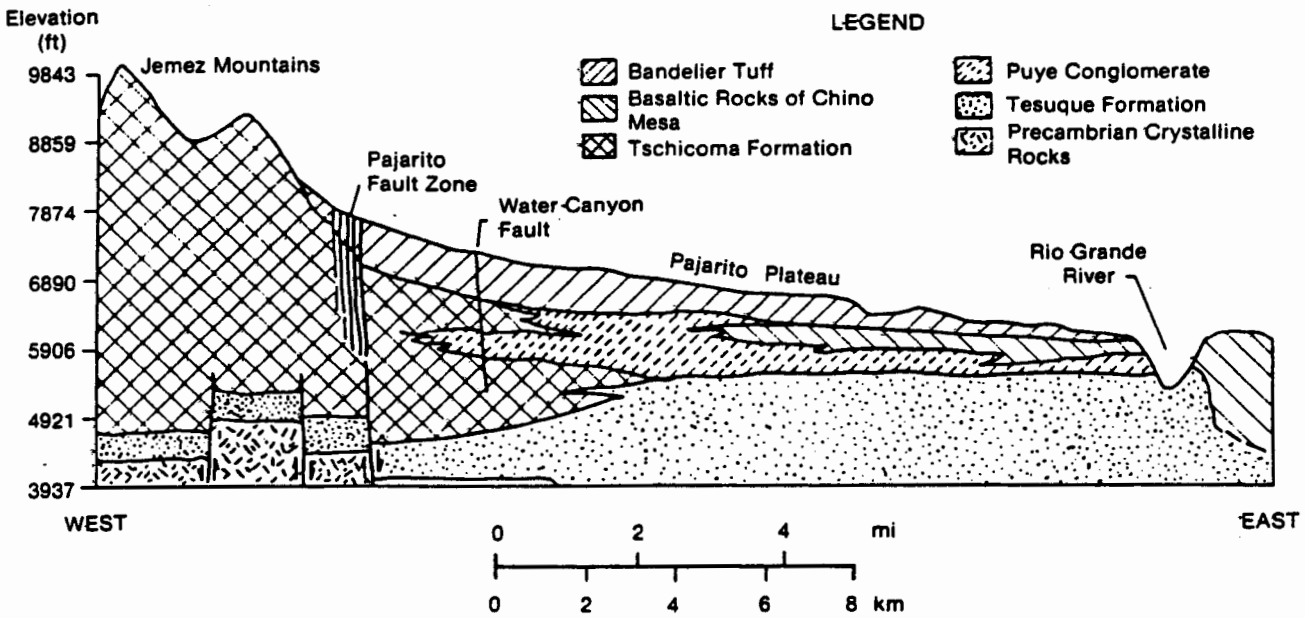

Figure 2-2. Geologic Cross Section from the Jemez Mountains on the West, Through the Pajarito Plateau, to the Rio Grande River on the East (modified from Abeele and others, 1981)

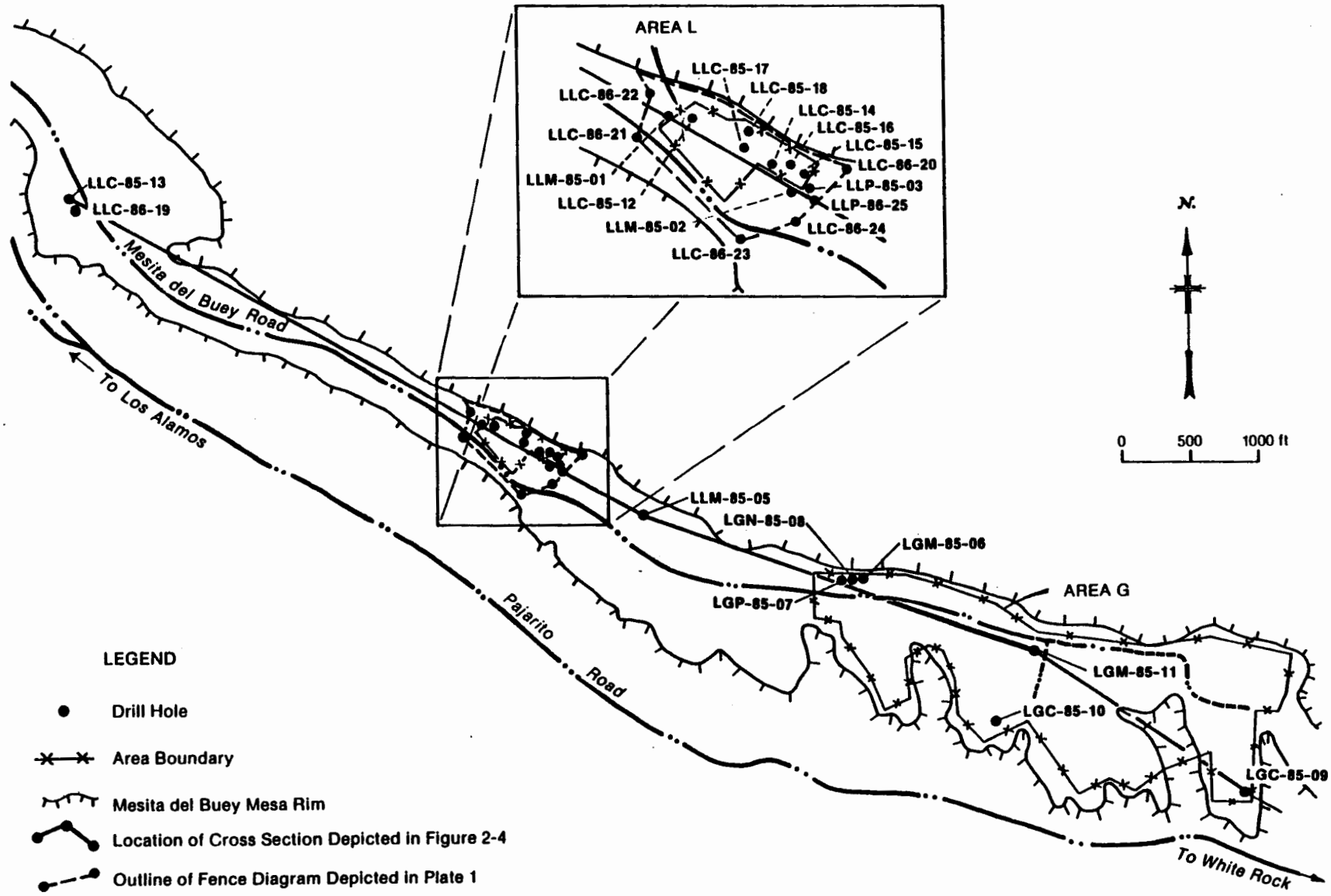

Figure 2-3. Locations of Drill Holes in Areas G and L, Technical Area 54, Los Alamos National Laboratory, New Mexico

rhyolitic, vitric-crystal ash-flow tuff. The maximum thickness of Unit 1a encountered in the Los Alamos drill holes was 64 ft; however, no drill hole penetrated the entire unit. At Mesita del Buey, Unit 1a consists of very uniform, nonwelded to slightly welded ash composed of brown glass shards and fine, flattened pumice lapilli, neither of which is devitrified. Also found in the ash are numerous but scattered lumps of light-tan pumice lapilli and latitic to rhyolitic lithic lapilli. In some of the deeper holes (1986 series), the lower, more tannish colored and slightly welded portions of the unit are noticeably damp immediately upon retrieval from the core barrel.

The contact between Units 1a and 1b is discerned in the core on the basis of the increased degree of welding and the presence of brown and gray pumice lapilli in Unit 1b. Unit 1b is a rhyolitic ash-flow tuff, ranging in color from light gray to pinkish gray near the top, and from pale red to moderate orange pink near the base. The lower portion of Unit 1b contains distinctive bipyramidal quartz crystals up to 4 millimeters (mm) in diameter and a bimodal distribution of latitic to rhyolitic lithic lapilli. The lithic lapilli are abundant in the size range 1 to 4 mm in diameter, and occur less commonly in the size range 15 to 60 mm. They decrease in size and abundance toward the top of Unit 1b, where the occurrence of lithic lapilli is rare. The degree of welding in Unit 1b generally varies from slightly welded at the base to moderately welded just above the base to slightly welded at the top. In 11 core holes where the entire section of Unit 1b was penetrated, the total thickness varies from approximately 29 ft (on the southeast) to 74 ft.

The contact between Units 1b and 2a was difficult to identify precisely during coring operations. In certain cases, the contact can be estimated on the basis of either a subtle color change in a slightly welded portion of the core, or the presence of brown, gray, and olive-colored pumice lapilli in the basal portion of Unit 2a. These pumice lapilli are generally larger than the predominantly brown pumice lapilli found in the upper portion of Unit 1b. In addition, the contact seems to occur in a zone where vapor-phase crystals of quartz and sanidine are small (less than 1 mm in diameter) and sparse. Microscopic criteria for distinguishing between these units are described in Section 2.3 of this report.

Unit 2a consists of a lower ash flow and an upper ash fall (Purtymun and Kennedy, 1971), although no ash-fall unit was encountered during this study. The unit ranges in color from light pink to pale red to gray. It contains relatively large (5 to 30 mm) gray-, brown-, and olive-colored pumice lapilli, and varies from slightly to moderately welded. Unit 2a varies in thickness from 67 ft in the northwest (Hole LLC-86-19) to 21 ft in the southeast (Hole LGC-85-09).

The contact between Units 2a and 2b is generally marked by a subtle color change within a slightly welded zone of tuff. Purtymun and Kennedy (1971) identify this contact on the basis of the occurrence of thin, lenticular deposits of reworked tuff. This zone of reworked tuff was observed in core from Holes LLC-86-21 and LLC-86-22. The transition from Unit 2a to Unit 2b at Mesita del Buey appears to be marked by a decrease in the variety of pumice lapilli occurring in the basal portion of Unit 2b; pumice lapilli in Unit 2b are dominantly gray in color, whereas the pumice lapilli in Unit 2a are gray-, brown-, and olive-colored. The contact between the two units is most easily seen in the outcrop; in many places the lenticular deposits of reworked tuff,

occasionally cross-bedded, are readily observable. In general, Unit 2a contains a greater amount of pumice lapilli and bombs than Unit 2b, resulting in sloping erosional surfaces. However, basal portions of Unit 2b often display an increase in the amounts of pumice lapilli and blocks, which can obviously confuse the issue when trying to discern this contact in the core. In outcrop, these basal, pumice-rich portions of Unit 2b are often continuous with the vertical cliff-forming nature of the rest of Unit 2b, down to its contact with Unit 2a, even though it is generally only slightly welded.

Unit 2b forms the cap rock at Mesita del Buey and consists of brownish-gray, light-gray, and pinkish-gray, slightly to moderately welded, rhyolitic ash-flow tuff with light-gray and occasional brown pumice lapilli. In some areas on the Pajarito Plateau, this subunit may contain up to eight distinct flow units, separated by sandy partings and pumice concentrations (Goff and Bolivar, 1983). Field descriptions, apparent density logs, and magnetic susceptibility logs obtained during this study indicate that, at Mesita del Buey, Unit 2b consists of several flows and is generally separated from Unit 2a by a lower zone of slightly welded tuff. The maximum and minimum thicknesses of Unit 2b encountered in the Los Alamos drill holes were 45 ft in the northwesternmost hole (LLC-85-13) and 28 ft in the southeasternmost hole (LGC-85-09).

2.2 WELDING AND CORRELATION OF ASH-FLOW UNITS AT MESITA DEL BUEY

Welding of tuffaceous rocks at Mesita del Buey ranges from nonwelded to moderately welded. Although the degree of welding is gradational between these ranges, generalized definitions of each welding descriptor were formulated for use when describing rocks in the study area. These are summarized below:

- Nonwelded - Completely disaggregated; little to no flattening of pumice lapilli observed.

- Slightly Welded - Slightly coherent, but crumbles easily in the hand; occasional pumice lapilli are noticeably flattened.

- Moderately Welded - Tuff crumbles with difficulty in the hand and occasionally must be struck with a hammer to break; flattening of most pumice lapilli to varying degrees is noticeable.

Although the units are defined on the basis of individual or composite flows, general variations in welding within the units can be correlated across Mesita del Buey. A cross section showing these variations is presented in Figure 2-4; the location of the cross section in the study area is shown in Figure 2-3. A general thinning of the ash-flow units can be seen on the cross section from northwest to southeast (away from the caldera). Moderate welding is most consistently found in the lower portion of Unit 1b near its contact with Unit 1a, and in the middle and upper portions of Unit 2b. In general, the moderately welded portions of Unit 2a break or crumble in the hand more easily than the moderately welded portions of Units 1b and 2b. The welding characteristics of Unit 2a, however, are not consistent in a lateral sense. Also not laterally consistent are the slightly welded zones; in certain cases,

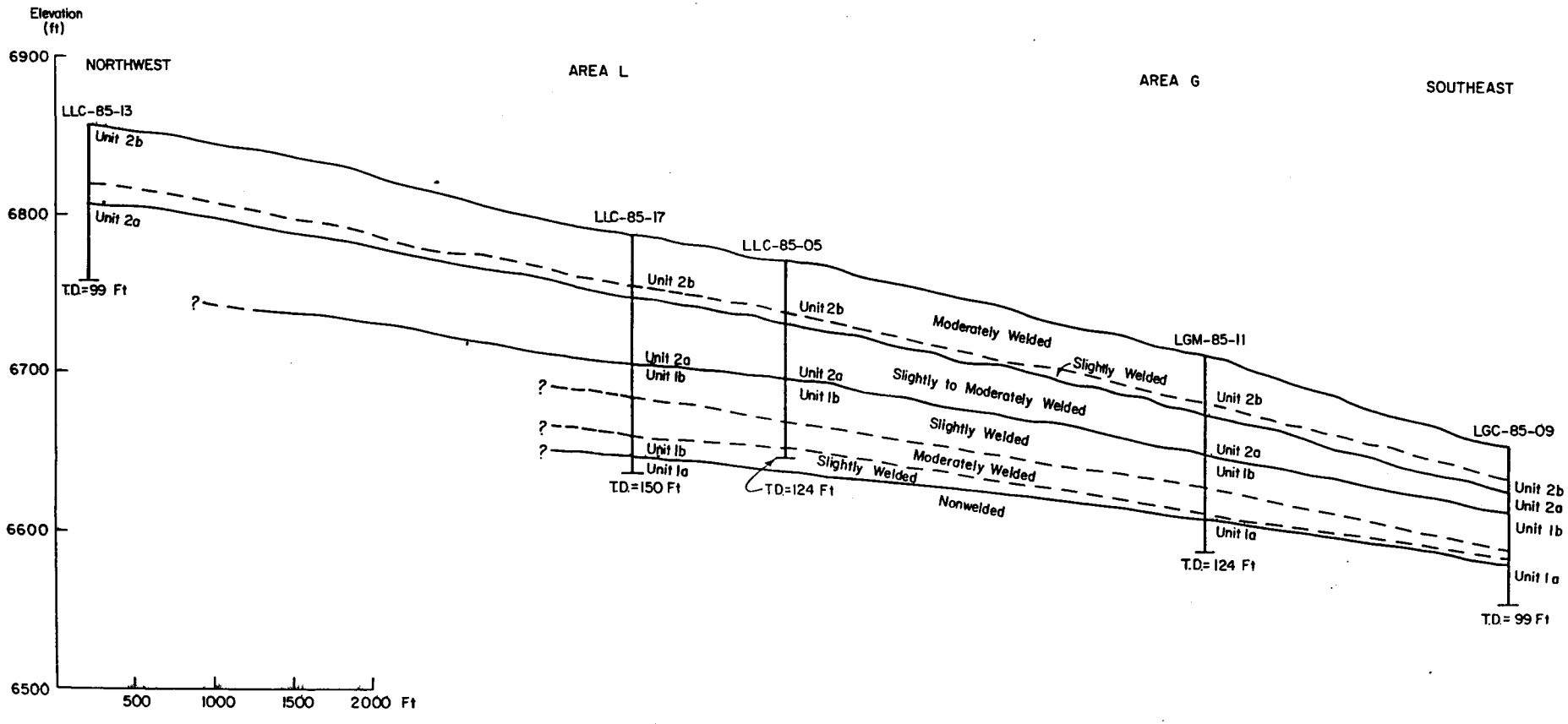

Figure 2-4. Cross Section Showing Parts of the Tshirege Member of the Bandelier Tuff, Drawn Through Mesita del Buey and Technical Area 54

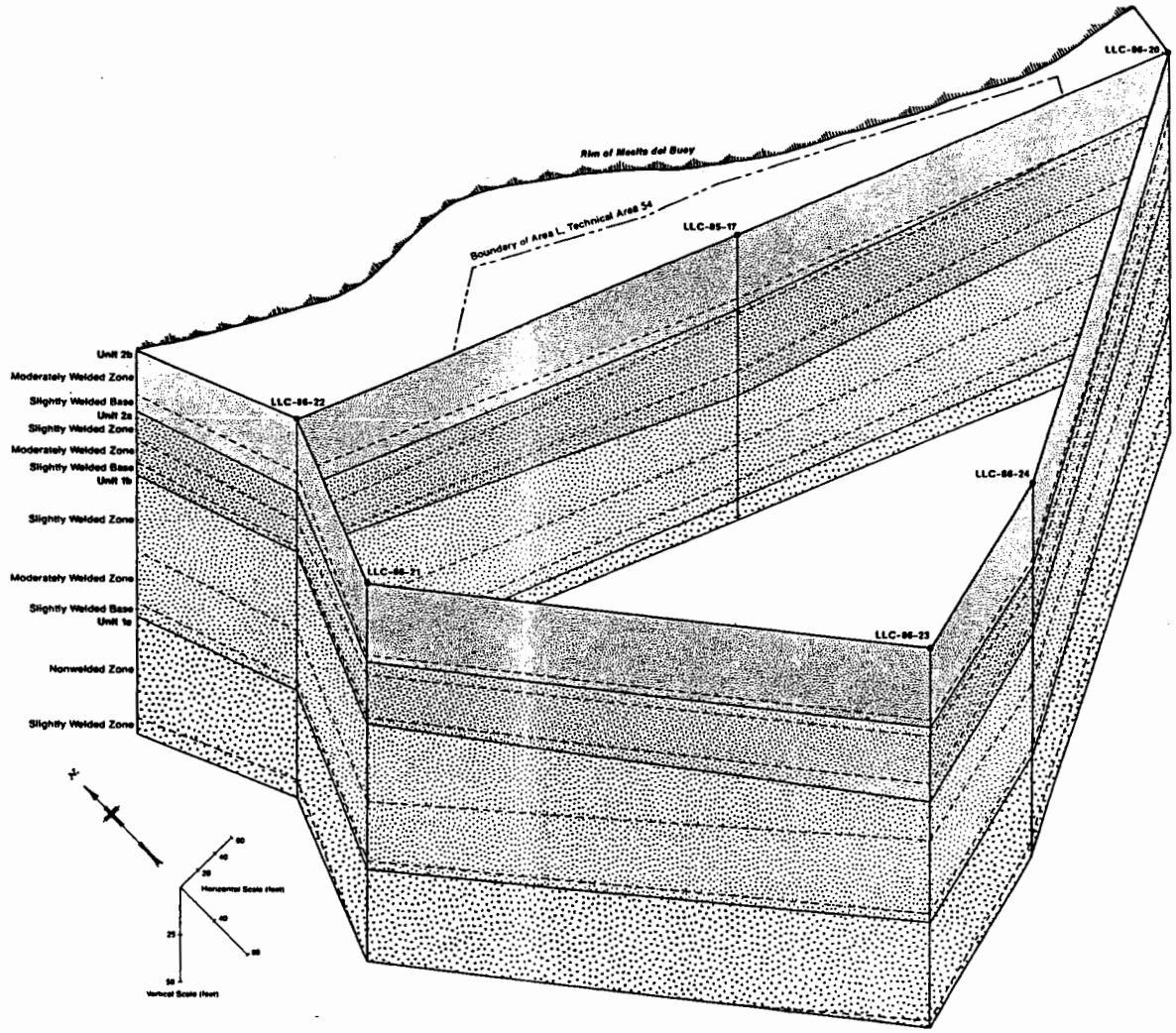

Figure 2-5. Fence Diagram Through Waste Disposal Area L Showing Subsurface Stratigraphy of the Bandelier Tuff

Units 2a and 2b are 0.6. In addition, it was found that tridymite is generally absent in samples from Unit 1b. Units 1 and 2 are therefore compositionally distinct.

Table 2-1. Volume-Percent Quartz and Sanidine Determined from Point-Count Analysis of Thin Sections

Sample Number	Hole Number	Depth (ft)	Volume-Percent Quartz	Volume-Percent Sanidine
UNIT 1b				
MCG-628	LLM-85-01	101	5.4	11.9
MCG-629	LLM-85-01	122	11.9	9.0
MCG-632	LLM-85-02	74	9.7	10.3
MCG-633	LLM-85-02	111	6.4	6.0
MCG-636	LGM-85-06	100	6.3	9.7
MCG-640	LGM-85-11	95	6.7	8.6
MCG-649	LGC-85-09	48	12.0	9.7
MCG-650	LGC-85-09	68	8.1	8.5
MCG-656	LLC-86-20	126	7.6	10.6
MCG-658	LLC-86-20	119	8.0	11.0
AVERAGE VALUES			8.2	9.5
UNIT 2a				
MCG-627	LLM-85-01	52	7.8	14.3
MCG-631	LLM-85-02	64	10.4	15.1
MCG-635	LGM-85-06	50	9.0	11.0
MCG-648	LGC-85-09	35	8.0	17.0
MCG-661	Outcrop	NA[a]	7.0	10.2
AVERAGE VALUES			8.4	13.5
UNIT 2b				
MCG-626	LLM-85-01	30	7.6	17.3
MCG-630	LLM-85-02	37	5.7	12.5
MCG-634	LGM-85-06	30	11.4	13.8
MCG-638	LGM-85-11	5	7.1	13.2
MCG-639	LGM-85-11	31	13.2	10.1
MCG-643	LLC-85-13	42	6.2	18.4
MCG-644	LLC-85-17	12	8.0	14.0
MCG-646	LGC-85-09	10	8.4	13.6
MCG-647	LGC-85-09	21	8.8	24.1
MCG-659	Outcrop	NA[a]	9.8	15.5
MCG-660	Outcrop	NA[a]	12.9	13.2
AVERAGE VALUES			9.0	15.1

[a]NA = Not Applicable.

Other significant recognition criteria are the microscopic characteristics of pumice lapilli. Pumice lapilli in Unit 1b either are devitrified and display spherulitic textures with occasional vapor-phase mineralization by a radial-acicular zeolite, or consist of fresh glass; they also vary in shape from flattened to nonflattened in many samples. Pumice lapilli in Units 2a and 2b, on the other hand, are ubiquitously replaced by sanidine, tridymite, and occasionally a zeolite; in general, they are all at least partially flattened. Moreover, the average percentage of pumice lapilli (determined by point-count analysis of thin sections) is generally higher in Unit 1b (21 percent) than in Unit 2a (16 percent) or Unit 2b (13 percent). Evidently, the less flattened, more abundant nature of the pumice lapilli in Unit 1b is the primary reason for the fact that Unit 1b is less dense than Units 2a and 2b (see discussion of apparent density logs in Section 2.4.3).

2.4 INTERPRETATION OF GEOPHYSICAL LOGS

Several different types of geophysical log were obtained utilizing different downhole probes. Details regarding equipment and procedures were described in the first interim report (Rush and Dexter, 1985); a complete set of geophysical logs for all holes drilled during the 1985 study is included in that report. Magnetic susceptibility and apparent density logs for holes drilled in 1986 are included in Appendix F.

The following geophysical-logging data were generated for many of the drillholes during this study:

- Natural Gamma, Epithermal Neutron (and derived moisture), and Vertical Deviation Logs
- Spectral Gamma and Caliper Logs
- Magnetic Susceptibility Logs
- Gamma-Gamma (Apparent Density) Logs

The caliper and vertical deviation logs were obtained prior to installation of instruments described in other parts of this report to determine sizes and types of downhole equipment that would be necessary to facilitate the installations. The vertical deviation in the 18 drill holes at Los Alamos averages 2.5 ft and ranges from 1 to 4 ft; in general, the diameters of the completed drill holes are between 7 and 8 inches.

Discussions of the remaining types of geophysical log are presented in the paragraphs that follow. These discussions focus primarily on interpreting the logs with a view to identifying the vertical variations of lithologies present in each drill hole. In general, most of the logs tend to confirm the presence of previously established boundaries and contacts within the ash-flow tuffs. In certain cases, however, information obtained from the geophysical logs required that modifications be made to the lithologic logs acquired during the drilling of the study-area holes. Original versions of the lithologic logs

were presented in the first interim report (Rush and Dexter, 1985); the subsequent modifications have been incorporated in the logs presented in this report (see Appendix A).

2.4.1 NATURAL GAMMA AND EPITHERMAL NEUTRON MOISTURE LOGS

The natural gamma probe counts the spectrum of gamma rays above approximately 50 kiloelectronvolts (keV). In the 18 holes drilled, gross-gamma radiation ranges from 300 to 700 counts per second (cps). The epithermal neutron system consists of a neutron detector used in conjunction with a neutron source. Values from the logs range from 600 to 1600 cps. Logs from both of these systems show the vertical distribution of these total-count ranges; few of the vertical changes in total count correlate with a known boundary within the ash-flow tuff. Only in two holes (LGC-85-09 and LGC-85-10) were confirmations of previously drawn contacts possible. Figure 2-6 presents the epithermal neutron, natural gamma, and lithologic logs for Hole LGC-85-10. As can be seen, changes in total count with depth suggest confirmation of contacts and boundaries drawn on the adjacent lithologic log. However, since some of the obvious vertical changes in total count do not correspond with known physical changes, it is not possible to identify contacts on the basis of the epithermal neutron and natural gamma logs alone.

Moisture logs were derived from the epithermal neutron data. These moisture logs have the same general shape as the moisture logs obtained by gravimetric methods (see Section 3.1.1). A comparison of the two methods is illustrated in Figure 2-7. In general, the values for moisture percent seen in the epithermal neutron log are higher than those seen in the gravimetric data. Although the epithermal neutron data are more detailed (data points were obtained every 0.5 ft whereas gravimetric samples were collected every 5 ft), it appears that the gravimetric data are more accurate. Uncertainties in the calculated (epithermal neutron) moisture content at each 0.5-ft interval are compounded by counting errors, errors associated with the calibration parameters, and errors associated with the fact that no hole-size corrections were applied to the data. The percent uncertainty represented by these errors often exceeds the calculated moisture value. In this study, for example, these errors are estimated to be ± 3.0 percent by volume (Marutzky, 1986).

2.4.2 SPECTRAL GAMMA LOGS

The spectral gamma probe counts energy produced by potassium (K), uranium (U), and thorium (Th); total counts obtained in the field were converted to concentrations of K in percent, and U and Th in parts per million (ppm).

The Bandelier Tuff drilled during this study averages approximately 4 percent potassium, 5 to 10 ppm uranium, and 20 to 30 ppm thorium. As with the logs described in the previous subsection, the spectral gamma logs can, at best, only help to confirm the existence of previously drawn contacts and boundaries. Since vertical changes in concentration are not consistent from one hole to another, the logs cannot be used to draw boundaries or modify previously drawn contacts.

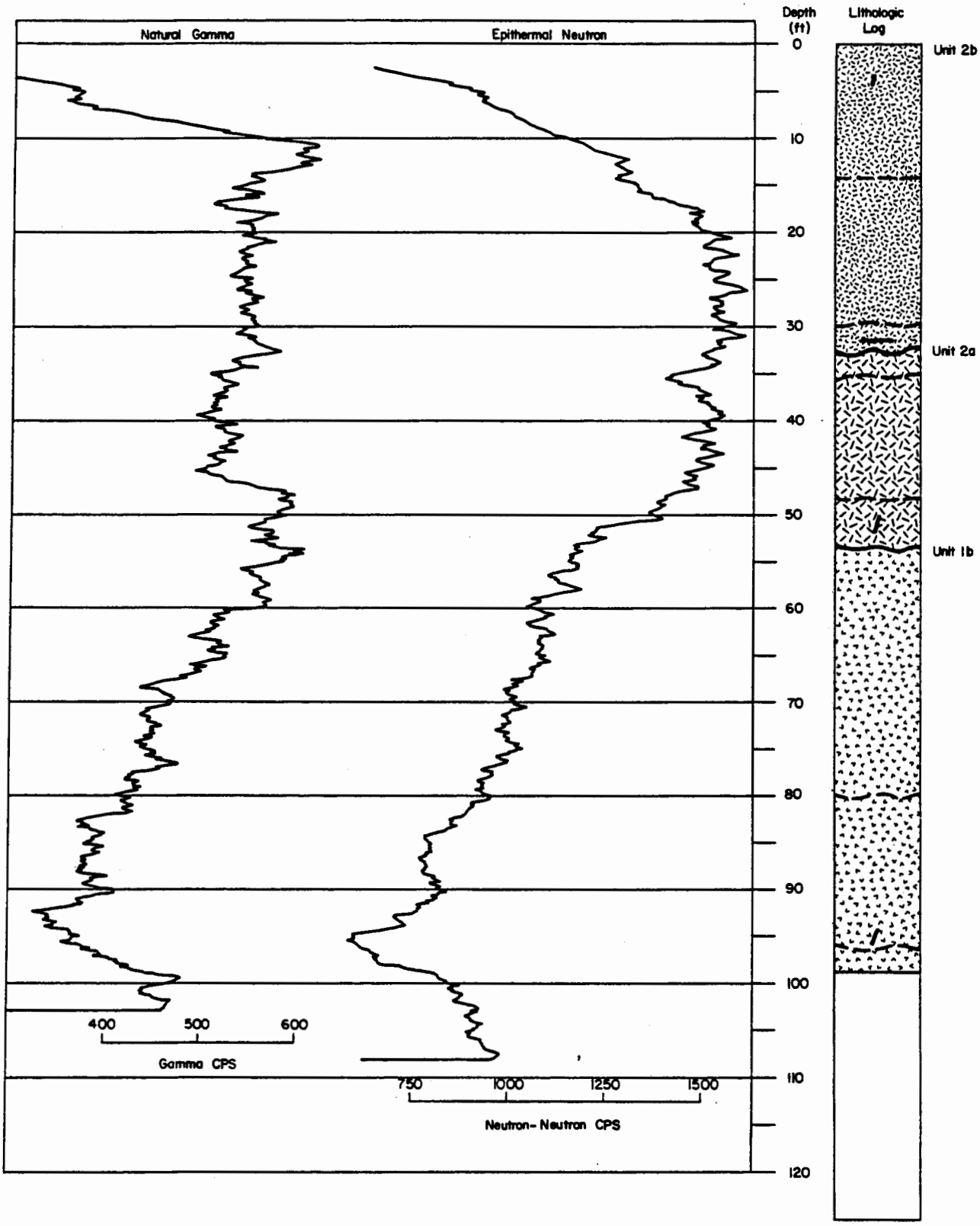

Figure 2-6. Epithermal Neutron, Natural Gamma, and Lithologic Logs for Hole LGC-85-10

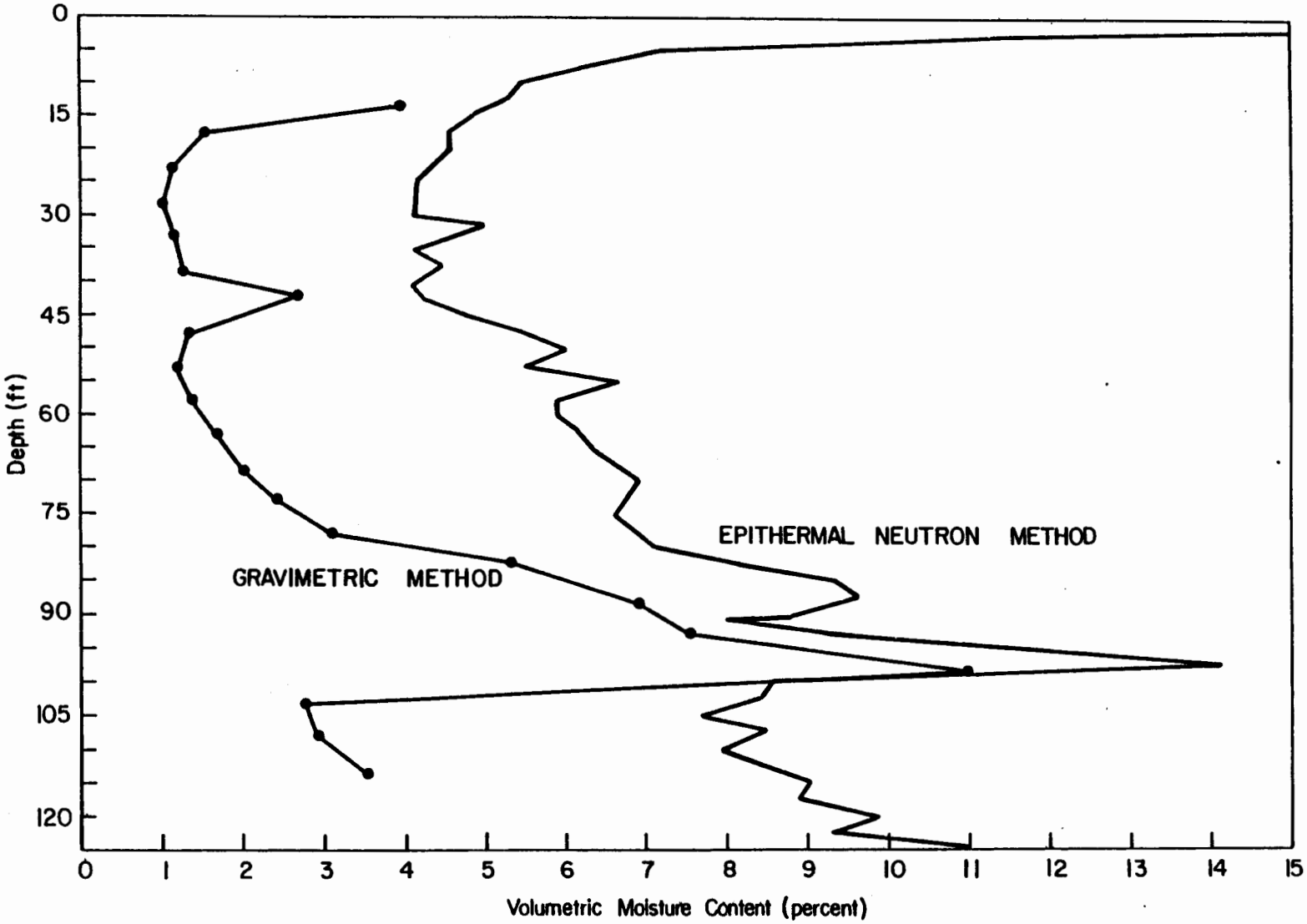

Figure 2-7. Comparison of Moisture Curves for Hole LGM-85-06, Derived by Geophysical and Gravimetric Methods

Figure 2-8 shows the spectral gamma and lithologic logs for Hole LGM-85-11. At first glance, there appears to be an inverse relationship between uranium and thorium. This is probably artificial and results from the use of a data-reduction program that strips away the energy contributions from uranium that overlap the energy window of thorium (and vice versa). At low concentrations of uranium and thorium, such as those displayed by the Bandelier Tuff in the study area, the stripping process results in apparent inverse relationships. As can be seen in Figure 2-8, however, this relationship is superseded by the simultaneous peaking of K, U, and Th at the boundary of Units 1b and 2a (61 ft), which is marked by an increase in uranium (to 10 ppm) and thorium (to 30 ppm). Similar increases in uranium and thorium at the contact of Units 1b and 2a were noted on spectral gamma logs from other holes as well, suggesting gross chemical differences between Unit 1 and Unit 2. This confirms the same conclusion drawn from the petrographic data on the basis of quartz and sanidine contents.

2.4.3 MAGNETIC SUSCEPTIBILITY AND GAMMA-GAMMA (APPARENT DENSITY) LOGS

The magnetic susceptibility (MS) and gamma-gamma (apparent density) logs proved to be the most valuable in terms of correlating physical and hydrologic properties in the study area. The MS probe is calibrated in micro-cgs* units and measures the degree to which the tuff is attracted to a magnet; essentially, this is an indirect measure of the iron content of the tuff. Because of considerable base-line drift due to temperature changes in the sensing coil of the probe, the shape of the curve, not the displayed values, is significant. The gamma-gamma probe collects data in counts per second that are immediately converted to apparent density in grams per cubic centimeter (g/cm^3) using the calibration data obtained during installation of the logging system. The density of the ash-flow tuffs is a function of welding, amounts of lithic and pumice lapilli, water content, and degree and amount of vapor-phase crystallization and devitrification.

Relationships between magnetic susceptibility, density, and lithology are shown schematically in Figures 2-9 through 2-11. For the most part, the MS logs show good correlations with contacts between individual ash flows, whereas the density logs show good correlations with boundaries based on welding characteristics. However, minute changes in magnetic susceptibility can delineate zones with different welding characteristics (see, for example, Figures 2-9 and A-9, Hole LGC-85-10, 83 to 97 ft), whereas minute changes in apparent density can delineate contacts between individual ash flows (Hole LGC-85-10 at a depth of 55 ft).

The MS and apparent density logs obtained from holes drilled Summer 1986 also correlate well with the lithologic logs. Since the 1986 holes penetrated the tuff at deeper levels, additional physical characteristics were substantiated. The moderately welded zone in Unit 1b was detected on the MS and apparent density logs. In Hole LLC-86-22, the core at a depth of 128 feet was noticeably damp upon retrieval (see Figure A-21, Appendix A). Although the apparent density log (see Appendix F) does not delineate the moderately welded zone very well (see comment on Figure A-21 stating that this zone is not as well defined as in other holes), a relatively dense zone is depicted from 125 to

*Centimeter-gram-second.

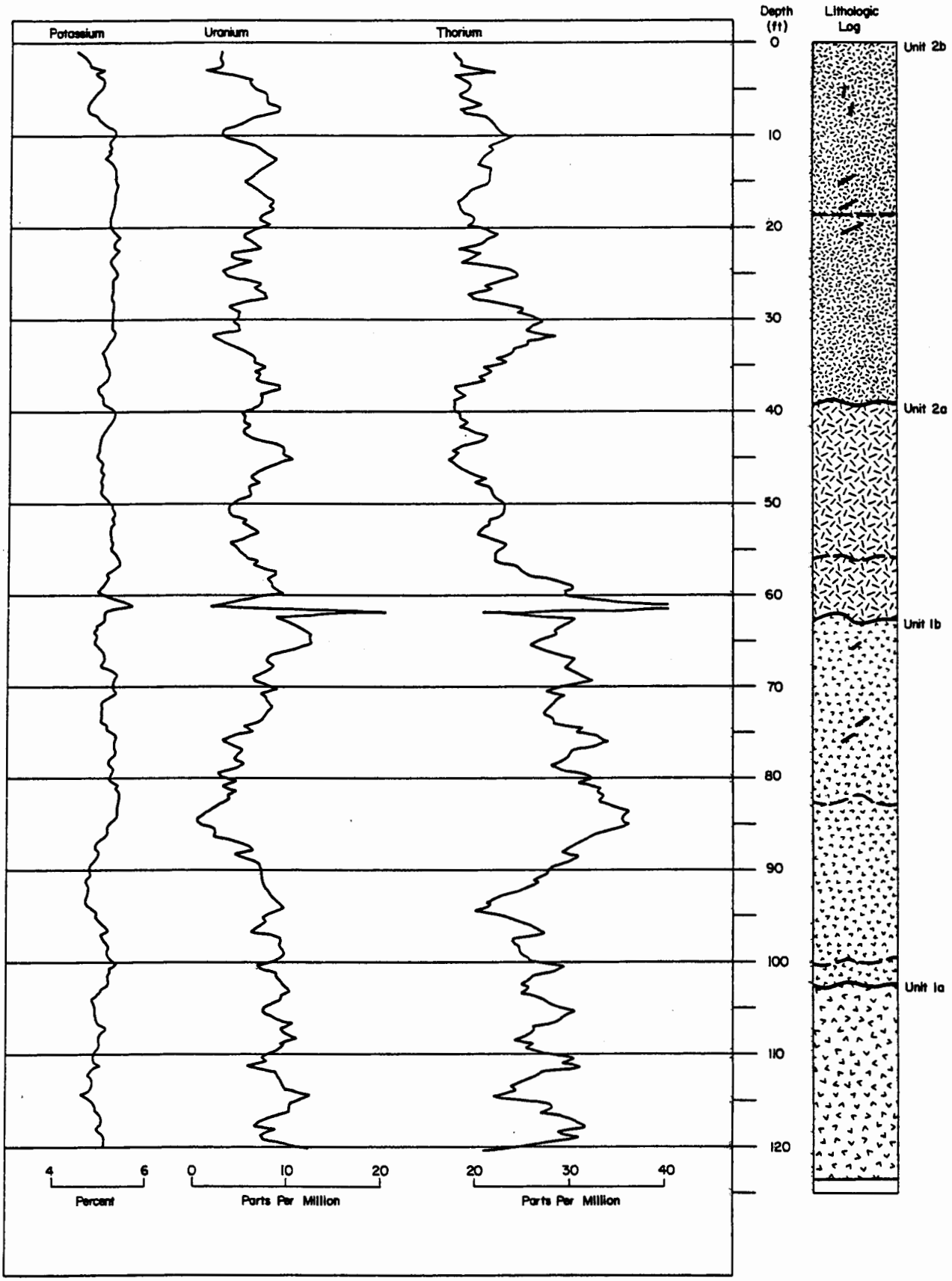

Figure 2-8. Spectral Gamma and Lithologic Logs for Hole LGM-85-11

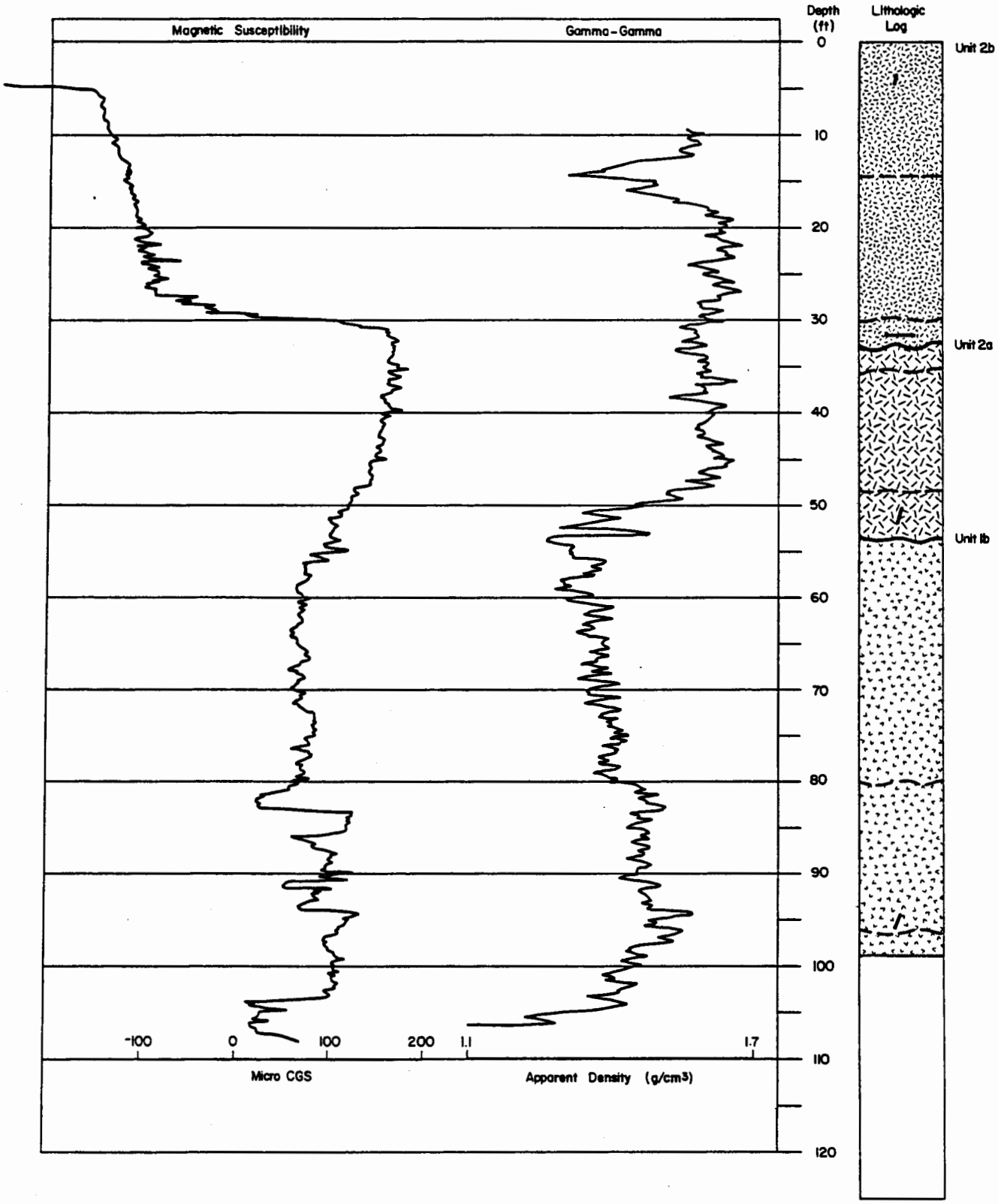

Figure 2-9. Magnetic Susceptibility, Apparent Density, and Lithologic Logs for Hole LGC-85-10

130 feet and defines the part of the zone with the highest moisture content. This 5-foot zone is in excellent agreement with the volumetric moisture data for this hole (see Figure 3-3, Hole LLC-86-22). The density log also indicates a gradual increase in density below a depth of 180 feet, where the Unit 1a tuff becomes noticeably damp and slightly welded. The MS log for this hole does not delineate this moderately welded zone, but does yield a striking match to the contact of Units 1a and 1b that was logged at approximately 142 feet during field operations; the MS log displays a large peak at a depth of 142 feet. In addition, the contact between Units 2a and 2b is substantiated by a large MS shift at 38 feet; the Units 2a and 1b contact is documented by a magnetic susceptibility spike at 72 feet. A large shift in magnetic susceptibility at a depth of 23 feet matches the subtle color change depicted on the lithologic log and probably represents the 'multiple-flow' nature of Unit 2b. The MS shift at a depth of 210 feet is probably significant, but core was not obtained below 198 feet so the shift cannot be interpreted; the MS shift could represent a simple color change in Unit 1a or the base of Unit 1a.

In some cases, the density log will indicate a contact between separate flows that is not visible on the MS log. For example, in Hole LGC-85-10 (Figure 2-9), the contact between separate flows within Unit 2b is marked only by an increase in the amount of pumice lapilli and is therefore visible only on the density log (at 14 ft). Concentrations of pumice lapilli are common at the tops, bottoms, and within ash-flow units. This feature is obvious on the density log in Figure 2-9; large negative peaks clearly demonstrate the increased concentration of pumice lapilli in the lower part of Unit 2a, from a depth of 50 to 54 ft. Another feature discernible on the density logs is the general decrease in the density of Unit 1b, which appears to be less dense on the whole than Units 2a or 2b. As noted earlier in the discussion of the petrologic data (Section 2.3), the decrease in the overall density of Unit 1b appears to be due to the fact that the pumice lapilli in the unit are more abundant and less flattened than those in Units 2b and 2a.

Occasionally the ability of the density logs to indicate contacts between distinct units, on the basis of minute density changes, is hampered by the presence of fractures. In Hole LLM-85-02 (Figure 2-10), the near-vertical fracture that extends from 35 to 40 ft obscures the minute changes in density that might be visible on the log were it not for the presence of the fracture. Induration of the tuff near the fracture, together with open spaces along the fracture, appears to result in both negative and positive apparent density peaks. A relationship between fractures and apparent density can also be seen in Figure 2-11 (Hole LGM-85-11) from a depth of 14 to 20 ft; large negative peaks on the apparent density log at 14, 16, and 19 ft correspond to observed fractures in core from this hole at 15.5, 17.5, and 20 ft. The differences in depth are probably due to the size of the core (2.5-inch diameter) versus the size of the hole that was probed (7- to 8-inch diameter). A potential application of the apparent density logs is in the determination of the extent to which fractures are open. Areas where fractures were logged via examination of the core are not always obvious on the density logs; fractures that are wholly to partially filled would probably not be characterized by a significant decrease in density.

The magnetic susceptibility log for Hole LGM-85-11 (Figure 2-11) indicates sharp boundaries which appear to define the gross differences between the four major subunits of the Tshirege Member; contacts between subunits at this

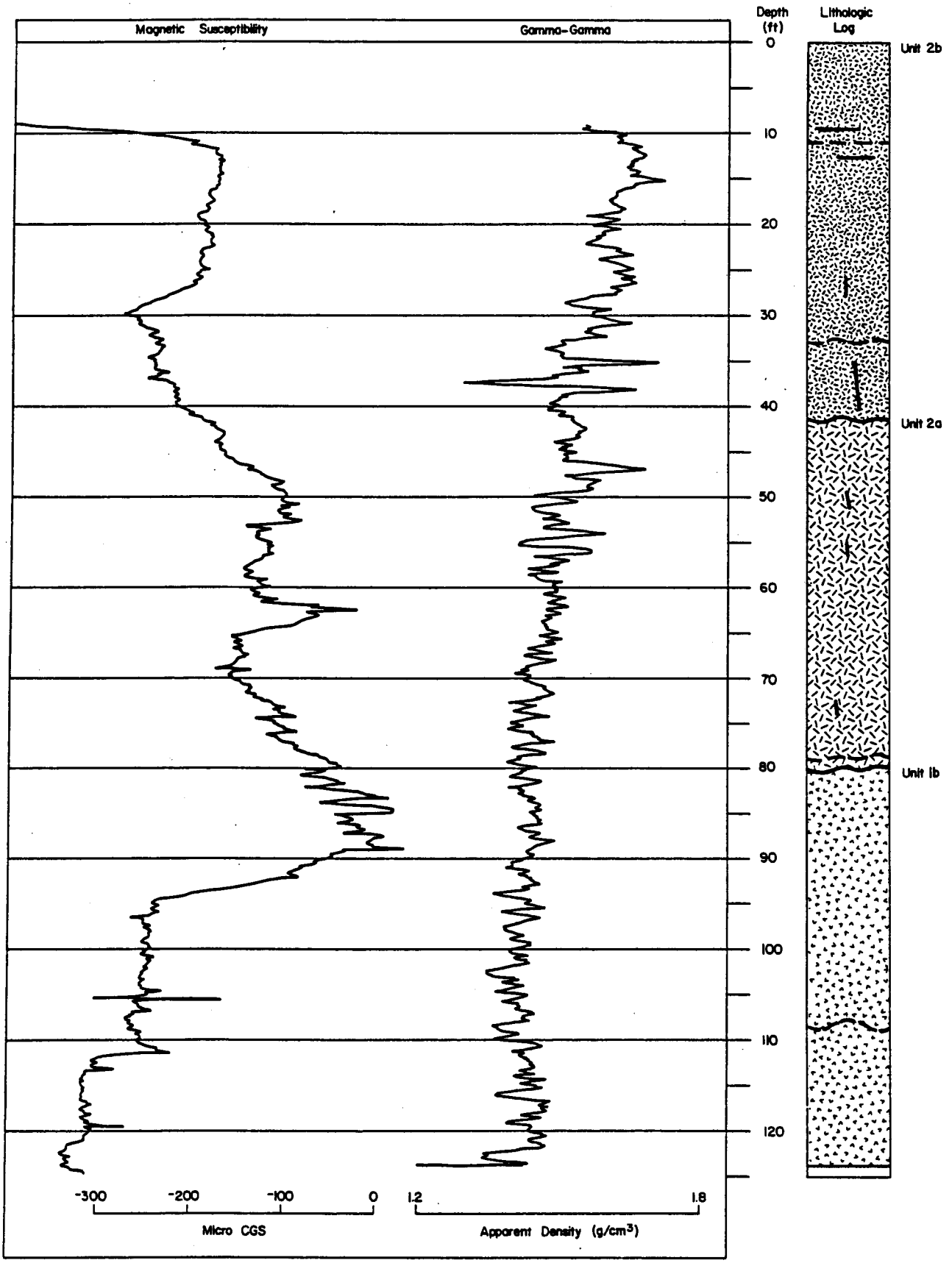

Figure 2-10. Magnetic Susceptibility, Apparent Density, and Lithologic Logs for Hole LLM-85-02

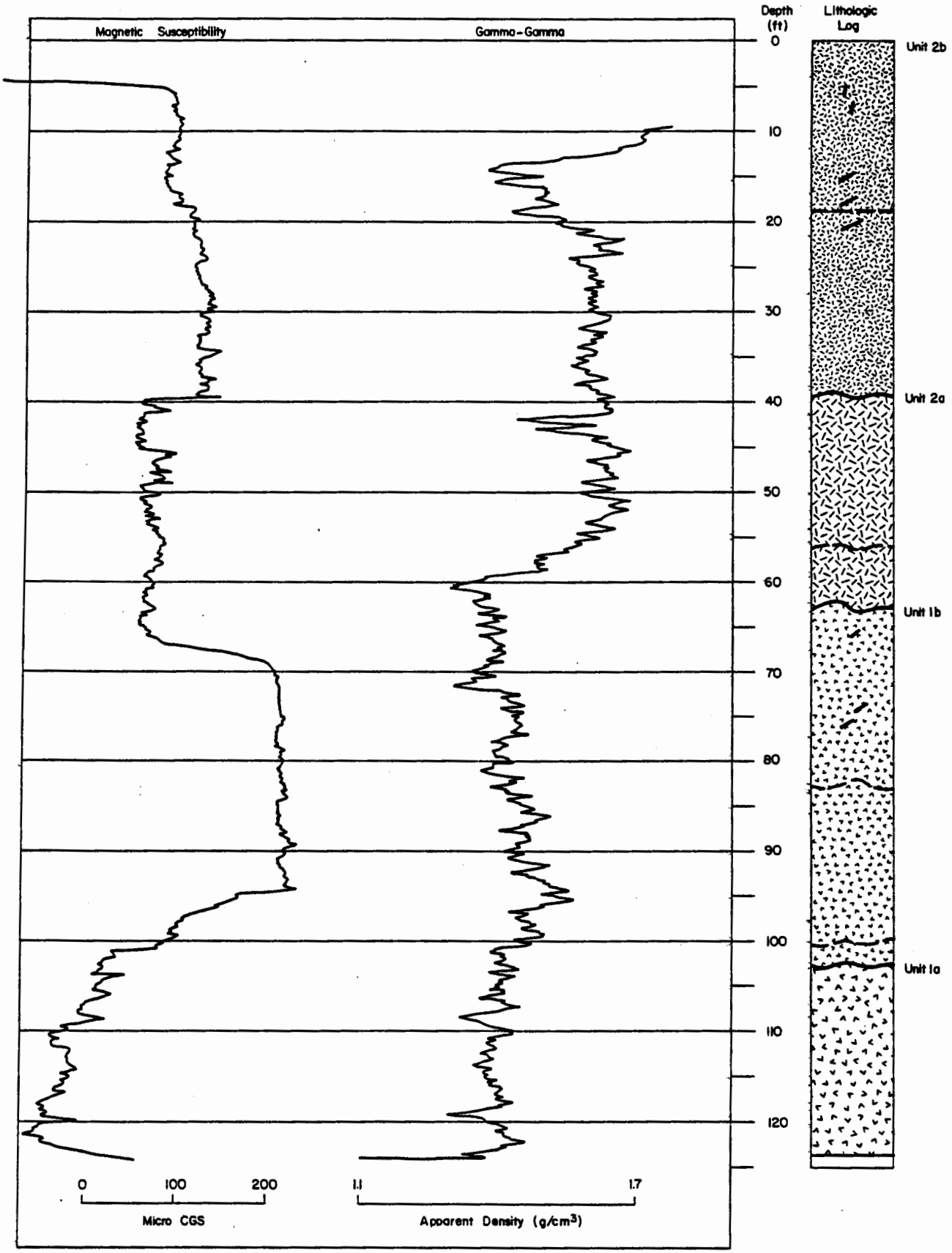

Figure 2-11. Magnetic Susceptibility, Apparent Density, and Lithologic Logs for Hole LGM-85-11

location were refined based on this information. The MS log for Hole LLM-85-02 (Figure 2-10), on the other hand, does not appear to define the contacts between major subunits; consequently, the log can only be used to confirm, rather than modify, the boundaries and contacts identified during drilling operations.

In conclusion, it should be emphasized that care must be taken when interpreting MS logs. Because of the common 'base-line drift' mentioned previously, apparent boundary changes in the form of an MS shift are possible. Therefore, the MS logs should not be used alone to identify contacts between ash-flow cooling units.

2.5 FRACTURES

2.5.1 SUBSURFACE CHARACTERISTICS

Fractures in the Tshirege Member at Mesita del Buey are predominantly tension joints formed as a result of contraction during initial cooling of the flows. Horizontal fractures, for the most part observed near the surface, are probably postdepositional fractures related to near-surface unloading along flow-foliation due to erosion of formerly overlying ash-flow tuff; most of these are filled with caliche and root material. During this study, horizontal fractures were observed only in Unit 2b. Only two fractures were observed in Unit 1a, which is composed of nonwelded to slightly welded tuff. (Note: The entire thickness of Unit 1a was not penetrated in this study.)

A summary of the number of fractures logged during the drilling program of this study is presented in Table 2-2. Although most of these fractures are nearly vertical (between 70 and 90 degrees), many fractures in both Units 2a and 2b have an apparent dip of about 45 degrees (see the lithologic logs in Appendix A). The greatest number of fractures occurs in Unit 2b; this agrees with data collected by Purtymun and others (1978). These authors found that more than 70 percent of the fractures they logged in both Units 2b and 2a were filled with brown clay or caliche. Similarly, observations made during the drilling program for this study indicated that most of the fractures appeared to be partially to completely filled with either caliche, brown clay, or limonitic material. Samples of some of the filled fractures were submitted to the GJPO Petrology Laboratory for X-ray diffraction analysis. Both bulk fractions and clay-sized separates of the fracture coatings were analyzed. The results demonstrated that the bulk fractions had the same composition as the host samples. Clay-sized fractions consisted predominantly of smectite (montmorillonite), with moderate to minor amounts of illite/mica and kaolinite.

Most of the fractures logged during this study occur in moderately welded zones within the tuffs. This is to be expected since these zones retained heat longer than the slightly welded zones. A feature observed in one fracture (cf. Figure 2-10, Hole LLM-85-02, 35 to 44 ft) deserves to be mentioned. This fracture displays an effect similar to surficial 'case-hardening,' as described by Abeele and others (1981, page 5); the tuff near the fracture is quite hard, but the tuff is only slightly welded less than 2 inches from the joint surface. This feature may signify preferential movement of water or

Table 2-2. Number of Fractures Logged in the Los Alamos Drill Holes

Unit of Tshirege Member	Number of Fractures[a]
Unit 2b	
Slightly Welded Zone	22
Moderately Welded Zone	81
Unit 2a	
Slightly Welded Zone	7
Moderately Welded Zone	45
Unit 1b	
Slightly Welded Zone	13
Moderately Welded Zone	26
Unit 1a	
Slightly Welded Zone	2

[a]Fracture zones are excluded where numerous fractures are present.

water vapor along open fractures during recent times, or may be a result of devolatization of the tuff during cooling. The fact that the gravimetric moisture data indicate an increase in moisture along several fractures (see Section 3.1.1) lends support to the former theory.

2.5.2 SURFACE CHARACTERISTICS

Because the distribution of fracture (joint) orientation may influence the anisotropy of the flow system associated with contaminants, a frequency-distribution study of joint orientations in Area L was conducted during the Summer of 1986. It was anticipated that results might further substantiate some of the apparent trends shown in part of the Petrex survey area (see Section 6). Joint orientations were measured using a Brunton compass and were plotted on a rose diagram (see Figure 2-12). Most of the 119 joints measured dip from 70 to 90 degrees.

A predominant northeast trend in the fracture orientations is depicted on the rose diagram (see Figure 2-12). However, because of the trend of Mesita del Buey and the configuration of its outcrop, a bias in the data resulted from the sampling limitation imposed by available exposures. Specifically, because the mesa trends northwest-southeast, the majority of the exposed fractures will be those oriented in a northeasterly direction; fractures having other orientations would be difficult to detect given the trend of the available exposures. Purtymun and Kennedy (1970) and Rogers (1977) reported diverse orientations on the mesa on the basis of measurements taken from trenches and pits away from the mesa rim. Purtymun and Kennedy concluded that 40 percent of the 1078 joints they measured in Unit 2b fall into three ranges of orientation: N. 30°-50° W., N. 60°-80° W., and N. 40°-60° E. Only the latter range was substantiated by measurements obtained during this study, but the diversity of trends found by Purtymun and Kennedy may help explain a similar

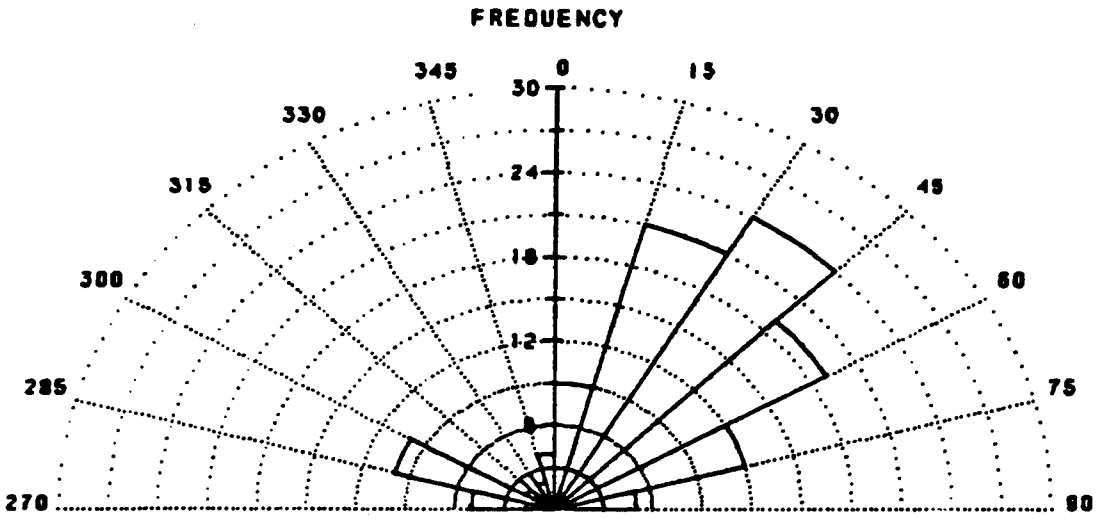

Figure 2-12. Rose Diagram of Joint Orientations of Exposed Fractures in Area L, Los Alamos National Laboratory (119 data points)

diversity in trends indicated by results of the Petrex survey (see Section 6). Therefore, although prominent northeast-trending fractures are recognized, it cannot be definitely concluded that the northeast orientation is the preferred avenue for contaminant transport.

The problem is further complicated by the fact that the physical nature of individual fractures may play an equally important, if not more important, role than the fracture orientation. As discussed previously, more than 70 percent of the fractures observed in the boreholes during this study, and by Purtymun and Kennedy (1970), are filled and therefore do not provide preferential pathways for contaminant migration. Fractures observed in freshly dug pits in Area G were noted by Rogers (1977) to range from tens of centimeters in width to tightly closed (or filled). According to Purtymun and Kennedy (1970), a single joint traced vertically through an ash flow may be closed in places and open in others, with openings ranging in width from 2 inches to less than 0.25 inch. Consequently, it is unlikely that any simple pattern of contaminant transport pathways can be inferred from fracture orientations. Rather, transport from the contaminant source to the surface probably follows tortuous routes determined by a combination of fracture orientations and degree of dilation, and interconnections of fractures related to the position of infill materials.

In summary, it appears that the mere occurrence of any 'preferred' fracture orientation is not sufficient to predict a simple, single direction of contaminant transport in Area L because transport is complicated by other fracture orientations and the closing of some fractures by secondary materials. The best method for determining the extent and dominant direction (if any) of contaminant transportation would be close monitoring and interpretation of chemical results from downhole pore-gas samples, in conjunction with more extensive Petrex surveys just under the rim of Mesita del Buey and in Area L.

Section 3

HYDROLOGIC CHARACTERIZATION OF THE VADOSE ZONE

This description of the hydrologic characteristics of the vadose zone in the study area is divided into three major subsections. Section 3.1 describes the general hydrologic characteristics of the tuff, including moisture content, which was determined gravimetrically; porosity, which was determined from helium-injection tests; and capillary force, determined from moisture characteristic curves. Permeability of the tuff is detailed in Section 3.2. Three field techniques were used to measure in-situ permeability, and two laboratory methods were used to measure permeability in core samples collected from the drill holes. Analyses of saturated and unsaturated hydraulic conductivity as a function of moisture content were also performed and are discussed in a separate subsection. A summary of all these permeability determinations concludes Section 3.2. Section 3.3 describes the gradient determinations, specifically measurements of temperature, water potential, and gas pressure, conducted to assess the driving forces of transport in the tuff.

This section of the report provides the geotechnical information specified in Tasks 1 through 4 of Paragraph 25 of the Compliance Order/Schedule. The specific subsections that address these tasks are highlighted with an asterisk and the corresponding task identified.

3.1 GENERAL CHARACTERISTICS

3.1.1 GRAVIMETRIC MOISTURE CONTENT

3.1.1.1 Purpose and Scope

Gravimetric moisture determinations were conducted to obtain a direct measurement of the in-situ water content of the tuff and to quantify the vertical moisture distribution. The moisture content as a function of depth is important when compared with results of permeability tests, water-potential measurements, and laboratory hydrologic testing as part of the quantification of moisture movement in the vadose zone.

This section describes the procedures for sample collection and moisture content calculations, and discusses the results of the gravimetric moisture-content determinations. Comparisons of the water-content results with other hydrologic measurements are presented in succeeding sections of this report (see Sections 3.1.3, 3.2.4, and 3.3.1).

3.1.1.2 Procedures

The specific procedure for the determination of gravimetric moisture consisted of the following steps. Core samples 1 ft in length were selected from the split-barrel sampler at 5-ft intervals and immediately placed in preweighed sample containers equipped with air-tight lids. The containers were weighed in the field and then delivered to the laboratory for drying. After drying for 24 hours at 105°C, the samples were reweighed to determine the moisture loss (Bendix Field Engineering Corporation, 1985a, 1985b).

Although gravimetric moisture determinations are relatively easy to perform, a number of precautions are necessary. For example, a major concern associated with the drilling was that the heat produced by the auger would drive water

out of the samples, resulting in inaccurate moisture-content measurements. Upon retrieval of the auger from the borehole, however, the temperature of the core barrel was observed to be cool. Apparently, the heat produced by the friction during drilling was minimal and confined to the outside of the auger, and therefore did not have a measurable effect on the moisture content in the core samples. Care was also taken to maintain the drying-oven temperature at 105°C to ensure that no structural water would be evolved and included in the apparent moisture content. Finally, the balance used to weigh the samples had a readability of 0.01 gram to ensure adequate accuracy for the low-moisture-content samples collected in this study.

3.1.1.3 Calculations

The amount of water in soil or rock can be expressed in the following ways:

- Water Content, Volume Fraction

$$\theta = V_l/V_t \tag{1}$$

- Water Content, Mass Basis

$$\theta_m = m_l/m_s \tag{2}$$

- Degree of Saturation

$$\theta_s = V_l/(V_l + V_g) \tag{3}$$

where

V_l = volume of liquid
V_t = total volume
m_l = mass of liquid
m_s = mass of solid
V_g = volume of the gas or air in the sample

Equations (1) and (2) are combined in order to convert from the mass basis to the volume fraction, a quantity that is generally more useful in field studies (Marshall and Holmes, 1979):

$$\theta = \theta_m \rho_b/\rho_l \tag{4}$$

where

ρ_b = dry bulk density
ρ_l = density of liquid

Values for mass were determined gravimetrically (Section 3.1.1.2). Values for dry bulk density were obtained from the gamma-gamma (apparent density) geophysical logs after subtracting the moisture content. Values for the density of water at different temperatures are readily available in the literature, but for most applications, it is sufficiently accurate to use the value 10^3 kg/m^3 (1.94 slugs/ft^3).

3.1.1.4 Results and Discussion

Gravimetric moisture determinations were performed in samples from 12 holes: LLM-85-01, LLM-85-02, LLM-85-05, LGM-85-06, LGM-85-11, LLC-86-19, LLC-86-20, LLC-86-21, LLC-86-22, LLC-86-23, LLC-86-24, and LLC-86-25 (see Figure 2-3 for drill-hole locations). The resulting volumetric moisture contents are plotted as a function of depth for all 12 holes in Figures 3-1, 3-2, 3-3, 3-4, and 3-5.

Four distinct characteristics are apparent upon examination of these data:

- Low overall moisture content.
- Varying depths of water infiltration.
- Relatively high moisture content exhibited by the lower portion of Unit 1b.
- Higher moisture content observed in the vicinity of certain fractures.

The low overall moisture content is demonstrated by the 2 to 4 percent average moisture for the central portion of the profile, while the lower portion of the profile, specifically Unit 1a, averaged a moisture content of 4 to 10 percent. At such low moisture contents, interconnection of pore water would be minimal and capillarity as a major transport mechanism would be negligible. As a result, it can be concluded that vapor transport would be the major mechanism for moisture movement in the tuff (see the discussion in Section 3.1.3.4).

Infiltration depth depends on the specific area. Holes located in Area L, for example, show an increase in moisture content relative to depth of less than 10 ft. In Area G, the corresponding depth is closer to 15 ft. This difference in the depth of moisture penetration is unexplained at this time.

All of the moisture data indicate an increase in moisture content in the lower portion of Unit 1b. In holes which fully penetrated Unit 1b, the increased moisture content correlates exactly with the moderately welded tuff encountered in Unit 1b (see lithologic logs in Appendix A). The degree of welding in the lower portion of Unit 1b was the highest observed in this study, with the exception of the upper portion of Unit 2b. As the degree of welding increases, the porosity of the formation decreases (Ross and Smith, 1961). It would be expected that as the porosity decreases so would the average pore-size radius, the result being an increase in capillary forces which would retain moisture in the more welded intervals of the tuff. The higher pumice content could also have a direct effect on the moisture-retention properties of Unit 1b. As welding increases, pumice clasts are flattened, both conditions resulting in a high concentration of gas tubes; these tubes form ideal capillary tubes which appear to exhibit strong capillary forces.

A higher moisture content is observed in samples located adjacent to certain fractures, indicating that some fractures do transport greater quantities of water vapor for absorption into the adjacent rock wall. Examples are the fractures located at 35 to 40 ft and 55 to 56 ft in Hole LLM-85-02, represented by the two moisture spikes at 38 and 55 ft, respectively (see

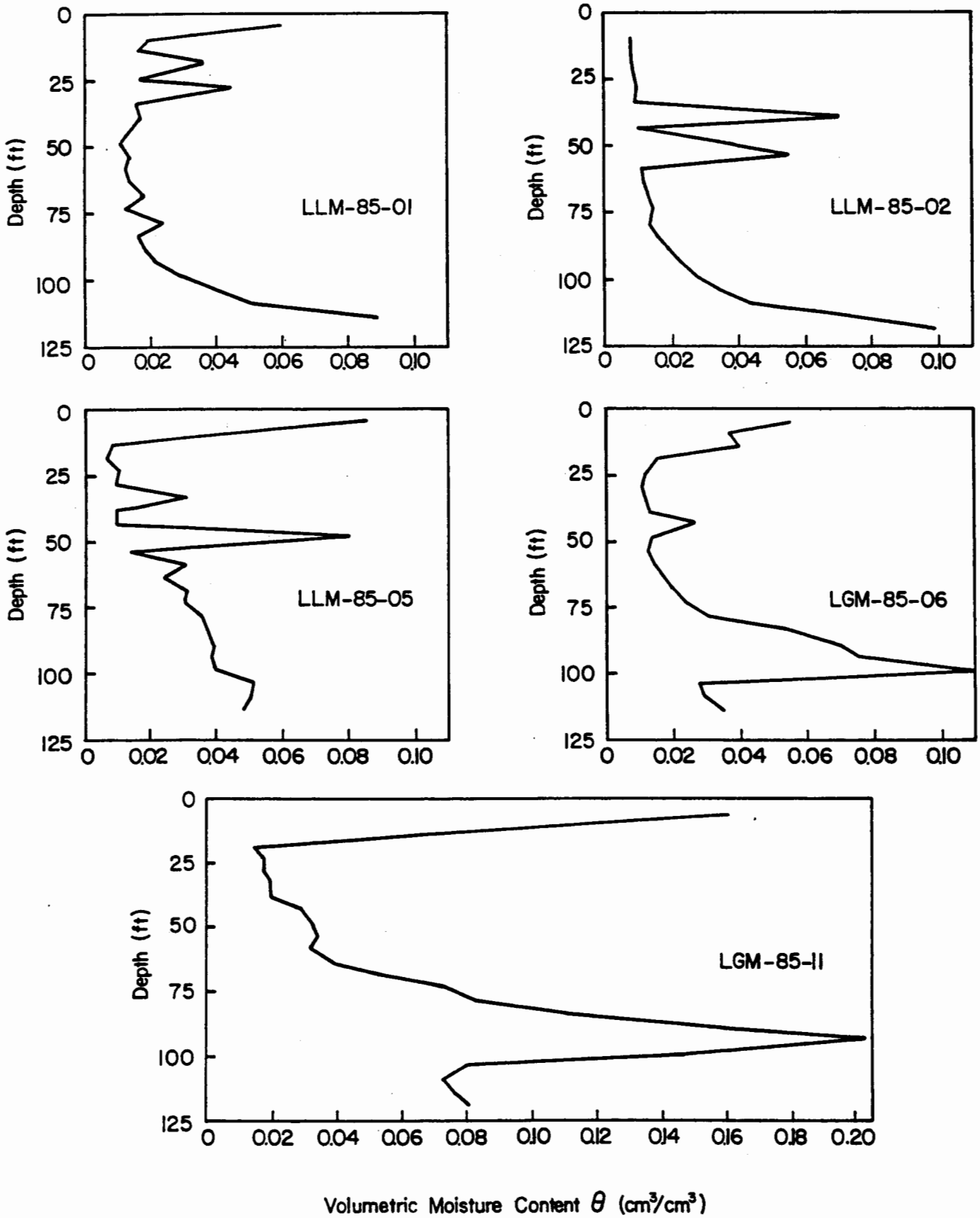

Figure 3-1. Plots of Volumetric Moisture Content as a Function of Depth for Drill Holes LLM-85-01, LLM-85-02, LLM-85-05, LGM-85-06, and LGM-85-11

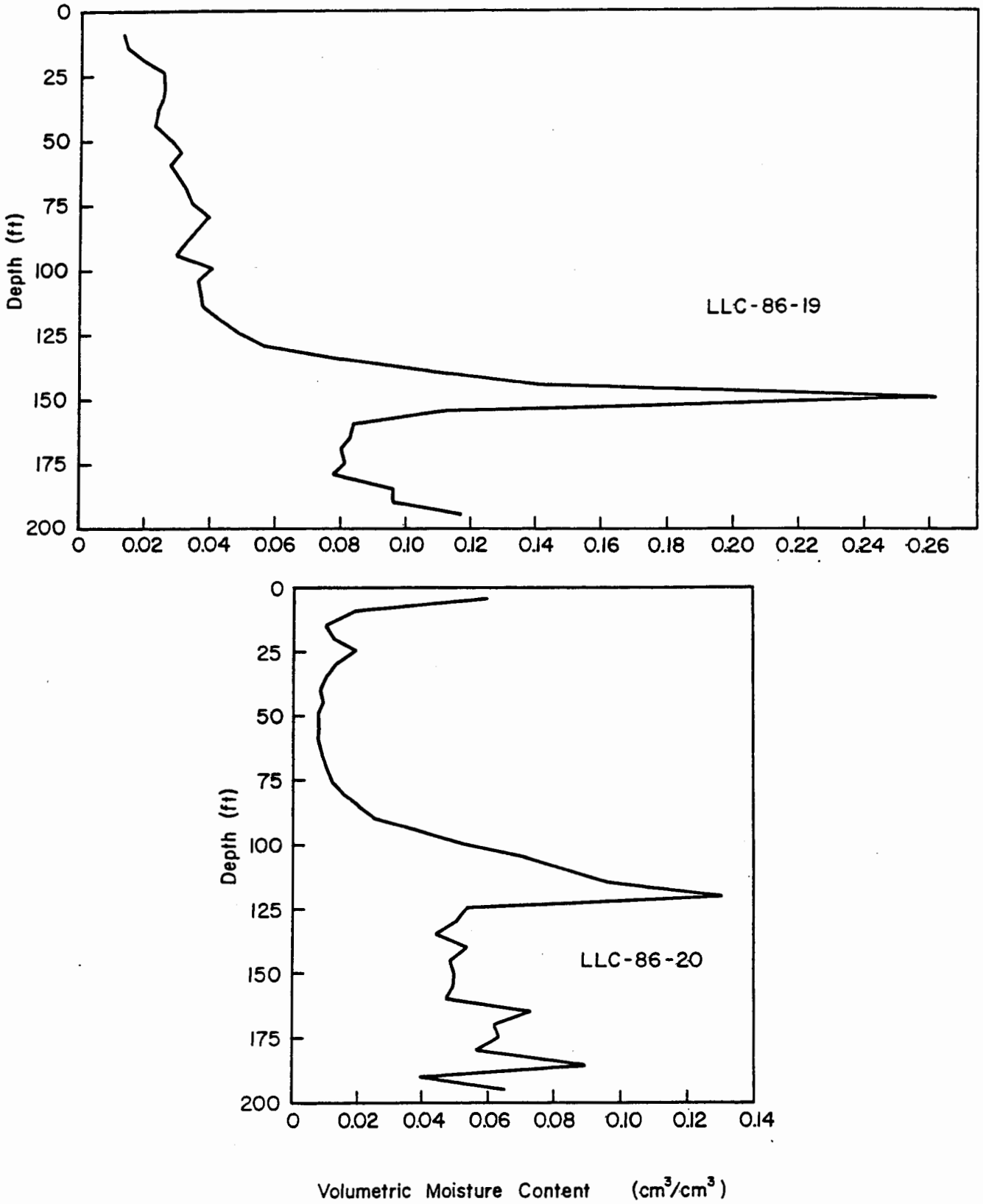

Figure 3-2. Plots of Volumetric Moisture Content as a Function of Depth for Drill Holes LLC-86-19 and LLC-86-20

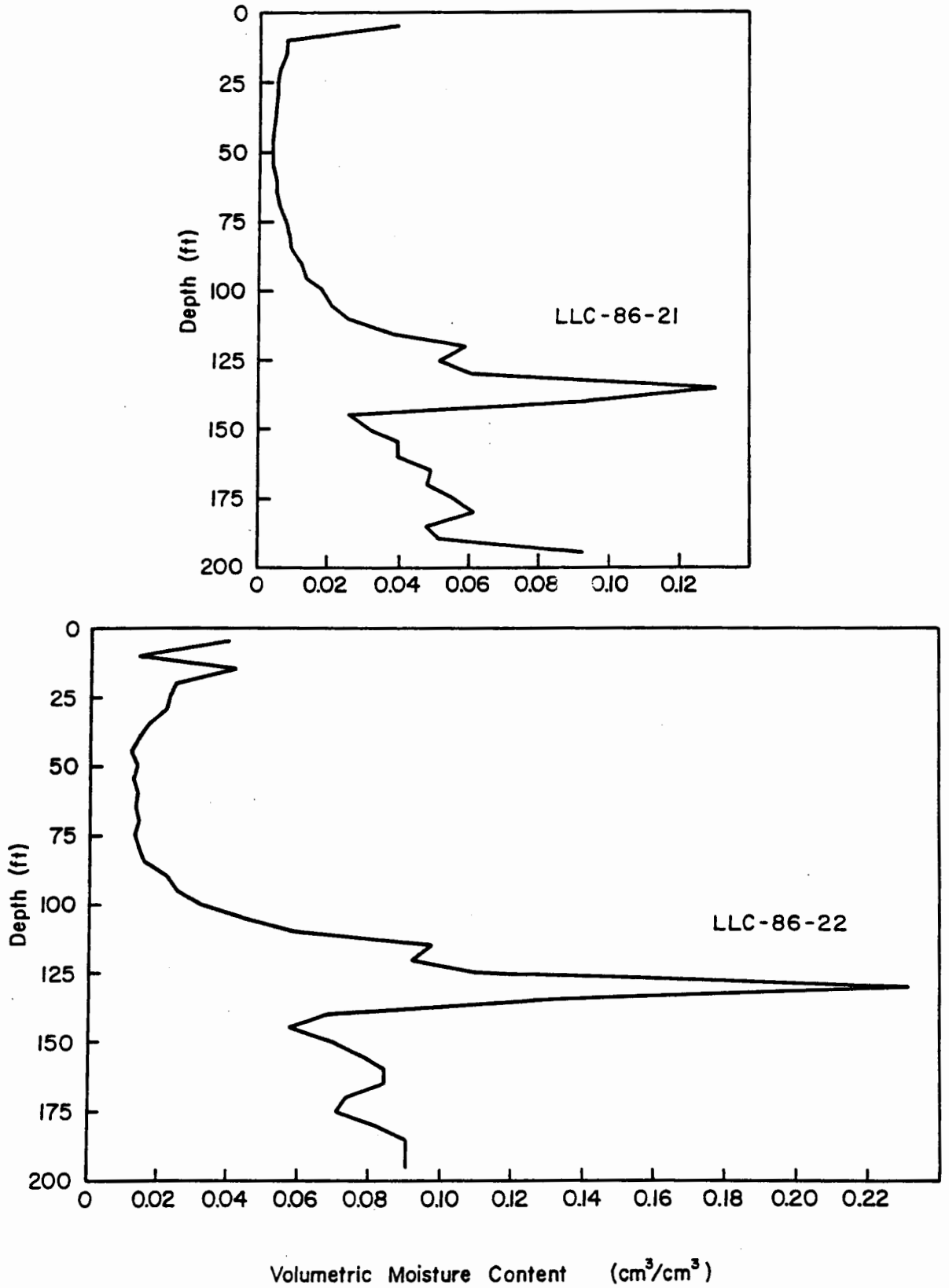

Figure 3-3. Plots of Volumetric Moisture Content as a Function of Depth for Drill Holes LLC-86-21 and LLC-86-22

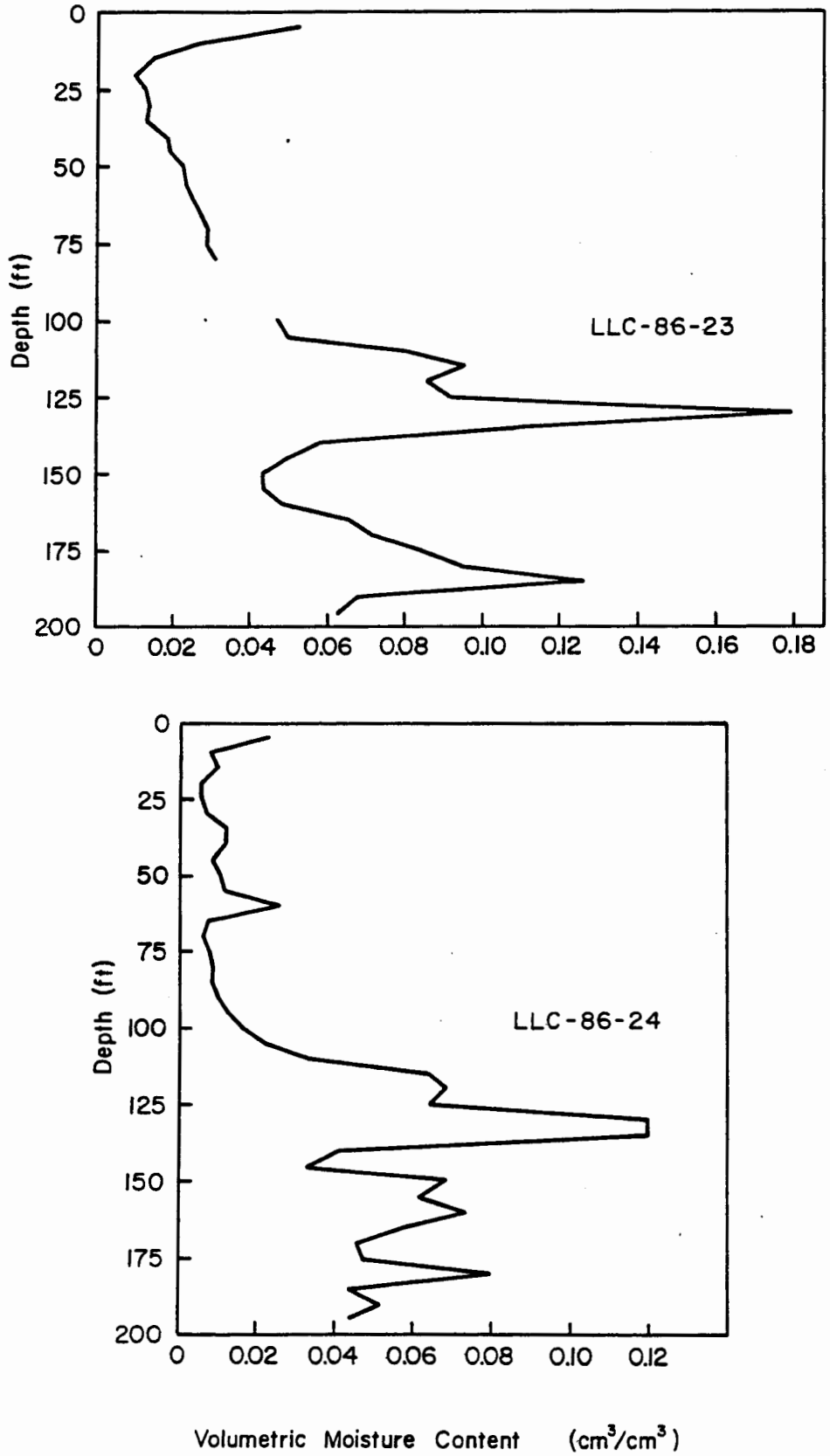

Figure 3-4. Plots of Volumetric Moisture Content as a Function of Depth for Drill Holes LLC-86-23 and LLC-86-24

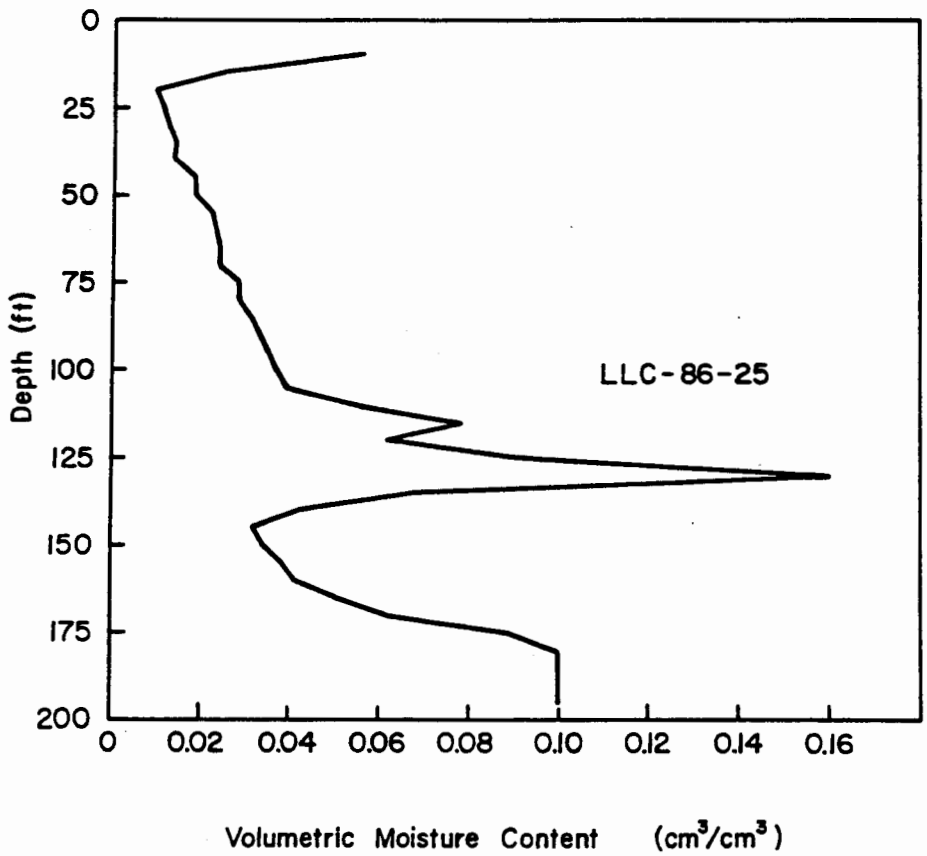

Figure 3-5. Plots of Volumetric Moisture Content as a Function of Depth for Drill Hole LLC-86-25

Figure 3-1). Not all of the fractures exhibit this moisture anomaly, however, suggesting that not all of the fractures are open and available as avenues of transport for water vapor (see Section 2.5).

3.1.2 POROSITY

3.1.2.1 Purpose and Scope

This section presents the results of helium-injection tests performed on 20 core samples for the purpose of measuring the porosity of the Bandelier Tuff. The laboratory work was performed by TerraTek Research Laboratory of Salt Lake City, Utah, at the direction of Bendix. The sample-preparation and laboratory-procedure sections that follow (3.1.2.2 and 3.1.2.3) are adapted from TerraTek's report (TerraTek Research Laboratory, 1985).

3.1.2.2 Sample Preparation

In order to obtain samples that were of the right size and shape for testing, it was necessary to plug the full diameter core material. This was done using air as the drill-bit coolant (to avoid any potentially adverse rock-fluid interaction). Plugging was done vertically due to the limited horizontal cross section of the core material. In all but one case (Sample MCG-616), attempts at sample plugging resulted in a partial disaggregation of the sample.

The samples thus obtained were placed in protective sheathing (one-inch-diameter heat-shrink Teflon tubing*), with stainless steel end screens used for support and prevention of grain loss, and to allow for gas or fluid flow in testing. The samples were then subjected to a confining stress equal to that found at their burial depth in order to compact the grains to an orientation similar to that experienced in the formation. This was done to ensure that any void space between the sheathing and the sample did not affect the pore volume of the sample.

3.1.2.3 Procedure for Helium-Injection Tests

The samples were oven-dried prior to testing and placed under a slight overburden pressure (approximately 100 psi) in a hydrostatic core holder. Porosity measurements consisted of injecting helium into the samples (50-psi charging or injection pressure), monitoring pressure/volume relationships, and calculating porosity values using Boyle's Law.

3.1.2.4 Results and Discussion

Table 3-1 presents the results for the porosity determinations. Porosity values range from approximately 39 to 74 percent. Using a classification scheme presented by Abeele and others (1981), the degree of welding based on the porosity would range from nonwelded to moderately welded. This classification agrees with field and petrographic observations.

---

*Diameter cited is after shrinking.

Table 3-1. Results of Porosity Determinations Using the Helium-Injection Method and Boyle's Law

Hole Number	Geologic Unit	Sample Number	Depth (ft)	Degree of Welding[a]	Pumice Content (percent)[b]	Bulk Volume (cm^3)	Pore Volume (cm^3)	Porosity (percent)
LGM-85-11	2b	MCG-618	3	Moderately Welded	19	25.68	13.94	54.3
LLM-85-02	2b	MCG-606	7	Moderately Welded	--[c]	25.62	10.62	41.5
LLM-85-05	2b	MCG-610	15	Moderately Welded	--[c]	24.96	13.14	52.6
LLM-85-01	2b	MCG-602	30	Moderately Welded	15	27.44	10.87	39.6
LGM-85-11	2b	MCG-619	30	Slightly Welded	13	24.61	12.67	51.5
LLM-85-02	2b	MCG-607	36	Moderately Welded	11	24.00	11.15	46.5
LGM-85-06	2b	MCG-614	29	Moderately Welded	7	25.31	10.76	42.5
LLM-85-05	2b	MCG-611	36	Slightly Welded	--[c]	24.08	17.72	73.6
LLM-85-01	2a	MCG-603	52	Slightly Welded	33	24.20	15.58	64.4
LGM-85-06	2a	MCG-615	51	Slightly Welded	14	25.73	10.34	40.2
LLM-85-02	2a	MCG-608	67	Moderately Welded	6	24.69	10.69	43.3
LLM-85-05	2a/1b	MCG-612	76	Slightly Welded	--[c]	24.37	18.08	74.2
LLM-85-01	1b	MCG-604	101	Slightly Welded	27	26.76	16.62	62.1
LGM-85-06	1b	MCG-616	99	Moderately Welded	27	28.26	13.42	52.6
LGM-85-11	1b	MCG-620	94	Moderately Welded	17	26.08	16.76	64.3
LLM-85-02	1b	MCG-609	117	Moderately Welded	--[c]	25.69	12.46	48.5
LLM-85-05	1b	MCG-613	123	Slightly Welded	--[c]	26.23	17.20	65.6
LLM-85-01	1b	MCG-605	124	Moderately Welded	20	25.62	12.53	48.9
LGM-85-11	1a	MCG-621	115	Nonwelded	--[c]	24.16	14.51	60.1
LGM-85-06	1a	MCG-617	115	Nonwelded	--[c]	26.32	14.82	56.3

[a]Based on field observations.

[b]The percentage of pumice fragments in the sample was determined by thin-section analysis using the point-count method.

[c]Not measured.

Since field determinations are very subjective, porosity appears to be a way of quantifying the degree of welding. The pumice content, however, must also be considered. The buoyancy of pumice in water is a consequence of its high porosity. As a result, a moderately welded sample could exhibit a relatively high porosity because of a high pumice content (e.g., compare Samples MCG-608 and MCG-620 in Table 3-1).

Ross and Smith (1961) demonstrate that porosity can be used to delineate degree of welding (Figure 3-6). However, it would be difficult to use porosity to classify the geologic units in the project area without greatly increasing the sampling frequency, because Units 2a and 2b are composed of more than one flow, each exhibiting significant variations in porosity and pumice content.

Based on the laboratory results, there appears to be no relationship between porosity and permeability (see Section 3.2). The reason could be that, for similar degrees of welding, an increase in the pumice content results in an increase in the porosity. Since the pumice lapilli contain a significant amount of dead-end pores, however, there is no significant increase in the effective permeability.

3.1.3 MOISTURE CHARACTERISTIC CURVES*

3.1.3.1 Purpose and Scope

A moisture characteristic curve is defined as the relationship between the capillary forces at varying degrees of saturation for a selected porous medium. This curve is particularly useful for the conversion of moisture data to capillary potential, and vice versa. This section of the report describes the procedure used to generate these curves, along with a discussion of the test results. The testing was performed by TerraTek Research Laboratory, and the description of the test procedures (Section 3.1.3.3) was adapted from their report (TerraTek Research Laboratory, 1985).

3.1.3.2 Sample Preparation

(See Section 3.1.2.2.)

3.1.3.3 Procedure for Centrifuge Tests

Prior to testing, the samples were vacuum-saturated with tap water. Complete saturation was verified by comparison with previous saturation data and the helium-injection data. Testing consisted of loading the samples into specially designed centrifuge cups and spinning them at six incremental speeds. Speeds ranged from a low of 130 revolutions per minute (rpm) to a high of 680 rpm. A stroboscope was used to monitor the speed of the centrifuge until it was stable. The speeds were converted mathematically to capillary pressure, and saturations were determined using displacement data. The average saturation derived from the displacement data was converted to a corrected wetting-fluid saturation value.

---

*Response to Task 2, Paragraph 25, Compliance Order/Schedule.

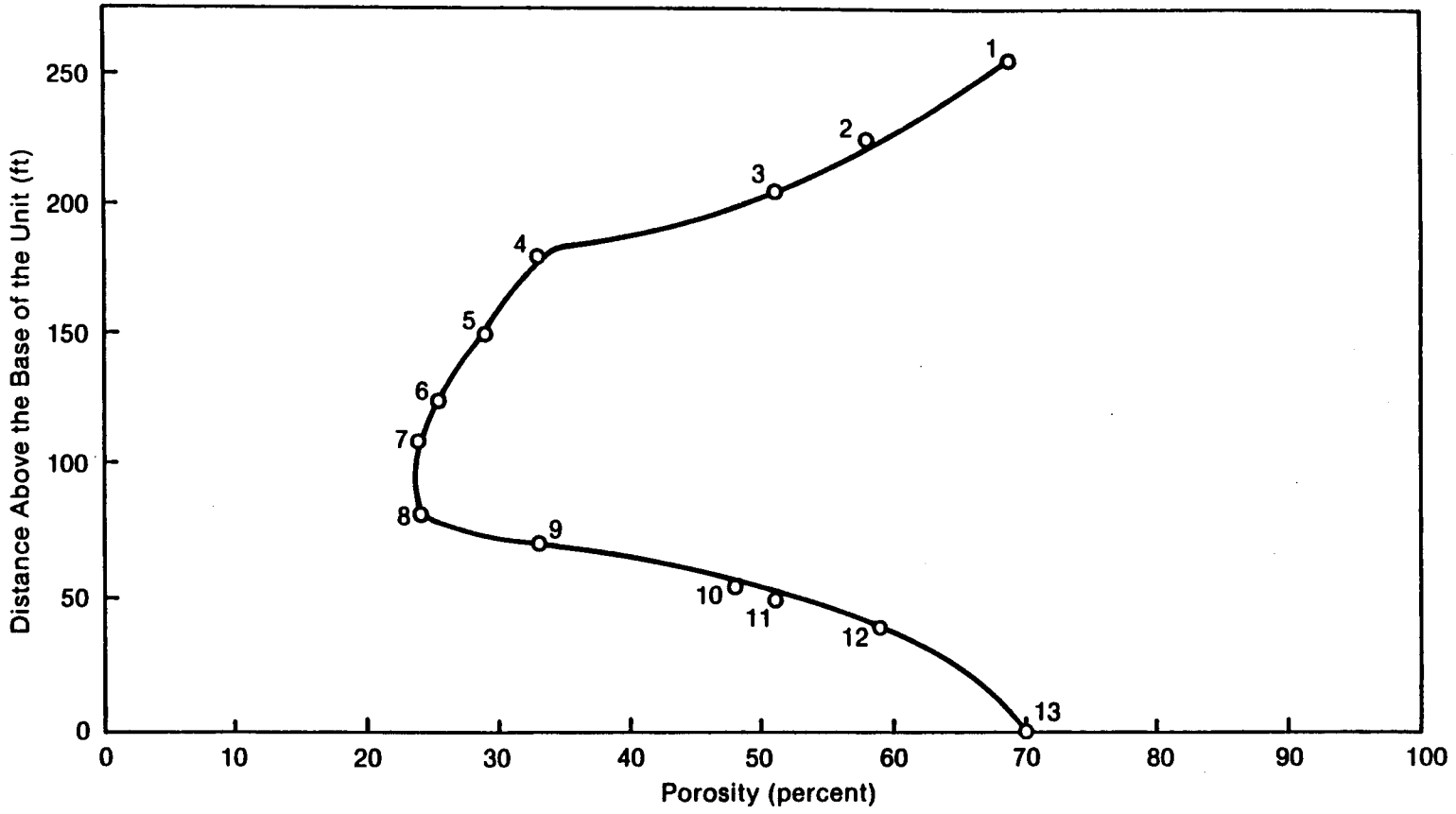

DATA PLOTTED IN THE GRAPH

Sample Number	Distance Below the Top of the Unit (ft)	Porosity (percent)	Sample Number	Distance Below the Top of the Unit (ft)	Porosity (percent)
1	0	69	8	175	24
2	30	58	9	185	33
3	50	51	10	200	48
4	75	33	11	205	51
5	105	29	12	215	59
6	130	25.5	13	255	70
7	145	24			

Figure 3-6. Porosity of Battleship Rock Ash-Flow Tuff, Valles Mountains, New Mexico (from Ross and Smith, 1961)

3.1.3.4 Results and Discussion

Moisture characteristic curves for 20 samples are presented in Appendix C. Only the drying curves were obtained because of the severe problems encountered when attempting to obtain imbibition (wetting) curves. Due to the highly porous nature of the samples, water was imbibed to such an extent that capillary-pressure determinations were impossible. Since the samples were too friable for mercury injection, it was decided to suspend attempts at obtaining these data.

After reviewing the moisture characteristic curves, the laboratory was requested to increase the centrifuge speed in order to evaluate lower water potentials (capillary pressures). Unfortunately, the samples disaggregated at these higher speeds. The laboratory was then requested to use the pressure-plate method to measure moisture characteristics, but those attempts were also unsuccessful due to sample disaggregation.

The most interesting data discernible from the moisture characteristic curves (Appendix C) are the extremely high moisture-retention (θ_r) values, which range up to 80 percent. The moisture-retention value is important because it represents the point at which capillarity as a transport mechanism breaks down. Since all of the moisture-content measurements for the Bandelier Tuff are significantly below this value, vapor transport is clearly the major mechanism of water transport.

The moisture characteristic data also demonstrate that only a minor amount of force is required to initiate the drainage of water from the saturated core sample, suggesting that the tuff has a low air-entry value. This information, coupled with the high residual moisture content, indicates that the tuff is characterized by a highly variable pore-size distribution.

It is interesting to compare the results of this study with those of a study performed by Abeele (1984), who presents moisture characteristic curves for crushed Bandelier Tuff. Residual saturation (θ_r) for the crushed tuff is approximately 0.2, as compared with an average of 0.5 for the solid rock cores. If it is assumed that both laboratory methods are reliable, then comparison of the unsaturated hydraulic properties of crushed versus natural tuff reveals a significant difference. One possible explanation is the destruction of the internal structure of the pumice lapilli in the crushed tuff. The gas tubes present in the pumice lapilli of uncrushed tuff are perfect little capillary tubes whose strong capillary forces retain significant amounts of water, resulting in higher θ_r values.

Knowledge of the average moisture-retention value enables one to calculate how much water must be supplied to the system in order for the capillary forces of the overlying tuff to be satisfied—a condition which must be met in order for recharge of liquid water to occur to the underlying groundwater system. Based on an average porosity of approximately 50 percent (Table 3-1) and an average moisture-retention value of approximately 50 percent (Appendix C), a recharge of 25 centimeters for each 1-meter thickness of tuff would be required to satisfy the capillary forces before recharge to the underlying groundwater system could occur. This scenario is quite unlikely in the study area due to the large amount of water required and the fact that the potential evapotrans-

piration rates in the Jemez Mountains area exceed the annual precipitation amount (Abeele and others, 1981).

3.2 PERMEABILITY DETERMINATIONS

3.2.1 BOREHOLE-INJECTION TESTS*

3.2.1.1 Purpose and Scope

Borehole-injection tests, or packer tests, were used to measure the in-situ permeability of different intervals in the Bandelier Tuff. The tests were performed in accord with procedures described by the U.S. Department of the Interior (1974) and the University of Missouri at Rolla (1981). Usually the tests are performed with water, but injection of water near the waste-disposal areas at Los Alamos was not allowed (see succeeding subsection on Background for further discussion). One hole, LLM-85-05, located between Areas G and L, was tested with both air and water in order to permit a comparison between the two fluids.

Following the discussion on background, a detailed description of the field tests is presented, including equipment and procedures. The equations used to calculate hydraulic conductivity and intrinsic permeability are presented next, followed by a discussion of the results, including a comparison of the air and water values obtained for Hole LLM-85-05.

3.2.1.2 Background

Two methods are available to measure the in-situ saturated hydraulic conductivity, K_s, of the tuff above the water table. These are borehole-infiltration tests and borehole-injection tests. Borehole-infiltration tests require maintenance of a constant head of water in an open or cased borehole until the flow rate becomes steady. The method is described in papers by Stephens and Neuman (1982a, 1982b) and Stephens and others (1983). Borehole-injection tests involve installing packers in the borehole to isolate measurement intervals, followed by injection of air or water into the formation.

Prior to initiation of the investigations described in this report, Los Alamos National Laboratory requested that water not be injected into boreholes in the vicinity of Areas G and L. Since the majority of the holes for this study are in or adjacent to these areas, borehole infiltration as a method for determining in-situ permeabilities was eliminated. Instead, borehole injection was used to measure in-situ permeability in the study area, largely because packers can be used to isolate sections of the borehole for testing and because air can be used in place of water. However, the method, whether using air or water, is subject to a number of limitations and assumptions which warrant further discussion.

*Response to Task 1, Paragraph 25, Compliance Order/Schedule.

First, it should be emphasized that the air-injection method is experimental and may permit only a qualitative characterization of subsurface permeabilities. Miller and others (1974), for example, used an air-injection technique to study the fracturing around a tunnel in volcanic rock and were able to conclude only that the permeability of the rock was either high or low. Therefore, before any quantitative interpretation can be made, air-injection results must be compared with results of laboratory and other field tests.

Using air as an injection fluid for packer tests may require compensation or correction for these factors: gas compressibility, changes in the volume of the gas with respect to temperature, and variation in the atmospheric water-vapor content. To overcome potential problems related to these factors, certain assumptions were made and appropriate procedures were implemented.

Compressive effects are minimal under steady-state conditions. Hence, the flow of air was kept at a constant rate and under low pressure during the injection step. In addition, boundary effects were disregarded because capillary action should have no impact on air flow.

To permit compensation for temperature effects on the volume of gas, a probe was placed downhole just above the packer assembly. A description of the temperature probe and meter is presented in the Equipment subsection (Section 3.2.1.3.1).

Based on the results of a study by Loughborough (1966), who compared the permeability of concrete using air and water vapor versus dried air, the potential effects of varying amounts of water vapor were disregarded. Loughborough's results demonstrated an average difference in permeability of only 5 percent. It is expected that this difference would be even less in a more permeable medium such as the Bandelier Tuff, indicating that it is reasonable to assume no effect.

Finally, in order to accurately calculate permeability for an air-injection test, values for the fluid injection pressure and flow rate must be known. Depending on the injection rate and the permeability of the formation, the resulting pressure can be very low. Equipment used to measure the low injection flow rates and pressures are described in the Equipment subsection (Section 3.2.1.3.1).

The use of water as an injection fluid also has certain limitations, specifically for tests above the water table. The U.S. Department of Interior (1974) points out that water-injection tests are more accurate below the water table than above, since the describing equations assume that horizontal flow is inherent throughout the system. Another potential source of error associated with water-injection tests is that existing formulas for computing permeability disregard the effects of capillary flow in the vadose zone. Instead, the formulas are based on various approximations of the classical free surface theory, which assumes that flow takes place entirely within a saturated region, an approximation which could lead to significant errors as pointed out by Stephens and Neuman (1982a).

3.2.1.3 Description of Field Tests

3.2.1.3.1 Equipment. Figures 3-7 and 3-8 illustrate the equipment used for the air- and water-injection tests, respectively. Although the two configurations differ somewhat, each has the same essential parts: flow meter, pressure gauge or gauges, conduit pipe, downhole temperature probe, and pneumatic packers.

For the air-injection tests, a New Jersey Air Flow Meter was used to measure the volume of air injected into the formation. Since the quantity of air injected varied from hole to hole, two different meters with different flow ranges were used. One had a range of 0 to 40 cubic feet per minute (cfm) with 1-cfm increments, while the other had a range of 50 to 300 cfm with 5-cfm increments. For the water-injection tests, a Neptune Water Meter with 0.1-gallon increments replaced the New Jersey Air Flow Meter.

For both the air- and water-injection tests, a Heise pressure gauge was used to measure the downhole, or back injection, pressure. The Heise gauge has a range of 0 to 60 psi with 0.2-psi increments, and is calibrated for atmospheric pressure at sea level (14.7 psi). Such a sensitive gauge was necessary to accurately measure the low pressures which resulted from the small volumes of fluid injected.

Galvanized conduit pipe, 1-3/8 inches in diameter, was used to conduct fluid down the hole. Threaded sections and couplings were secured with Teflon tape to prevent leakage.

The probe used to measure downhole fluid temperatures was located in a small chamber at the base of the conduit pipe, just above the pneumatic packers. Both the chambers and the section of pipe to which it was welded contained holes that permitted small amounts of air to flow between the two. The temperature probe was connected to a YSI Model 42SC Tele-thermometer located at the surface. The Tele-thermometer had a range of -40 to 150°C with increments of 1°C.

Each 6-ft interval was isolated using a set of Tigre Tierra Model 610 Pneumatic Packers. The 4-ft-long packers expand up to 10 inches in diameter and can be inflated to 470 psi.

3.2.1.3.2 Procedure. The borehole-injection tests were conducted by isolating 6-ft intervals in the uncased boreholes using the pneumatic packers. The packers were inflated to 200 psi to ensure a good seal. (Several tests were performed before this inflation pressure was determined.) A known quantity of air or water was injected until a measurable pressure was obtained on the Heise gauge. The pressure, flow rate, and temperature were then periodically recorded until all readings were constant with respect to time. The flow rate was then increased and the procedure repeated. Once the higher flow rate became constant, the process was repeated using the lower flow rate to check reproducibility.

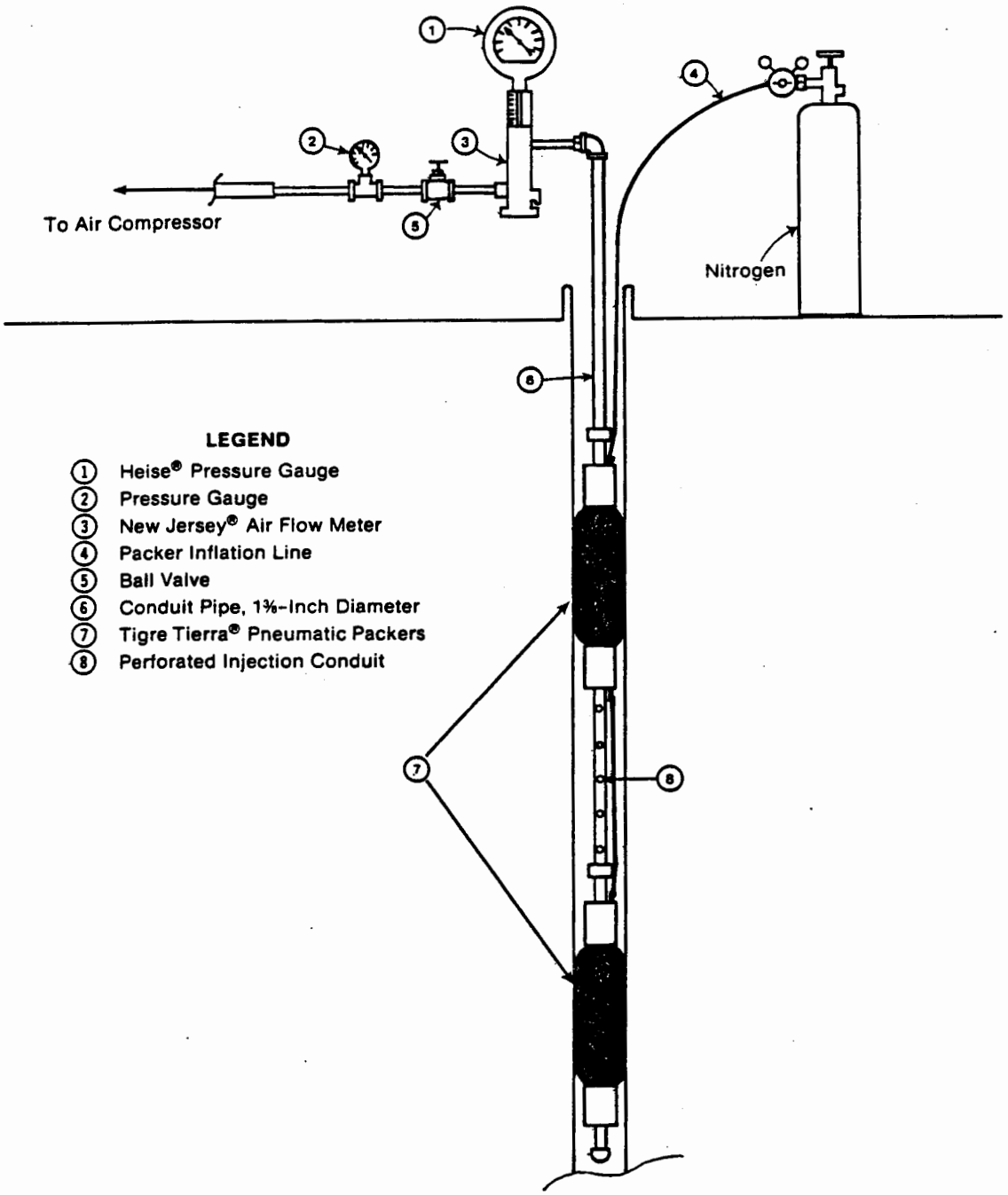

Figure 3-7. Air-Injection Apparatus Used for In-Situ Permeability Measurements

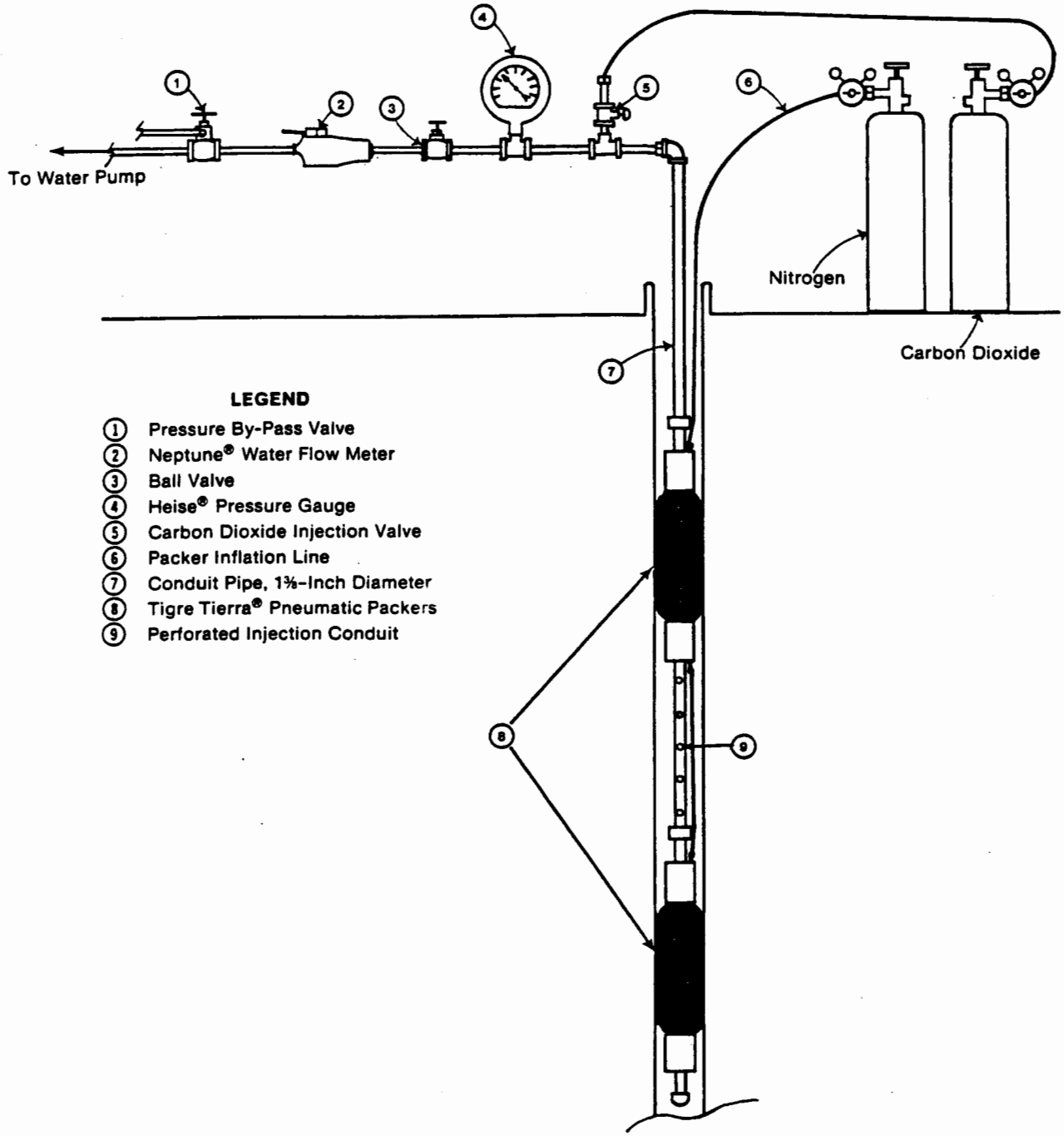

Figure 3-8. Water-Injection Apparatus Used for In-Situ Permeability Measurements

During the tests, the borehole was monitored for discharge of either air or water. If a discharge occurred, it was assumed that the packers were leaking and that the test was invalid.

3.2.1.4 Calculations

The rate at which a fluid can be injected into a geologic formation at a given pressure and through a known area is a function of the permeability of the formation. This relationship can be expressed in the following equation (U.S. Department of the Interior, 1974):

$$K = (Q/2\pi SH) \ln (S/r) \tag{5}$$

where

K = hydraulic conductivity (L/t)
Q = injection rate (L^3/t)
S = length of the test interval (L)
H = differential head of the fluid (L)
r = radius of the borehole (L)

Since the differential head is a combination of the height of the fluid column above the test interval and the pressure p at which the fluid is injected, p may be expressed as the height of the column of any fluid by the relationship

$$H = p/\gamma \tag{6}$$

where γ is the specific weight of the fluid.

Equation (5) is sufficient for the calculation of hydraulic conductivity when water is the injection fluid. However, modifications to Equation (5) are required when air is the injection fluid, because the specific weight of air is strongly dependent on the temperature and pressure. The specific weight of air can be determined from the equation of state for an ideal gas,

$$\gamma = gp_a/RT_a \tag{7}$$

where

γ = specific weight of the fluid (m/L^2t^2)
g = gravitational acceleration (L/t^2)
p_a = absolute pressure (force/L^2)
R = a gas constant
T_a = absolute temperature in degrees Rankine or Kelvin

For air, the value of R is 287 N-m/(kg)(°K) [1715 ft-lb/(slug)(°R)]. Substituting Equations (6) and (7) for the appropriate variables in Equation (5) yields

$$K = (Qgp_a/2\pi SpRT_a) \ln (S/r) \tag{8}$$

Since the flow rate of a gas through the New Jersey meter is also dependent on temperature and pressure, a combined correction factor, C_f, is required to calculate the actual flow rate. Inserting the combined correction factor into

Equation (8) yields the final equation for calculating the in-situ air-derived hydraulic conductivity,

$$K = (QC_f g p_a / 2\pi S p R T_a) \ln (S/r) \tag{9}$$

In order to compare the hydraulic conductivity derived from air injection versus that derived from water injection, it is convenient to use the term intrinsic permeability, k. Intrinsic permeability is a function of only the medium, whereas hydraulic conductivity is a function of both the medium and the fluid. The term k is widely used in the petroleum industry where the existence of gas, oil, and water in multiphase flow systems makes the use of a fluid-free conductance parameter attractive.

Intrinsic permeability and hydraulic conductivity can be related to one another by the equation (Nutting, 1930)

$$k = K\mu/\rho g \tag{10}$$

where

- k = intrinsic permeability (L^2)
- K = hydraulic conductivity (L/t)
- μ = absolute viscosity of the fluid ($F \cdot t/L^2$, where F = force)
- ρ = density of the fluid (m/L^3)
- g = gravitational acceleration (L/t^2)

Equation (10) will suffice for calculating k values from water-derived K values. However, modifications to Equation (10) are required for gas-derived conductivities because of the dependence of the density term on the pressure and temperature. Once again, the equation of state in the following form is used:

$$\rho = p_a/RT_a \tag{11}$$

Equation (11) is substituted for ρ in Equation (10) to yield the relationship between k and K for a gas,

$$k = K\mu RT_a/p_a g \tag{12}$$

Comparing the intrinsic permeability values calculated from the air- and water-injection tests can aid in the evaluation of any bias inherent in the individual methods.

3.2.1.5 Results and Discussion

Hydraulic conductivity values derived from the air-injection tests (Table 3-2) range from 10^{-3} to 10^{-5} centimeter per second (cm/s) [10^{-5} to 10^{-6} foot per second (ft/s)]. Conversions to intrinsic permeability indicate that the range of values is similar to those exhibited by a silty to clean sand (Freeze and Cherry, 1979). Based on field observations of the tuff, these permeability values appear to be reasonable.

Table 3-2. Hydraulic Conductivity Determined from Air-Injection Tests in Los Alamos Drill Holes

Hole Number	Geologic Unit	Test Interval[a] (ft)	Interval Description	Fractures Present?	Hydraulic Conductivity (K)	
					cm/s x 10^{-3}	ft/s x 10^{-5}
LLM-85-01	2b	9-15	Upper 2b, Moderately Welded	No	1.2	4.1
LLM-85-01	2b	30-36	Lower 2b, Moderately to Slightly Welded	No	0.70	2.3
LLM-85-02	2b	9-15	Upper 2b, Moderately Welded	Yes	0.094	0.31
LLM-85-02	2b	24-30	Middle 2b, Moderately Welded	No	0.11	0.37
LLM-85-05	2b	24-30	Mid-Lower 2b, Moderately Welded	No	0.91	3.0
LGM-85-11	2b	9-15	Upper 2b, Moderately Welded	No	1.5	5.0
LGM-85-11	2b	14-20	Middle 2b, Moderately Welded	Yes	1.4	4.7
LGM-85-11	2b/2a	35-41	Contact 2b/2a, Slightly Welded	No	0.12	0.40
LLM-85-01	2a	51-57	Middle 2a, Slightly Welded	No	0.33	1.1
LLM-85-01	2a	72-78	Lower 2a, Slightly Welded	Yes	0.14	0.45
LLM-85-02	2a	45.5-51.5	Upper 2a, Slightly Welded	Yes	0.14	0.45
LLM-85-02	2a	66.5-72.5	Mid-Lower 2a, Moderately Welded	No	0.14	0.45
LLM-85-05	2a	45-51	Upper 2a, Slightly Welded	Yes	2.8	9.3
LLM-85-05	2a	55-61	Middle 2a, Slightly Welded	Yes	1.9	6.2
LGM-85-06	2a	38-44	Upper 2a, Slightly Welded	Yes	0.067	0.22
LLM-85-05	2a/1b	75-81	Contact 2a/1b, Slightly Welded	No	0.052	0.17
LGM-85-11	2a/1b	56-62	Contact 2a/1b, Slightly Welded	No	0.52	1.7
LLM-85-01	1b	93-99	Mid-Upper 1b, Slightly Welded	No	0.082	0.27
LLM-85-02	1b	87-93	Upper 1b, Slightly Welded	No	0.085	0.28
LLM-85-05	1b	82-88	Upper 1b, Slightly Welded	No	0.061	0.20
LGM-85-06	1b	60-66	Upper 1b, Slightly Welded	No	0.64	2.1
LGM-85-06	1b	81-87	Middle 1b, Slightly to Moderately Welded	No	0.52	1.7
LGM-85-11	1a/1b	99-105	Contact 1a/1b, Slightly Welded	No	0.030	0.098
LGM-85-11	1b	77-83	Middle 1b, Slightly to Moderately Welded	No	0.23	0.77
LGM-85-11	1a	108-114	Upper 1a, Nonwelded	No	0.088	0.2

[a]Depth below ground level.

In general terms, the permeability of the tuff decreases with stratigraphic depth. Unit 2b shows an average air-derived hydraulic conductivity of 8.5 x 10^{-4} cm/s (2.8 x 10^{-5} ft/s); Unit 2a, 7.9 x 10^{-4} cm/s (2.6 x 10^{-5} ft/s); Unit 1b, 2.3 x 10^{-4} cm/s (7.7 x 10^{-6} ft/s); and Unit 1a, 8.8 x 10^{-5} cm/s (2.9 x 10^{-6} ft/s), this last being the only measurement obtained for Unit 1a.

The highest air-derived hydraulic conductivity was determined for a fractured zone in Unit 2a [2.8 x 10^{-3} cm/s (9.3 x 10^{-5} ft/s)]. However, the average K value determined for fractured zones [9.4 x 10^{-4} cm/s (3.1 x 10^{-5} ft/s)] was only slightly greater than values determined from the majority of air-injection tests in unfractured tuff. These results suggest that secondary fracture permeability does not appear to be significantly greater than the primary permeability of the tuff.

Water-derived hydraulic conductivities, presented in Table 3-3, are in the same range as those reported by Abeele (1984) for crushed tuff, i.e., 1.4 x 10^{-4} cm/s (4.6 x 10^{-6} ft/s). These values, like those derived from the air-injection tests, generally decrease with depth.

The reliability of the air-injection method is demonstrated by comparing the intrinsic permeability values calculated from both the air and water test for the same intervals (Table 3-4); results from the two lower zones in particular are in good agreement with one another. The largest discrepancy between the two methods is seen in the results for the interval 24 to 30 ft, where the value calculated from the water-injection test is an order of magnitude lower than the value calculated from the air-injection test. This water-injection test, however, was not performed in the same fashion as the others. Specifically, carbon dioxide was not injected prior to the tests as it was for the lower intervals. The purpose of injecting carbon dioxide is to minimize the effects of trapped air in the formation. Thus, permeability values might be less for tests performed without carbon dioxide injection. It would appear that these results support the use of carbon dioxide for water-injection tests in the vadose zone, as recommended by Stephens and others (1983).

Table 3-3. Hydraulic Conductivity Values Determined from Water-Injection Tests in Hole LLM-85-05

Test Interval (ft)[a]	Hydraulic Conductivity (K) cm/s	ft/s
10-16	9.4 x 10^{-4}	3.1 x 10^{-5}
24-30[b]	1.0 x 10^{-3}	3.3 x 10^{-5}
75-81	6.4 x 10^{-4}	2.1 x 10^{-5}
82-88	4.6 x 10^{-4}	1.5 x 10^{-5}

[a]Depth below ground level.
[b]Injection with carbon dioxide prior to water injection was not performed for this test interval.

Table 3-4. Comparison of Intrinsic Permeability Values Determined from Water-Injection and Air-Injection Tests in Hole LLM-85-05

Test Interval (ft)[a]	Intrinsic Permeability (k)			
	Air-Injection Test		Water-Injection Test	
	cm^2	ft^2	cm^2	ft^2
24-30[b]	1.8×10^{-7}	1.9×10^{-10}	1.3×10^{-8}	1.4×10^{-11}
75-81	7.5×10^{-9}	8.1×10^{-12}	8.4×10^{-9}	9.1×10^{-12}
82-88	9.0×10^{-9}	9.7×10^{-12}	6.0×10^{-9}	6.5×10^{-12}

[a]Depth below ground level.
[b]Injection with carbon dioxide prior to water injection was not performed for this test interval.

3.2.2 VACUUM TESTS*

3.2.2.1 Purpose and Scope

Vacuum tests were conducted in selected intervals of the Bandelier Tuff in order to obtain additional measurements of the in-situ permeability. These tests also involve sealing off the measurement interval using pneumatic packers and monitoring the changes in air pressure and flow rate after creating a pressure gradient. Unlike the air-injection tests, however, the pressure gradient is negative and is created by means of a vacuum pump. Detailed descriptions of the equipment and procedures, followed by discussions of the calculations and results, are presented in the succeeding paragraphs.

3.2.2.2 Description of Field Tests

3.2.2.2.1 Equipment. The vacuum-testing apparatus used for this study (see Figure 3-9) was designed to isolate a specified interval in the drill hole, to evacuate air by means of pumping, and to measure the resultant pressure response, flow rate, and air temperature. Isolation of the 1-meter-long (3.3 ft) test interval was accomplished by means of pneumatic packers similar to those used in the injection tests. A vacuum hose attached to the packer conduit pipe extended upward to the ground surface and was connected to a two-way valve that isolated the drill hole from the rest of the vacuum-testing equipment.

A capacitance manometer connected between the valve and the packers measured downhole pressure changes induced by pumping. The manometer was a tensioned-metal-diaphragm vacuum gauge having the capacity to measure pressure in the range of 1×10^{-4} torr to 1000 torr. (A torr is a unit of pressure equal to 1333.22 microbars, or the pressure required to support a column of mercury 1 millimeter high under standard conditions.) A pressure display module was connected to the manometer to provide direct readout of pressure in torr or millimeters.

*Response to Task 1, Paragraph 25, Compliance Order/Schedule.

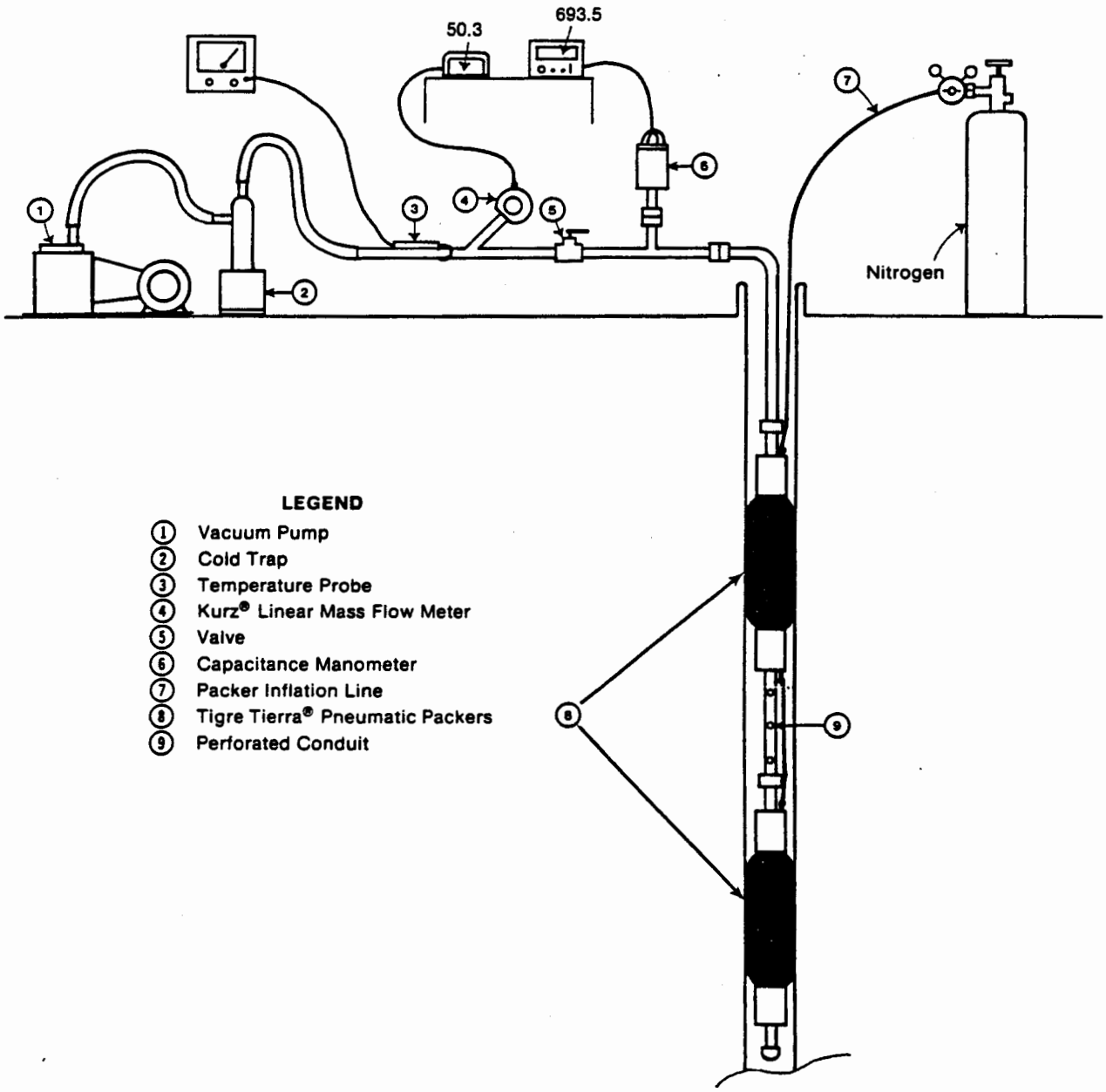

Figure 3-9. Vacuum-Testing Apparatus Used for In-Situ Permeability Measurements

The probe used to measure downhole air temperature was located in line with the system, in a small chamber welded to a section of pipe. Small holes connect the chamber and the pipe, allowing small amounts of air to flow between the two. The temperature probe was connected to a YSI Model 42SC Tele-thermometer, which has a range of -40 to 150°C with increments of 1°C.

A linear mass flow meter was located adjacent to the temperature probe in order to measure the gas flow rate induced by pumping. The meter consisted of two platinum windings: One winding was an ambient temperature detector; the other was heated to a constant temperature above that of the ambient or surrounding gas. A measure of the power required to maintain this temperature difference is a measure of the heat transfer from the winding, which in turn is a measure of the quantity of gas flowing past the sensor. The range of the meter was 0 to 1000 liters per minute (lpm), with an accuracy of 2 percent of the reading over a 10-to-1 range plus an additional one-half percent at full scale.

3.2.2.2.2 Procedure. Once a test interval had been selected, the pneumatic packers were lowered to the desired depth and inflated to isolate that particular section of the drill hole. The vacuum valve was closed, and the formation pressure prior to pumping was recorded in the field notebook.

With the vacuum pump running, the valve was opened to start the test. Pressure readings versus time were recorded at 5-second intervals. Pumping of the test section was continued as long as was necessary under the specified conditions dictated by the medium and the dead volume of the equipment. Generally, pumping was terminated after achieving steady-state flow. For tests in the Bandelier Tuff, it was observed that quasi steady-state conditions were obtained prior to 1 minute of pumping. Therefore, for all tests, the interval was pumped for a period of 1 minute. The temperature was recorded during the pumping phase of the tests, and the flow rate was recorded just prior to the end of the pumping phase.

After 1 minute of pumping, the vacuum valve was closed and the pressure buildup phase was begun. Pressure readings were once again recorded at 5-second intervals until the system returned to the prepumping pressure, signifying the end of the test.

3.2.2.3 Calculations

The vacuum-testing technique is based on methods used by the petroleum industry. In a paper presented by Horner (1951), the pressure buildup that results from closing gas wells is used to calculate the permeability of the subsurface formation. This method was modified by Jakubick (1983) for use in unsaturated materials by initiating the pressure buildup by means of vacuum pumping rather than by shutting-in the well. The equations used for the calculations in this study, however, were taken directly from Horner's paper, because Jakubick does not present the theory for his equations which are different from the original work by Horner. Moreover, Jakubick does not define the gas-constant term he used, nor does he maintain consistency in the units used in his equations.

Single-phase radial flow to a well completed in a reservoir, assumed to be homogeneous, horizontal, and of uniform thickness, may be expressed by the equation

$$(\partial^2 p/\partial r^2) + [(1/r)(\partial p/\partial r)] = (fc\mu/k)(\partial p/\partial t) \tag{13}$$

where

p = reservoir pressure
r = distance from the center line of the well
f = formation porosity
c = fluid compressibility
μ = fluid viscosity
k = intrinsic permeability of the formation
t = time

Horner presents the so-called 'point solution' to Equation (13) which yields

$$p = p_o + \{(q\mu/4\pi kh)E_i[-(r^2 f\mu c/4kt)]\} \tag{14}$$

where

p_o = initial reservoir pressure
q = a constant rate of production for the well
h = length of the test interval
E_i = the exponential integral

Considering a single well brought into production at t_o, which subsequently produced at a constant rate q, the well pressure p_w at the time $[(t_o + \varphi)/\varphi]$ may be obtained by superimposing two solutions of the form of Equation (14). For small values of its argument, the E_i function may be approximated by a logarithmic function. The result is the basic buildup equation for a single well in an infinite reservoir,

$$p_w = p_o - \{(q\mu/4\pi kh) \ln [(t_o + \varphi)/\varphi]\} \tag{15}$$

where is the time after close-in of the well.

For analysis of the data, it is convenient to change the natural logarithm, ln, to the base ten logarithm, $\log_{10}$, by the relationship

$$\ln x = (\log_{10} x)(\ln 10) \tag{16}$$

which yields

$$p_w = p_o - \{[(\ln 10)q\mu/4\pi kh] \log [(t_o + \varphi)/\varphi]\} \tag{17}$$

Analysis of the vacuum-test data using Equation (17) involves fitting a straight line through the data points. The slope of the line, m, from Equation (17) is defined as

$$m = -[(\ln 10)q\mu/4\pi kh] \tag{18}$$

The next step in the analysis involves plotting the well-pressure (p_w) data versus the log of $[(t_o + \varphi)/\varphi]$ and determining the slope of the resultant line. This graph is commonly referred to as a Horner plot. Once the slope of the line is determined, Equation (18) can be rearranged in terms of the intrinsic permeability as follows:

$$k = -[(\ln 10) q\mu/4\pi mh] = -[0.1832339(q\mu/mh)] \quad (19)$$

3.2.2.4 Results and Discussion

Intrinsic permeabilities determined from vacuum tests in the Bandelier Tuff (Table 3-5) range from 10^{-8} to 10^{-9} cm^2 (10^{-11} to 10^{-12} ft^2). The correlation coefficients for the linear regression used to fit a straight line through the data points on the Horner plots indicate a good linear relationship for the data; the lowest coefficient is 0.92 (see Table 3-5).

In general, the vacuum-test results, like those from the air-injection tests, indicate that permeability tends to decrease with depth. The lowest value, for example, was observed in the lower, moderately welded portion of Unit 1b. Results of the three tests performed in fractured zones indicate that there is no significant difference in permeability between fractured versus unfractured zones.

Table 3-6 compares intrinsic permeabilities derived from the air-injection tests versus the vacuum tests for similar intervals. The comparison demonstrates that the two methods yield results of the same order of magnitude. The vacuum-test results, however, are lower. A discussion of possible variations in vacuum-test and air-injection methods is presented in Section 3.2.5.

3.2.3 LABORATORY MEASUREMENTS*

3.2.3.1 Purpose and Scope

Laboratory measurements of permeability were also obtained on 20 core samples to provide a comparison with the field-test results. These determinations were conducted by TerraTek Research Laboratory using two procedures, one to measure permeability via gas injection and correction for gas slippage (Klinkenberg Correction Method) and the other to measure the gas-water relative permeability (Dynamic Method). The descriptions of these procedures are taken from TerraTek's report (TerraTek Research Laboratory, 1985). They are followed by a discussion of the laboratory results. A comparison of the laboratory and field data is presented in Section 3.2.5.

3.2.3.2 Sample Preparation

(See Section 3.1.2.2.)

*Response to Task 1, Paragraph 25, Compliance Order/Schedule.

Table 3-5. Permeability Values Determined from Vacuum Tests in Los Alamos Drill Holes

Hole Number	Geologic Unit	Test Interval[a] (ft)	Interval Description	Correlation Coefficient[b]	Fractures Present?	Intrinsic Permeability (k)	
						$cm^2 \times 10^{-9}$	$ft^2 \times 10^{-12}$
LLM-85-01	2b	30-33.3	Lower 2b, Moderately Welded	0.9409	No	39	42
LLM-85-02	2b	10-13.3	Upper 2b, Moderately Welded	0.9325	Yes	14	15
LLM-85-02	2b	25-28.3	Middle 2b, Moderately Welded	0.9267	Yes	22	24
LLM-85-05	2b	15-18.3	Middle 2b, Moderately Welded	0.9948	No	24	2.6
LGM-85-06	2b	10-13.3	Upper 2b, Moderately Welded	0.9675	No	38	41
LGM-85-11	2b/2a	35-38.3	Contact 2b/2a, Moderately Welded	0.9779	No	5.5	5.9
LLM-85-01	2a	70-73.3	Lower 2a, Nonwelded	0.9799	No	43	46
LLM-85-05	2a	40-43.3	Upper 2a, Slightly Welded	0.9196	No	8.4	9.1
LLM-85-05	2a	50-53.3	Middle 2a, Slightly Welded	0.9812	No	8.6	9.3
LLM-85-05	2a	60-63.3	Middle 2a, Moderately Welded	0.9882	No	8.6	9.3
LLM-85-06	2a	40-43.3	Middle 2a, Moderately Welded	0.9895	Yes	2.4	2.6
LLM-85-01	1b	80-83.3	Upper 1b, Slightly Welded	0.9946	No	5.6	6.0
LLM-85-01	1b	94-97.3	Upper 1b, Slightly Welded	0.9959	No	3.5	3.8
LLM-85-02	1b	87-90.3	Upper 1b, Slightly Welded	0.9966	No	9.3	10
LGM-85-06	1b	82-85.3	Middle 1b, Slightly Welded	0.9931	No	1.0	1.1
LGM-85-06	1b	100-103.3	Lower 1b, Moderately Welded	0.9932	No	0.84	0.90
LGM-85-11	1b	77-80.3	Middle 1b, Slightly Welded	0.9851	No	8.2	8.8
LGM-85-06	1b	60-63.3	Upper 1b, Slightly Welded	0.9903	No	8.7	9.4
LGM-85-11	1a	110-113.3	Upper 1a, Nonwelded	0.9963	No	2.7	2.9
LLM-85-02	1b	87-90.3	Upper 1b, Slightly Welded	0.9966	No	8.6	9.3
LLM-85-06	1b	87-90.3	Mid-Lower 2b, Moderately Welded	0.9609	No	2.4	2.6

[a]Depth below ground level.

[b]Correlation coefficient for the linear regression used to fit a straight line through the data points on the Horner plots (see Section 3.2.2.3).

Table 3-6. Comparison of Intrinsic Permeability Values Determined from Air-Injection and Vacuum Tests in Los Alamos Drill Holes

Hole Number	Test Interval (ft)[a]		Intrinsic Permeability (k)			
	Air-Injection Test	Vacuum Test	Air-Injection Test		Vacuum Test	
			$cm^2 \times 10^{-9}$	$ft^2 \times 10^{-12}$	$cm^2 \times 10^{-9}$	$ft^2 \times 10^{-12}$
LLM-85-01	30-36	30-33.3	130	140	39	42
LLM-85-02	9-15	10-13.3	10	11	15	16
LLM-85-02	24-30	25-28.3	16	17	22	24
LGM-85-11	35-41	35-38.3	17	18	5.5	5.9
LLM-85-01	72-78	70-73.3	19	21	43	46
LLM-85-01	93-99	94-97.3	7.6	8.2	3.5	3.8
LLM-85-02	87-93	87-90.3	3.3	9.5	9.3	10
LGM-85-06	60-66	60-63.3	120	130	8.7	9.4
LGM-85-06	81-87	82-85.3	84	90	1.0	1.1
LGM-85-11	99-105	100-103.3	3.3	3.6	0.84	0.90
LGM-85-11	77-83	77-80.3	32	35	8.2	8.8
LGM-85-11	108-114	110-113.3	7.2	7.8	2.7	2.9

[a]Depth below ground level.

3.2.3.3 Procedures

3.2.3.3.1 Klinkenberg Correction Method. Following porosity determinations, gas permeability measurements were performed on the 20 samples. These measurements were corrected for gas slippage, i.e., movement of gas along a boundary, using the Klinkenberg Correction Method. The measurement technique consisted of applying a confining pressure of approximately 100 psi and a slight pore pressure, and maintaining an approximate pressure drop of 2 psi across the sample during testing. Nitrogen gas was injected into the samples at four mean pressures (4, 9, 14, and 19 psi), and the permeability was calculated for each of these pressures. A plot was made of permeability versus the reciprocal mean pressures, and the intercept of a best-fit line through these four points, with the permeability axis at zero reciprocal mean pressure (infinite mean pressure), yielded the gas permeability corrected for gas slippage (Klinkenberg Correction).

3.2.3.3.2 Dynamic Method. Following completion of the gas permeability measurements, all 20 samples were subjected to gas-water relative permeability testing to determine intrinsic permeabilities (described in Section 3.2.3.4 below) and effective permeabilities (described in Section 3.2.4.1). Testing was begun by vacuum-saturating the samples with tap water (density = 0.995 g/cm^3 at room temperature). Complete saturation was verified by comparing these saturated-weight data with helium-injection data. Following saturation, each sample was placed in a hydrostatic core holder and subjected to a confining pressure of approximately 100 psi. Testing consisted of displacing the water from the samples with humidified nitrogen. (The gas was humidified to prevent drying or dehydration.) Incremental production of gas and water was monitored against time and flow rate at a constant injection pressure. These production data were used to calculate the gas-water relative permeabilities according to Johnson, Bossler, and Naumann's (1959) extension of Welge's (1952) derivation of relative permeability.

3.2.3.4 Results and Discussion

The laboratory permeability results (Table 3-7) are relatively uniform and consistent between the two methods, except for Sample MCG-607. The Klinkenberg result for this sample is probably unreliable as evidenced by its low correlation coefficient (0.714) and its poor comparison with the Dynamic Method result.

The results from both methods indicate only minor differences with depth or between geologic units. Klinkenberg permeabilities are approximately twice those determined by the Dynamic Method, but that is not considered significant for these types of measurement. More importantly, the average intrinsic permeability for both the Klinkenberg Correction Method and the Dynamic Method is 10^{-9} cm^2 (10^{-11} ft^2), a result that compares favorably with the field-test results.

Table 3-7. Intrinsic Permeability Values Determined from Laboratory Analysis of Core Samples

Hole Number	Geologic Unit	Sample Number	Depth of Sample (ft)[a]	Interval Description	Intrinsic Permeability/ Klinkenberg Method		Correlation Coefficient[b]	Intrinsic Permeability/ Dynamic Method	
					$cm^2 \times 10^{-9}$	$ft^2 \times 10^{-12}$		$cm^2 \times 10^{-9}$	$ft^2 \times 10^{-12}$
LGM-85-11	2b	MCG-618	3	Moderately Welded[c]	6.2	6.7	0.989	5.5	5.9
LLM-85-02	2b	MCG-606	7	Moderately Welded	6.6	7.1	0.745	4.5	4.9
LLM-85-05	2b	MCG-610	15	Moderately Welded	6.5	7.0	0.893	5.7	6.2
LLM-85-01	2b	MCG-602	30	Moderately Welded	2.7	2.9	0.958	1.1	1.2
LGM-85-11	2b	MCG-619	30	Moderately Welded	3.2	3.5	0.949	2.9	3.1
LLM-85-02	2b	MCG-607	36	Moderately Welded	11.0	12.0	0.714	1.2	1.3
LGM-85-06	2b	MCG-614	29	Moderately Welded	6.4	6.9	0.847	4.9	5.3
LLM-85-05	2b	MCG-611	36	Slightly Welded	3.5	3.8	0.984	2.4	2.6
LLM-85-01	2a	MCG-603	52	Slightly Welded	4.1	4.4	0.969	2.7	2.9
LGM-85-06	2a	MCG-615	51	Slightly Welded	2.5	2.7	0.954	0.86	0.93
LLM-85-02	2a	MCG-608	67	Moderately Welded	2.0	2.2	0.958	1.0	1.1
LLM-85-05	1b	MCG-612	76	Slightly Welded	2.1	2.3	0.944	1.3	1.4
LLM-85-01	1b	MCG-604	101	Slightly Welded	3.0	3.2	0.939	2.6	2.8
LGM-85-06	1b	MCG-616	99	Moderately Welded	18.0	19.0	0.917	13.0	14.0
LGM-85-11	1b	MCG-620	94	Moderately Welded	4.4	4.7	0.958	1.1	1.2
LLM-85-02	1b	MCG-609	117	Moderately Welded	3.3	3.6	0.973	1.7	1.8
LLM-85-05	1b	MCG-613	123	Slightly Welded	4.2	4.5	0.902	1.6	1.7
LLM-85-01	1b	MCG-605	124	Moderately Welded	6.0	6.5	0.850	2.3	2.5
LGM-85-11	1a	MCG-621	115	Nonwelded	3.4	3.7	0.933	1.8	1.9
LGM-85-06	1a	MCG-617	115	Nonwelded	1.4	1.5	0.970	0.93	1.0

[a]Below ground level.
[b]Determined for Klinkenberg permeabilities.
[c]Weathered.

3.2.4 HYDRAULIC CONDUCTIVITY AS A FUNCTION OF MOISTURE CONTENT*

3.2.4.1 Laboratory Tests

As noted above, the Dynamic Method was also used to determine permeability as a function of moisture content for the 20 samples of Bandelier Tuff (see Section 3.2.3.3.2). These values, called effective permeabilities, are plotted as a function of total air saturation in the graphs presented in Appendix D. Since the abscissa corresponds to total air saturation, the maximum effective permeabilities for water depicted on the curves occur at an air saturation of 0.000, which is equivalent to a water saturation (Θ_s) of 1.000. Therefore, as the water saturation decreases, the effective permeability for water decreases, and the effective permeability for air increases.

The effective permeability values for the rock-core samples from the Bandelier Tuff range from 86.1 to 1301 millidarcys [(8.5×10^{-10} to 1.3×10^{-8} cm^2) or (9.1×10^{-13} to 1.4×10^{-11} ft^2)]. Residual water saturation following gas injection ranged from 0.64 to 0.95. Since moisture contents in the study area are much lower than this range (generally less than 10 percent), the effective permeabilities determined using the Dynamic Method are not indicative of the permeabilities one would expect to observe at depth in Areas G and L. These data are therefore only applicable to the estimation of near-surface conditions following a heavy rainfall, when moisture contents might exceed residual water saturation.

3.2.4.2 van Genuchten's Method

3.2.4.2.1 Purpose and Scope. A model described by van Genuchten (1978) was used to calculate the unsaturated hydraulic conductivity functions for the Bandelier Tuff. Inputs to the model are the saturated hydraulic conductivities and data from the moisture characteristic curves for the 20 core samples analyzed in the laboratory tests. The output function is a closed-form analytical expression that generates a plot of hydraulic conductivity versus moisture content and/or water potential. The output function is only valid over the moisture and water-potential ranges tested.

3.2.4.2.2 Procedure. A model described by Mualem (1976) was used to predict unsaturated hydraulic conductivities from the moisture characteristic curves (Appendix C) and the saturated hydraulic conductivities. Mualem's derivation yields an integral formula for determining the unsaturated hydraulic conductivity as a function of moisture content, which enables one to derive closed-form analytical expressions provided suitable equations for the moisture characteristic curves are available. The resulting conductivity expressions generally contain three independent, dimensionless parameters—α, n, and m—which are calculated using the nonlinear least-squares curve-fitting program described by van Genuchten (1978). The information required to calculate these parameters consists of saturated hydraulic conductivities and data obtained from the moisture characteristic curves, namely, the saturated and residual soil-moisture contents (Θ_s, and Θ_r, respectively) and the slope for the curve at midpoint [$(\Theta_s + \Theta_r)/2$].

---

*Response to Task 3, Paragraph 25, Compliance Order/Schedule.

All of this information was assembled into a data base and used as input into van Genuchten's model, which generates values for α, n, and m. The model then inputs these values into Mualem's integral formulas and plots the following two functions: $K(\theta)$ versus θ (moisture content) and $K(\psi)$ versus ψ (water potential). The intrinsic permeabilities determined using the Klinkenberg Correction Method (Table 3-7) were then used to calculate water-saturated hydraulic conductivities for input to the model. (See Section 3.2.1.4 for conversion of intrinsic permeability to hydraulic conductivity.) These values were used largely because they more closely reflect the in-situ permeabilities for air and water in the study area.

3.2.4.2.3 Results and Discussion. The modeling results are presented as graphs of unsaturated hydraulic conductivity versus volumetric moisture content [$K(\theta)$ versus θ] and of hydraulic conductivity versus water potential [$K(\psi)$ versus ψ]. Representative outputs from the model for 7 of the 20 samples are presented in Figures 3-10 through 3-13.

Unfortunately, these results are of limited value because they are based on partial moisture characteristic curves which do not extend over the range of water potentials and moisture contents measured in the field. For example, the water-potential values of the curves extend roughly to -0.3 bar (-300 cm of water), while those measured in the field range from -1 to -15 bar (see Section 3.3.1.3). Similarly, values for moisture content (θ) range from 0.4 to 0.6 on the curves, while those determined in the field are generally less than 0.1. As a consequence, the calculated unsaturated hydraulic conductivities are also outside the range of the field values.

Nevertheless, the calculated values can be used for near-surface infiltration studies when the moisture and water-potential ranges fall within those of the moisture characteristic curves. It should be noted, however, that these curves were obtained by drying the soil and therefore represent only the drying branch of the hysteresis loop. The drying branch has a higher moisture content for a given water potential than does the wetting branch; hence, a given soil is more retentive for drying than it is for wetting (Case and Welch, 1979).

3.2.5 PERMEABILITY SUMMARY

Table 3-8 compares the overall average intrinsic permeabilities of the geologic units as determined by the three methods used in this study, namely, in-situ borehole injection, in-situ vacuum testing, and laboratory testing of core samples. In contrast to the laboratory results, which show relative uniformity throughout the tuff, results of both field methods indicate a decrease in permeability with stratigraphic depth. This contrast is probably due in part to the fact that it was necessary to select the laboratory samples from those exhibiting the highest degree of consolidation; such samples would have lower permeabilities than the bulk formation from which they were taken. Furthermore, the laboratory tests measure a significantly smaller interval than that measured in the field. It was therefore concluded that the field-test results were the more reliable indicators of bulk permeabilities and that the permeabilities of the individual geologic units do indeed decrease with stratigraphic depth.

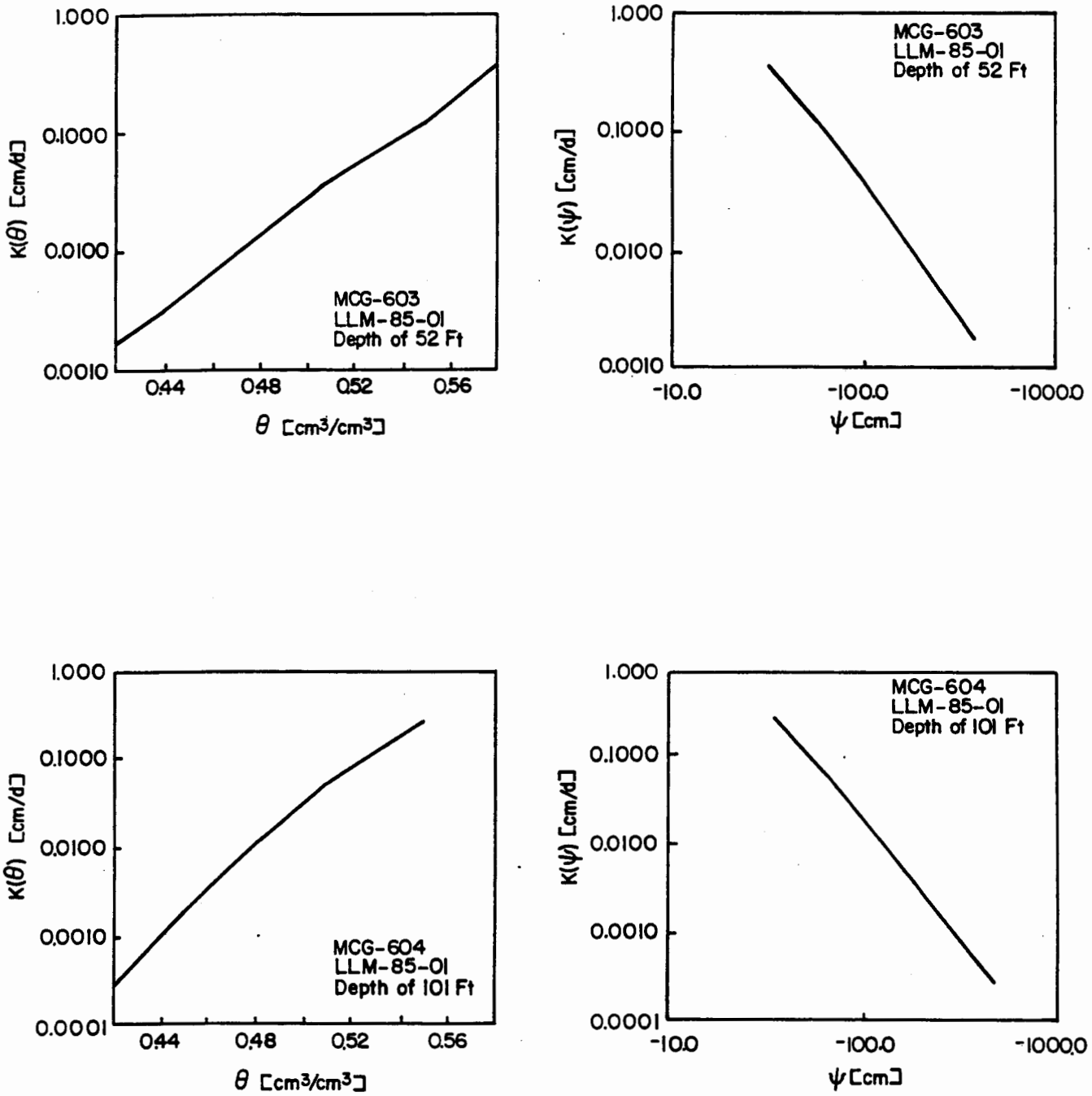

Figure 3-10. Unsaturated Hydraulic Conductivities as Functions of Moisture Content and Water Potential for Samples MCG-603 and MCG-604

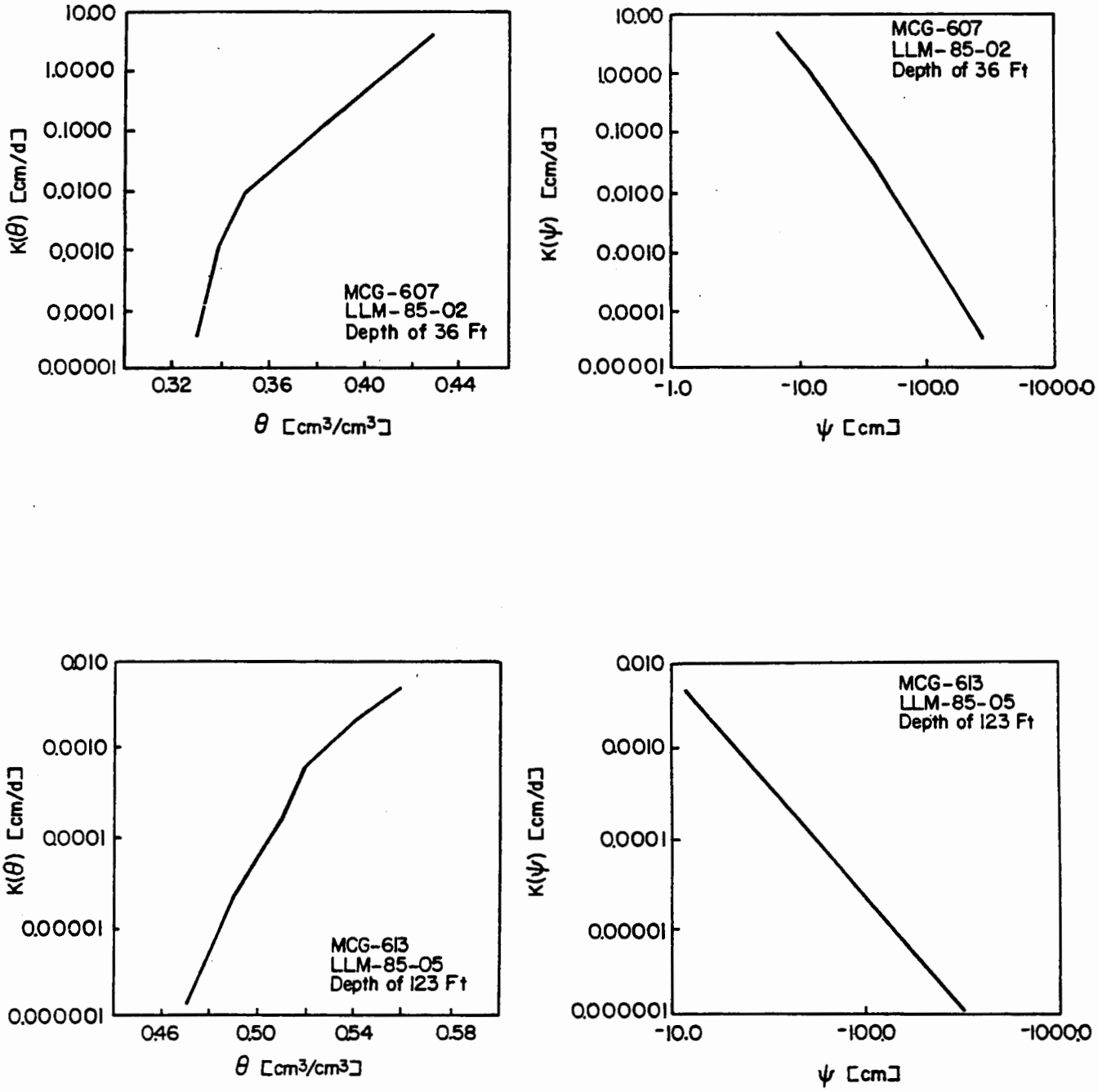

Figure 3-11. Unsaturated Hydraulic Conductivities as Functions of Moisture Content and Water Potential for Samples MCG-607 and MCG-613

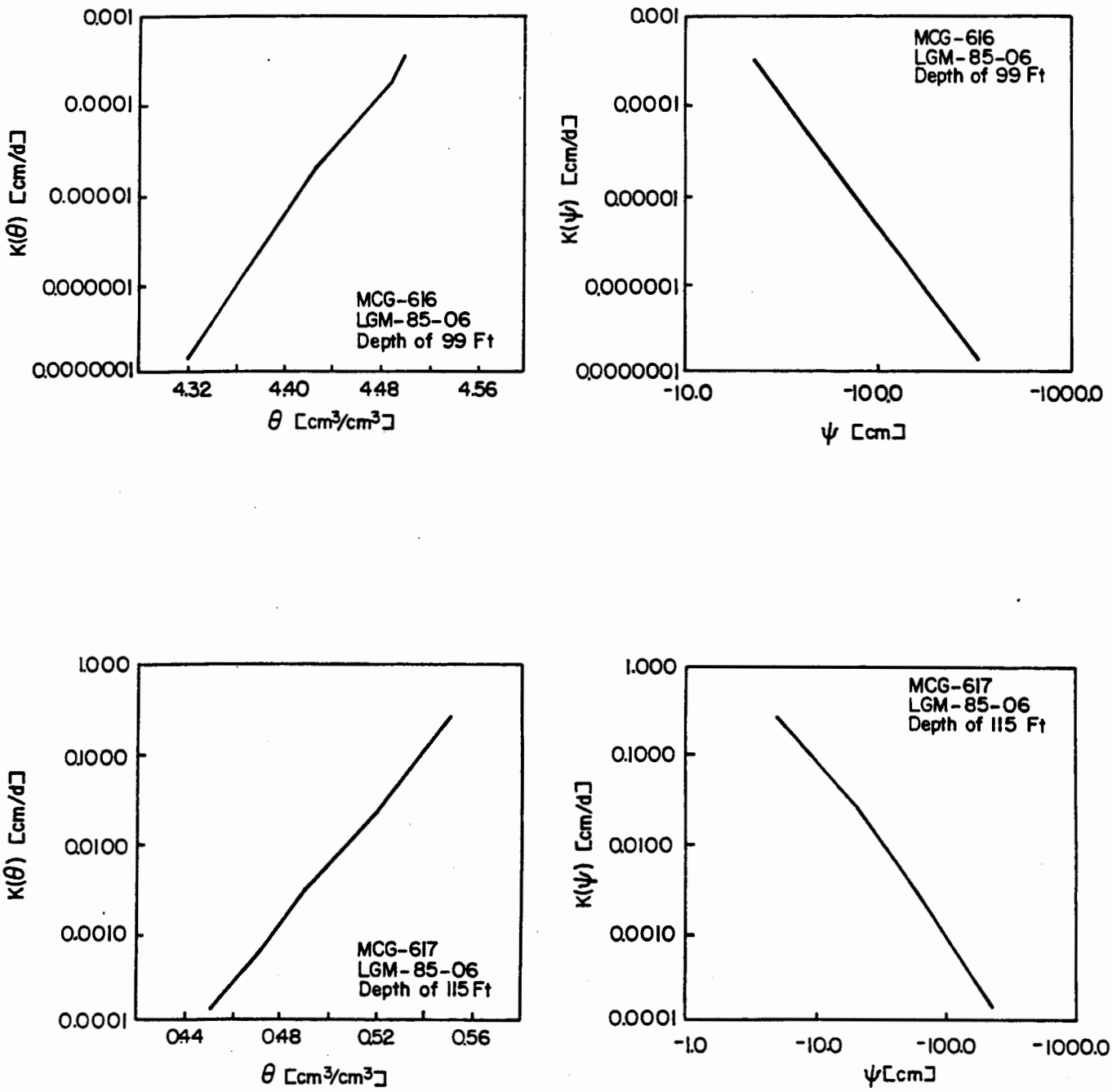

Figure 3-12. Unsaturated Hydraulic Conductivities as Functions of Moisture Content and Water Potential for Samples MCG-616 and MCG-617

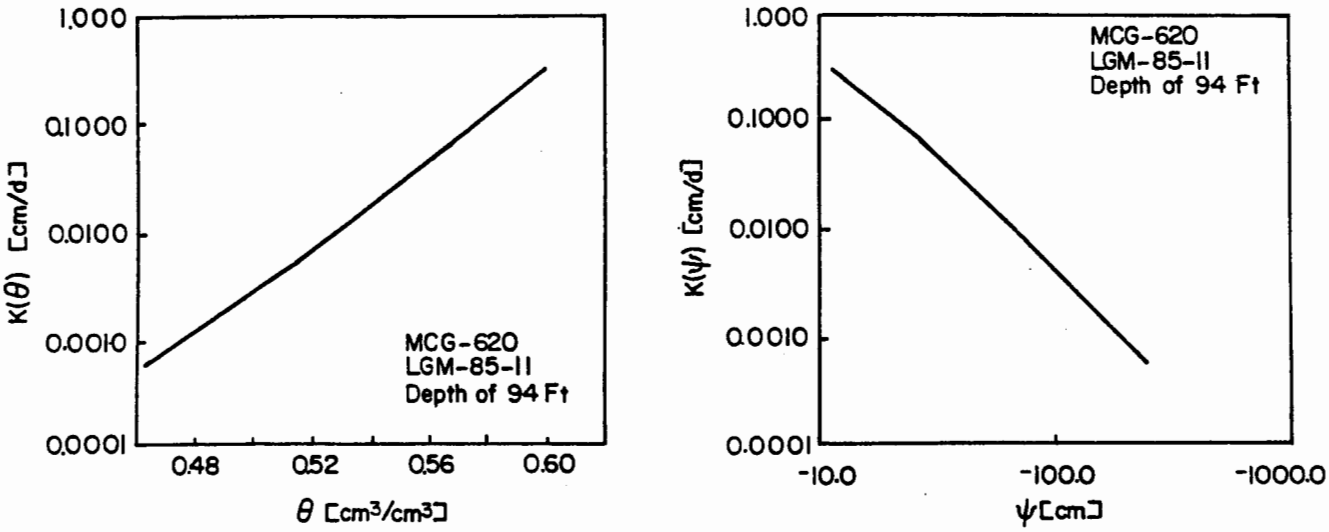

Figure 3-13. Unsaturated Hydraulic Conductivities as Functions of Moisture Content and Water Potential for Sample MCG-620

Table 3-8. Comparison of Average Intrinsic Permeability Values for the Major Geologic Units of the Bandelier Tuff in the Study Area

Unit	Intrinsic Permeability					
	Air-Injection Test		Vacuum Test		Laboratory Analysis	
	$cm^2 \times 10^{-9}$	$ft^2 \times 10^{-12}$	$cm^2 \times 10^{-9}$	$ft^2 \times 10^{-12}$	$cm^2 \times 10^{-9}$	$ft^2 \times 10^{-12}$
2b	93	100	23	25	5.7	6.2
2a	62	67	13	14	2.8	3.0
1b	26	28	5.7	6.2	5.7	6.2
1a	7.2[a]	7.8[a]	2.7[a]	2.9[a]	2.4	2.6

[a]Intrinsic permeability for this unit is based on only one measurement.

It should be noted that the lower average permeabilities determined by the vacuum test for Units 2b and 2a are probably due to the inability to perform the test in the more permeable portions of these units. A vacuum could not be established in the upper portions, so the test failed and no data were obtained. Thus, the average vacuum-test data do not include values for the most permeable zones in the units, resulting in average results which are biased low.

Results from all of the determinations do not permit a conclusive assessment of the effect of fractures on permeability. The moisture-content data indicate that the potential exists for fractures to cause preferential water movement; however, the enhancement may be less than the sensitivity of the measurement techniques. It follows that a better assessment would require additional testing, using methods having greater sensitivity. Similarly, additional tests, also having greater sensitivity, would be needed in order to fully assess the effects on permeability of such other sources of variation as pumice content.

3.3 GRADIENT DETERMINATIONS

3.3.1 TEMPERATURE AND WATER-POTENTIAL MEASUREMENTS*

3.3.1.1 Purpose and Scope

Temperature and water-potential measurements were made at the site to assess the magnitude and direction of the thermal and water-potential gradients in the study area. Knowledge of the gradients is used to determine whether temperature and water potential play a significant role in the transport of contaminants to the water table. A description of the instruments used to acquire these data, together with information on calibration, installation, and data reduction, is presented below, and is followed by a discussion of the results. The results are presented in the form of graphs plotting temperature and water potential versus time and depth.

*Response to Task 4, Paragraph 25, Compliance Order/Schedule.

3.3.1.2 Field Instrumentation

3.3.1.2.1 Description of the Thermocouple Psychrometers. Thermocouple psychrometers were used to obtain the water-potential measurements at Los Alamos because the low soil-water potential (less than -1 bar) precluded the use of tensiometers. The instruments actually measure voltage which is converted to soil-water potential by means of a calibration model (Brown and Bartos, 1982). Psychrometers are particularly convenient because they simultaneously measure temperature.

The thermocouple psychrometers used in this study were Models PCT-55 and PST-55 manufactured by Wescor, Inc., of Logan, Utah. The only difference between the two models is that the PST series is shielded with a stainless steel screen instead of a ceramic cup, and therefore has a faster response time. A diagram of a typical screen-shielded psychrometer is shown in Figure 3-14.

Operation of the psychrometers is based on the Peltier effect, in which a thermocouple is cooled below the dew point by passing an electric current across a junction composed of two dissimilar metal conductors. After water has condensed on the cooling junction, the electric current is discontinued and the junction immediately begins to warm up. The rate of warming is rapid at first, and then slows down until the latent heat of vaporization is overcome, at which time water condensed on the junction evaporates. The point at which the warming rate is at a minimum is known as the psychrometric plateau. The electromotive force (emf) generated across the junction during the psychrometric plateau is a measure of the relative humidity of the system (Spanner, 1951).

The relative humidity ($\bar{P}/P_o$) in soil is related to soil-water potential by the equation (Case and Welch, 1979)

$$\psi = (\rho k_B T/m) \ln (\bar{P}/P_o) = \psi_o \ln (\bar{P}/P_o) \qquad (20)$$

where

ρ = the density of water at temperature T
k_B = Boltzman's constant (1.38×10^{-16} erg/°K)
m = the mass of a water molecule (approximately 3×10^{-23} g)
$\bar{P}$ = the average vapor pressure in the soil
P_o = the pressure of the water vapor above a surface of infinite radius of curvature
$\psi_o \simeq 10^3$ bars at 300°K

3.3.1.2.2 Laboratory Calibration. Each psychrometer must be calibrated individually due to the variable thicknesses of the welded junction and wires used in fabrication. Saline solutions are convenient to use for calibration, since tables that relate salt concentrations and temperature to relative humidity are readily available (Lang, 1967). The ratio of microvoltage to theoretical water potential at a given temperature for a particular psychrometer provides the correction coefficient necessary for determining actual water potential in rock and soil systems.

In this study, reagent-grade sodium chloride was dissolved in deionized water to provide calibration solutions ranging in strength from 0.1 to 1.0 molal.

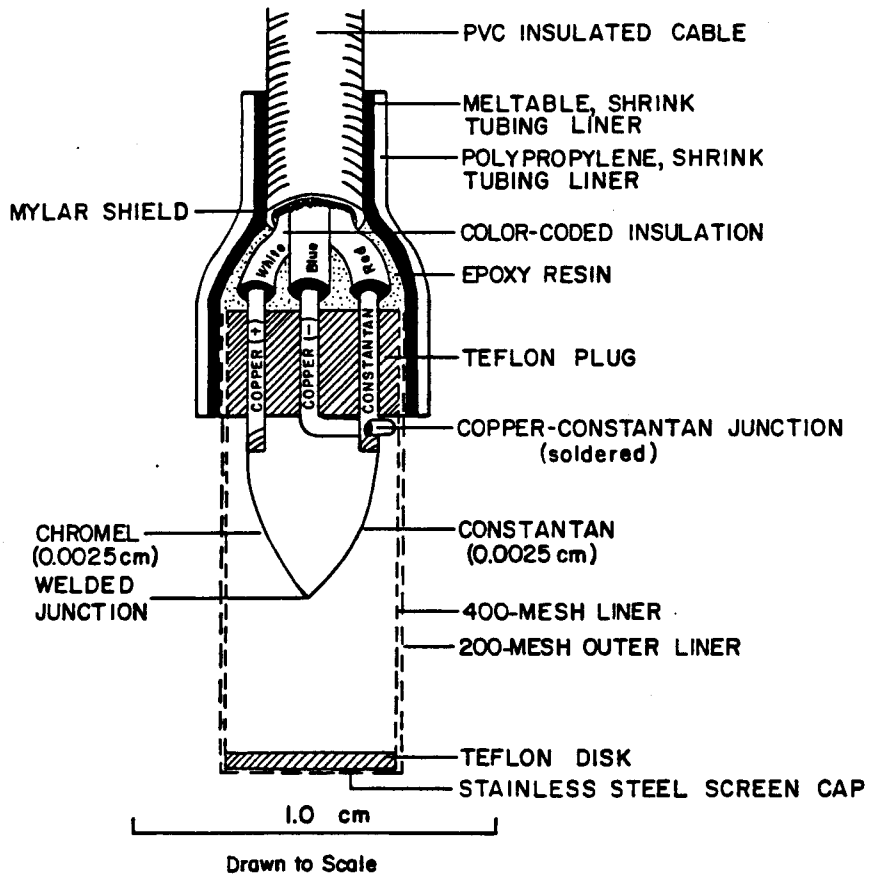

Figure 3-14. Sketch of the Single-Junction Stainless Steel Screen-Shielded Thermocouple Psychrometer (from Brown and Collins, 1980)

Each psychrometer was calibrated using at least three molal concentrations, independently, in the following manner. One milliliter of solution was decanted into a sample chamber. A psychrometer was then sealed into the chamber to create a closed system with a known water potential (see Figure 3-15). The sealed chamber was then placed in a wooden rack and equilibrated for at least 24 hours. Following equilibration, the voltage output of the thermocouples was read in psychrometric (wet-bulb) mode using either a Wescor HR33T Dewpoint Microvoltmeter or a Wescor HP-115 Microprocessor-Controlled Data Collection System. Each molal concentration (water potential) was read a minimum of three times for temperature and microvolts. These readings were then converted to water potential using the calibration model described below.

3.3.1.2.3 Psychrometer Calibration Model. The psychrometer calibration model developed by Brown and Bartos (1982) was used to accurately convert psychrometer outputs to water potential. This model is far more versatile than hand-drawn calibration curves because it can convert water potentials from -1 to -80 bar over a wide range of temperature and zero offset readings. Inputs to the model are temperature, cooling time, zero offset, psychrometer output in microvolts, and calibration coefficients, the last required for conversion of microvolts to water potential. The calibration coefficient B is defined as

$$\sum B = \sum WP / \sum \widehat{WP} \qquad (21)$$

where $\sum WP$ is the sum of the actual water potentials (sodium chloride solutions) used during calibration, and $\sum \widehat{WP}$ is the sum of the water potentials estimated by the model. Calibration coefficients for each of the psychrometers installed in Holes LLP-85-03 and LGP-85-07 are presented in Tables 3-9 and 3-10, respectively. A listing of the Fortran V program for the model is reproduced as Appendix E. The output from the model is the water potential for the soil conditions as sensed by the psychrometer.

3.3.1.2.4 Field Installation. On 22 October 1985, a total of 38 thermocouple psychrometers were installed at the study area, 23 in Hole LLP-85-03 and 15 in Hole LGP-85-07. Completion diagrams are provided in Appendix A. Because of the presence of surface casing in Hole LLP-85-03, a shallow boring was drilled adjacent to the main hole and five psychrometers were installed in this second hole close to the ground surface (depicted in Appendix A as being in the same hole). Installation was accomplished by taping the psychrometers to a string of Schedule 40, 2-inch-I.D., polyvinylchloride (PVC) pipe and carefully lowering the string into the hole. The annulus surrounding the PVC pipe was then backfilled with auger cuttings from that drill hole. It was assumed that the density of this backfill was similar to the in-situ density of the tuff, and that the relative humidity of the backfill, as sensed by the psychrometers, would equilibrate with the relative humidity of the adjacent tuff. Installation depths are included with the data presented in Tables 3-9 and 3-10, for Holes LLP-85-03 and LGP-85-07, respectively.

3.3.1.3 Results and Discussion

Psychrometer data were collected for Holes LLP-85-03 and LGP-85-07 over the period 22 October to 20 November 1985. The values for temperature and water potential were viewed in two ways, as plots of temperature or water potential versus time, and as plots of temperature or water potential versus depth.

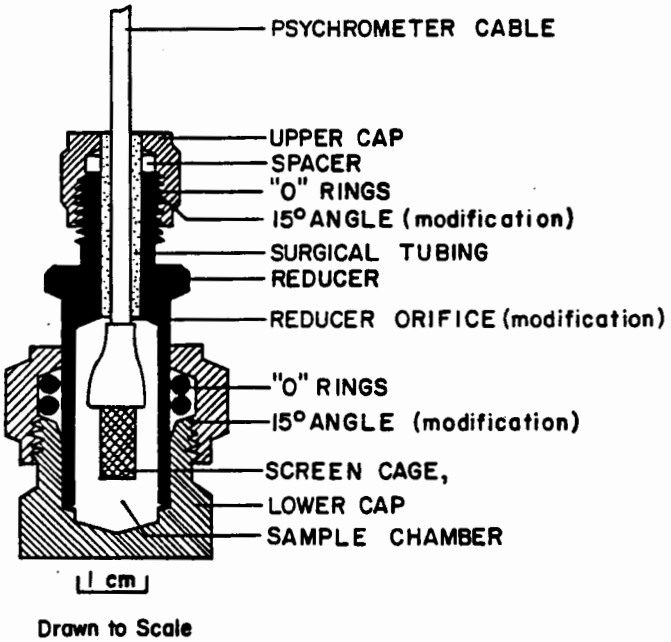

Figure 3-15. Sketch of the Stainless Steel Calibration Chamber Showing Seals and Screen-Shielded Thermocouple Psychrometer (from Brown and Collins, 1980)

Table 3-9. Installation Depths and Calibration Coefficients for Psychrometers in Hole LLP-85-03

Model Number[a]	Serial Number	Scanner/Channel	Calibration Coefficient for Water-Potential Model	Installation Depth (ft)
PCT-55	29414	I/1	—	Surface
PCT-55	29416[b]	I/2	0.85	2.0
PST-55	29474[b]	I/3	0.84	4.0
PST-55	29473[b]	I/4	0.84	6.0
PCT-55	29420[b]	I/5	0.89	8.0
PST-55	29469[b]	I/6	0.84	10
PCT-55	29418	I/7	0.81	13
PST-55	29483	I/8	0.88	13
PCT-55	29424	I/9	0.85	24
PST-55	29479	I/10	0.87	24
PCT-55	29406	I/11	0.90	41
PST-55	29462	I/12	1.00	41
PCT-55	29409	II/1	1.00	50
PST-55	29475	II/2	0.94	50
PCT-55	29405	II/3	0.85	56
PST-55	29477	II/4	1.03	56
PCT-55	29425	II/5	0.84	66
PST-55	29455	II/6	0.96	66
PST-55	29481	II/7	0.89	76
PCT-55	29422	II/8	0.94	76
PST-55	29476	II/9	0.90	86
PST-55	29458	II/10	1.00	96
PCT-55	29427	II/11	1.00	96

[a]The PCT series psychrometers are shielded with a ceramic cup, while the PST models are shielded with a stainless steel screen.

[b]Psychrometers in the upper 10 ft are located in a shallow boring adjacent to the main hole.

Table 3-10. Installation Depths and Calibration Coefficients for Psychrometers in Hole LGP-85-07

Model Number[a]	Serial Number	Scanner/Channel	Calibration Coefficient for Water-Potential Model	Installation Depth (ft)
PCT-55	29415	III/1	0.89	4.5
PST-55	29459	III/2	0.89	6.5
PCT-55	29410	III/3	0.85	8.5
PST-55	29461	III/4	0.91	10
PCT-55	29411	III/5	0.91	12
PST-55	29463	III/6	0.86	14
PCT-55	29417	III/7	0.84	17
PST-55	29466	III/8	0.87	19
PCT-55	29403	III/9	0.92	22
PST-55	29467	III/10	0.92	27
PCT-55	29407	III/11	1.00	32
PST-55	29465	III/12	1.04	37
PST-55	29464	III/13	0.95	42
PCT-55	29404	III/14	0.85	47
PST-55	29468	III/15	0.89	52

[a]The PCT series psychrometers are shielded with a ceramic cup, while the PST models are shielded with a stainless steel screen.

Selected plots of the former are presented in Figures 3-16 through 3-19. Air temperature versus time at Hole LLP-85-03 is plotted in Figure 3-20. Box plots of water potential and temperature versus depth for the entire time period are presented in Figures 3-21 through 3-24. Since the box plots present the data in quartiles, the outlying values represent minimum and maximum values. The boxes enclose the 25- and 75-percent values, and the vertical lines connecting the boxes intersect the median-temperature or water-potential values for the time period.

The plot of air temperature versus time (Figure 3-20) demonstrates that a dramatic diurnal temperature variation exists at the site, and that the highs and lows generally decreased over this monitoring period. Plots of formation temperature versus time (Figures 3-17 and 3-19) for the psychrometers located within 15 ft of the ground surface demonstrate that the near-surface temperatures also decreased in response to the decrease in air temperature. Furthermore, as expected, a phase lag is evident when comparing the decreasing temperatures measured by successively deeper psychrometers.

The plots of temperature versus depth (Figures 3-22 and 3-24) reveal a temperature bulge that probably represents the heat stored in the ground due to Summer heating. The position of the bulge indicates that the median gradient in temperature for this monitoring period is downward from about 10 to 20 ft and upward from about 10 ft.

The plots of water potential versus time for given depths (Figures 3-16 and 3-18) demonstrate that water potentials are subject to diurnal variations of about ±1 bar per day, and that there was little, if any, change in the average

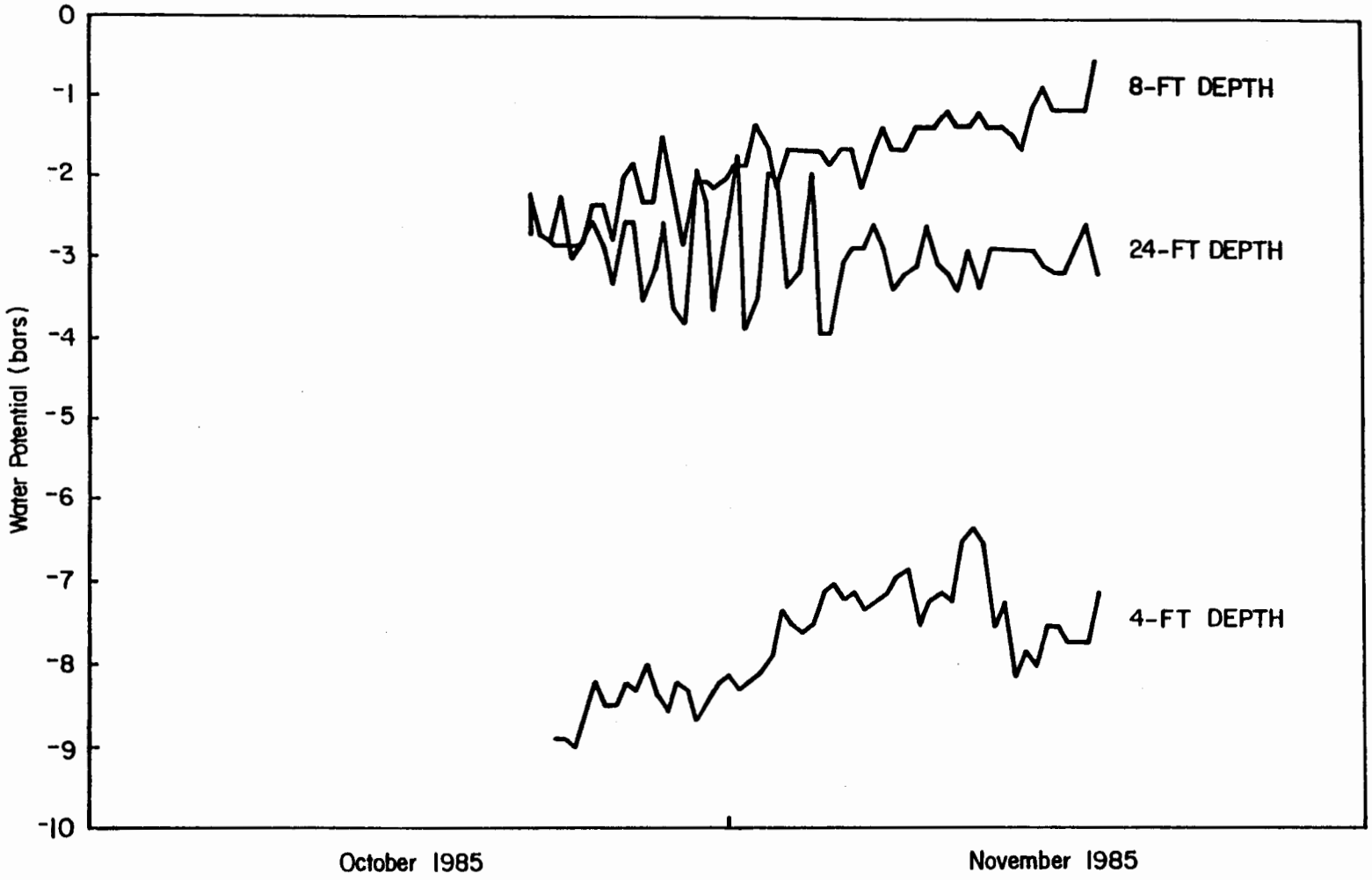

Figure 3-16. Water Potential Versus Time for Selected Psychrometers in Hole LLP-85-03

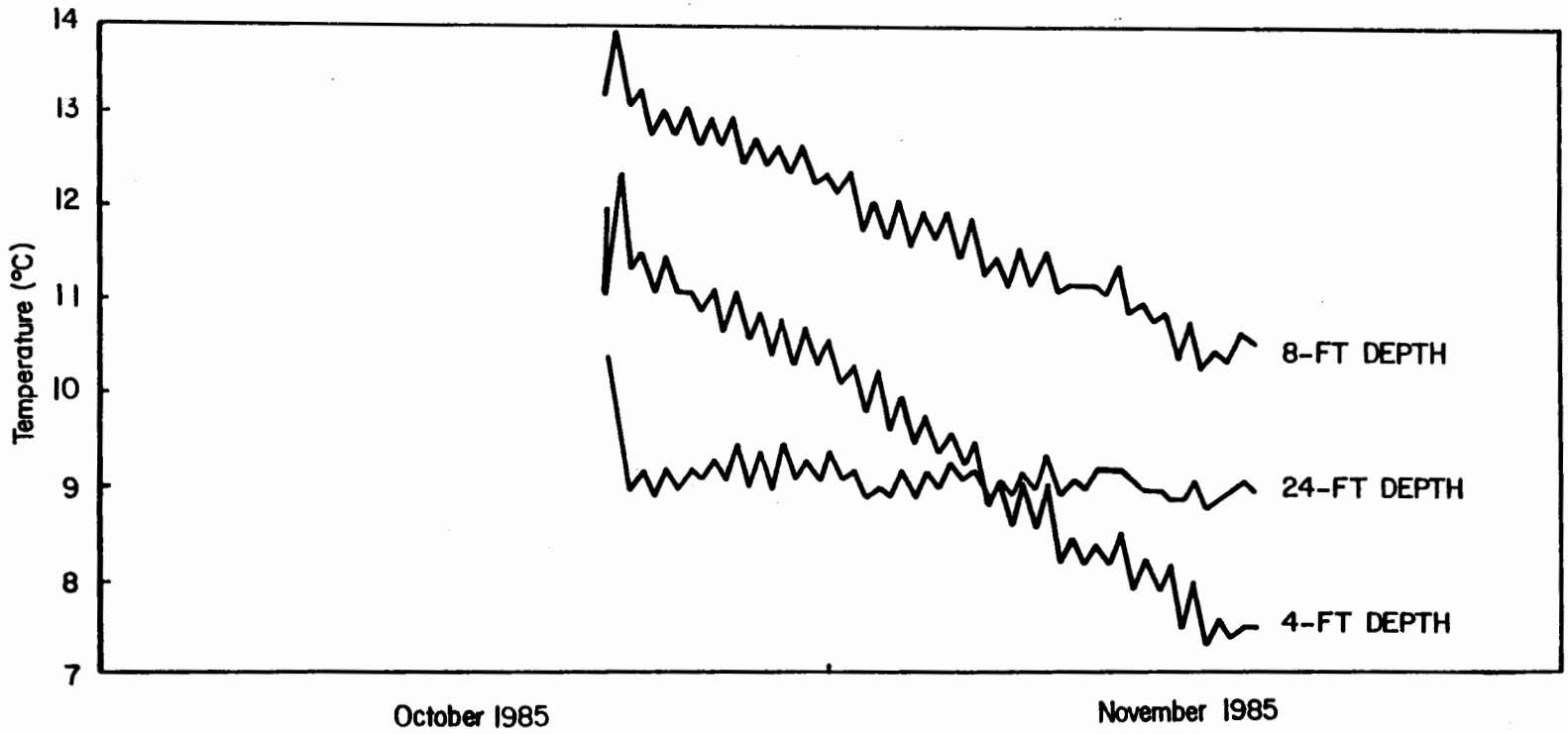

Figure 3-17. Temperature Versus Time for Selected Psychrometers in Hole LLP-85-03

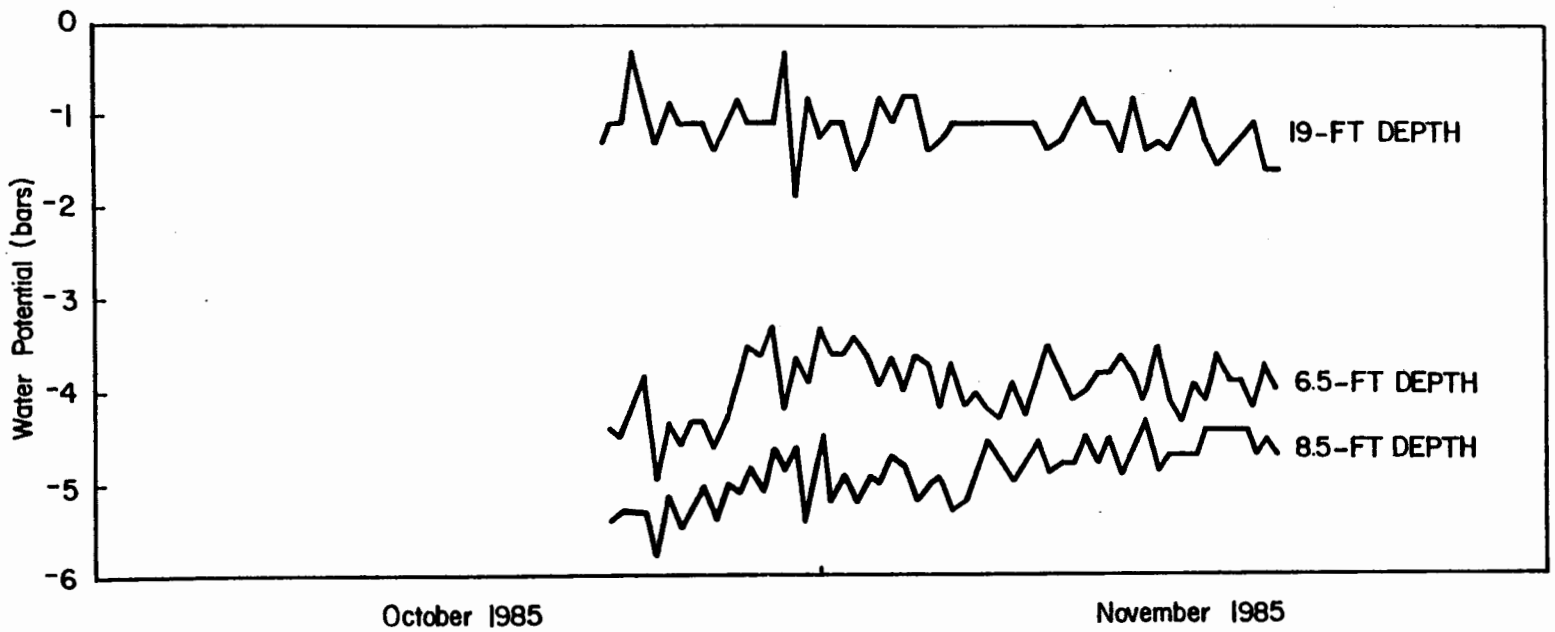

Figure 3-18. Water Potential Versus Time for Selected Psychrometers in Hole LGP-85-07

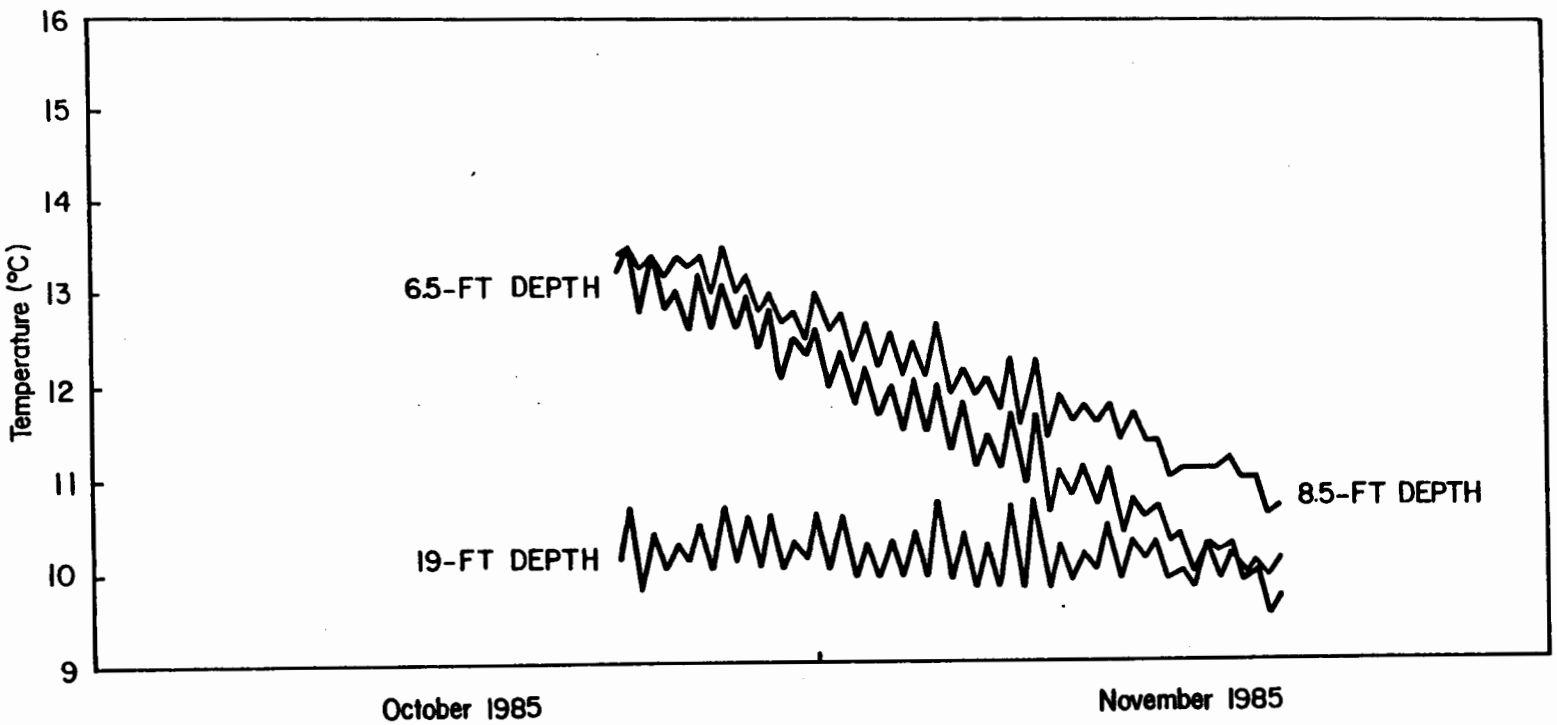

Figure 3-19. Temperature Versus Time for Selected Psychrometers in Hole LGP-85-07

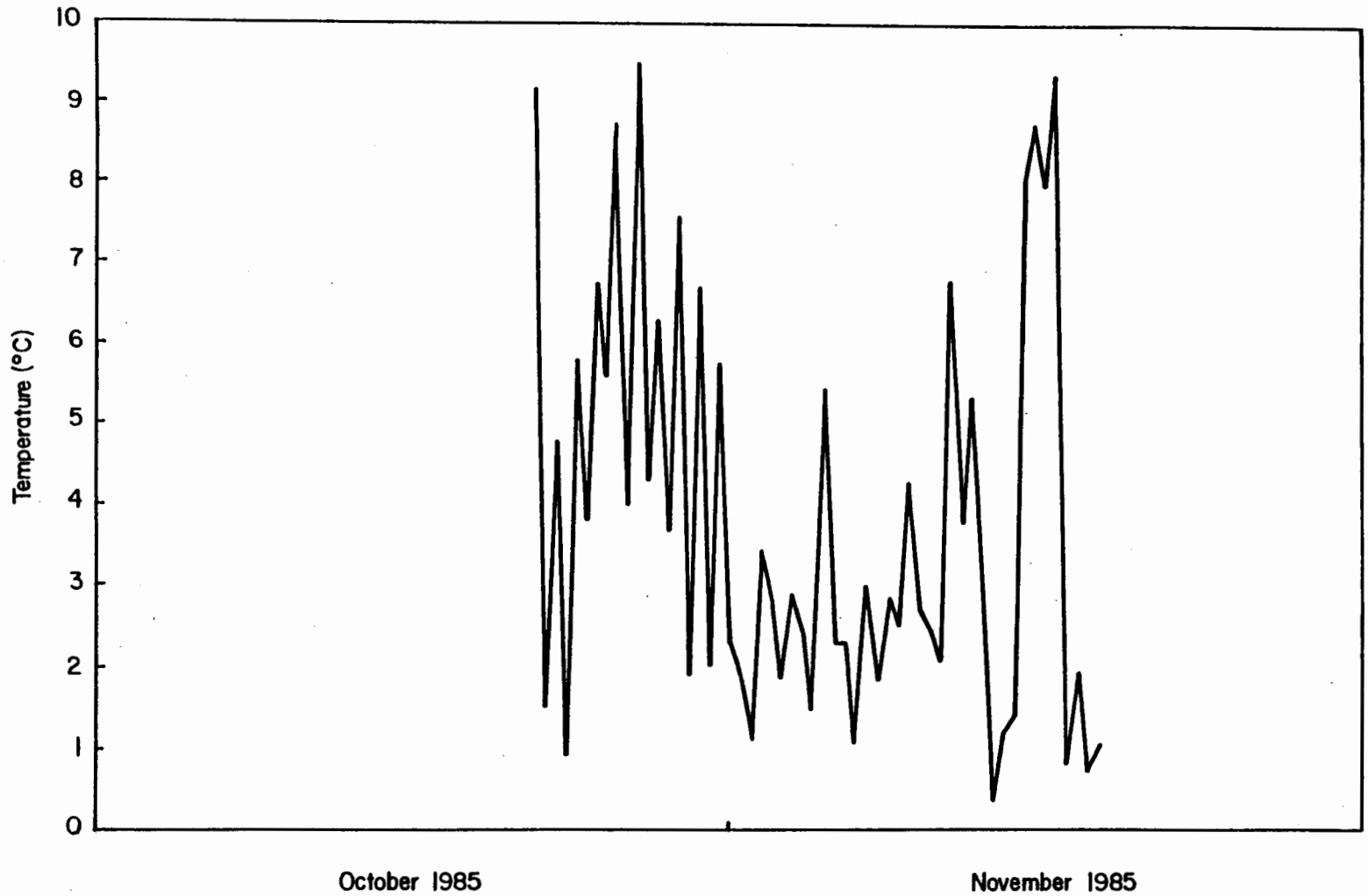

Figure 3-20. Air Temperature Versus Time at Hole LLP-85-03

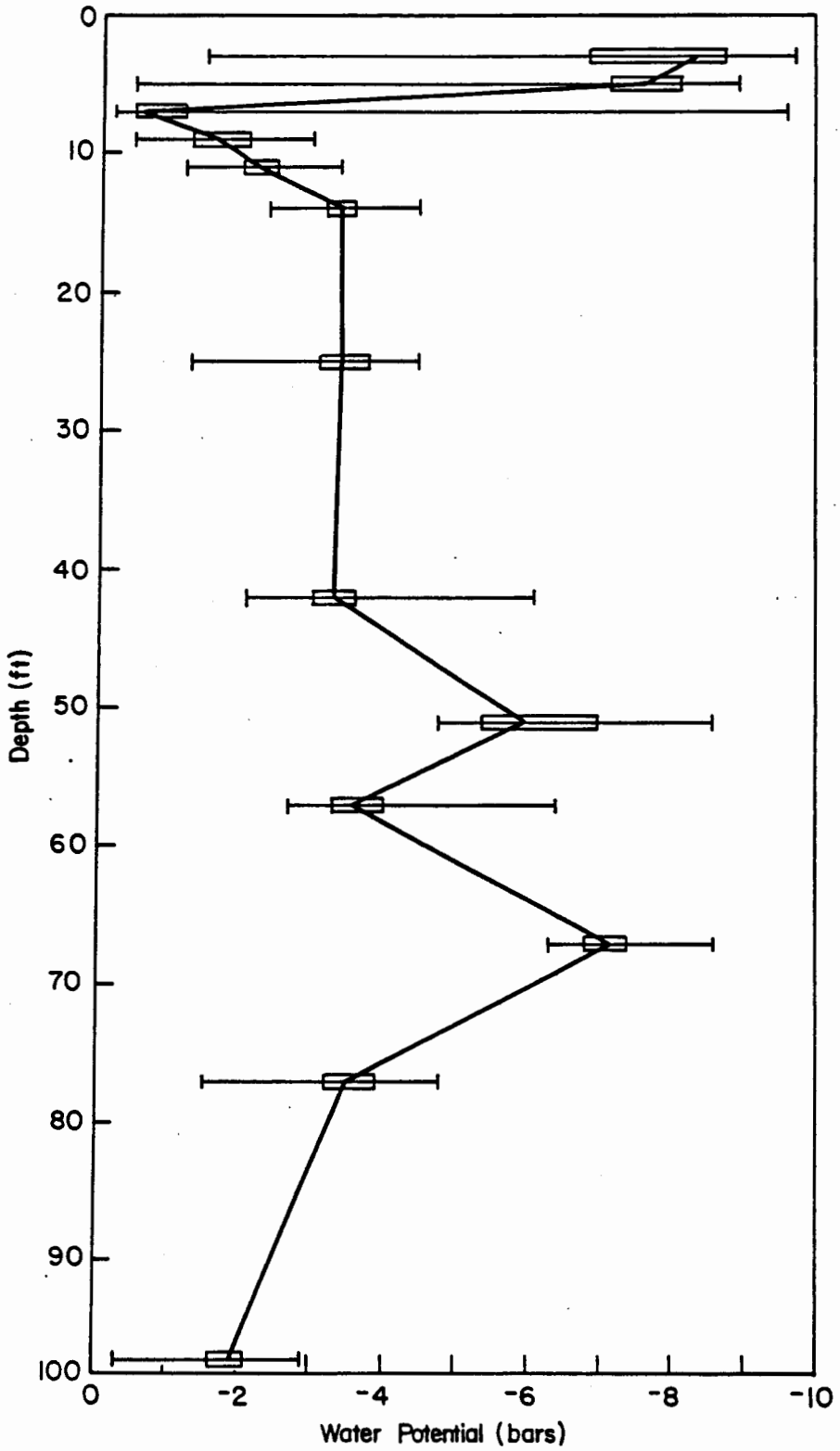

Figure 3-21. Water Potential Versus Depth for Hole LLP-85-03

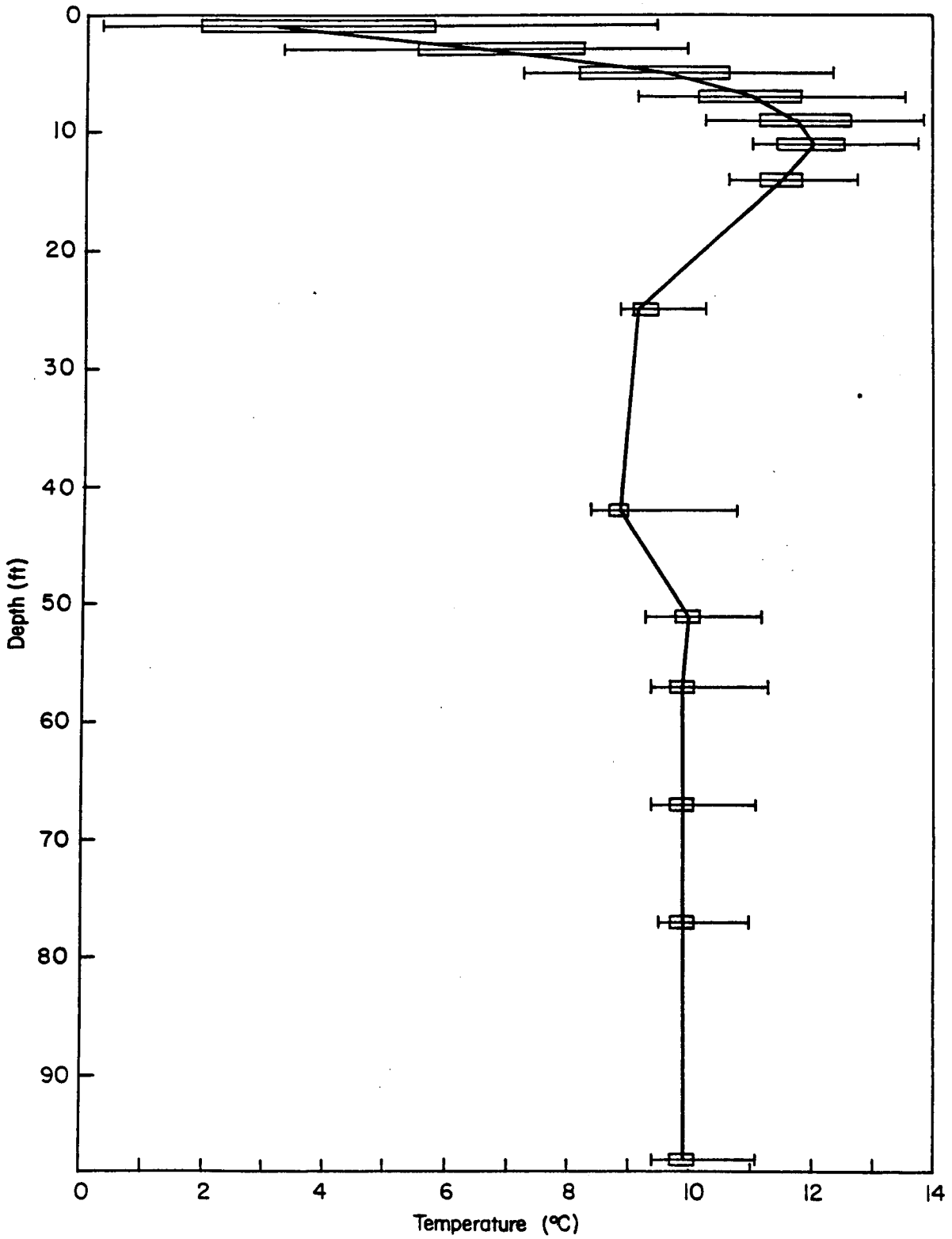

Figure 3-22. Temperature Versus Depth for Hole LLP-85-03

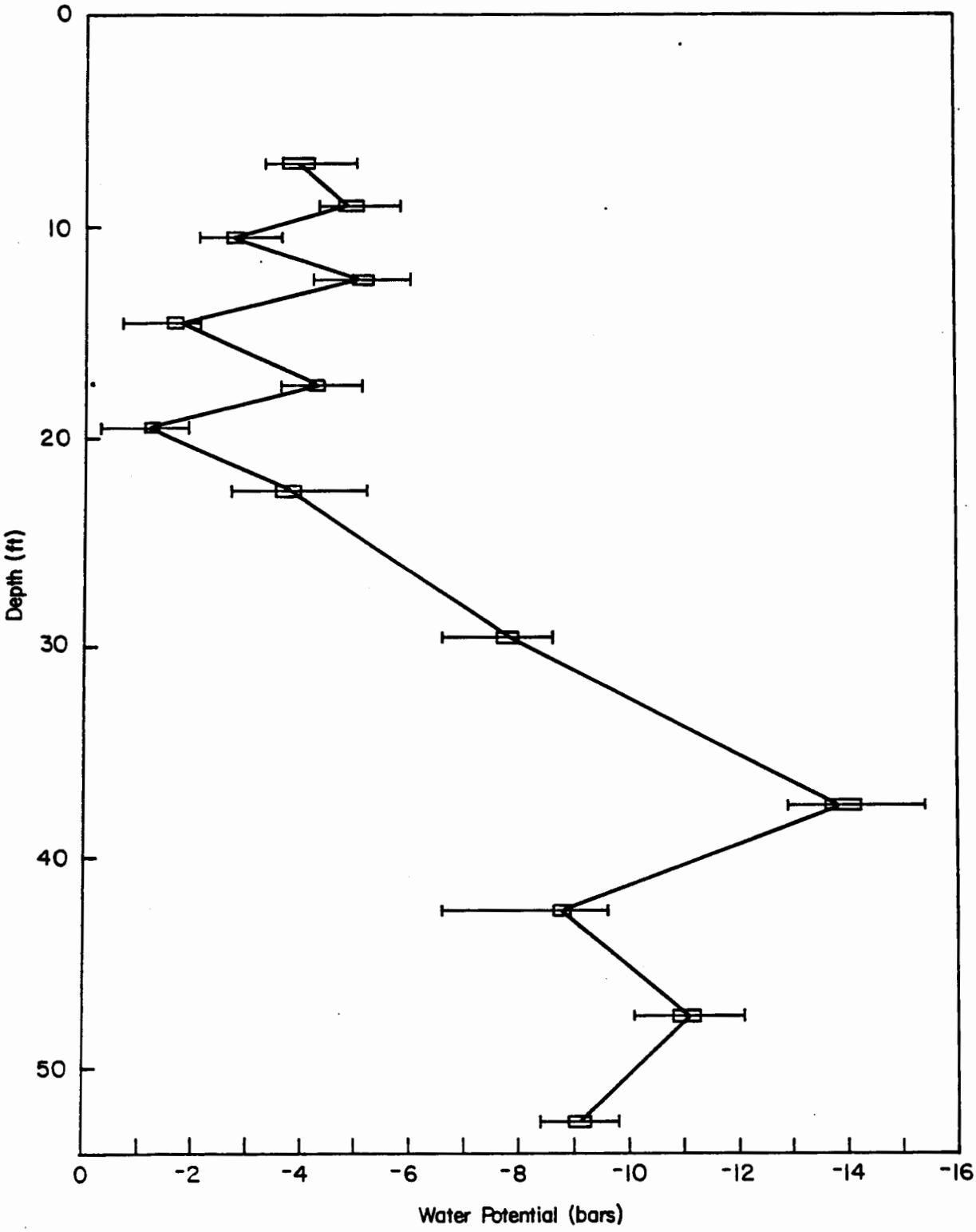

Figure 3-23. Water Potential Versus Depth for Hole LGP-85-07

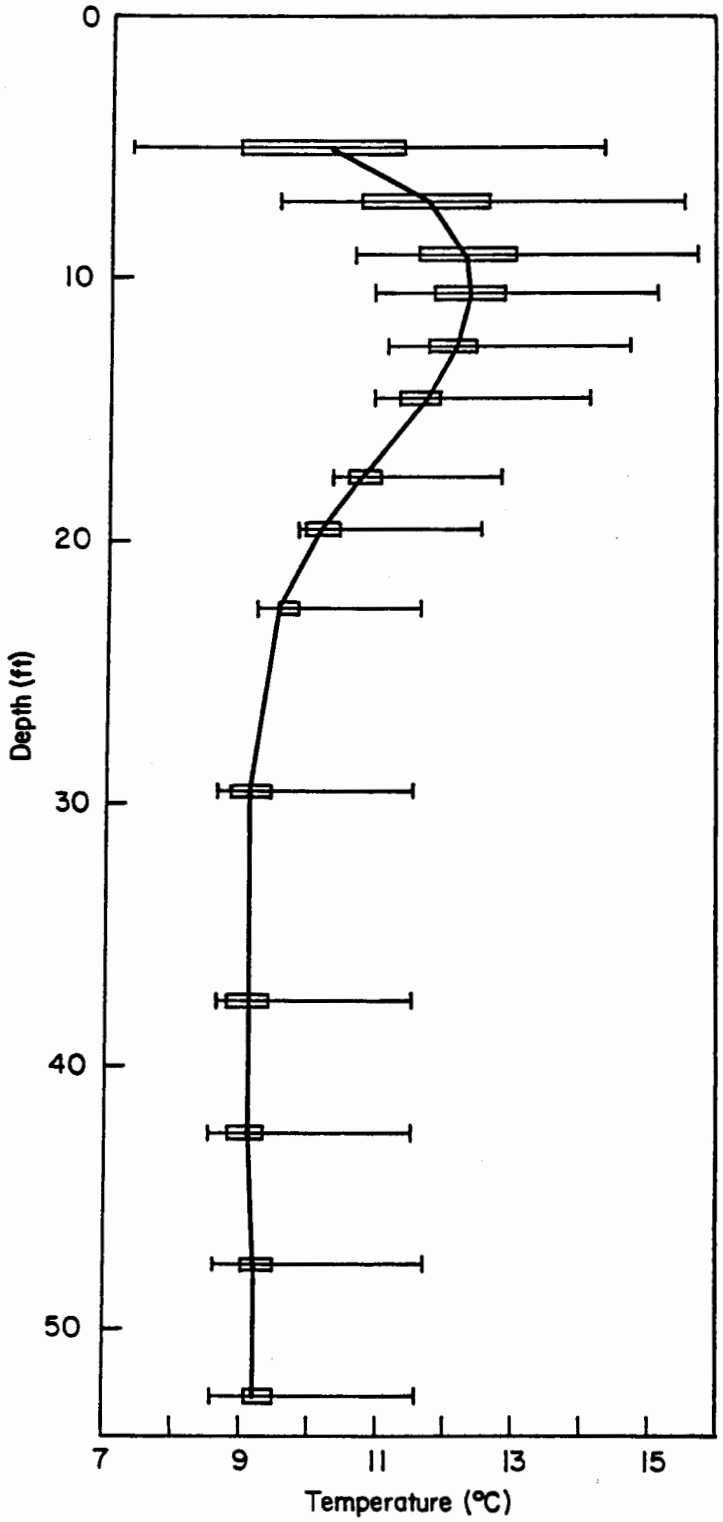

Figure 3-24. Temperature Versus Depth for Hole LGP-85-07

water potential during this monitoring period. Median water potentials range from approximately -0.5 bar to -8.7 bar in Hole LLP-85-03 (Figure 3-21) and from approximately -1.2 bar to -13.8 bar in Hole LGP-85-07 (Figure 3-23).

The large range of maximum and minimum values observed during this monitoring period limit gradient estimations to those that can be measured between successive psychrometers, i.e., within a single depth interval. Accurate assessments of an overall gradient in the study area will most likely require longer equilibration and monitoring times.

3.3.2 ATMOSPHERIC/ROCK-PORE PRESSURE MONITORING SYSTEM

3.3.2.1 Purpose and Scope

The purpose for installing the Atmospheric/Rock-Pore Pressure Monitoring System was to quantify the gas-pressure gradients in the Bandelier Tuff. Although these data were not required by the Compliance Order/Schedule, they can contribute significantly to the initial site assessment since differences in gas pressure can affect contaminant transport in the vapor phase.

Equipment and system installation are described in the paragraphs that follow. The subsection entitled Results and Discussion presents only a preliminary interpretation of the data; a broader, more reliable assessment of gas-pressure gradients would most likely require acquisition of pressure readings over a period of at least 1 year.

3.3.2.2 Equipment

The pressure-measurement system installed at Los Alamos consists of four electrical pressure transducers connected to an electro-piezo scanner/recorder. The transducers contain an absolute-electrical-pressure sensor equipped with a strain-gauged stainless steel diaphragm. A stainless steel disc filter permits direct burial of the transducers. Measurement capacity ranges from 0 to 25 pounds per square inch at sea level (psis), with a readability of 0.02 percent of scale. (Psis is calibrated in psi with zero being atmospheric pressure at sea level.)

The electro-piezo scanner/recorder is a portable, battery-operated system that automatically records ten transducer channels. The dates, times, and outputs from each of the transducers are recorded on the integral printer. This versatile scanner/recorder can permanently record the transducer outputs, or can provide the outputs to an external device such as a computer, data terminal, paper punch, or magnetic tape recorder. The pressure-measurement system can be programmed to scan continuously or to scan at variable intervals. In the case of the latter, the recorder can be sealed and left unattended and will still record data at the preselected intervals.

3.3.2.3 Installation Design

The completion diagram for the pressure-transducer instrumentation installed in Hole LLP-85-03 is presented in Appendix A. The four transducers were installed at the following depths: ground surface, 26 ft, 54 ft (near a fracture), and 90 ft. The transducer located at ground surface measures the

atmospheric pressure, while the buried transducers measure rock-pore gas pressures.

3.3.2.4 Results and Discussion

Pressure-measurement data were collected over the period 17 October through 15 November 1985 (Figure 3-25), except for the 7 days from 6 through 12 November when the system was inadvertently shut down. As noted previously, these limited data permit only a preliminary interpretation at this time. Characteristics which are discernible in Figure 3-25 include the following:

- Both the atmospheric and rock-pore pressures undergo daily fluctuations.
- The rock-pore pressure at 54 ft is consistently higher than the surrounding pressures, potentially a result of the nearby fracture.
- An increase in the atmospheric pressure for a period of several days is not reflected in the rock-pore pressures for the same period.

A broader assessment of the gas-pressure gradients in the study area requires acquisition of additional data, particularly with regard to identifying potential sources of variation in the data other than actual pressure variations.

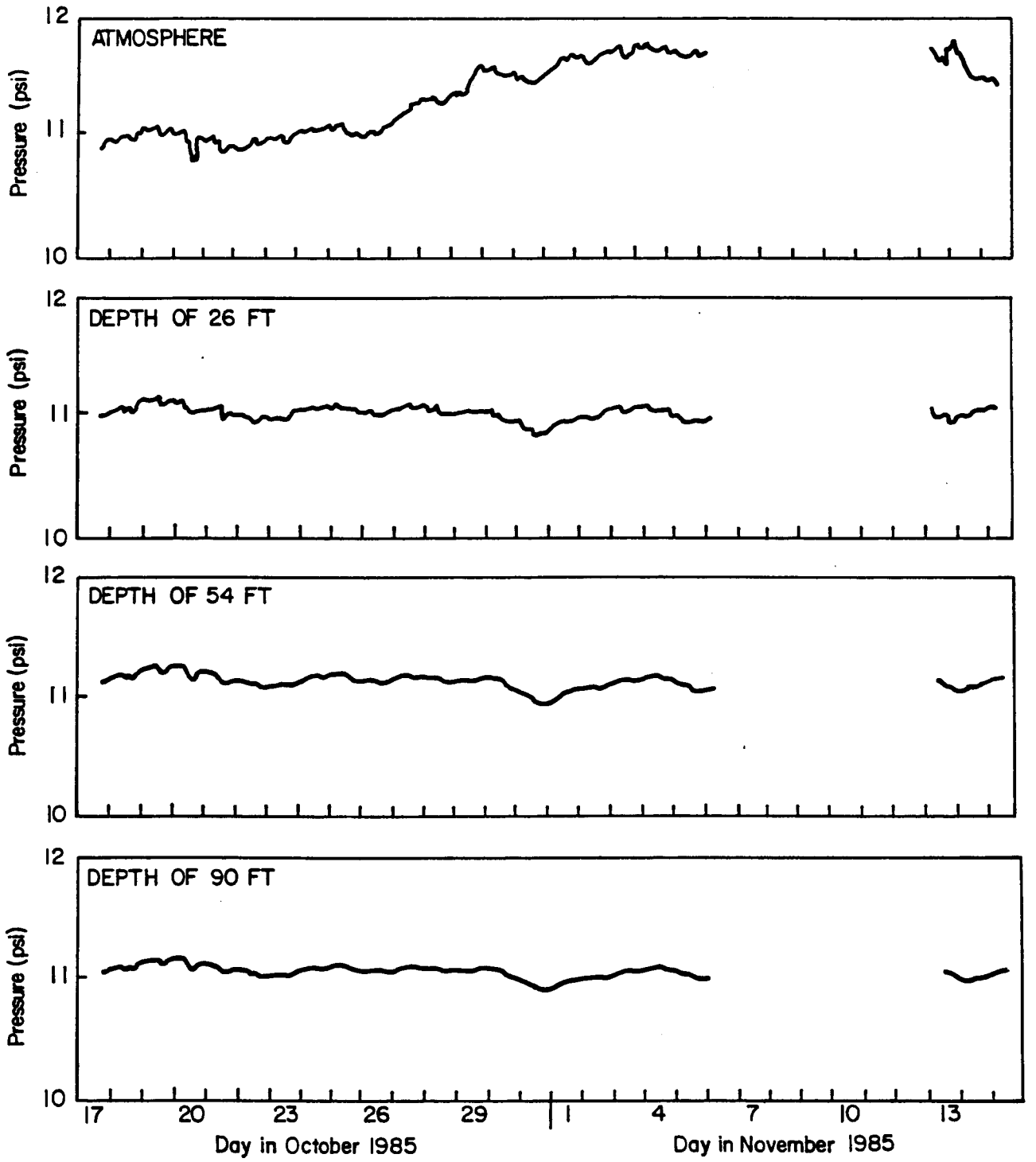

Figure 3-25. Results from the Pressure Transducers Installed in Hole LLP-85-03 (Note: The system was inadvertently shut down over the period 6-12 November 1985.)

Section 4

NEUTRON MOISTURE MEASUREMENTS

Note: This section responds to Task 4, Paragraph 25, of the Compliance Order/Schedule. The section was prepared by personnel of Los Alamos National Laboratory.

4.1 PURPOSE AND SCOPE

The moisture content of the Bandelier Tuff is being measured with a neutron probe in order to characterize the infiltration and redistribution of water in the tuff. Use of the neutron probe for moisture monitoring was specifically requested by the State of New Mexico in Task 4, Paragraph 25, of the Compliance Order/Schedule. Although data acquired with the probe were not yet available at the time of this writing, it is possible that the method will be of little value at Los Alamos due to the low moisture content of the tuff (see gravimetric moisture results in Section 3.1.1).

Two holes were identified for acquisition of biweekly neutron moisture readings, LLN-85-04 and LGN-85-08 (see Figure 2-3 for locations). Descriptions of the casing installations, probe calibration, and monitoring program are provided below. Data presentation and interpretation will be addressed in a subsequent report when data become available.

4.2 CASING INSTALLATIONS

The neutron access tubes, or casings, were constructed of cold drawn aluminum tubes, each 12 ft in length and having a wall thickness of 0.049 inch, an outside diameter of 2.5 inches, and an inside diameter of 2.402 inches. This inside diameter is approximately 0.25 inch larger than the outside diameter of the probe (1.865 inches), which prevents the probe from binding as it is maneuvered inside the casing. To further ensure free movement of the probe while it is being raised or lowered in the hole, the casing has no internal seams or obstructions.

Prior to transport to the field, the 12-ft lengths of tubing were welded together to make 24-ft sections and the sections pressure-tested to ensure a watertight seal. A cap was welded to one end of each of two sections, these to be installed at the bottom of the two holes. In the field, the 24-ft sections were joined together using 'no-hub' couplings rather than welding. This was done because the tubing wall is so thin that a watertight weld would be nearly impossible to accomplish with portable welding equipment. A no-hub coupling is a watertight rubber coupling, held in place by a corrugated stainless steel cover, on the ends of which are stainless steel hose clamps used for gripping the aluminum tubing.

The casings were installed in the drill holes in the following manner. The section with the bottom cap was lowered into the hole and held in place with a pipe vise. A second 24-ft section was joined to the first with a no-hub coupling. Silicon sealant was applied wherever rubber was exposed to slow decomposition of the material underground. Once the two sections were coupled, they were lowered into the ground and again held in place with the pipe vise while a second no-hub coupling was installed to join the now 48-ft section of tubing to another 12- or 24-ft section. This process was repeated until the bottom of the hole was reached. Any tubing remaining above ground level was cut off.

A diagram of the casing installation for Hole LLN-85-04 is presented in Figure 4-1. The depth of the uncased hole was 108 ft, so the casing required four 24-ft sections and one 12-ft section, joined together with four no-hub

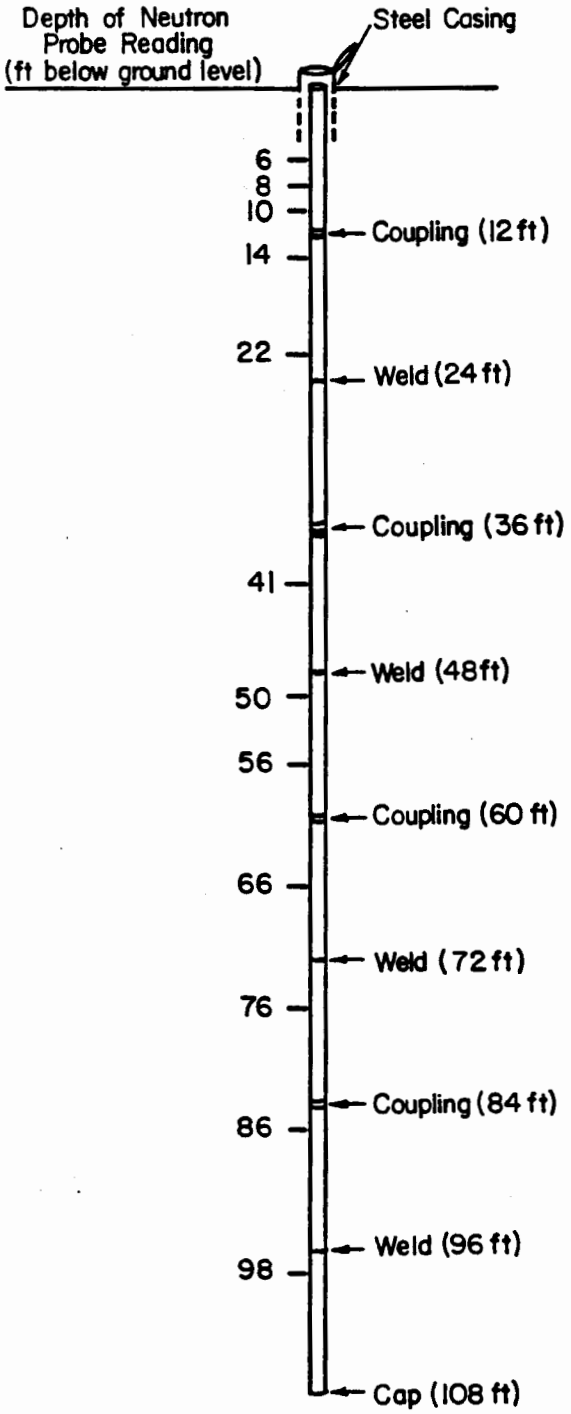

Figure 4-1. Casing Installation and Depths of Neutron Probe Measurements in Hole LLN-85-04

couplings. Hole LGN-85-08 (Figure 4-2) had an uncased depth of 50 ft, so the casing required two 24-ft sections and one 12-ft section, joined together with two no-hub couplings.

4.3 CALIBRATION OF THE NEUTRON PROBE

The neutron probe used at Los Alamos is a Campbell Pacific moisture gauge. Calibration of the instrument was accomplished by using it to measure moisture in five samples of Bandelier Tuff, each with a different but known moisture content. Instrument responses were recorded and used to generate a calibration curve.

The five samples of tuff consisted of three with varying moisture contents, one with no moisture, and one representing saturated conditions. The first three were prepared in the following manner. Crushed Bandelier Tuff was oven-dried at 250°C for 48 hours. A predetermined amount of dry tuff was then weighed and water added to it. The moistened tuff was packed in 15-cm lifts in a 55-gallon drum to achieve a bulk density of 1.5 g/cm^3, which is the average bulk density of the consolidated Bandelier Tuff at Los Alamos. The amounts of water added to the lifts varied from one drum to another, such that the volumetric water content of each drum was different. Samples were collected from each lift in each drum and analyzed gravimetrically to determine the moisture content and to ensure that the moisture content was constant throughout the entire drum.

The fourth drum was prepared in the same way as the first three except that no water was added. The fifth drum was also prepared as described above, except that water was added not to the lifts, but into the bottom of the drum through a 3/8-inch Tygon tube until the tuff was saturated to the drum surface. Samples from these drums were also analyzed so that the moisture contents would be known. Following preparation, all five drums were sealed by placing plastic sheeting between the drum surface and the cover. Silicon sealant was then applied on the edges to prevent evaporation.

Calibration measurements were taken by lowering the probe to the center of each drum and acquiring four 1-minute counts. These data and the known moisture contents were then subjected to a linear-regression analysis, which yields a calibration curve for the instrument. At the time of this writing, the calibration curve was not complete and is therefore not included in this report.

4.4 MONITORING PROGRAM

Biweekly neutron-moisture measurements were initiated in both drill holes on 17 December 1985. The depths of the probe readings are shown in Figures 4-1 and 4-2. The measurement depths in Hole LLN-85-04 correspond to the psychrometer-measurement depths in Hole LLP-85-03, while those in Hole LGN-85-08 correspond to psychrometers in Hole LGP-85-07 (see Appendix A for completion diagrams of Holes LLP-85-03 and LGP-85-07). In certain cases, identical correspondence was not possible due to the presence of the welds and couplings in the neutron-probe holes. As noted previously, no data are available at this time.

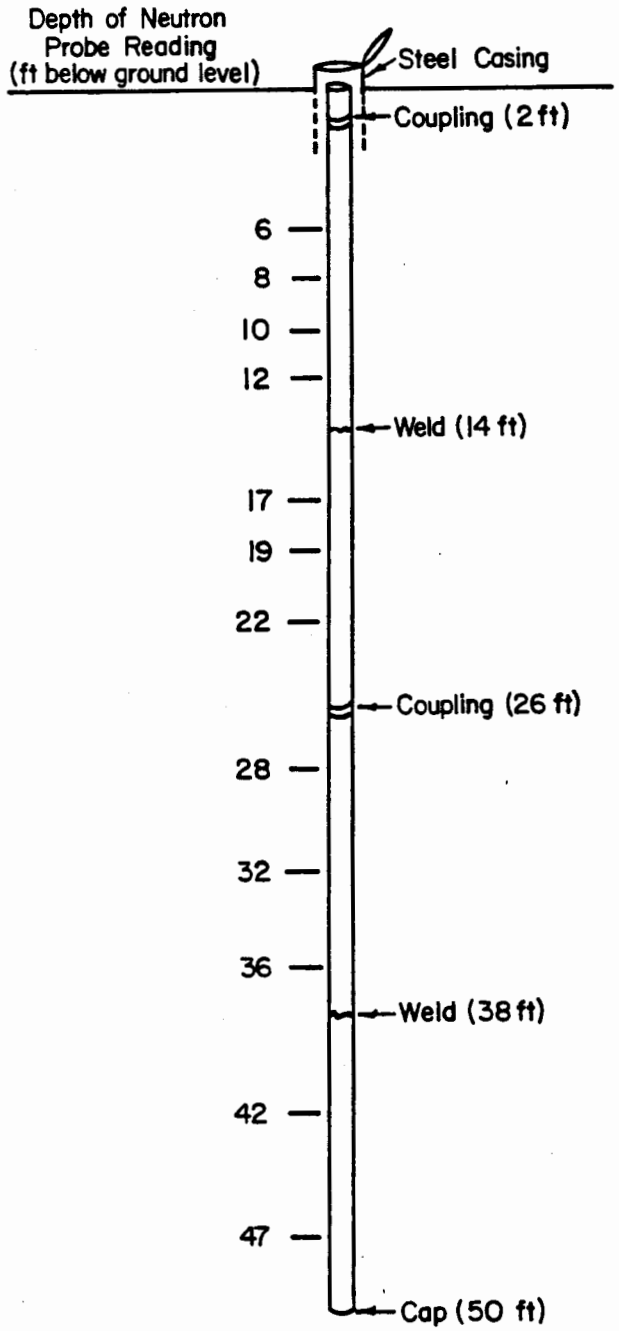

Figure 4-2. Casing Installation and Depths of Neutron Probe Measurements in Hole LGN-85-08

Section 5

PORE-GAS SAMPLING SYSTEM

Note: This section responds to Task 5, Paragraph 25, of the Compliance Order/Schedule.

5.1 PURPOSE AND SCOPE

Samples of pore gas from 14 drill holes are being collected and analyzed in order to characterize the subsurface atmosphere in Areas G and L. The design and installation of the samplers are described in this section; included is a hole-by-hole description of the sampling-port locations and the rationale for choosing each location. At the time of this writing, laboratory analysis of the samples collected to date were not available. Data presentation and interpretation will therefore not be addressed in this report.

5.2 DESIGN

Two pore-gas sampling port designs were implemented for this study. The first design was utilized during the installations completed during Summer 1985, while the second design was used during the installation completed during Fall 1986. During Summer 1985, the pore-gas sampling ports were constructed using low-pressure mobile-phase filters which were welded to standard 2-inch-I.D. galvanized pipe (Bendix Field Engineering Corporation, 1985b). The filters consist of 2-micrometer, porous, stainless steel elements; uphole access is provided via connection to 1/4-inch stainless steel tubing and stainless steel compression fittings. A diagram of a pore-gas sampling port is presented in Figure 5-1. During Summer 1986, the pore-gas samplers were simply assembled by connecting the mobile-phase filters to 1/4-inch stainless steel tubing with stainless steel compression fittings. No elbows were used. Consequently, the sampling port and line assembly were built for installation without the galvanized pipe used in Summer 1985.

5.3 INSTALLATION

In Summer 1986, 70 pore-gas sampling ports were installed in seven 200-ft-deep boreholes. The borehole locations were cited based upon the Petrex Survey (Section 6) results. As requested by Los Alamos National Laboratory, the sampling ports were installed at 20-ft intervals to a depth of 200 ft. A total of 10 sampling ports were placed into each hole. Installation diagrams are presented in Appendix A; drill hole locations are shown in Figure 2-3. In Summer 1985, a total of 23 sampling ports were installed in seven drill holes in the study area; installation procedures were described in the second report (Bendix Field Engineering Corporation, 1985b). Installation diagrams are presented in Appendix A; drill-hole locations are shown in Figure 2-3. The following paragraphs describe the locations of the ports within each hole and the rationale for choosing these locations.

- Hole LGC-85-09. Since this was the only pore-gas sampling hole that penetrated Unit 1a, two ports were installed in that unit, one in the relatively moist section (below 88 ft) and the other in the relatively dry section, just above 80 ft. The third port was installed at about 63 ft to coincide with a fracture present in Unit 1b, and because the maximum waste-disposal depth in this area is approximately 60 ft. The fourth port was installed at 37 ft to coincide with fractures present in Unit 2a.

- Hole LGC-85-10. The deepest sampling port was installed at 95 ft to coincide with a near-vertical fracture present in the more densely welded

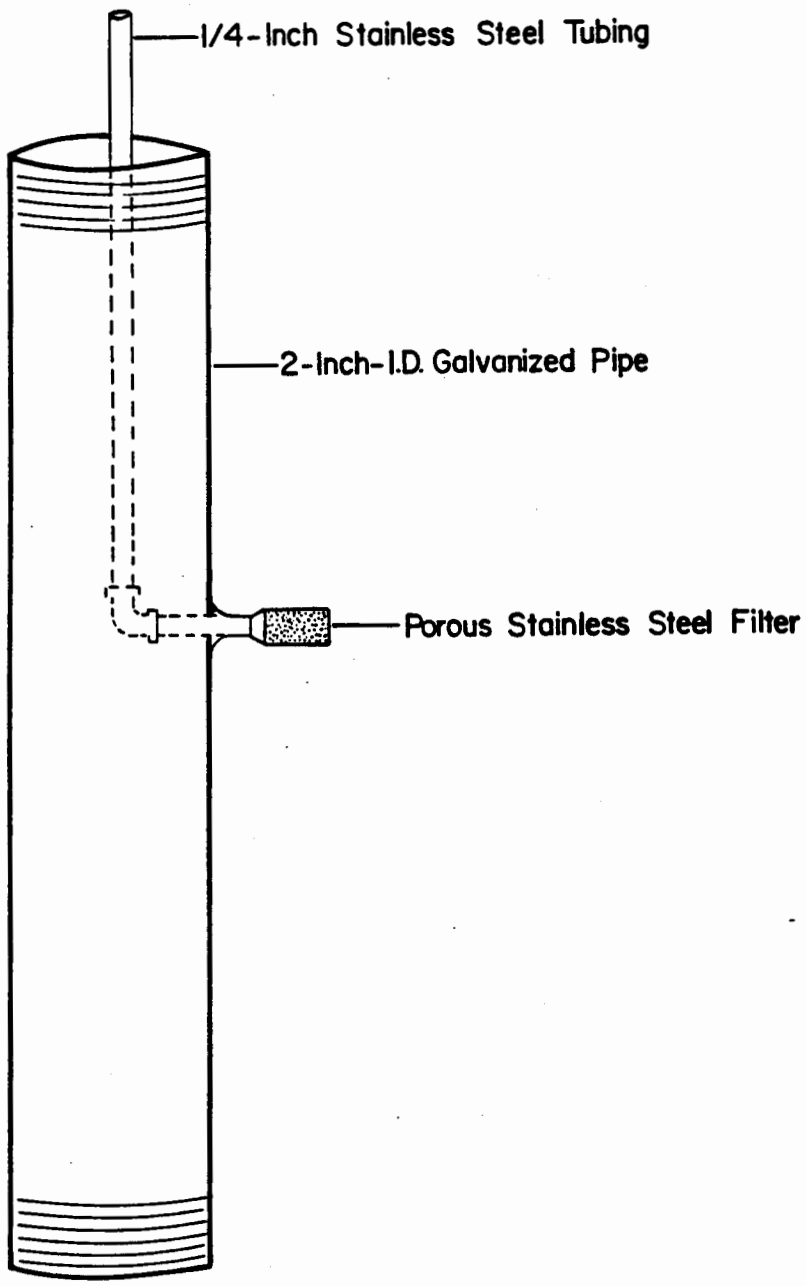

Figure 5-1. Diagram of a Pore-Gas Sampling Port

portion of Unit 1b. The middle port was installed at about 53 ft to coincide with a fracture present in Unit 2a. The uppermost port was installed at 31 ft to coincide with a horizontal fracture and the Unit 2a/Unit 2b contact.

- Hole LLC-85-12. The deepest sampling port was installed at about 41 ft to coincide with a vertical fracture and the Unit 2a/Unit 2b contact. The middle port was installed at about 27 ft to sample the interval between 24 and 29 ft. This interval lies within Unit 2b and consists of a light-gray ash flow with numerous horizontal fractures. In addition, the Organic Vapor Meter (OVM) registered high readings [114 parts per million (ppm) downhole] when the bottom of the auger string reached 24 ft, and again when the bottom of the string reached 29 ft (160 ppm). The uppermost gas-sampling port was installed at about 6 ft to coincide with several fractures present from 5 ft to 8 ft.

- Hole LLC-85-13. This is a 'background' hole located west of Area L. Only Units 2a and 2b were penetrated in this hole. The deepest sampling port was installed at about 65 ft in a moderately welded portion of Unit 2a. The middle port was installed at about 43 ft to coincide with several fractures and the Unit 2a/Unit 2b contact. The uppermost port was installed at about 21 ft to coincide with a near-vertical fracture present in Unit 2b.

- Hole LLC-85-14. The deepest sampling port was installed at about 86 ft to coincide with a fracture zone extending from 84 to 89 ft within Unit 1b. A relatively high OVM reading was recorded for this zone, which is separated from upper zones with high OVM readings by a zone of 'background' OVM readings. The second port was installed at about 46 ft to coincide with a nonfracture zone extending from 44 to 49 ft in Unit 2a where relatively high OVM readings were obtained. The third port was installed at about 31 ft to coincide with the interval 28 to 34 ft because the contact between two physically different zones of Unit 2b is present at 32 ft and field OVM readings were higher when crossing this interval. The contact is defined primarily by the transition into slightly welded or more easily drilled ash-flow tuff. Fractures are also present just above this contact. The uppermost sampling port was installed at about 13 ft to coincide with a moderately welded, nonfracture zone within Unit 2b. This zone, extending from 12 to 14 ft, exhibited relatively high OVM readings. In addition, sampling in this zone would permit comparison with results from known fracture zones.

- Hole LLC-85-15. The deepest port was installed at about 82 ft to sample pore gas in the interval 80 to 86 ft because a relatively high OVM reading was obtained near this interval. The other two sampling ports were installed at about 32 ft and 19 ft to coincide with the areas where the highest OVM readings were obtained in this hole.

- Hole LLC-85-16. The deepest sampling port was installed near the bottom of this hole to coincide with areas exhibiting high OVM readings. These areas are separated from the zones of additional high readings by 75 ft of relatively low OVM readings. The other two ports were installed near ground surface to coincide with zones that are both fractured and displayed relatively high OVM readings.

Section 6

PETREX SURVEY

6.1 PURPOSE AND SCOPE

A Petrex survey, utilizing the K-V Fingerprint Technique, was conducted at Waste Disposal Area L as a screening tool to guide the placement of additional pore-gas sampling wells. The survey was also used to qualitatively define the extent of migration of volatile organic compounds away from waste-disposal shafts and trenches. The K-V Fingerprint Technique, marketed by Petrex, Golden, Colorado, permits passive or static gas sampling and analysis of the soil to identify organic compounds and determine the relative number of ions sorbed onto the sampling element per unit time. The ion counts per unit time represent a relative flux of ions venting to the ground surface. The volatile organic compounds studied were trichloroethylene (TCE), tetrachloroethylene (PCE), benzene, and toluene.

6.2 SAMPLING AND ANALYSIS

The sampling device used in the Petrex survey consists of a 0.02-inch-diameter by 4-inch-long wire filament, which is coated with a monolayer of charcoal and inserted in a glass tube. The tube is then placed in a 12- to 14-inch deep hole and covered with soil. The sampling tube remains in the ground for a sufficient period to expose the filament, and is then removed. For this investigation, a period of 10 days was used. The volatile organic compounds sorbed onto the charcoal filament from the soil atmosphere are purged in a pyrolyzer, using the filament as a heat source. The volatilized compounds are then passed to a mass spectrometer for analysis.

A total of 101 samplers were installed at a 30-foot grid in and around Waste Disposal Area L. The sampler spacing was selected to be broad enough to provide information on the lateral extent of the plume and narrow enough to contour the ion-count data. The designated spacing interval of the samplers was also chosen to be close enough to determine the orientation of any plumes.

Natural background measurements were also performed to provide a perspective from which to analyze the sampling results. The natural background was determined by placing an array of five samplers at 30-foot intervals along a northerly projection away from background Hole LLC-85-13 (see Figure 2-3). The background samplers were removed from the soil 10 days after emplacement.

6.3 RESULTS

Four maps were constructed to show the relative vapor ion counts emanating from Waste Disposal Area L. Figures 6-1 through 6-4 show results of the Petrex survey for the organic compounds trichloroethylene, tetrachloroethylene, benzene, and toluene, respectively.

The toluene ion counts were the highest of the compounds surveyed. Toluene ion counts exceed 60,000 at a number of locations, and more than 90,000 at one location at the east-central margin of the survey grid. The counts for benzene were the next highest, although they were much lower than the counts

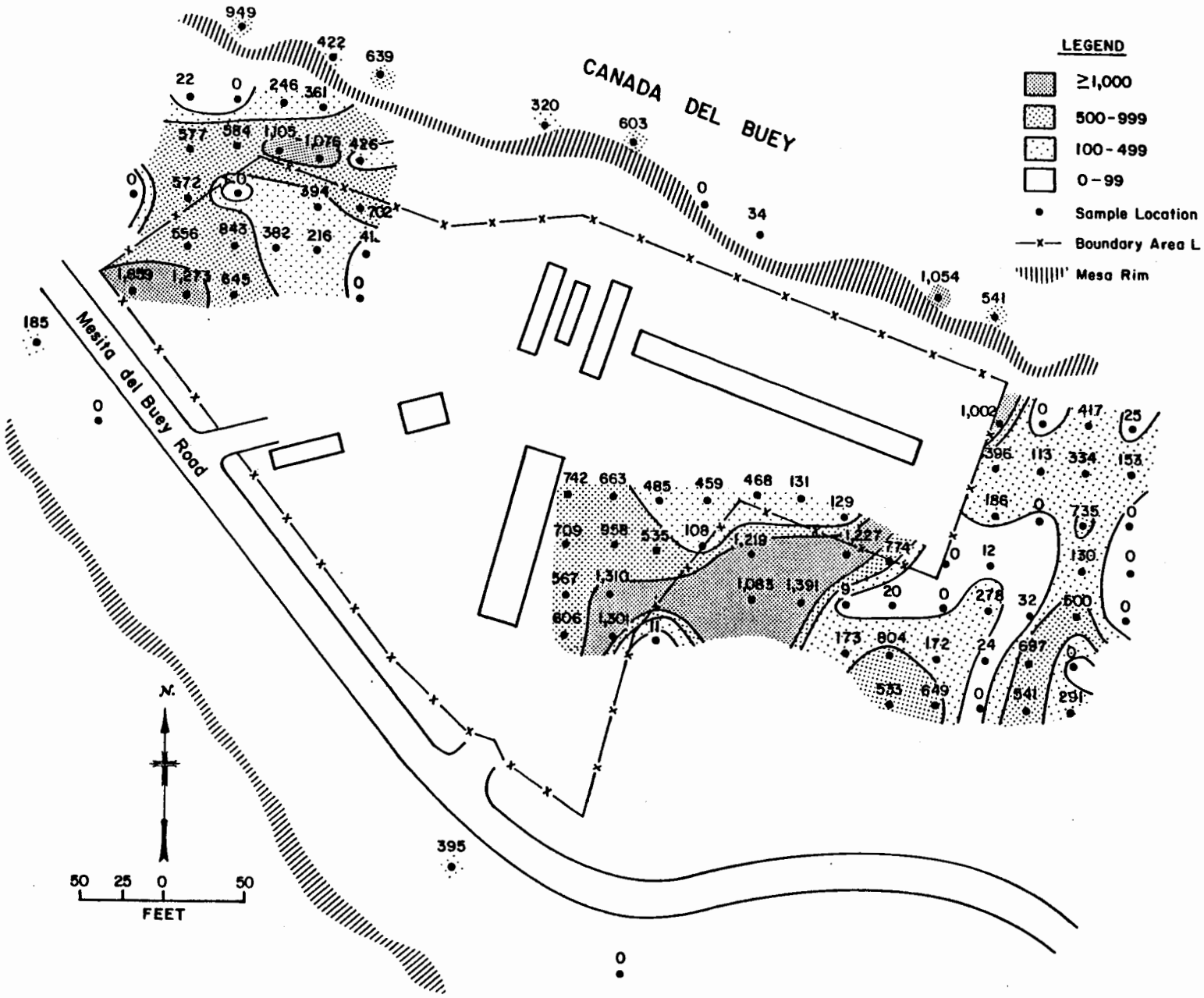

Figure 6-1. Normalized Trichloroethylene Ion-Count Map, Waste Disposal Area L, Los Alamos National Laboratory, New Mexico

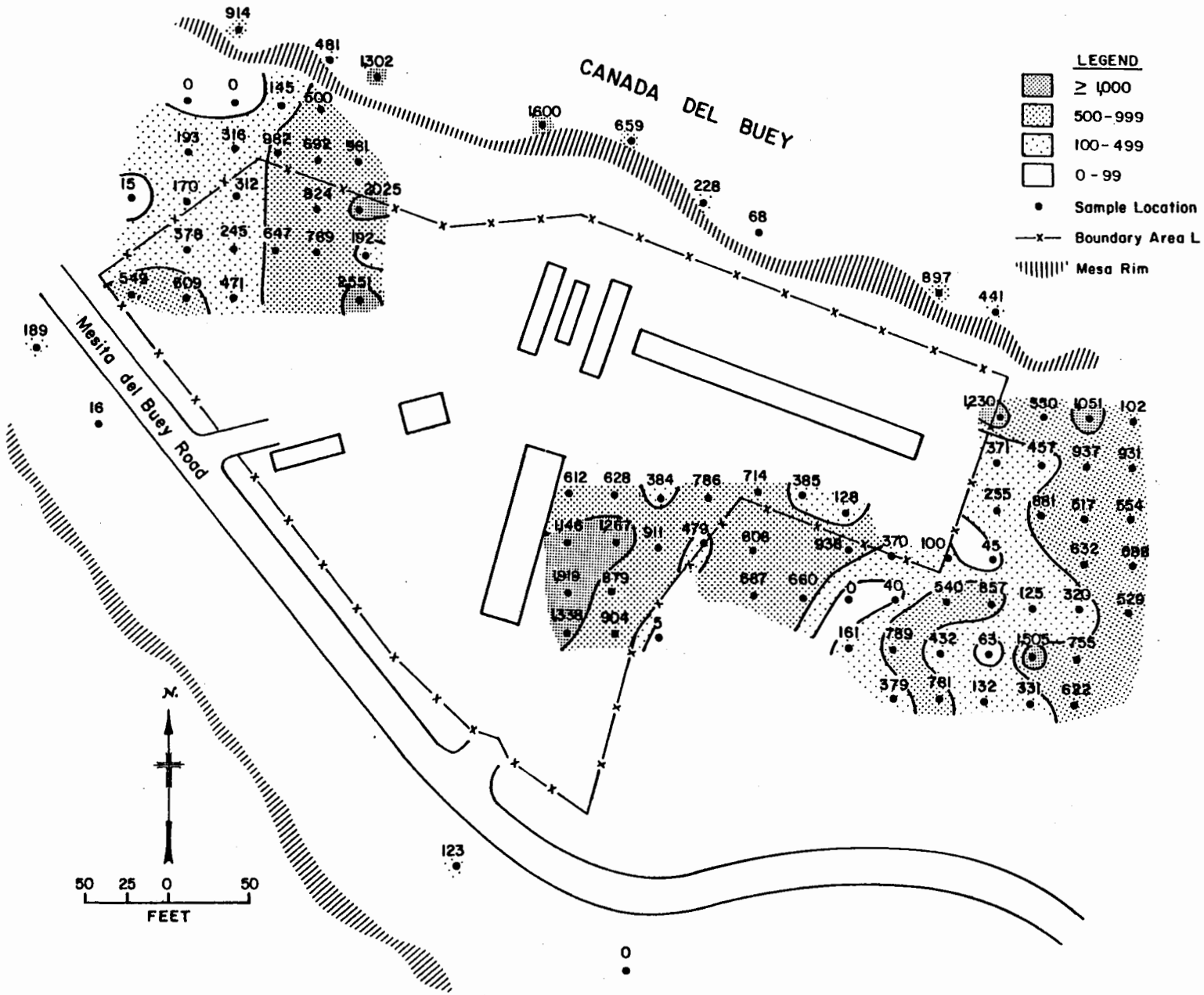

Figure 6-2. Normalized Tetrachloroethylene Ion-Count Map, Waste Disposal Area L, Los Alamos National Laboratory, New Mexico

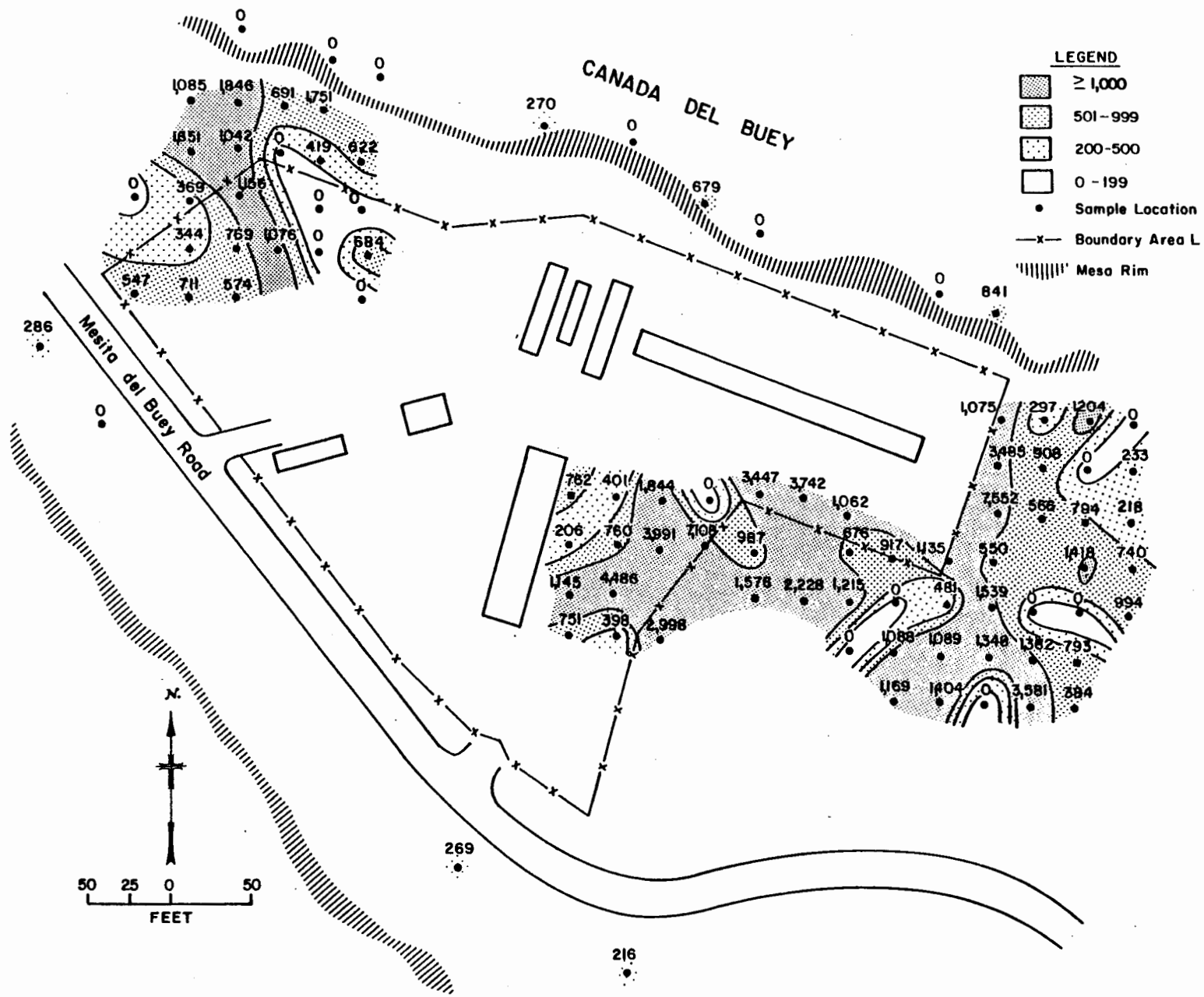

Figure 6-3. Non-Normalized Benzene Ion-Count Map, Waste Disposal Area L, Los Alamos National Laboratory, New Mexico

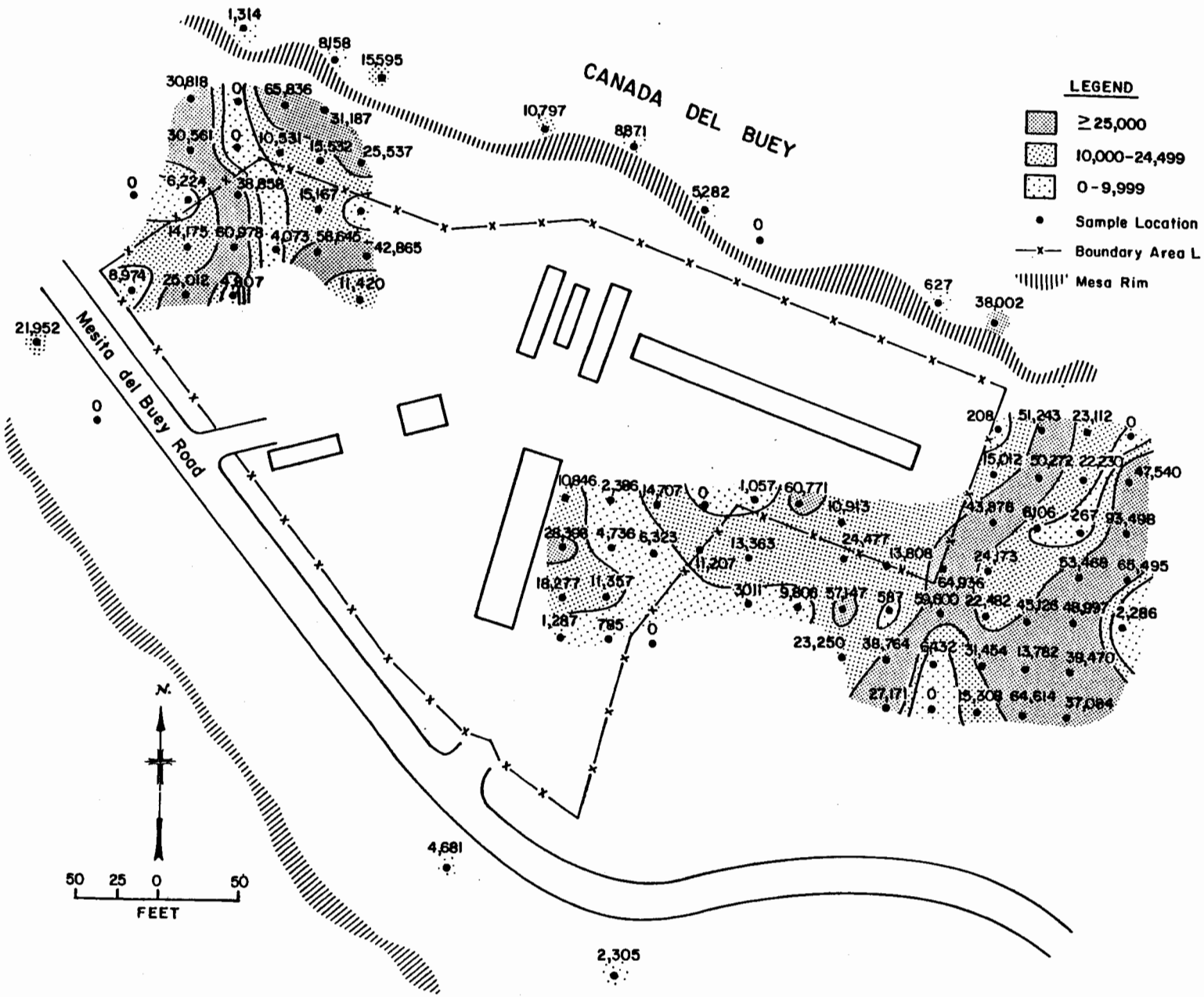

Figure 6-4. Non-Normalized Toluene Ion-Count Map, Waste Disposal Area L, Los Alamos National Laboratory, New Mexico

for toluene. Trichloroethylene and tetrachloroethylene had the lowest total ion counts.

The trichloroethylene and tetrachloroethylene data presented in Figures 6-1 and 6-2, respectively, were normalized by dividing the specific ion counts by the total ion counts less atmospheric compounds. The benezene and toluene ion counts are non-normalized and represent total uncorrected specific ion counts. The ion counts for a specific compound are not absolute and, therefore, should not be used to compare individual compounds as a means of determining relative abundances of the compounds present. The ion counts of a particular compound, however, may be used to show the relative flux distribution of specific ions.

Background ion counts for benzene and toluene ranged from 0 to 1,078 and 0 to 27,998, respectively. The background values are quite high when compared to the ion counts taken at Waste Disposal Area L. The gases given off by plant roots in the soil zone are suspected of having a chemical structure similar to benzene and toluene; the plant-root gases overprint and likely predominate over the counts observed at Area L. Since the range in background counts is so high for benzene and toluene, it is likely that even a wider range of background counts could be expected if more than five samplers were used to survey the background. The existing five-sample array of background counts is, therefore, insufficient to characterize the background accurately because the maximum observed counts could be well below the probable maximum background value. Furthermore, analytical results of core samples collected during the drilling phase of the project have not indicated that benzene or toluene were even present in the pore-gas fraction of the rock (Rocky Mountain Analytical Laboratory, 1986). The benzene and toluene maps (see Figures 6-3 and 6-4), consequently, are not recommended for use in delineating the vapor-phase contamination at Area L.

Background ion counts for trichloroethylene and tetrachloroethylene were found to be very low to nonexistent. As a result, the ion counts shown in Figures 6-1 and 6-2 more accurately reflect the relative flux of these vapors emanating from Area L. Trichloroethylene and tetrachloroethylene would, therefore, be good compounds to define the extent of migration away from the waste-disposal shafts and trenches.

From the distribution of the ion-count data observed in Figures 6-1 through 6-2, there is no readily apparent single trend in the data at any location surveyed. There are locally high ion-count locations, which may simply indicate proximity to waste trenches and pits. The distribution of ion counts, however, is not concentric around the source. Locally contoured areas with high ion counts, some of which are linear trends, may indicate areas where the fracture intensity or the fracture aperture is relatively large. Where the trends do exist, it may indicate preferential movement through open joints, which would be more effective in transmitting organic vapors than the intervening blocks of tuff.

It should be noted that the lateral extent of the ion-count plume could not be defined conclusively because substantial ion counts were detected at the margins of the sample area. It can be assumed that these elevated ion counts extend beyond the limits of the present survey. Consequently, additional pore-gas sampling holes were located beyond the limits of the existing Petrex grid to aid in defining the extent of the organic vapor contamination plume. No analytical data on the newly installed, pore-gas monitoring ports were available at the time of this report.

Section 7

CONCLUSIONS

The time constraints imposed on this study of Waste Disposal Areas G and L at Los Alamos permitted only a brief period for data acquisition and interpretation. As a consequence, the assessment presented herein of the vadose zone underlying Mesita del Buey is for the short term only. Nevertheless, some conclusions can be drawn from the data obtained thus far, the most important being that the dominant mode of transport in the interval of the Bandelier Tuff examined for this study is by vapor phase. In other words, the low moisture content of the tuff and the high moisture-retention values observed in the moisture characteristic curves indicate that interconnection of liquid water, and therefore movement of water in the liquid phase, is nonexistent. Additional conclusions are discussed in the paragraphs that follow.

- The geologic framework through which transport occurs can be characterized as a complex network of pumice and lithic clasts surrounded by a glass-shard/crystal matrix, with occasional fractures dissecting the porous media. Factors such as porosity, degree of welding, and pumice content have a direct effect on the unsaturated hydraulic characteristics.

- Taken together, the high values for porosity and moisture retention (both average approximately 50 percent) indicate that the tuff behaves much like a sponge. A quantity of water equal to approximately one quarter of the rock volume is required to satisfy capillary forces before recharge to the underlying groundwater system can occur. Based on the normal precipitation and the high evapotranspiration rates in the study area, this scenario is unlikely.

- Results from field and laboratory tests indicate that the overall range of intrinsic permeability for the Bandelier Tuff is 10^{-8} to 10^{-9} cm^2 (10^{-11} to 10^{-12} ft^2). These values are considered to represent moderate permeability.

- Permeability and porosity are not directly related, probably because of the tuff's pumice content; highly porous pumice lapilli contain a significant amount of dead-end pore space which greatly reduces permeability.

- The unsaturated hydraulic conductivities calculated using van Genuchten's model are of little value since the laboratory could only obtain moisture characteristic curves in the range 0 to -0.3 bar, with moisture contents (θ) of about 0.4 to 0.6. The calculated unsaturated hydraulic conductivities range from about 2 centimeters per day at saturation to about 1.0×10^{-6} centimeter per day at a water potential of -0.3 bar. In the field, however, water potentials range from -1 to -15 bar, and the moisture contents are below 0.1. Thus, the unsaturated hydraulic conductivities of the tuff in the field are actually much lower than the values calculated using van Genuchten's method.

- Unit 1b has a relatively higher degree of welding than the other units of Bandelier Tuff examined in this study. This higher degree of welding, coupled with the unit's high pumice content, results in strong capillary forces which are assumed to be responsible for the significant increase in moisture content in the lower portion of Unit 1b. Increases in the degree of welding are believed to reduce the pore-size radii, resulting in an increase in the capillary forces. Similarly, because there is a high

pumice content, there is a correspondingly high concentration of gas tubes; these tubes form ideal capillary tubes which appear to exhibit strong capillary forces.

- Test results indicate that permeability in and along fractures is very similar to the permeability of the surrounding porous media. Detection of the differences in the permeability, however, may be beyond the sensitivity of the testing methods, since several fracture zones show an increase in moisture content relative to the adjacent porous media.

- In certain cases, the magnetic susceptibility logs can be useful for estimating or confirming lithologic contacts. The gamma-gamma (apparent density) logs are useful for determining the degree of welding and possibly the relative pumice content of the various ash-flow units.

- Moisture characteristic curves for crushed tuff samples differ significantly from those obtained for core samples. As a consequence, interpretations of in-situ hydrogeologic transport cannot be reliably based on hydraulic data for crushed tuff.

- Petrex survey results indicate that organic-vapor ion-count contours are not distributed concentrically surrounding the contaminant source at Area L. Venting of organic vapors may occur in discrete zones where fracture apertures and/or intensities are locally elevated.

- A dominant northeast trend of fractures was determined by measuring joints on Mesita del Buey; however, a bias in the data resulted from sampling limitations imposed by available exposures. Occurrence of 'preferred' fracture orientation is not a sufficient single criteria for predicting direction of contaminant migration; transport from a contaminant source to the surface probably follows tortuous routes determined by a combination of fracture orientations and degree of dilation, and interconnections of fractures related to the position of infill materials.

- The best method for determining the extent and direction of contaminant transportation would be close monitoring and interpretation of analytical results from pore-gas samples, together with more extensive Petrex surveys just under the rim of Mesita del Buey and in Waste Disposal Area L.

Section 8

REFERENCES

Abeele, W. V., 1984. Hydraulic Testing of Crushed Bandelier Tuff, LA-10037-MS, UC-11, Los Alamos National Laboratory, New Mexico.

Abeele, W. V., M. L. Wheeler, and B. W. Burton, 1981. Geohydrology of Bandelier Tuff, LA-8962-MS, UC-11, Los Alamos National Laboratory, New Mexico.

Bailey, R. A., R. L. Smith, and C. S. Ross, 1969. Stratigraphic Nomenclature of Volcanic Rocks in the Jemez Mountains, New Mexico, Bulletin 1274-P, U.S. Geological Survey.

Bendix Field Engineering Corporation, 1985a. Environmental Sciences Procedure Manual, Environmental Programs Division, Grand Junction, Colorado, internal document.

Bendix Field Engineering Corporation, 1985b. Vadose Zone Characterization of Technical Area 54, Waste Disposal Areas G and L, Los Alamos National Laboratory - Report 2: Downhole Instrumentation and Pore-Gas-Sampling/Data-Collection Procedures, GJ-43, Bendix Field Engineering Corporation, Grand Junction Operations, U.S. Department of Energy, Grand Junction Projects Office, Grand Junction, Colorado.

Brown, R. W., and D. L. Bartos, 1982. A Calibration Model for Screen-Caged Peltier Thermocouple Psychrometers, Research Paper INT-293, U.S. Department of Agriculture, Intermountain Forest and Range Experiment Station.

Brown, R. W., and J. M. Collins, 1980. 'A Screen-Caged Thermocouple Psychrometer and Calibration Chamber for Measurements of Plant and Soil Water Potential,' Agronomy Journal, Vol. 72, pp. 851-854.

Case, C. M., and A. Welch, 1979. 'Pore Size Distribution, Suction and Hysteresis in Unsaturated Groundwater Flow,' Journal of Hydrology, Vol. 43, pp. 99-120.

Chemical Rubber Company, 1986-1987. Handbook of Chemistry and Physics: 47th Edition, Robert C. Weast (editor-in-chief), Cleveland, Ohio.

Cook, E. F., 1965. Stratigraphy of Tertiary Volcanic Rocks of Eastern Nevada, Report No. 11, Nevada Bureau of Mines.

Environmental Improvement Division, 1985. Compliance Order/Schedule: Los Alamos National Laboratory, State of New Mexico, Santa Fe.

Freeze, R. A., and J. A. Cherry, 1979. Groundwater, Prentice-Hall, Inc., Englewood Cliffs, New Jersey.

Fukui, L. M., 1985. Petrography of the Tshirege Member of the Bandelier Tuff, Mesita del Buey, Los Alamos County, New Mexico, prepared for the Environmental Programs Division, Bendix Field Engineering Corporation, Grand Junction, Colorado.

_____ 1986. Petrography of the Tshirege Member of the Bandelier Tuff, Mesita del Buey, Los Alamos County, New Mexico: Second Report, prepared for the Environmental Programs Division, Bendix Field Engineering Corporation, Grand Junction, Colorado.

Goddard, E. N., P. D. Trask, R. K. DeFord, O. N. Rove, J. T. Singewald, Jr., and R. M. Overbeck, 1975. Rock Color Chart, Geological Society of America, Boulder, Colorado.

Goff, F. E., and S. L. Bolivar, 1983. Field Trip Guide to the Valles Caldera and Its Geothermal Systems, LA-9963-OBES, Los Alamos National Laboratory, New Mexico.

Horner, R. D., 1951. 'Pressure Build-Up in Wells,' in Proceedings of the Third World Petroleum Congress, Section II, E. J. Bill, Leiden, Holland.

Jakubick, A. T., 1983. Permeability Measurements of the Near-Field of Excavations by Transient Pressure Testing, Atomic Energy of Canada, Technical Report, Whiteshell Nuclear Research Establishment, Pinawa, Manitoba.

Johnson, E. F., D. P. Bossler, and V. D. Naumann, 1959. 'Calculations of Relative Permeability from Displacement Experiments,' Transactions of the American Institute of Mining, Metallurgical, and Petroleum Engineers, Vol. 216, pp. 370-372.

Kearl, P. M., J. J. Dexter, and M. Kautsky, 1986. Vadose Zone Characterization of Technical Area 54, Waste Disposal Areas G and L, Los Alamos National Laboratory, New Mexico - Report 3: Preliminary Assessment of the Hydrologic System, GJ-44, Bendix Field Engineering Corporation, Grand Junction Operations, U.S. Department of Energy, Grand Junction Projects Office, Grand Junction, Colorado.

Lai, Sung-Ho, J. M. Tiedje, and A. E. Erickson, 1976. 'In Situ Measurement of Gas Diffusion Coefficient in Soil,' Soil Science Society of America Journal, Vol. 40, pp. 3-6.

Lang, A. R. G., 1967. 'Osmotic Coefficients and Water Potentials of Sodium Chloride Solutions from 0 to 40°C,' Australian Journal of Chemistry, Vol. 20, No. 9, pp. 2017-2023.

Loughborough, M. T., 1966. 'Permeability of Concrete to Air,' Ontario Hydro Research Quarterly, First Quarter, Ontario, Canada.

Marshall, T. J., and J. W. Holmes, 1979. Soil Physics, Cambridge University Press, New York.

Marutzky, S. J., 1986. Personal Communication with S. J. Marutzky, Bendix Field Engineering Corporation, Grand Junction, Colorado, 18 February 1986.

McBeth Division, Kollmorgen Corporation, 1975. Munsell™ Soil Color Chart, McBeth Division, Kollmorgen Corporation, Baltimore, Maryland.

Miller, C. H., D. R. Cunningham, and M. J. Cunningham, 1974. 'An Air Injection Technique to Study Intensity of Fracturing Around a Tunnel in Volcanic Rocks, Bulletin of the Association of Engineering Geologists, Vol. II, No. 3.

Mualem, V., 1976. 'A New Model for Predicting the Hydraulic Conductivity of Unsaturated Porous Media,' Water Resources Research, Vol. 12, No. 3, pp. 513-522.

Nutting, P. G., 1930. 'Physical Analysis of Oil Sands,' Bulletin of the American Association of Petroleum Geologists, Vol. 14, pp. 1337-1349.

Purtymun, W. D., and W. R. Kennedy, 1971. Geology and Hydrology of Mesita del Buey, LA-4660, UC-41, Los Alamos National Laboratory, New Mexico.

Purtymun, W. D., M. L. Wheeler, and M. A. Rogers, 1978. Geologic Description of Cores from Holes P-3 MH-a through P-3 MH-5, Area G, Technical Area 54, LA-7308-MS, Informal Report, Los Alamos Scientific Laboratory, New Mexico.

Rocky Mountain Analytical Laboratory Division, ENSECO, Inc., 1986. Analytical Results for Bendix Field Engineering Corporation, Rocky Mountain Analytical Laboratory Division, ENSECO, Inc., Arvada, Colorado.

Rogers, M. A., 1977. History and Environmental Setting of LASL Near-Surface Land Disposal Facilities for Radioactive Wastes, LA-6848-MS, Vol. 1, Los Alamos Scientific Laboratory.

Ross, C. S., and R. L. Smith, 1961. Ash-Flow Tuffs: Their Origin, Geologic Relationship, and Identification, USGS Professional Paper 366, Government Printing Office, Washington, D.C.

Rush, S. M., and J. J. Dexter, 1985. Vadose Zone Characterization of Technical Area 54, Waste Disposal Areas G and L - Report 1: Drilling and Logging Activities, GJ-37, Bendix Field Engineering Corporation, Grand Junction Operations, U.S. Department of Energy, Grand Junction Projects Office, Grand Junction, Colorado.

Spanner, D. C., 1951. 'The Peltier Effect and Its Use in the Measurement of Suction Pressure,' Journal of Experimental Botany, Vol. 2, No. 5, pp. 145-167.

Stephens, D. B., and S. P. Neuman, 1982a. 'Vadose Zone Permeability Tests: Summary,' Journal of the Hydraulics Division, American Society of Civil Engineers, Vol. 108, No. HY5, pp. 623-639.

Stephens, D. B., and S. P. Neuman, 1982b. 'Vadose Zone Permeability Tests: Steady State Results,' Journal of the Hydraulics Division, American Society of Civil Engineers, Vol. 108, No. HY5, pp. 640-659.

Stephens, D. B., S. Tyler, K. Lambert, and S. Yates, 1983. 'Field Experiments to Determine Saturated Hydraulic Conductivity in the Vadose Zone,' in Role of the Unsaturated Zone in Radioactive and Hazardous Waste Disposal, J. W. Mercer, P.S.C. Rao, and M. I. Wendell (eds.), Ann Arbor Scientific Publications, Ann Arbor, Michigan.

Streckeisen, A., 1967. 'Classification and Nomenclature of Igneous Rocks,' in Neues Jahrbuch fur Mineralogie, Abhandlungen, Vol. 107, pp. 144-240.

TerraTek Research Laboratory, 1985. Laboratory Analysis of Rock Core: Bandelier Formation, TR86-49, Salt Lake City, Utah.

U.S. Department of the Interior, 1974. Earth Manual: A Water Resource Technical Publication, Second Edition, Government Printing Office, Washington, D.C.

University of Missouri at Rolla, 1981. Seminar for Drillers and Exploration Managers, Orlando, Florida.

van Genuchten, Rien, 1978. Calculating the Unsaturated Hydraulic Conductivity with a New Closed-Form Analytical Model, Princeton University Water-Resources Program Report 78-WR-08.

Welge, H. J., 1952. 'A Simplified Method for Computing Oil Recovery by Gas or Water Drive,' Transactions of the American Institute of Mining, Metallurgical, and Petroleum Engineers, Vol. 195, pp. 91-98.

Wescor (undated). Instruction Manual for the Model HP-115 Microprocessor Controlled Water Potential Data System, Wescor, Inc., Logan, Utah.

Wescor, 1982. CI-30 Audio Cassette Interface, Wescor, Inc., Logan, Utah.

Appendix A

LITHOLOGIC LOGS AND INSTRUMENT COMPLETION DIAGRAMS

LITHOLOGIC LOGGING

A lithologic log was prepared in accord with established field procedures for each of the 23 holes cored with the continuous sampling system (Bendix Field Engineering Corporation, 1985a, 1985b). These logs are presented in chronological order by hole number as Figures A-2 through A-24. The colors used to describe the core matrices are taken from the Rock Color Chart of Goddard and others (1975) and the Munsell™ Soil Color Chart, Macbeth Division of Kollmorgen Corporation, Baltimore, Maryland (1975); the code in parentheses following a color description corresponds to the charts.

For most of the holes, the lithologic logs also show the numbers and depth intervals of samples collected for subsequent field or laboratory analysis. Samples identified by the three-letter prefix MCG- followed solely by a three-digit number were collected for gravimetric analysis. Those MCG-numbered samples denoted by a single asterisk (*) were collected for petrologic analysis, and those denoted by a double asterisk (**) were collected for laboratory analysis of moisture characteristics. Samples identified with the number 85 followed by a decimal point and five additional digits were collected for EP-toxicity and volatile-organic analyses by Los Alamos National Laboratory for drilling conducted during Summer 1985. Splits of these samples are identified by the addition of the letter A immediately following the sample number. Samples identified with the prefix R5 were collected for volatile-organic analyses by Rocky Mountain Analytical Laboratory, Arvada, Colorado. Results of these analyses were presented to Los Alamos National Laboratory 7 October 1986.

Lithologic logs for holes drilled during 1986 (designated with an '86' in the log number) and Holes LLM-85-01 and LLM-85-02 have a specific installation column for instrument-completion diagrams (except LLC-86-25). The lithologic logs for the remainder of the holes in which instruments were installed show instrument-completion diagrams in the column originally used for sample identification. The reader is referred to the first report (Rush and Dexter, 1985) for information on sample numbers and intervals for those holes. It is important to note, however, that the lithologic data have been updated since publication of the first report. Consequently, the graphic log and description for a particular hole as they appeared in the first report may not match the information presented in this appendix.

INSTRUMENT COMPLETIONS

A total of 93 pore-gas sampling ports were installed in 14 boreholes in the study area. Completion diagrams of the installations are presented in Figures A-2, A-3, A-8, A-9, A-11 through A-15, and A-19 through A-23.

A total of 38 thermocouple psychrometers were installed at the study area, 23 in Hole LLP-85-03 and 15 in Hole LGP-85-07. Because of the presence of surface casing in Hole LLP-85-03, a shallow boring was drilled adjacent to the main hole and five psychrometers were installed in this second hole close to the ground surface (depicted in Figure A-4 as being in the same hole). Completion diagrams of the thermocouple-psychrometer installations are shown in Figures A-4 and A-7. Four pressure transducers were installed in Hole LLP-85-03, although the one at ground surface is actually in the shallow

adjacent boring described above. The completion diagram is shown in Figure A-4.

Installation details were described in the second interim report (Bendix Field Engineering Corporation, 1985b). The legends for the instrument installations are presented in Figure A-1.

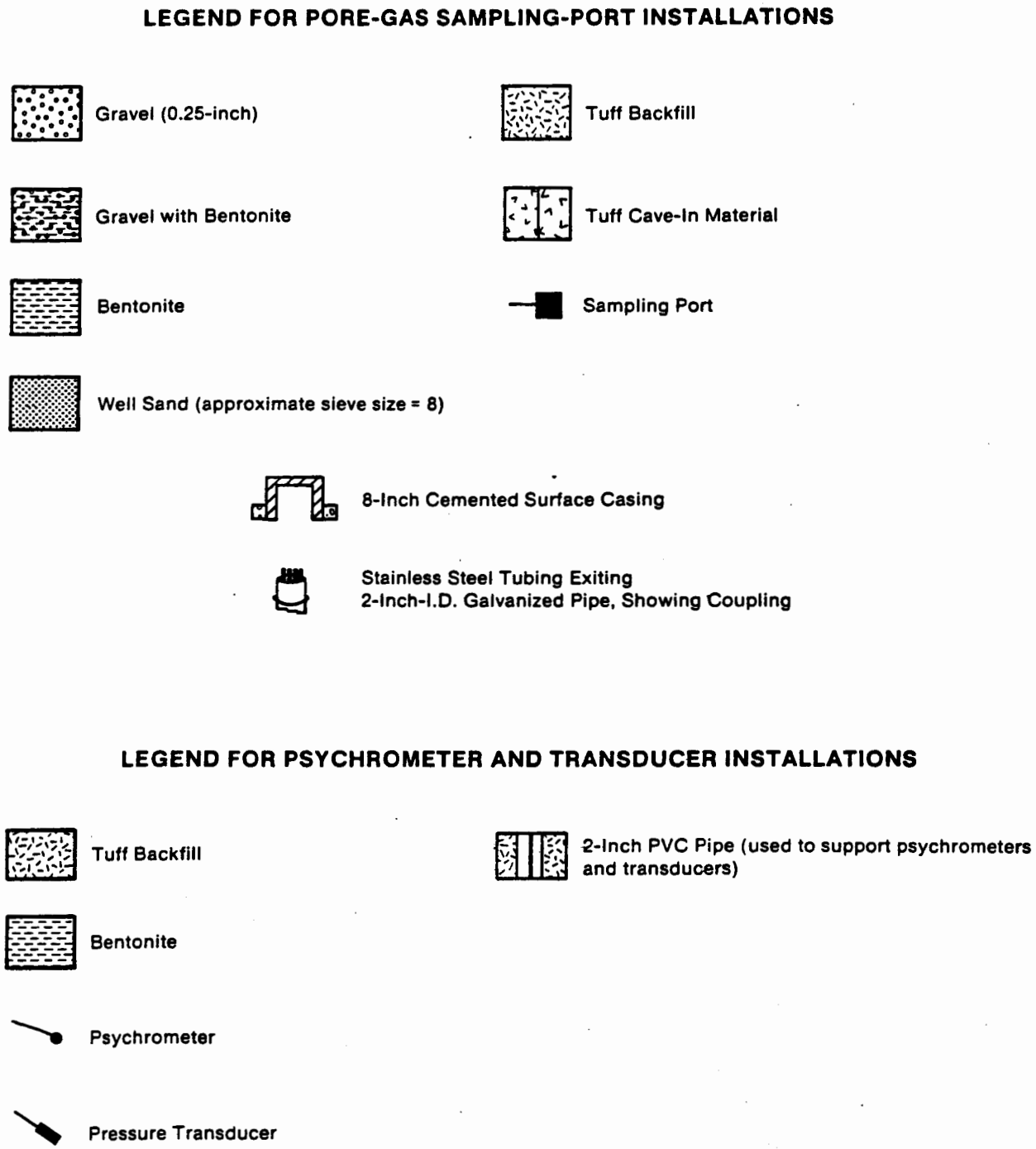

Figure A-1. Legends for the Instrument Installations

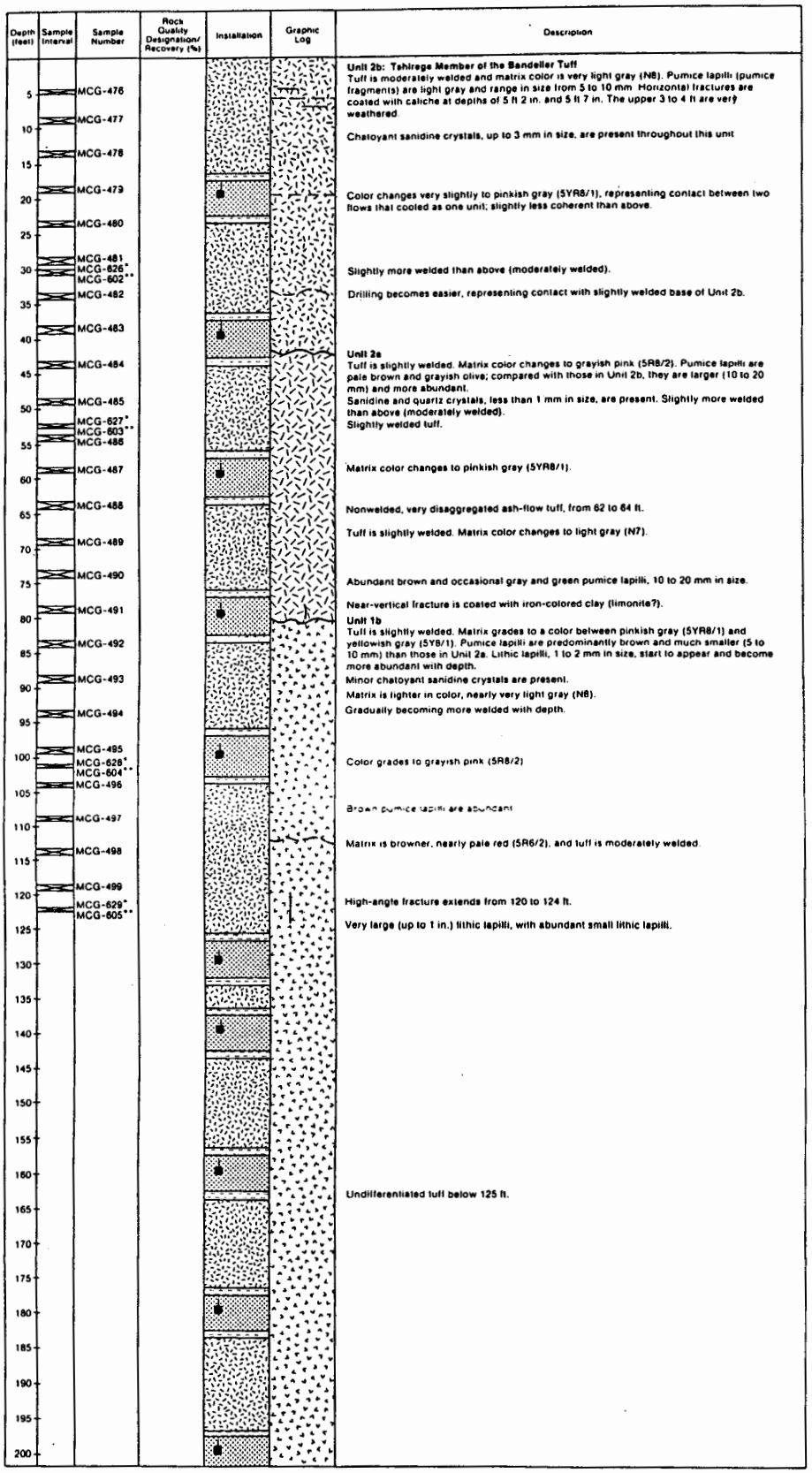

Figure A-2. Lithologic Log of Hole LLM-85-01

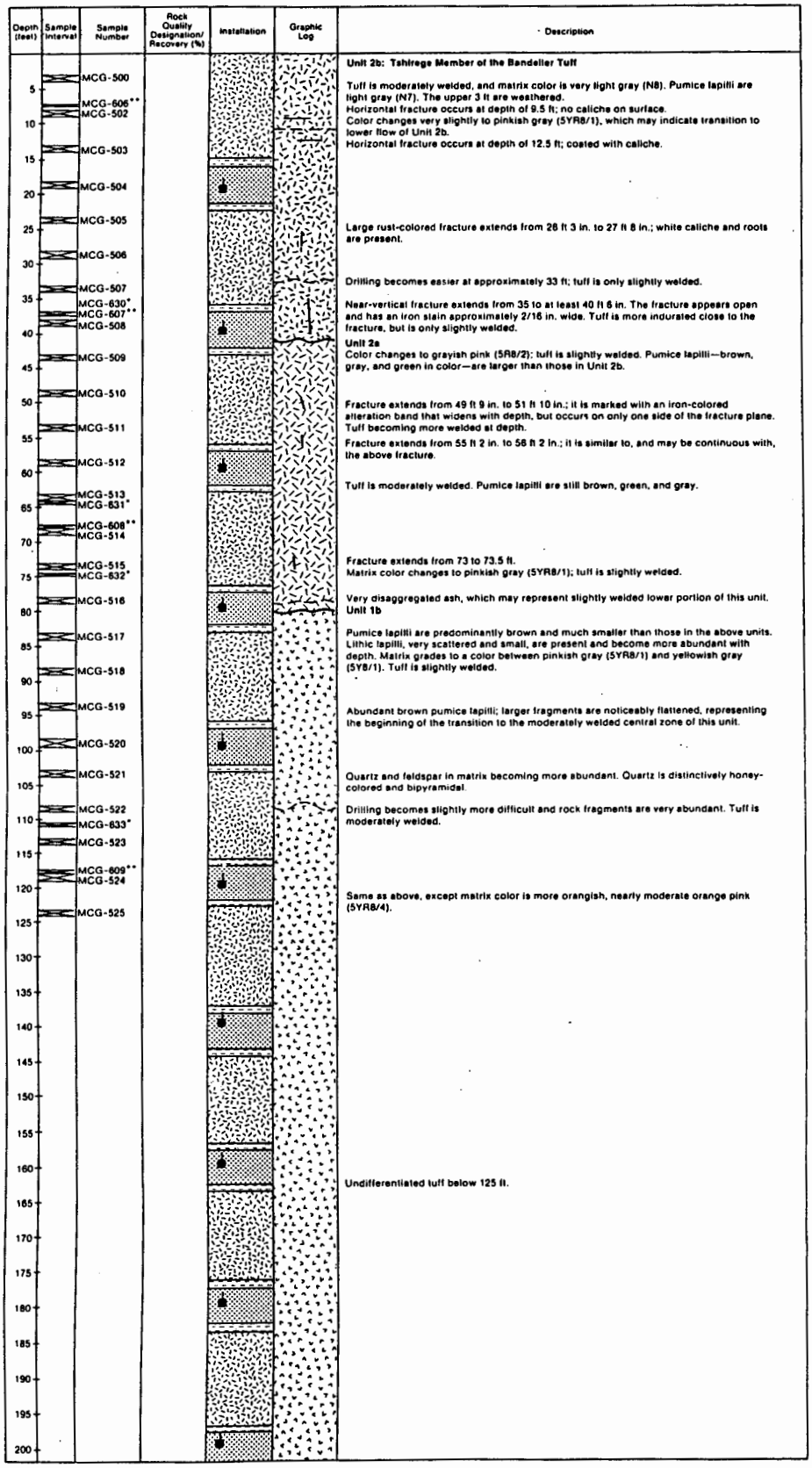

Figure A-3. Lithologic Log of Hole LLM-85-02

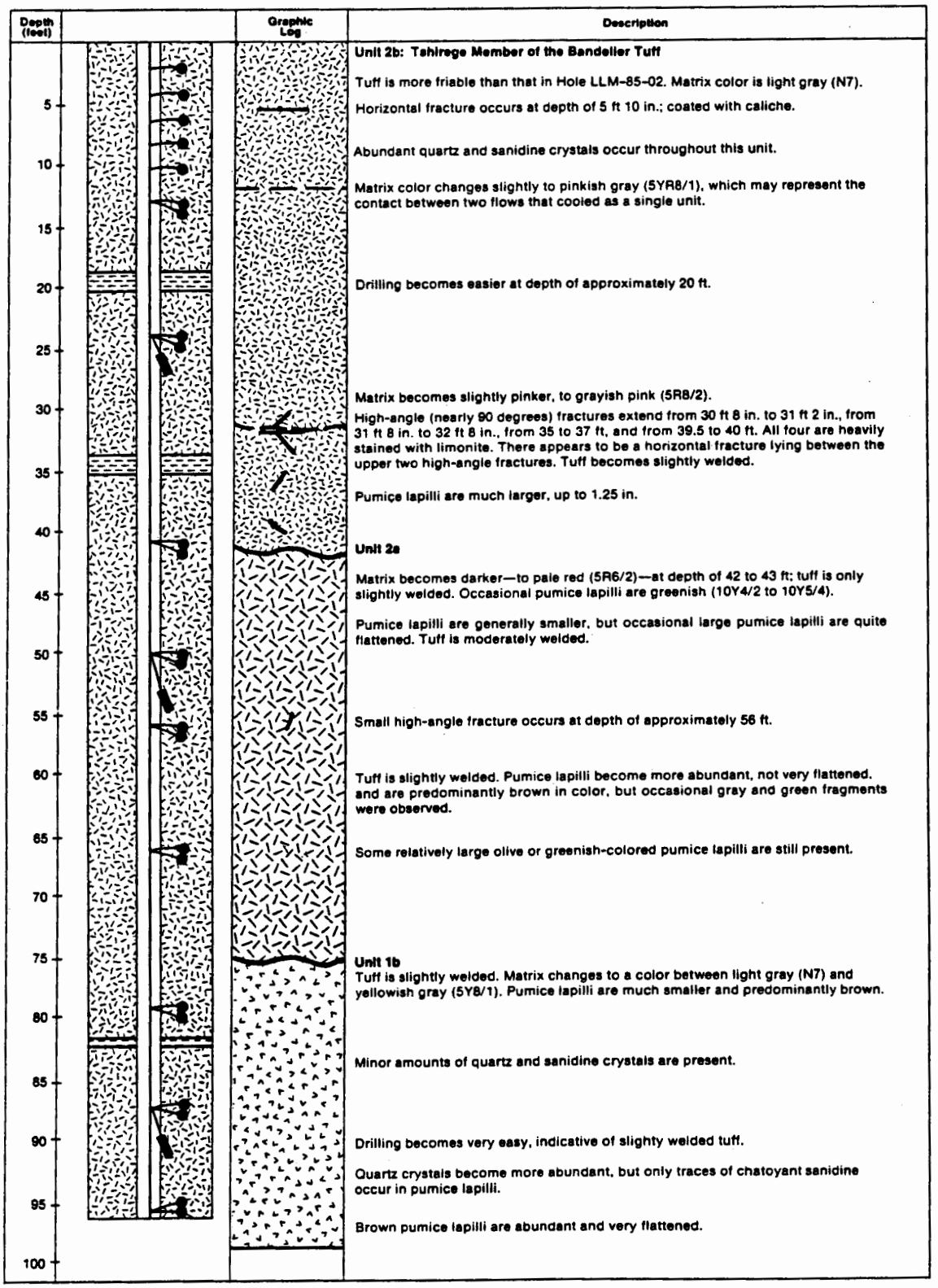

Figure A-4. Installation of Thermocouple Psychrometers and Pressure Transducers in Hole LLP-85-03 (Note: The psychrometers in the upper 10 ft are located in a shallow boring adjacent to the main hole.)

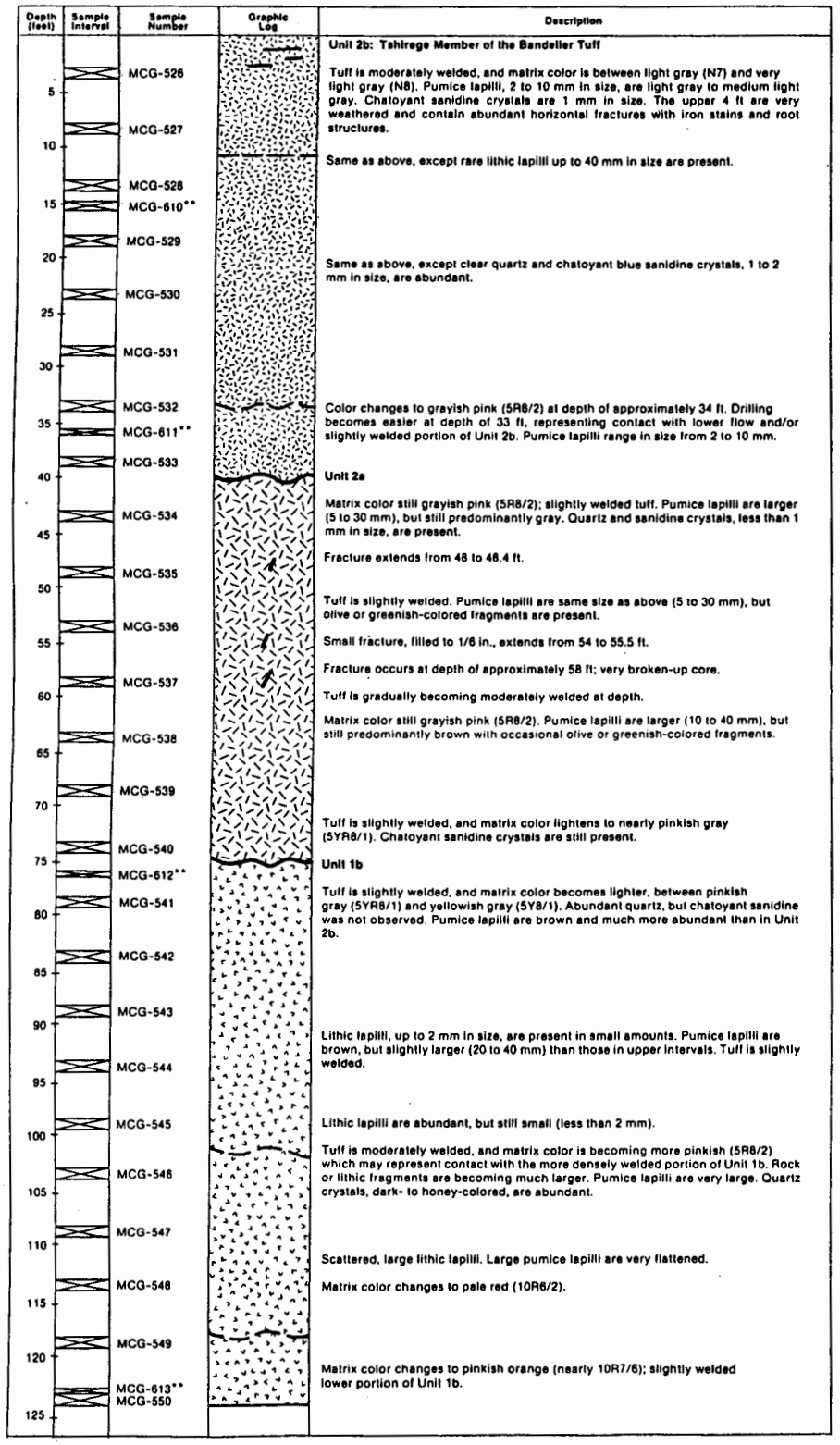

Figure A-5. Lithologic Log of Hole LLM-85-05

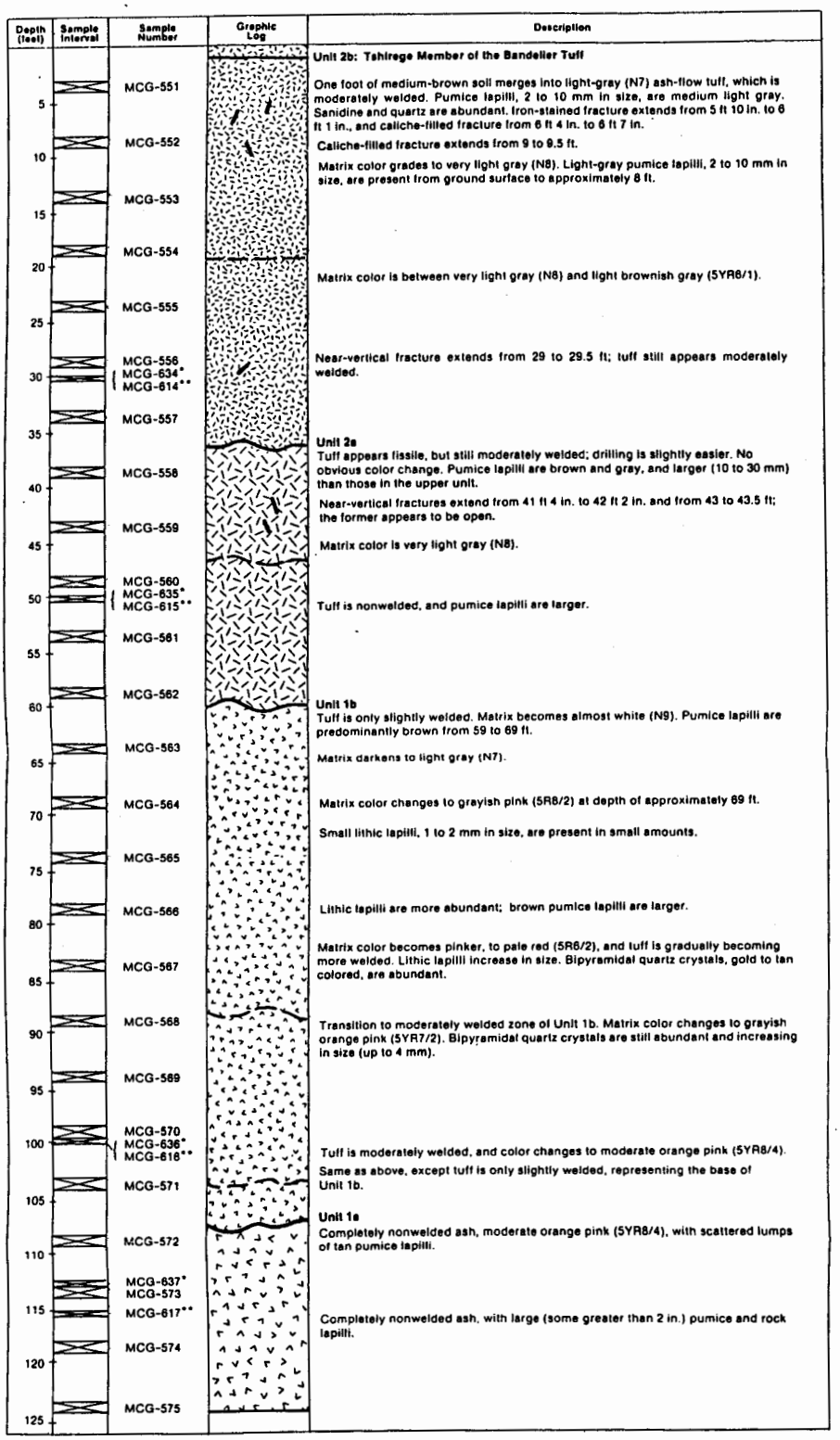

Figure A-6. Lithologic Log of Hole LGM-85-06

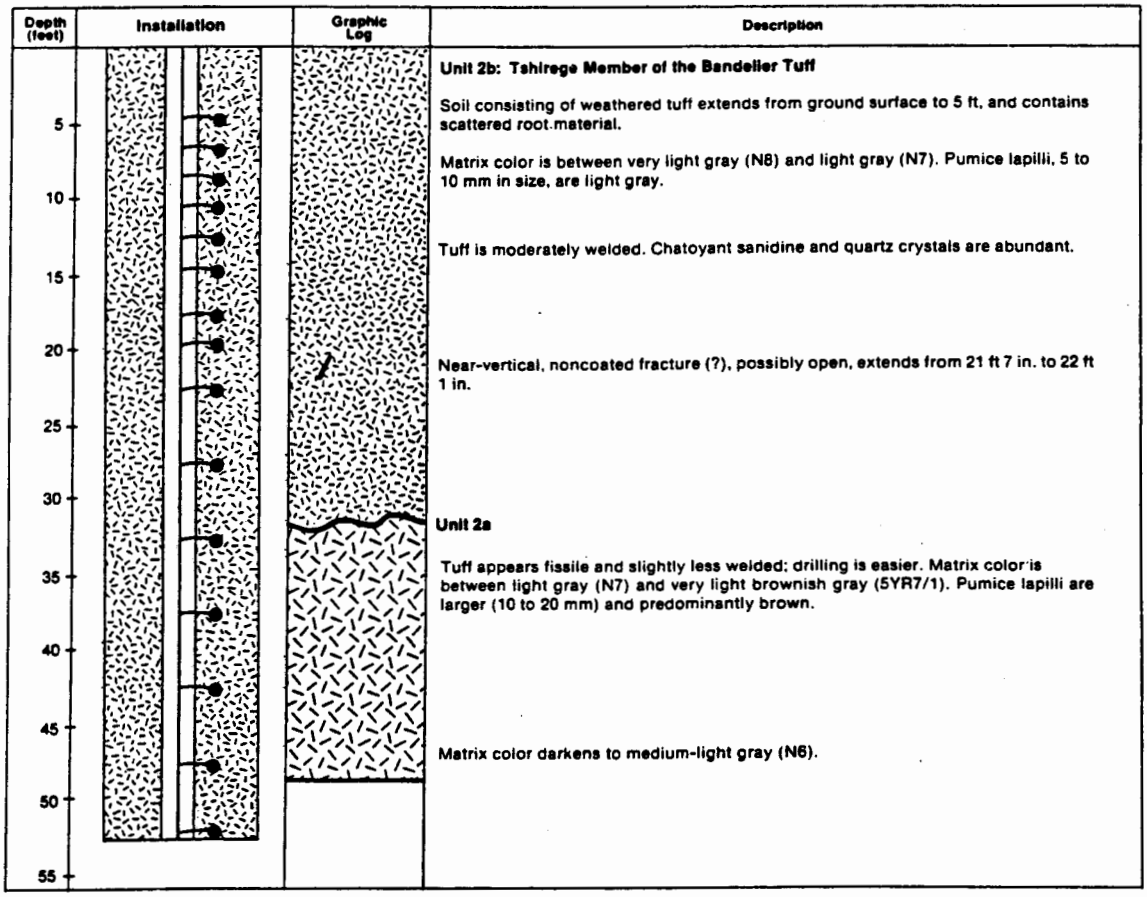

Figure A-7. Installation of Thermocouple Psychrometers in Hole LGP-85-07

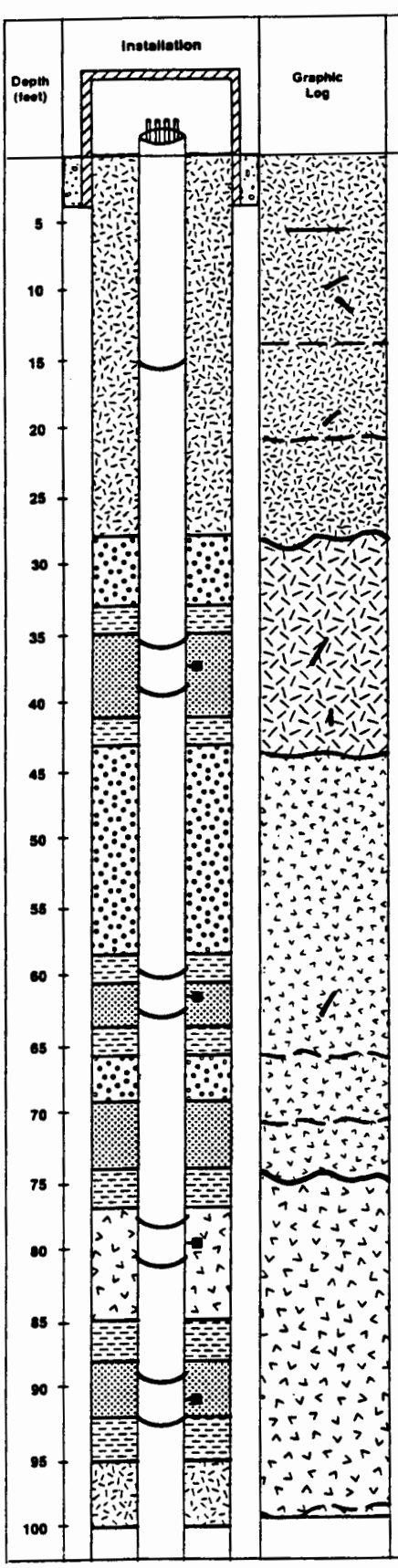

Description

Unit 2b: Tshirege Member of the Bandelier Tuff

The upper 5 ft are weathered and loose, and predominantly brown in color.

Possible horizontal fracture occurs at depth of 6 ft 10 in.; very slight discoloration to brown on the surface. Tuff is moderately welded.

Matrix color is very light gray (N8).

Fractures extend from 9 ft 6 in. to 9 ft 9 in. and from 10 ft 1 in. to 10 ft 4 in.; both appear to dip approximately 45 degrees and have slight brown coloring on the surfaces.
Concentrations of larger pumice lapilli may represent the boundary between separate flows within this unit.
Matrix color changes to pinkish gray (5YR8/1).
Tuff appears slightly fissile, but is still moderately welded.
Possible noncoated fracture extends from 19 ft to 19 ft 3 in.

Slightly less welded than above.

Matrix color becomes very slightly pinkish, with very small, brown pumice lapilli, probably indicating a transitional contact with Unit 2a.

Unit 2a
Matrix color is definitely pinkish. Sanidine and quartz are present. Approximately 75% of the pumice lapilli are brown, 25% green (olive).

Matrix color changes to light brownish gray (5YR6/1).
Tuff is moderately welded.
Near-vertical, iron-stained fracture extends from 35 ft 4 in. to 36 ft 4 in.

Near-vertical, noncoated fracture extends from 40 ft to 40 ft 8 in.
Slightly welded tuff.

Unit 1b
Matrix color changing to very light gray (N8) to almost white (N9) at depth of 43 to 44 ft; tuff is only slightly welded. Pumice lapilli are predominantly brown; occasional large pumice fragments appear flattened. Sanidine crystals are abundant.

Matrix color changes to white (N9) at depth of 52 ft.

Pumice lapilli are still brown, but becoming larger in the interval 59 to 63 ft. Lithic lapilli are abundant, up to ½ in. in size at depth of 59 ft. Quartz crystals are honey-colored. Slightly welded tuff is grading to moderately welded unit below.
Near-vertical fracture, slightly iron-stained, extends from 61 to 62 ft.

Drilling becomes more difficult, and tuff is moderately welded. Lithic lapilli are larger. This more welded material probably represents the central portion of the Unit 1b cooling zone. Fresh glass shards were observed.
Matrix color grades from pinkish gray (5YR8/1) to very pale orange (10YR8/2) to light brown (5YR6/4).
Tuff is slightly welded, and looks like the rest of Unit 1b except the color is becoming very orange. Lithic lapilli are still very abundant, and quartz crystals are still honey-colored.

Unit 1a
Completely nonwelded, orange-colored ash with large pumice lapilli. The latter are distinctively light brown or cream-colored. Only scattered lithic lapilli were observed, one 1 in. in size and another 1/16 in. in size.

Matrix color is moderate orange pink (5YR8/4).

Same as above, except dampness observed at depth of approximately 88 ft.

Same as above, except matrix color changes to light tan [approximately 5Y8/1 (yellowish gray)] and green pumice lapilli are scattered throughout.

Figure A-8. Installation of Pore-Gas Sampling Ports in Hole LGC-85-09

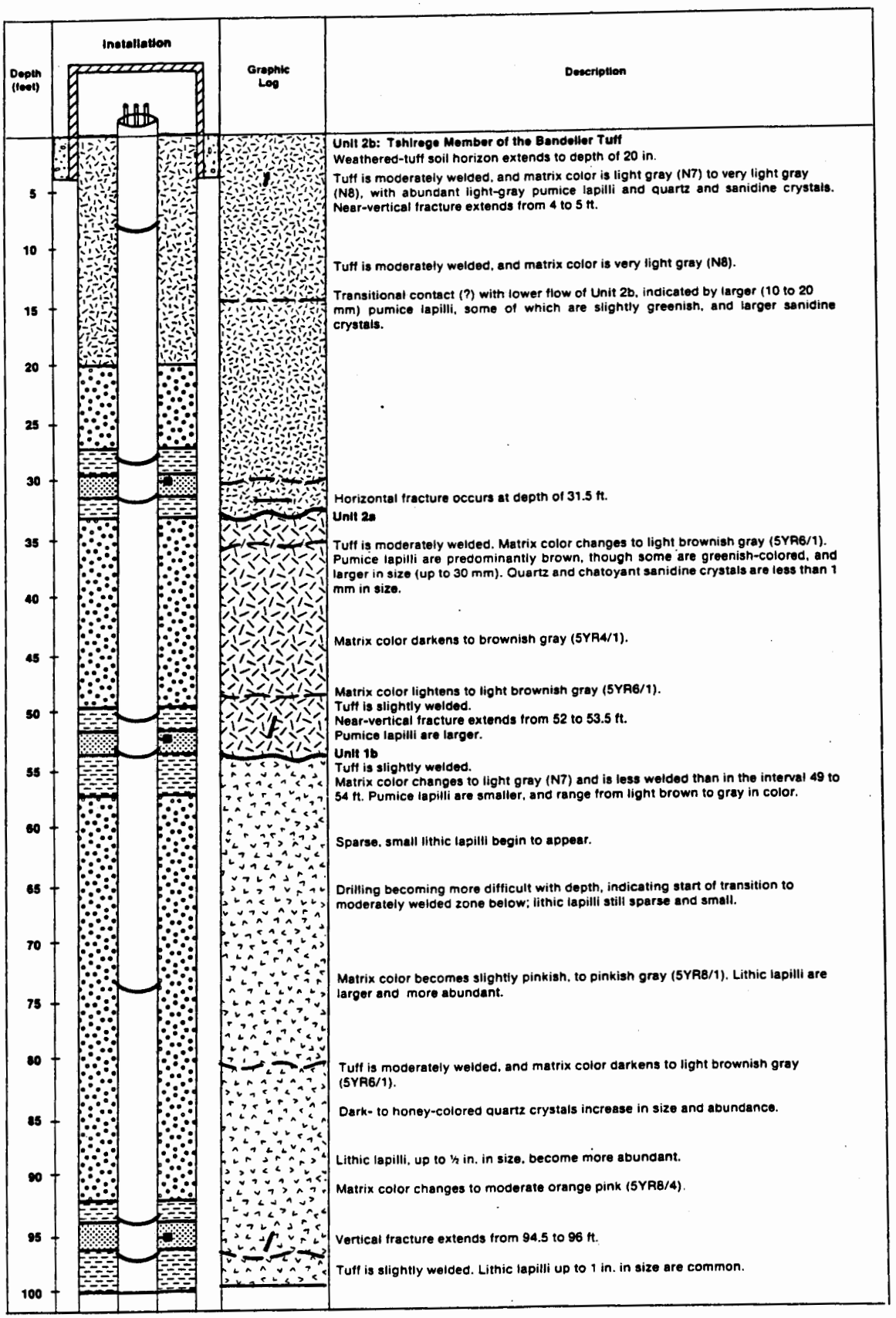

Figure A-9. Installation of Pore-Gas Sampling Ports in Hole LGC-85-10

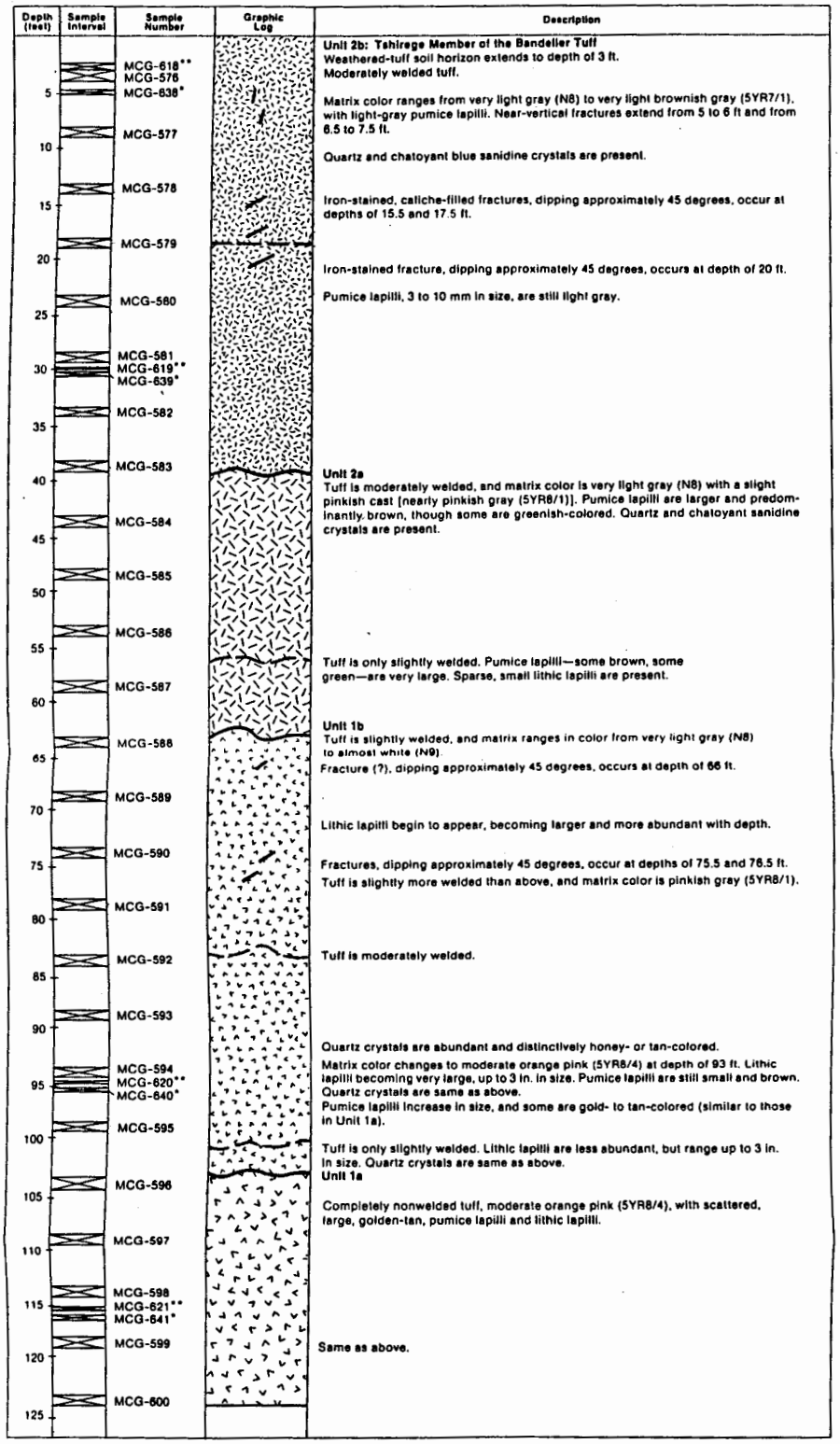

Figure A-10. Lithologic Log of Hole LGM-85-11

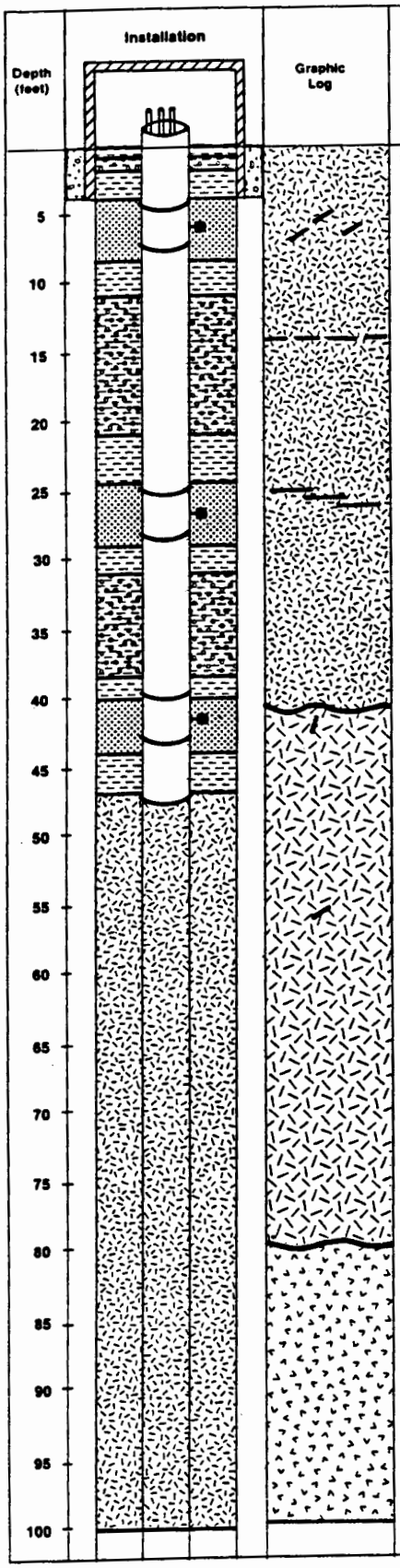

Description

Unit 2b: Tshirege Member of the Bandelier Tuff

Soil consists of weathered tuff and some fill (tuff).

Matrix is light gray (N7), with common quartz and chatoyant sanidine crystals. Iron-stained fractures, dipping 45 degrees, occur at depths of 5 ft, 6 ft, and 6 ft 8 in. Pumice lapilli are medium light gray, except for a very few which are light green.

Same as above.

Horizontal fractures occur at depths of 24 ft 8 in., 25 ft, 25 ft 7 in., and 26 ft.

Pumice lapilli are gray and range from 2 to 10 mm in size.

Tuff appears only slightly welded (from surface), possibly the result of weathering due to the hole's proximity to the edge of the mesa.

Unit 2a

Tuff is moderately welded and matrix color changes to pinkish gray (5YR8/1). Pumice lapilli are larger (10 to 20 mm) and predominantly brown. Vertical fracture, with roots, occurs at depth of 41 ft.

Pumice lapilli are brown and greenish-colored.

Matrix color darkens slightly, to nearly light brownish gray (5YR6/1).

Fracture, dipping approximately 45 degrees, occurs at depth of 55.6 ft. Quartz crystals are dominant phenocrysts.

Matrix color lightens, back to pinkish gray (5YR8/1). Lithic lapilli are small (1 to 2 mm) and very sparse. Minor amount of sanidine crystals.

Sanidine and quartz crystals are abundant and present in equal amounts.

Pumice lapilli—some brown, some green—are larger than above.

Tuff is slightly to moderately welded. Matrix color is very light gray (N8).

Unit 1b

Tuff is slightly to moderately welded, and matrix is becoming lighter, to a color between very light gray (N8) and white (N9). Pumice lapilli range up to 30 mm in size.

Sanidine and quartz crystals are present in approximately equal amounts. Quartz crystals are distinctively honey- or tan-colored. Pumice lapilli range up to 40 mm in size. No lithic lapilli were observed.

Figure A-11. Installation of Pore-Gas Sampling Ports in Hole LLC-85-12

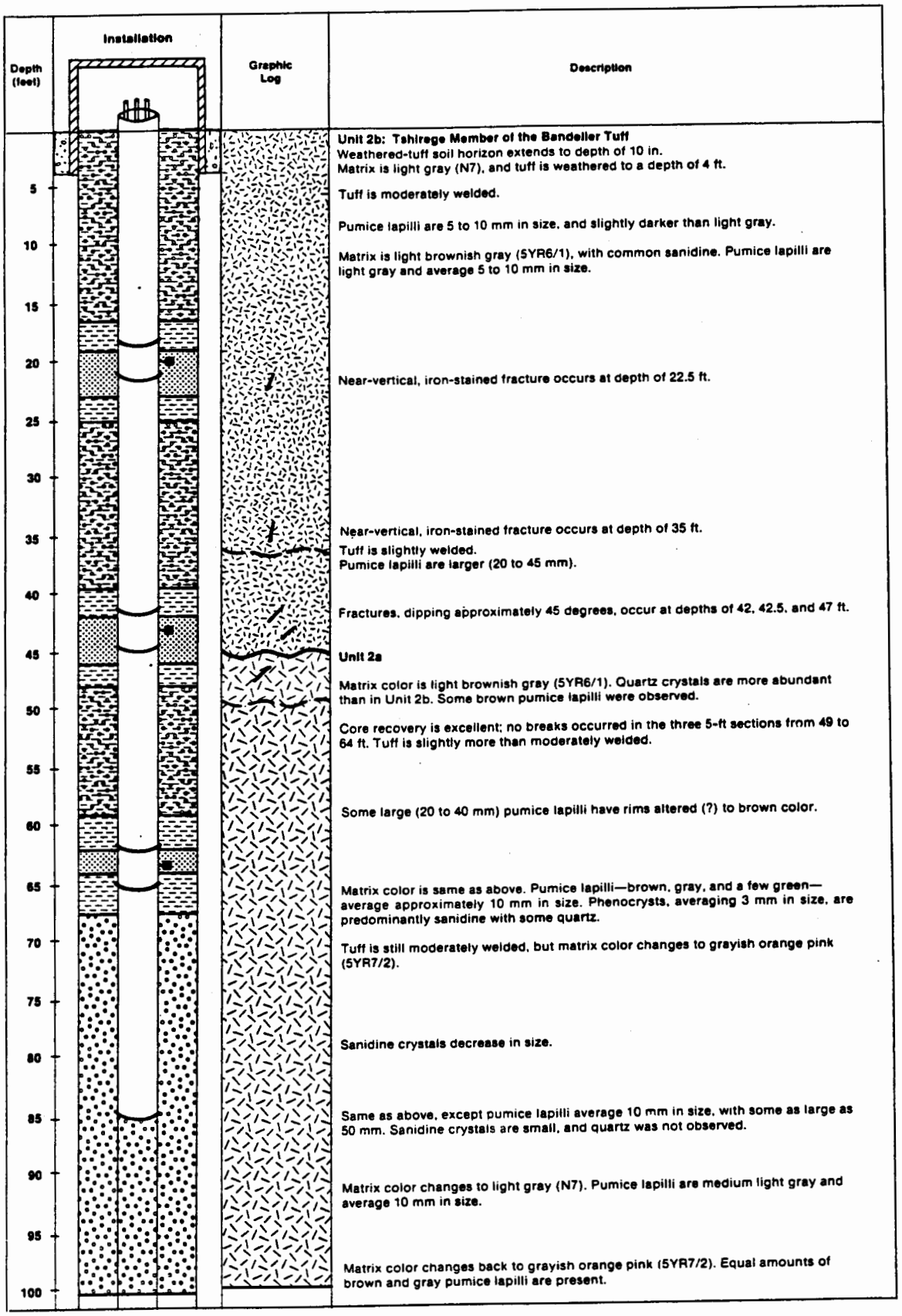

Figure A-12. Installation of Pore-Gas Sampling Ports in Hole LLC-85-13

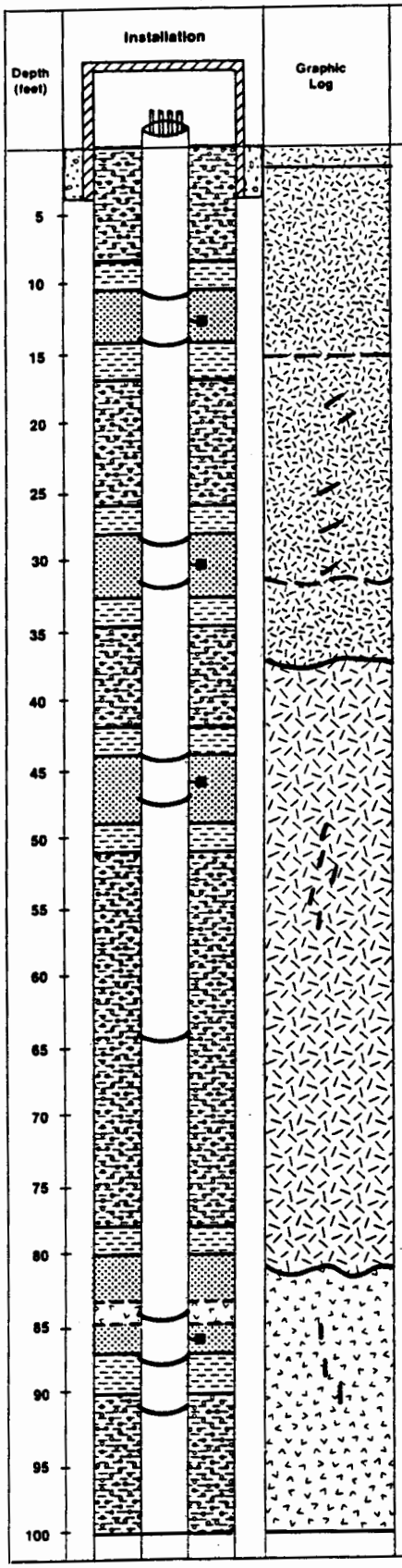

Description

Unit 2b: Tshirege Member of the Bandelier Tuff

Tuff is moderately welded, and matrix color is light brownish gray (5YR6/1). Horizontal fracture occurs at depth of 1.5 ft. Pumice lapilli are small and gray. Quartz and sanidine crystals are small and clear.

Matrix color changes to very light gray (N8), which probably represents the contact with the lower flow of Unit 2b.

Fractures, dipping approximately 45 degrees, occur at depths of 18 ft 2 in. and 19 ft 3 in.

Lithic lapilli are sparse and range up to 30 mm in size.

Matrix color changes back to light brownish gray (5YR6/1) at depth of 26 ft. Fractures, dipping approximately 45 degrees, occur at depths of 25 and 28 ft.

Pumice lapilli—some brown, some gray—range in size from 10 to 40 mm.

Drilling becomes much easier at depth of 32 ft, representing the contact with the slightly welded base of Unit 2b. Matrix color changes to grayish orange pink (5YR7/2). Fracture, dipping approximately 45 degrees, occurs at depth of 31 ft.

Unit 2a

Tuff is slightly welded, and matrix color is light brownish gray (5YR6/1). Pumice lapilli—some brown, some green—range in size from 10 to 30 mm.

Tuff is slightly welded, and matrix color changes to grayish pink (5R8/2). Lithic lapilli are sparse and average 5 to 10 mm in size, with some up to 40 mm. Pumice lapilli are same as above.

Near-vertical fractures occur at depths of 49, 52, 53, 54, and 57 ft. This may be one fracture, observed entering and exiting the core.

Tuff is moderately welded, and matrix changes to a color between grayish pink (5R8/2) and grayish orange pink (5YR7/2). Pumice lapilli are predominantly brown, and average 10 to 40 mm in size. Lithic lapilli are still sparse, but larger (20 to 40 mm).

Matrix color changes to grayish orange pink (5YR7/2); otherwise same as above except fewer lithic lapilli.

Same as above, except lithic lapilli are more abundant.

Same as above, except no lithic lapilli were observed.
Tuff is slightly welded. Matrix color lightens to grayish pink (5R8/2). Pumice lapilli—brown and green—are larger (20 to 50 mm). Sanidine and quartz crystals are very small and clear.

Unit 1b

Tuff is slightly welded. Matrix color changes to light gray (N7). Brown pumice lapilli are smaller (10 to 25 mm). Lithic lapilli and quartz crystals are common, the latter ranging up to 3 mm in size. Near-vertical fractures occur at depths of 85, 88, and 89 ft.

Same as above, except quartz crystals are larger (4 mm) and more abundant.

Figure A-13. Installation of Pore-Gas Sampling Ports in Hole LLC-85-14

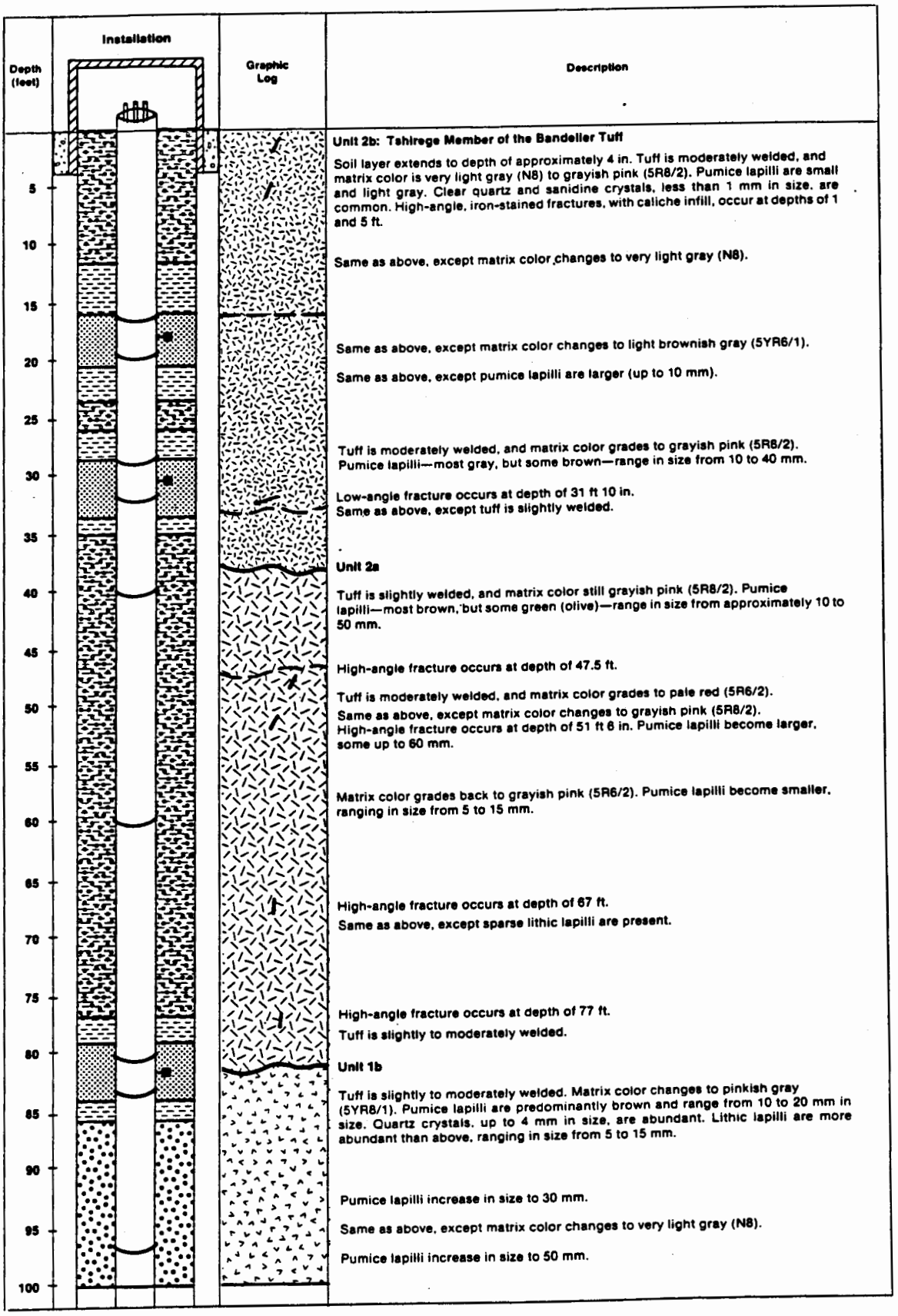

Figure A-14. Installation of Pore-Gas Sampling Ports in Hole LLC-85-15

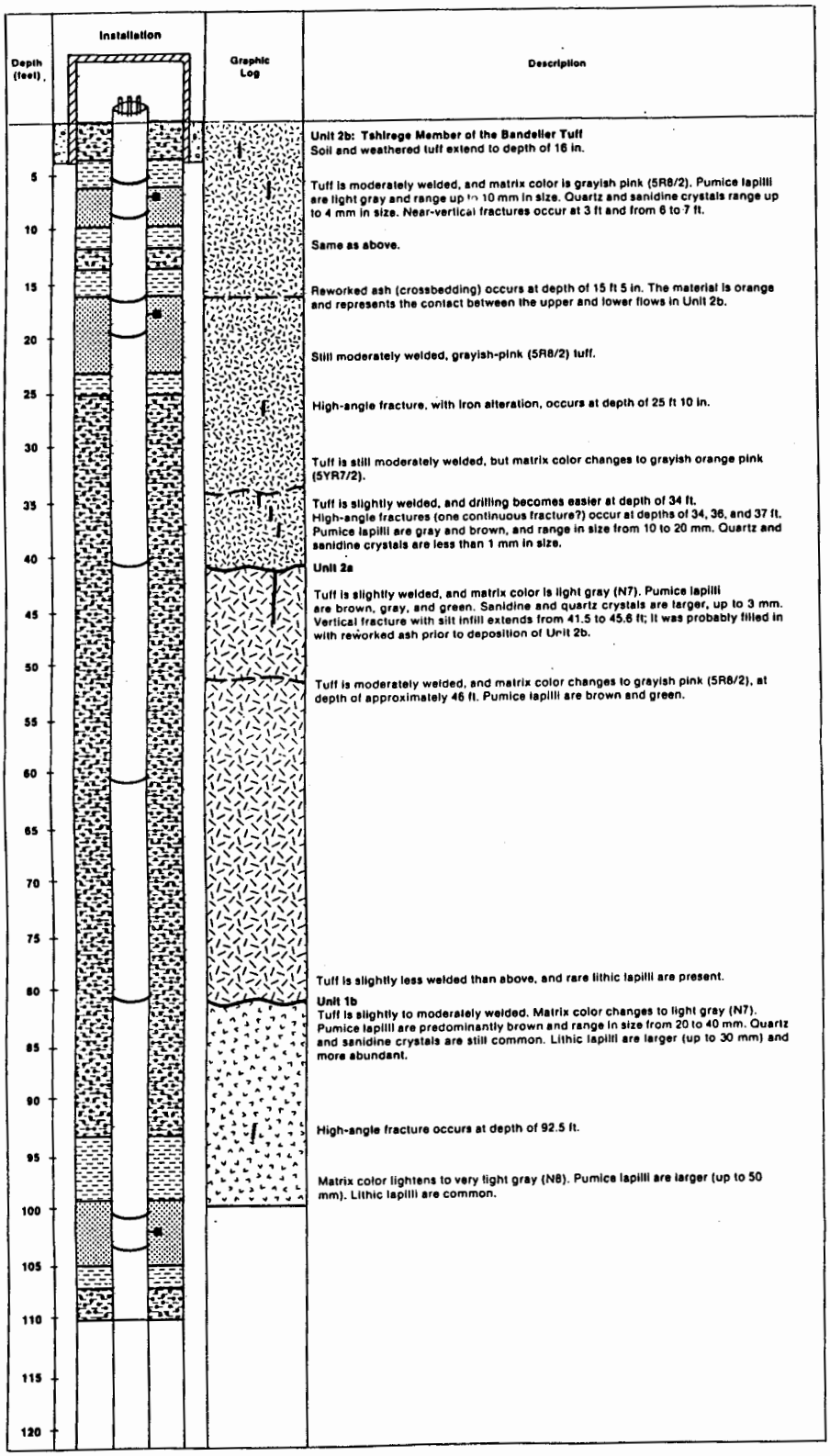

Figure A-15. Installation of Pore-Gas Sampling Ports in Hole LLC-85-16

Depth (feet)	Sample Interval	Sample Number	Graphic Log	Description
				Unit 2b: Tshirege Member of the Bandelier Tuff
				Soil and weathered tuff extend to approximately 3 ft.
5				Tuff is moderately welded, and matrix color is light gray (N7). Pumice lapilli are gray and range in size from 5 to 10 mm. Quartz and sanidine crystals, less than 1 mm in size, are abundant.
		85.05230 85.05113		
10		MCG-644*		Same as above. Altered, high-angle fracture, with silt infill and roots, occurs at depth of 11 ft 2 in.
15				Matrix color is grayish pink (5R8/2) and pumice lapilli are larger (up to 30 mm), representing transition to lower flow of Unit 2b. Quartz and sanidine crystals same as above.
		85.05231 85.05114		
20				
25				Same as above, except sparse lithic lapilli are present and quartz and sanidine crystals increase in size to 3 mm.
		85.05232 85.05115		
30				High-angle fracture extends from 27 to 28.5 ft.
35				Slightly welded base of Unit 2b; drilling becomes easier. Pumice lapilli increase in size to 50 mm, while quartz and sanidine crystals decrease in size to less than 1 mm.
		85.05233 85.05116		**Unit 2a**
40				Tuff is slightly welded. Matrix color is pale red (5R6/2). Pumice lapilli are brown and green, and range in size from 10 to 30 mm. Quartz and sanidine crystals range up to 2 mm in size.
45				Tuff is moderately welded; matrix color lightens to grayish pink (5R8/2) at depth of approximately 45 ft.
		85.05234 85.05117		
50				Same as above.
55				
		85.05235 85.05118		
60				Same as above, except pumice lapilli are larger (up to 40 mm) and quartz and sanidine crystals are smaller (less than 1 mm). High-angle fracture occurs at depth of 61 ft.
65				
		85.05236 85.05119		
70				Same as above, except tuff is slightly welded.
75				
		85.05237 85.05120		
80				Same as above.
				Unit 1b
85				Tuff is slightly welded, and matrix color changes to light gray (N7). Lithic lapilli are present in minor amounts, ranging in size to 20 mm. Pumice lapilli—most brown, but some green—range up to 40 mm in size. Quartz crystals are larger and honey-colored.
		85.05238 85.05121		
90				
95				
		85.05239 85.05122		
100				Tuff is slightly to moderately welded, and matrix color changes to grayish orange pink (10R8/2). Pumice lapilli are brown and range up to 50 mm in size. Quartz and sanidine crystals, ranging up to 2 mm in size, are common. Lithic lapilli, ranging up to 50 mm in size, are also common.
105				
		85.05240 85.05125		Tuff becoming moderately welded.
110		MCG-645*		Same as above, except small (2 to 4 mm) lithic lapilli are abundant.
115				Matrix color changes to more intense grayish orange pink (5YR7/2). Quartz crystals are gold, bipyramidal, and more abundant than above. Small (less than 1 to 2 mm) lithic lapilli are very abundant, but those as large as 60 mm are sparse.
		MCG-550* 85.05241 85.05126		
120				Same as above, except matrix color changes to light brown (5YR6/4).
				High-angle fracture extends from 122 to 123 ft.
125				
		MCG-601* 85.05242 85.05127		Tuff is slightly welded, and matrix color changes to moderate orange pink (5YR8/4). Pumice lapilli are grayish orange (similar to those in Unit 1a) and range up to 50 mm in size. Rest of matrix is similar to above.
130				
135				Occasional greenish pumice lapilli are present.
		85.05243 85.05128		
140				**Unit 1a**
145				Completely nonwelded ash, moderate orange pink (5YR8/4) in color. Large grayish-orange (10YR7/4) pumice lapilli are abundant. Lithic lapilli range up to 50 mm in size.
		85.05244 85.05129		
150				

Figure A-16. Lithologic Log of Hole LLC-85-17

Depth (feet)	Sample Interval	Sample Number	Graphic Log	Description
				Unit 2b: Tshirege Member of the Bandelier Tuff
				Weathered tuff (fill?) extends to depth of 4 ft.
5				Tuff is moderately welded, and matrix color is light gray (N7). Pumice lapilli are gray and range from 5 to 10 mm in size. Quartz and sanidine crystals, up to 1 mm in size, are abundant.
		85.05245		
10		85.05130		Low-angle fracture occurs at depth of 11 ft.
15				Pumice lapilli are larger, which may indicate transition to lower flow of Unit 2b.
		85.05246		
20		85.05131		Same as above, except quartz and sanadine crystals increase in size to 3 mm.
25				
		85.05247		
30		85.05132		
35				Tuff is slightly to moderately welded. Matrix color changes to pale red (5R6/2) at depth of 33 ft. Pumice lapilli are larger (10 to 20 mm), while quartz and sanidine crystals are smaller (less than 1 mm). High-angle fracture, with iron alteration, extends from 33 to 35 ft.
		85.05248		
40		85.05133		**Unit 2a** Tuff is slightly to moderately welded. Matrix color is still pale red (5R6/2). Quartz crystals are larger (up to 3 mm). Pumice lapilli change from gray to brown and green.
45				
		85.05249		
50		85.05134		Same as above, except quartz crystals decrease in size to less than 1 mm.
55				
		85.05250		
60		85.05135		Same as above, except sparse lithic lapilli, 5 to 10 mm in size, are present.
65				
70				No core was recovered for the interval 64 to 74 ft.
75				Same as above, but tuff is only slightly welded.
		85.05252		
80		85.05137		High-angle fracture extends from 78 to 79 ft. **Unit 1b** Tuff is slightly welded. Matrix color changes to light gray (N7) at depth of 79 ft, and to very light gray (N8) at depth of 84 ft. Pumice lapilli are predominantly brown. Lithic lapilli are sparse.
85				
		85.05253		
90		85.05138		
95				Same as above.
		85.05254		
100		85.05139		

Figure A-17. Lithologic Log of Hole LLC-85-18

Depth (feet)	Sample Interval	Sample Number	Rock Quality Designation/ Recovery (%)	Installation	Graphic Log	Description
						Unit 2b: Tshirege Member of the Bandelier Tuff
5			?/0			Soil horizon extends to about 10 in. in depth. Matrix is light gray (N7). Pumice lapilli are light gray to gray and have iron-stained alteration rims. Tuff is moderately welded.
10		R5-1	90/100			Near horizontal iron-stained fracture at depth of 10 ft. Abundant phenocrysts of quartz (3-5 mm) and sanidine (1-3 mm).
15		R5-2	80/90			Matrix color changes to grayish orange pink (5YR 7/2). Scattered lithic lapilli up to 10 mm are present.
20		R5-3	0/100			Color as above; tuff is slightly welded.
25			100/100			Pumice lapilli slightly darker than above (5YR 6/1) and are occasionally flattened. Scattered lithic lapilli up to 30 mm are present. Tuff becomes moderately welded. Near-vertical fractures with iron-staining are present at depths of 23 and 25 ft.
30		R5-4	30/100			Tuff becoming slightly welded. Small, 1- to 2-mm spots of rust colloration are present.
35			0/100			**Unit 2a**
40		R5-5	0/100			Tuff appears fissile and is nearly non-welded. Matrix color is still grayish orange pink (5YR 7/2). Tuff still contains abundant spots of local iron-staining.
45			0/100			Tuff is slightly welded. Pumice lapilli appear slightly larger than above, and some are greenish-gray in color.
50		R5-6	0/100			Vertical fracture with only minor iron-staining from a depth of 50 to 53 ft.
55			14/100			Tuff is more coherent than above, but still only slightly welded. Scattered pumice lapilli are up to 30 mm in size but most average around 3-4 mm.
60		R5-7	0/100			As above; tuff is slightly welded.
65			0/100			
70		R5-8	5/90			Lithic lapilli around 2 mm in size begin to appear. Pumice lapilli are mostly gray and display alteration rinds of rust-color.
75			5/100			Tuff becomes moderately welded.
80		R5-9	60/100			Occasional lithic fragments up to 30 mm. Matrix color becoming grayer (5YR 7/1). Iron rust-spots (1 to 2 mm) are still common. Pumice lapilli appear slightly flattened.
85			100/20			Tuff becomes slightly welded. Pumice lapilli average 6 to 8 mm, are not flattened, and are about 70% gray and 30% greenish-colored. Trace of 1- to 2-mm sanidine is present.
90		R5-10	15/100			
95			0/100			Rare lithic lapilli are up to 30 mm in size. Matrix color between pinkish gray and pinkish white (5YR 7/2 to 5YR 8/2).
100		R5-11	20/100			**Unit 1b**
105			13/100			Matrix color is pinkish white (5YR 8/2). Tuff is slightly welded. Brown-colored pumice lapilli predominate. Minor amounts of quartz and sanidine are present.
110		R5-12	0/100			Matrix color is white (5YR 8/1).
115			26/100			Pumice lapilli are dominantly brown in color. Lithic lapilli from less than 1 to 5 mm becoming abundant.
120		R5-13	18/100			Scattered white colored pumice lapilli are present. Quartz phenocrysts (many obviously bipyramidal) are becoming more abundant. Minor sanidine phenocrysts are present; these are not chatoyant, but can be identified on the basis of striated crystal faces.
125			26/100			Golden color of quartz phenocrysts is due to iron staining of the tuff immediately surrounding the quartz.
130		R5-14	20/100			Matrix color darkening slightly to pinkish white (5YR 8/2). Lithic lapilli becoming larger, up to 35 mm, but most fall into size range of 1-5 mm.
135			20/100			Transition to moderately welded portion of Unit 1b.
140		R5-15	40/100			Matrix color changes to orange (5YR 7/4). Tuff feels damp to the touch immediately upon retrieval.
145			30/100			Core must be struck with a hammer to break and is moderately welded.
150		R5-18	84/100			Probable vertical fracture present from 152 to 153 ft.
155			30/100			Tuff becomes slightly welded.
160		R5-19 MCG-653	0/80			**Unit 1a** Tuff is non-welded. Lithic lapilli predominantly from 2-5 mm in size with some up to 30 to 60 mm. Quartz phenocrysts, similar to above units, increase in number. Matrix color as above. Pumice lapilli are a distinctive tan color. Scattered reddish-yellow (5YR 6/6) pumice lapilli.
165			0/80			
170		R5-20	0/100			Matrix color changes to a tannish color (7.5YR 7/4) at 169.5 ft.
175		MCG-652	0/100			Occasional tan pumice lapilli up to 45 mm.
180		R5-21	0/100			
185			0/100			
190		R5-22 MCG-651	0/100			Color changes to pink (5YR 7/3).
195			0/100			Tuff becomes slightly welded at 194 ft.
200		R5-23				

Figure A-18. Lithologic Log of Hole LLC-86-19

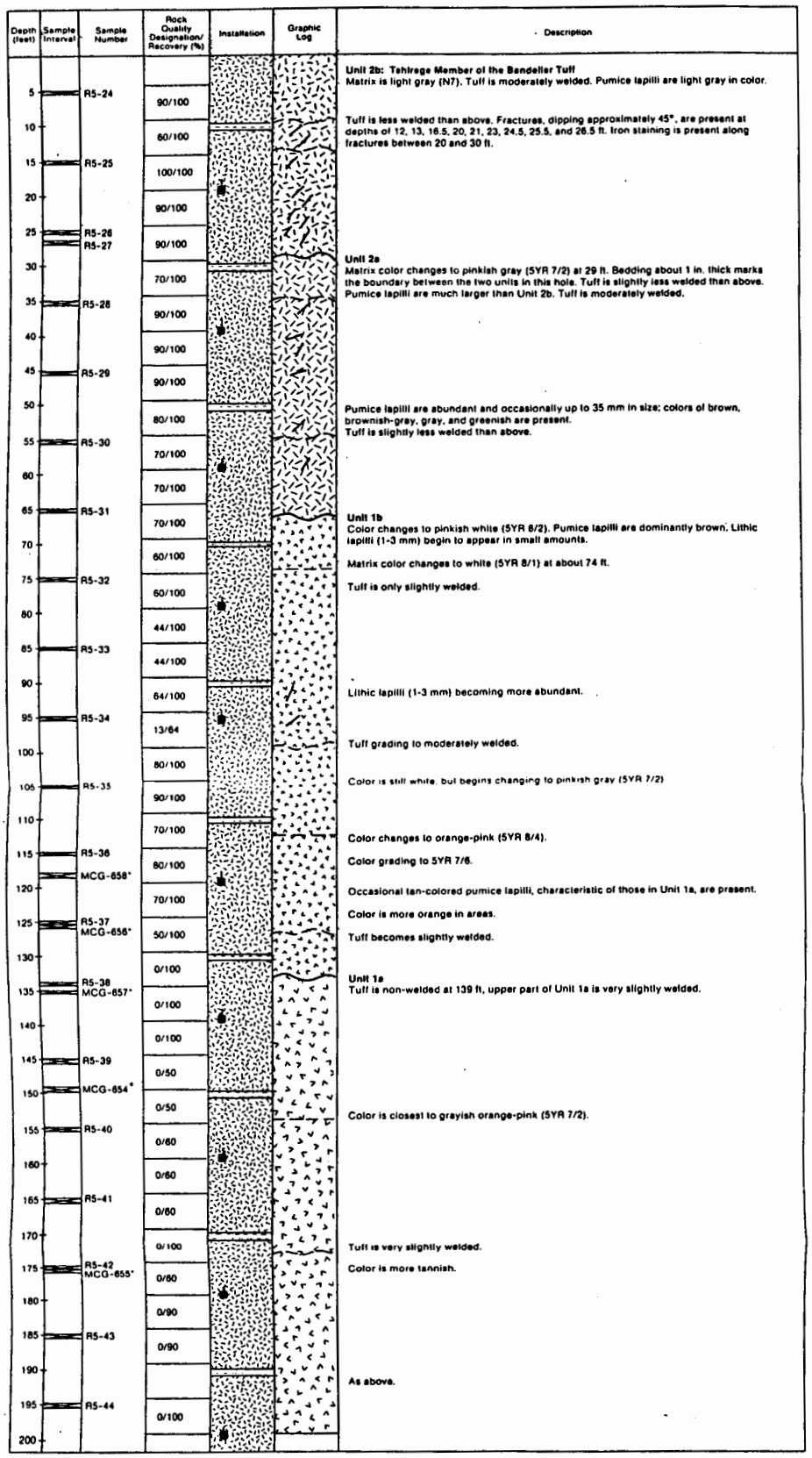

Figure A-19. Lithologic Log of Hole LLC-86-20

Depth (feet)	Sample Interval	Sample Number	Rock Quality Designation/ Recovery (%)	Installation	Graphic Log	Description
						Unit 3b: Tshirege Member of the Bandelier Tuff Matrix color is pinkish white (5YR 8/2). Tuff is moderately welded. High-angle fracture(s) are present at 6 and 8 ft depths, both with caliche infill.
5			90/100			
10			100/100			Color grades to white (5YR 8/1).
15		R5-48	90/100			Pumice lapilli are gray, visibly flattened, and average from 2-6 mm in size.
20			72/100			Tuff is slightly less welded than above, but still moderately welded.
25		R5-49	70/100			Matrix color as above.
30			90/100			Tuff is moderately welded. Lithic fragments, few up to 10 mm, most 2-4 mm, are present. High-angle fracture(s) are present at 33 and 34 ft depths. Pumice lapilli becoming larger (some greater than 2 cm diameter) and more abundant at a depth of 30 ft.
35		R5-50	90/100			Tuff grades into slightly welded base. Pumice lapilli are smaller and mostly flattened.
40			20/100			**Unit 2a** Reworked tuff zone from 41 to 41.13 ft marks boundary between two units. Matrix color still white, but closer to 7.5YR N 8/1. Pumice lapilli become larger, many up to 20 mm, and are slightly flattened. Slightly welded upper portion of unit grades to moderately welded at approximately 49 ft depth.
45		R5-51	30/100			
50			78/100			
55		R5-52	60/100			
60			60/100			Pumice lapilli dominantly gray in color.
65		R5-53	64/100			
70			48/100			Tuff becomes slightly welded.
75		R5-54	50/100			**Unit 1b** Contact marked by vivid color change to pinkish gray (5YR 7/2) at 73.2 ft. Pumice lapilli are dominantly brown in color. Very small (1 to 2 mm) lithic lapilli are present but sparse. Fracture (45°) with no infill at around 79 ft. Quartz phenocrysts are rare and mostly < 1 mm. Lithic lapilli still sparse but up to 4 mm.
80			42/100			
85		R5-55	20/100			Fracture(s) present at 85, 87, and 88 ft, none with infill, all around 45°.
90			20/100			Matrix color changes gradually to pinkish white (5YR 8/2).
95		R5-56	18/100			Lithic lapilli range in size up to 7 mm. Quartz phenocrysts become more abundant. Matrix color is closer to white (5YR 8/1).
100			18/100			
105		R5-57	18/100			Pumice lapilli are larger. Lithic lapilli are more abundant and range up to 15 mm in size.
110			22/100			Pumice lapilli are smaller and range from 5 to 20 mm. Lithic lapilli are dominantly from 1-3 mm in size; few range up to 10 mm. Matrix color changes to pinkish white (5YR 8/2). Tuff becomes moderately welded at a depth of 114 ft.
115		R5-58	90/100			
120			20/100			Tuff is highly fractured from 120 to 133 ft, but is still moderately welded. Fractures have no infill.
125		R5-59	30/100			
130			50/100			Color changes to pinkish orange (5YR 7/4) at 133 ft. Fractures, dipping at 45°, are present at 134.5 and 138 ft.
135		R5-60	40/100			
140			90/100			Tannish pumice lapilli typical of Unit 1a begin appearing. Fracture(s) present at 140 and 141 ft, dipping around 45°.
145		R5-61	0/100			Tuff becomes slightly welded at around 145 ft.
150			0/100			**Unit 1a** Tuff grades from slightly welded to nonwelded at 154 ft. Lithic lapilli are smaller and less abundant. Abundant tannish pumice lapilli are present.
155		R5-62	0/80			
160			0/90			Matrix color gradually changing to pinkish gray (5YR 7/2) at around 163 ft.
165		R5-63	0/80			Pumice lapilli are abundant and range in size from 5-25 mm. Lithic lapilli are scattered and range in size up to 5 mm.
170			0/80			
175		R5-64	0/60			
180			0/60			As above.
185		R5-65	0/60			
190			0/60			
195		R5-66	0/40			
200						

Figure A-20. Lithologic Log of Hole LLC-86-21

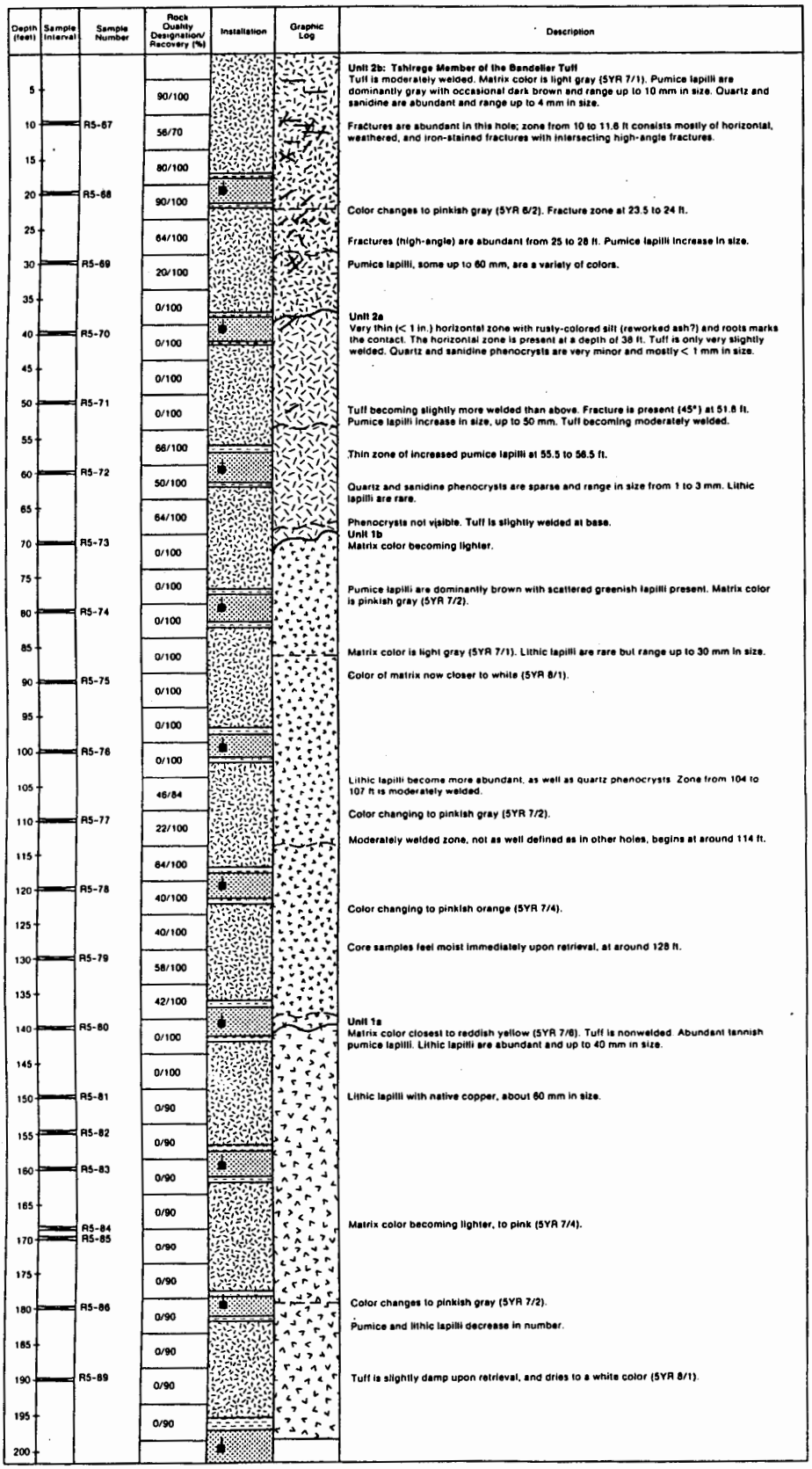

Figure A-21. Lithologic Log of Hole LLC-86-22

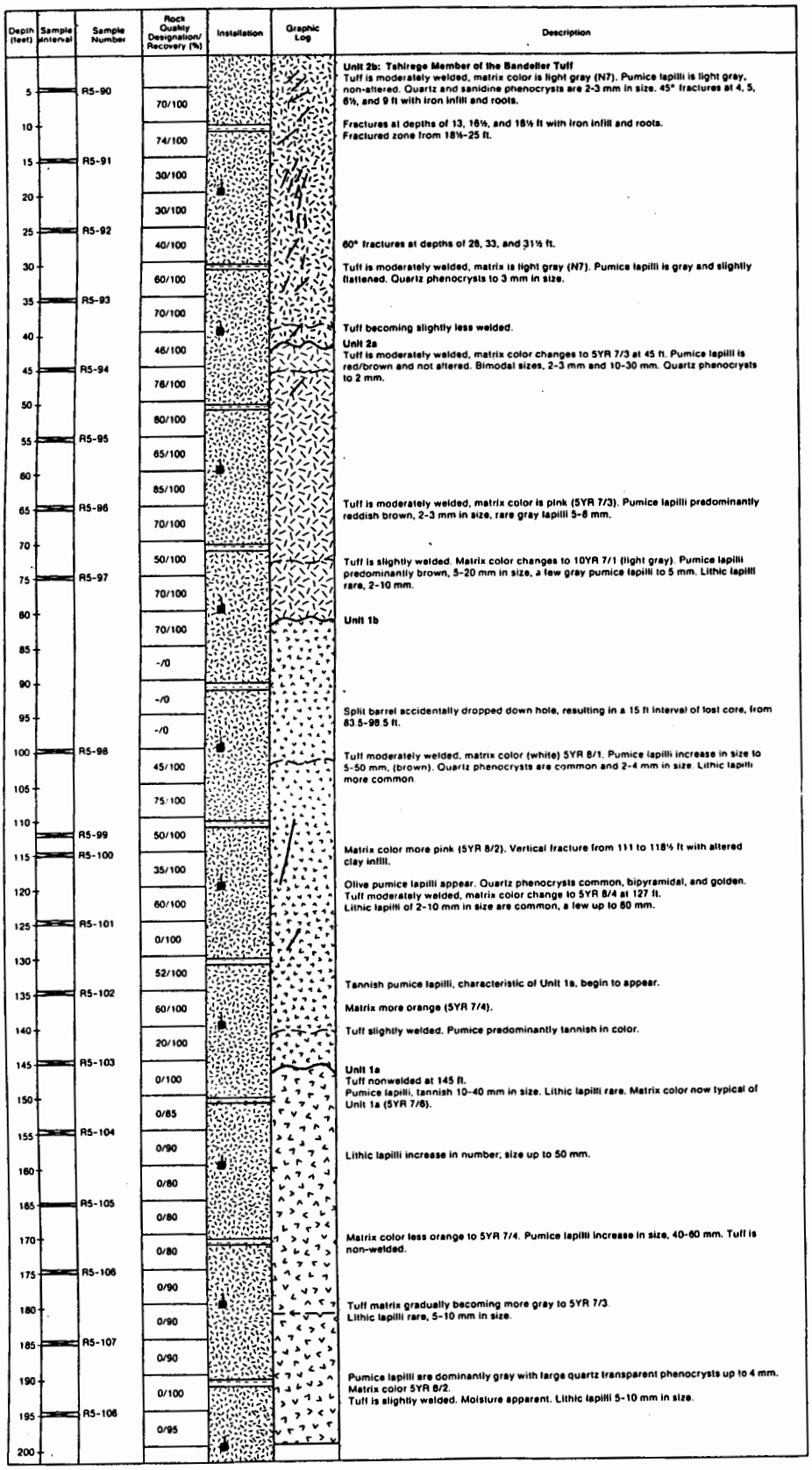

Figure A-22. Lithologic Log of Hole LLC-86-23

Depth (feet)	Sample Interval	Sample Number	Rock Quality Designation/ Recovery (%)	Installation	Graphic Log	Description
						Unit 2b: Tshirege Member of the Bandelier Tuff Tuff is moderately welded, matrix color is light gray (5YR 7/1). Horizontal fractures at 5 and 7 ft, both with iron staining. 60° fracture at 7½ ft, with iron staining.
5		R5-111	80/100			
10			90/100			Pumice lapilli, from 5-10 mm in size, gray in color. Quartz phenocrysts < 1 mm. Chatoyant sanidine < 1 mm. Horizontal fractures at 14½ ft with iron staining.
15		R5-112	90/100			
20			30/100			
25		R5-113	70/100			Two parallel vertical fractures from 20½ to 25 ft. 75° fracture at 27 ft. Pumice lapilli increase in size to 20 mm.
30			40/100			Vertical fracture from 31 to 34 ft with 10 mm thick clay infill. Organic odors noted.
35		R5-116 R5-114	40/100			60° fractures at 36, 40, and 43 ft.
40			70/100			Tuff is slightly welded. Metric color changes to 5YR 6/2 at 44 ft (pinkish gray).
45		R5-115	70/100			**Unit 2a** Pumice lapilli, red and brown, abundant, 10-30 mm in size. 60° fracture at 47 ft with iron stainings.
50		R5-117	20/100			Vertical fracture at 52½ ft with clay infill and roots. Tuff is moderately welded.
55		R5-118	20/100			Vertical fracture at 58½ ft. Pumice lapilli, gray, 10-40 mm in size. 65° fracture at 60 ft.
60			60/100			
65		R5-119	30/100			
70			50/100			Tuff is less welded, still moderate. Matrix less pink, color to 7.5YR 7/1. Pumice lapilli slightly flattened and brown.
75		R5-120	20/100			Tuff is now slightly welded. Lithic lapilli rare, 5-10 mm in size.
80			20/100			**Unit 1b** Matrix color more orange to 5YR 7/2.
85		R5-121	40/100			
90			60/100			Vertical fracture from 87½-88 ft. Highly-fractured zone from 88 to 89 ft.
95		R5-122	50/100			Tuff is slightly welded. Matrix becomes white (5YR 8/1).
100			54/100			
105		R5-123	54/100			Tuff becomes moderately welded. Pumice lapilli are dominantly brown, to 60 mm in size, with some olive-colored pumice lapilli. Lithic lapilli are common, 5-15 mm in size. Quartz and sanidine phenocrysts are more abundant.
110			54/100			
115		R5-124	60/100			
120			50/100			Abrupt matrix color change at 127 ft to pinkish orange (5YR 8/4).
125		R5-125	50/100			
130			50/100			Quartz phenocrysts are euhedral and bipyramidal.
135		R5-126	50/100			Pumice lapilli are tannish and flattened; 10-40 mm in size. Vertical fracture at 138½-140 ft. Lithic lapilli common, 10-30 mm in size.
140			40/100			Tuff becomes slightly welded.
145		R5-127	0/100			**Unit 1a** Tuff is nonwelded at a depth of 44 ft. Lithic lapilli are rare. Matrix color is reddish yellow (5YR 7/8).
150			0/50			
155		R5-128	0/80			
160			0/80			Matrix color not as bright and is closer to 5YR 7/6 (still reddish yellow).
165		R5-129	0/80			Pumice lapilli are tannish in color and range in size from 10-30 mm.
170			0/80			Matrix more tan to 5YR 7/4 (pink). Lithic lapilli increase in number and range in size from 5-20 mm.
175		R5-130	0/80			
180			0/80			
185		R5-131	0/80			Matrix color is pink (5YR 8/3).
190			0/70			Tuff becomes slightly welded. Lithic lapilli are still common.
195		R5-132	0/70			
200						

Figure A-23. Lithologic Log of Hole LLC-86-24

Depth (feet)	Sample Interval	Sample Number	Rock Quality Designation/ Recovery (%)	Graphic Log	Description
					Unit 2b: Tshirege Member of the Bandelier Tuff Moderately welded tuff. Matrix color is light gray (5YR 7/1). Pumice lapilli are gray and range in size from 5-10 mm. Quartz and sanidine phenocrysts are visible but are less than 1 mm in size.
5		R5-135	60/100		
10			100/100		Fracture, dipping around 45°, at depth of 10.7 ft. Matrix changes color to pinkish white (5YR 8/2) at 13 ft.
15		R5-136	80/100		
20			80/100		Quartz phenocrysts are up to 4 mm in size. High angle fractures are present at depths of 20, 21, 22.5 ft; iron staining is present on surface.
25		R5-137	50/100		Fracture zone from 23 to 26 ft; organic vapor odors were detected. Matrix color is gray (5YR 6/1). Quartz and sanidine crystals are abundant.
30			60/100		
35		R5-138	80/100		Tuff is still moderately welded. Fractures dipping about 45° are present at depths of 30.5, 33, 34, and 35 ft; organic vapor odors are stronger than above. **Unit 2a**
40			60/100		Matrix is pinkish gray (5YR 7/2). Tuff is slightly less welded than above.
45		R5-139	60/100		
50			60/100		Fractures were noted at 50 and 55 ft depths, both dipping about 45°.
55		R5-140	50/100		Quartz and sanidine are abundant and are up to 2mm in size.
60			40/100		Pumice lapilli becoming larger, up to 30 mm.
65		R5-141	64/100		Matrix color is light gray (5YR 7/1). Phenocrysts are not visible. Fractures are present at 65.7 and 66.6 ft.
70			40/100		Tuff is slightly welded. **Unit 1b**
75		R5-142	34/100		Matrix color changes to pinkish white (5YR 8/2). Tuff is slightly welded. Lithic lapilli up to 2 mm were noted. Quartz phenocrysts are less than 1 mm in size. Pumice lapilli are mostly brown in color.
80			20/100		Matrix color closer to white (5YR 8/1).
85		R5-143	30/100		Lithic lapilli increase in size (up to 30 mm).
90			20/100		Pumice lapilli range in size from 10 to 30 mm.
95		R5-144	20/100		
100		R5-145	16/100		Rig shutdown because of strong organic vapors in breathing zone.
105		R5-146	20/100		Matrix color as above. Quartz phenocrysts becoming more abundant and range in size up to 3 mm. Pumice lapilli range in size from 10-20 mm. Lithic lapilli more prominent; some up to 20 mm in size. High angle fractures are present at depths of 105, 106, 107, and 112.5 ft.
110		R5-147	40/100		
115		R5-148	60/100		Tuff becomes moderately welded.
120		R5-149	70/100		Matrix color is pinkish orange (5YR 8/4). Fractures are present at depths of 122, 127, and 127.5 ft, with a dip of approximately 45°.
125		R5-150	60/100		Matrix color darkens to reddish yellow (5YR 7/6).
130		R5-151	60/100		Tannish pumice lapilli such as those common in Unit 1a begin to appear at around 130 ft.
135		R5-152	30/100		Tuff becomes slightly welded.
140		R5-153	0/90		**Unit 1a** Matrix color as above only mottled up to 5YR 7/8 in spots. Tuff is nonwelded.
145		R5-154	0/95		
150		R5-155	0/40		
155		R5-156	0/30		Large tannish pumice lapilli are common, few up to <60 mm in size.
160		R5-157	0/40		Matrix color changes to pinkish gray (5YR 7/2) at 161 ft.
165		R5-158	0/40		
170		R5-159	0/70		
175		R5-160	0/60		Matrix color closer to 5YR 7/3. Tannish pumice lapilli appear slightly flattened.
180		R5-161	0/80		Matrix color is pink (5YR 7/2).
185		R5-162	0/100		Tuff becomes slightly welded. Pumice lapilli (the typical tannish color) are extremely flattened.
190		R5-163	0/100		High-angle fractures are present at depths of 191 and 192 ft.
195		R5-164	0/70		Matrix color changes to pinkish gray.
200					

Figure A-24. Lithologic Log of Hole LLC-86-25

Appendix B

PETROGRAPHIC REPORTS

NOTE

Appendix B comprises two sections to reflect work completed during two fiscal years; each section addresses the analysis of petrographic samples from a particular set of drill-hole and outcrop samples. Section B.1 contains results of samples obtained from Holes LLM-85-01, -02, -06, -09, -11, -13, -14, and -17, which were cored as part of the Fiscal Year (FY) 1985 fieldwork. Sample numbers corresponding to this suite of samples are MCG-550, -601, and -626 through -650 (a total of 27 samples). Section B.2 consists of results of samples from Holes LLC-86-19 and LLC-86-20, cored during the FY 1986 field season, and from outcrops on the study site (also obtained during FY 1986). Sample numbers corresponding to these samples are MCG-651 through -661 (a total of 11 samples).

B.1 FISCAL YEAR 1985 FIELDWORK

A total of 27 drill-core samples from the Tshirege Member of the Bandelier Tuff were submitted to the GJPO Petrology Laboratory for petrographic characterization. Nine samples were from Unit 2b, four from Unit 2a, eight from Unit 1b, two from Unit 1a, and four were lithic lapilli from various units. Analytical procedures and results are described below.

The samples as received consisted of sections of 5-cm-diameter drill core. From these samples, portions were removed using a core splitter for polished thin-section preparation. The samples were impregnated with blue-colored epoxy to emphasize the porosity in the thin sections.* Each thin section, with the exception of the nonwelded samples from Unit 1a, was subjected to point-count analysis (300 counts) to determine mineral and component abundance. Tuffaceous rocks were named according to the classification of Cook (1965). As shown in Figure B-1, the rocks from this study plot in the following fields: II (lithic-crystal tuff), III (lithic-vitric), IV (crystal-lithic), V (vitric-lithic), VII (crystal-vitric), and VIII (vitric-crystal).

The optical identifications of major and minor minerals, especially devitrification products, were confirmed using X-ray diffraction (XRD). The clay-sized fractions were separated from fracture coatings in Samples MCG-629, -630, -643, -644, and -648. These clay-sized separates were smeared or sedimented onto glass slides and analyzed in four different states: air-dried, glycolated, heated to 330°C, and heated to 550°C.

The compositional modifiers to tuffaceous rock names are based on the bulk XRD data. These modifiers were assigned according to the classification of Streckeisen (1967).

Petrographic descriptions of the samples are presented on the pages following Figure B-1. They are presented in consecutive order by sample number, although the drill-hole number, depth of the sample, and geologic unit are also identified near the top of the page. The volume percent of each mineral component is given, together with the petrographic description. Phenocrysts and groundmass are further subdivided into individual components, and these subcomponents are followed by a number in parentheses which indicates their volume percentage of the main component. The petrographic descriptions were taken from a report entitled Petrography of the Tshirege Member of the Bandelier Tuff, Mesita del Buey, Los Alamos County, New Mexico (Fukui, 1985).

*There is considerable discrepancy between porosity measured in thin section and that determined by means of helium injection (cf. Section 3.1.2). The significantly lower porosity determined in thin section is due to the fact that most of the thin sections were cut parallel to the core axis (parallel to the direction of flattening), resulting in erroneous extrapolation based on the cross section of the gas tubes rather than on their true shape.

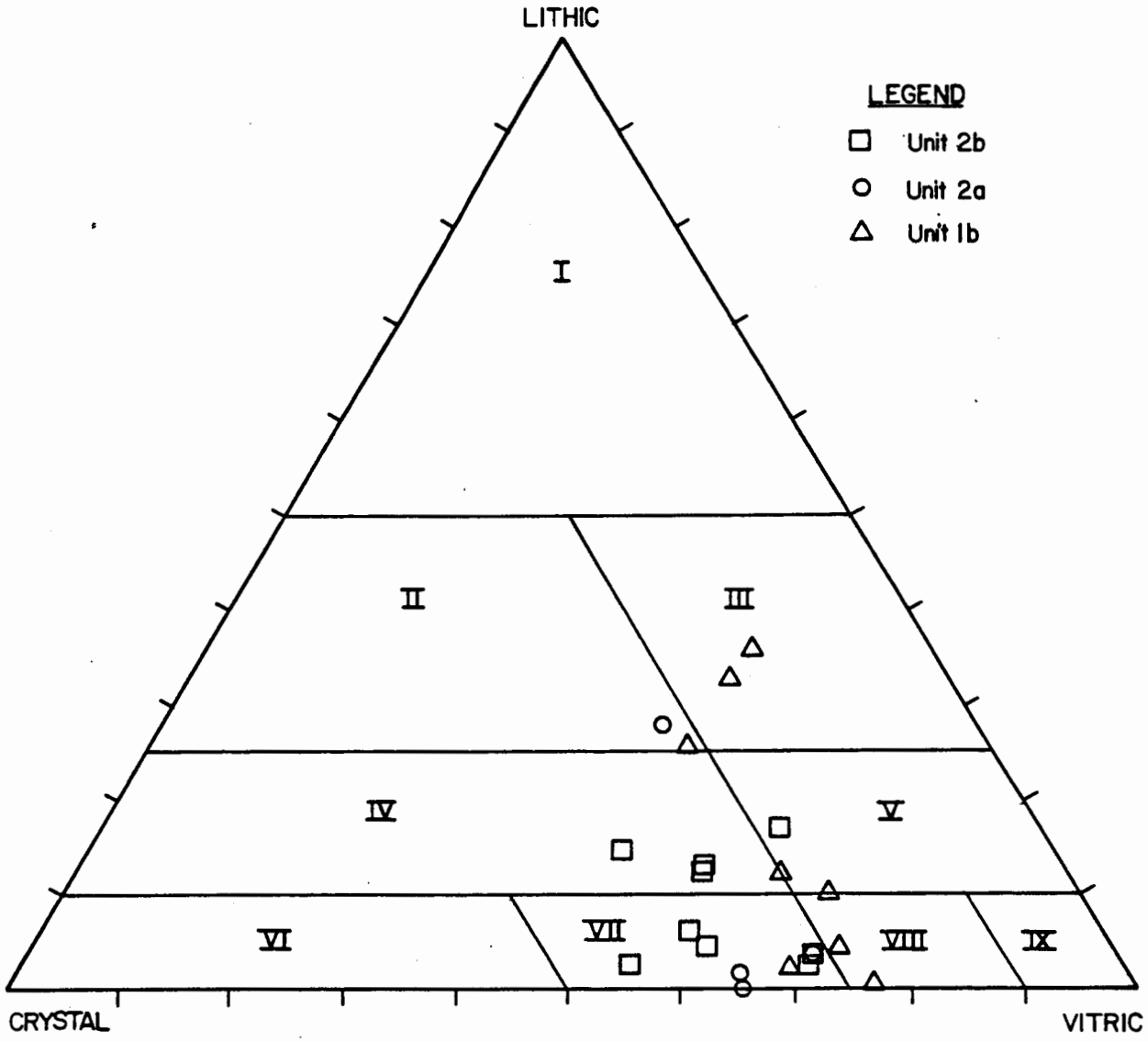

Figure B-1. Classification of Cook (1965) Used to Name Tuffaceous Rocks in This Study on the Basis of the Normalized Vitric (including pumice), Crystal, and Lithic Components Determined from the Modal Analysis

LANL VAPOR TRANSPORT STUDY
REQUEST NO.: 402553
PROJECT NO.: 6L0001000

SAMPLE NO.: MCG-550
DRILL HOLE LLM-85-17 UNIT 1B (LITHIC)
DRILL HOLE DEPTH (FT): 118

PHENOCRYST RATIO (Q/K/P): 1/6.67/0.33 DEGREE OF WELDING: Dense
POROSITY (VOL %): 10 OXIDATION STATE OF Fe-Ti OXIDES: C3-C4

ROCK NAME: Rhyolitic Vitric Tuff

GENERAL DESCRIPTION IN THIN SECTION: Densely welded glass with lithophysae filled by sanidine, tridymite, opaques, and late-stage alpha quartz. A few fine- to medium-grained phenocrysts are present.

MINERAL COMPONENT	VOL. %	COMMENTS
Groundmass	60	Densely welded glass with well-developed spherulitic devitrification. Glass is brown in part.
Vapor-Phase Minerals	28	
Sanidine	(73)	Porous, microcrystalline linings of lithophysae.
Tridymite	(18)	Fine grained, euhedral. Partially fills interiors of lithophysae. Wedge-shaped twins are common.
Alpha Quartz	(5)	Fine grained, anhedral. Late-stage filling of lithophysae.
Opaques	(4)	Fine grained, anhedral. Associated with sanidine stage of lithophysae filling. Magnetite/ilmenite altering to hematite.
Pore Space	10	Associated with vapor-phase crystallites.
Phenocrysts	2	
Sanidine	(83)	Fine to medium grained, euhedral to anhedral.
Alpha Quartz	(13)	Fine to medium grained, anhedral to euhedral. Embayed grains are present.
Plagioclase	(4)	Fine to medium grained, subhedral.
Opaques	(tr)	Fine grained, anhedral to subhedral. Magnetite intergrown with ilmenite.

LANL VAPOR TRANSPORT STUDY
REQUEST NO.: 402553
PROJECT NO.: 6L0001000

SAMPLE NO.: MCG-601
DRILL HOLE LLM-85-17 UNIT 1B (LITHIC)
DRILL HOLE DEPTH (FT): 128

POROSITY (VOL %): 1

OXIDATION STATE OF Fe-Ti OXIDES: C4

ROCK NAME: Hornblende Basalt Porphyry

GENERAL DESCRIPTION IN THIN SECTION: Fine- to medium-grained phenocrysts in a hyalopilitic groundmass. Glomeroporphyritic.

MINERAL COMPONENT	VOL. %	COMMENTS
Phenocrysts	32	
Plagioclase	(61)	Fine to medium grained, euhedral. Oscillatory zoning. Andesine. Embayed grains.
Hornblende(?)	(20)	Fine to medium grained, euhedral. Totally replaced by hematite and chlorite.
Biotite	(7)	Fine to medium grained, euhedral to subhedral. Partial replacement by hematite.
Pyroxene	(6)	Fine to medium grained, euhedral to subhedral. Hypersthene. Partial replacement by chlorite/serpentine.
Opaques	(5)	Fine grained, euhedral to subhedral. Magnetite with exsolved ilmenite; magnetite is oxidizing to hematite.
Olivine	(tr)	Medium grained, anhedral. Totally oxidized to hypersthene and magnetite.
Groundmass	68	Hyalopilitic.
Plagioclase	(94)	Felty laths.
Opaques	(2)	Magnetite oxidizing to hematite.
Glass	(1.5)	Brown-colored.
Pore Space	(1.5)	Microvugs in groundmass(?).
Biotite	(1)	Altered to chlorite and hematite.

LANL VAPOR TRANSPORT STUDY
REQUEST NO.: 402553
PROJECT NO.: 6L0001000

SAMPLE NO.: MCG-626
DRILL HOLE LLM-85-01 UNIT 2B
DRILL HOLE DEPTH (FT): 30

PHENOCRYST RATIO (Q/K/P): 1/2.26/0
POROSITY (VOL %): 23

DEGREE OF WELDING: Slight to Moderate
OXIDATION STATE OF Fe-Ti OXIDES: C4

ROCK NAME: Rhyolitic Crystal-Vitric Tuff

GENERAL DESCRIPTION IN THIN SECTION: Fine- to medium-grained phenocrysts (crystals) in a slightly to moderately welded glass groundmass. Intact glass bubble walls and Y-shaped shards are present.

MINERAL COMPONENT	VOL. %		COMMENTS
Groundmass		44	
Glass	(66)		Incipient axiolitic devitrification.
Pumice	(34)		Up to 2.59 mm. Replaced/mineralized by sanidine and tridymite. Phenocryst ratio (Q/K) = 1/3.
Phenocrysts		27	
Sanidine	(64)		Fine to medium grained, anhedral to subhedral.
Quartz	(28)		Fine to medium grained, anhedral to subhedral.
Opaques	(5)		Fine-grained, euhedral to subhedral. Ilmenite/magnetite altering to hematite.
Amphibole(?)	(3)		Fine grained, anhedral to subhedral. Lamprobolite, partially altered, with opaque rims.
Plagioclase	(tr)		Fine to medium grained, anhedral. Accidental crystal.
Biotite	(tr)		Fine grained, anhedral to subhedral.
Pore Space		23	
Lithic Fragments		5	Up to 10.4 mm. Consisting of an andesite, a rock similar to the host, and a plagioclase-sanidine fragment.
Zeolite		1	Very fine grained, euhedral. Isotropic; phase is probably analcime. Occurs in pore space.

LANL VAPOR TRANSPORT STUDY
REQUEST NO.: 402553
PROJECT NO.: 6L0001000

SAMPLE NO.: MCG-627
DRILL HOLE LLM-85-01 UNIT 2A
DRILL HOLE DEPTH (FT): 52

PHENOCRYST RATIO (Q/K/P): 1/1.79/0
POROSITY (VOL %): 13

DEGREE OF WELDING: Slight to Moderate
OXIDATION STATE OF Fe-Ti OXIDES: C2

ROCK NAME: Rhyolitic Crystal-Vitric Tuff

GENERAL DESCRIPTION IN THIN SECTION: Fine- to medium-grained phenocrysts in a groundmass that exhibits slight to moderate welding. Pumice fragments are generally coarser than those in Sample MCG-626 and the quartz phenocrysts are more embayed.

MINERAL COMPONENT	VOL. %		COMMENTS
Groundmass		62	
Pumice	(53)		Up to 13.9 mm. Replaced/mineralized by sanidine and tridymite. Phenocryst ratio (Q/K): 1/3. Some fragments altering to clay.
Glass	(47)		Incipient axiolitic devitrification.
Phenocrysts		23	
Sanidine	(62)		Fine to medium grained, subhedral to anhedral.
Quartz	(34)		Fine to medium grained, subhedral to euhedral. Some grains are embayed.
Opaques	(3)		Fine grained, euhedral to subhedral. Magnetite with exsolved ilmenite.
Pyroxene	(1)		Fine grained, anhedral to euhedral. Augite.
Pore Space		13	
Lithic Fragments		2	Up to 2.64 mm. Includes crystal-vitric tuffs with clay replacing the glass; strongly welded.
Unknown Component		tr	Rounded grain, 0.56 mm in longest axis, consisting of a thin rim of magnetite with randomly oriented clay (chlorite?) flakes and epidote or pyroxene grains.

LANL VAPOR TRANSPORT STUDY
REQUEST NO.: 402553
PROJECT NO.: 6L0001000

SAMPLE NO.: MCG-628
DRILL HOLE LLM-85-01 UNIT 1B
DRILL HOLE DEPTH (FT): 101

PHENOCRYST RATIO (Q/K/P): 1/2.25/0.06 DEGREE OF WELDING: Moderate
POROSITY (VOL %): 18 OXIDATION STATE OF Fe-Ti OXIDES: C2

ROCK NAME: Rhyolitic Vitric-Lithic Tuff

GENERAL DESCRIPTION IN THIN SECTION: Fine- to medium-grained phenocrysts in a moderately welded groundmass with incipient axiolitic devitrification. This sample contains more lithic fragments than Sample MCG-626 (Unit 2b) or Sample MCG-627 (Unit 2a).

MINERAL COMPONENT	VOL. %	COMMENTS
Groundmass	56	
Glass	(51)	Incipient axiolitic devitrification. Intact bubble walls and Y-shaped shards are present.
Pumice	(49)	Up to 8.89 mm. Spherulitic devitrification (rather than replaced by sanidine and tridymite as in Samples MCG-626 and -627). Phenocryst ratio (Q/K) = 1/3.67.
Phenocrysts	18	
Sanidine	(66)	Fine to medium grained, anhedral to euhedral.
Quartz	(30)	Fine to medium grained, anhedral to euhedral. Some grains are embayed.
Plagioclase	(2)	Medium grained, subhedral. Associated with pyroxene and magnetite-ilmenite. Zoned grain.
Opaques	(2)	Fine grained, anhedral to euhedral. Magnetite with exsolved ilmenite.
Pyroxene	(tr)	Fine grained, anhedral. One grain is coated by celadonite.
Pore Space	18	
Lithic Fragments	8	Up to 17.0 mm. Largest fragment is a thoroughly welded, crystal-vitric tuff. Other tuffs are altered to clay; basalts/andesites are present.

(continued on next page)

LANL VAPOR TRANSPORT STUDY
REQUEST NO.: 402553
PROJECT NO.: 6L0001000

SAMPLE NO.: MCG-628 (continued)
DRILL HOLE LLM-85-01 UNIT 1B
DRILL HOLE DEPTH (FT): 101

MINERAL COMPONENT	VOL. %	COMMENTS
Unknown Component	tr	Rounded grain, 0.62 mm in longest axis, consisting of clay (chlorite?) flakes in random orientation and magnetite with exsolved ilmenite. Magnetite is altering to hematite. Grain could be an altered mafic.

LANL VAPOR TRANSPORT STUDY
REQUEST NO.: 402553
PROJECT NO.: 6L0001000

SAMPLE NO.: MCG-629
DRILL HOLE LLM-85-01 UNIT 1B
DRILL HOLE DEPTH (FT): 122

PHENOCRYST RATIO (Q/K/P): 1/0.75/0
POROSITY (VOL %): 12

DEGREE OF WELDING: Moderate
OXIDATION STATE OF Fe-Ti OXIDES: C2-C3

ROCK NAME: Rhyolitic Vitric-Lithic Tuff

GENERAL DESCRIPTION IN THIN SECTION: Fine- to medium-grained phenocrysts in a moderately welded groundmass. Most shards show incipient alteration to clay. This sample is similar to MCG-628 except for the lack of significant devitrification of glass shards.

MINERAL COMPONENT	VOL. %		COMMENTS
Groundmass		55	
Glass	(63)		Shards are a mottled-brown color; this may be incipient alteration to clay. Intact bubble walls and Y-shaped shards are present.
Pumice	(37)		Up to 10.0 mm. Spherulitic devitrification. Phenocryst ratio (Q/K) = 1/4.25. One pumice fragment contains a pyroxene phenocryst.
Phenocryst		22	
Quartz	(54)		Fine to medium grained, anhedral to euhedral. Most grains are embayed.
Sanidine	(41)		Fine to medium grained, subhedral to euhedral.
Opaques	(5)		Fine grained, anhedral to euhedral. Magnetite with exsolved ilmenite.
Pyroxene	(tr)		Fine grained, anhedral to euhedral. Usually associated with opaques.
Pore Space		12	
Lithic Fragments		11	Up to 5.70 mm. Several thoroughly welded vitric-crystal tuffs with spherulitic devitrification are present. Also present are andesitic crystal-vitric tuffs that are moderately welded.

LANL VAPOR TRANSPORT STUDY
REQUEST NO.: 402553
PROJECT NO.: 6L0001000

SAMPLE NO.: MCG-630
DRILL HOLE LLM-85-02 UNIT 2B
DRILL HOLE DEPTH (FT): 37

PHENOCRYST RATIO (Q/K/P): 1/2.24/0.06 DEGREE OF WELDING: Moderate
POROSITY (VOL %): 16 OXIDATION STATE OF Fe-Ti OXIDES: C2

ROCK NAME: Rhyolitic Vitric-Lithic Tuff

GENERAL DESCRIPTION IN THIN SECTION: Fine- to medium-grained phenocrysts in a moderately welded groundmass. Shards show incipient axiolitic devitrification and clay coatings. Pumice fragments are mostly replaced by sanidine and tridymite as in Samples MCG-626 and -627.

MINERAL COMPONENT	VOL. %		COMMENTS
Groundmass		50	
Glass	(77)		Incipient axiolitic devitrification; glass is coated by clay. Y-shaped shards are present.
Pumice	(23)		Up to 8.74 mm. Replaced/mineralized by sanidine and tridymite. Phenocryst ratio (Q/K) = 1/4.
Phenocrysts		19	
Sanidine	(66)		Fine to medium grained, anhedral to euhedral. Some grains are embayed.
Quartz	(30)		Fine to medium grained, anhedral to euhedral. Some grains are embayed.
Plagioclase	(2)		Fine grained, subhedral.
Opaques	(2)		Fine grained, anhedral to euhedral. Magnetite with exsolved ilmenite.
Pyroxene	(tr)		Fine grained, anhedral to subhedral.
Amphibole	(tr)		Fine grained, anhedral.
Zircon	(tr)		Fine grained, euhedral.
Pore Space		16	
Lithic Fragments		14	Up to 15.8 mm. Several strongly welded, crystal-vitric tuffs with little or no devitrification of glass.

(continued on next page)

LANL VAPOR TRANSPORT STUDY
REQUEST NO.: 402553
PROJECT NO.: 6L0001000

SAMPLE NO.: MCG-630 (continued)
DRILL HOLE LLM-85-02 UNIT 2B
DRILL HOLE DEPTH (FT): 37

MINERAL COMPONENT	VOL. %	COMMENTS
Zeolite(?)	tr	Very fine grained, euhedral (radial acicular). Occupies pore space; too small for optical identification.
Unknown Component	tr	Euhedral grain shape (pyroxene?), 0.51 mm, at edge of thin section; consists of thin rim of magnetite and randomly oriented flakes of clay (chlorite?).

LANL VAPOR TRANSPORT STUDY
REQUEST NO.: 402553
PROJECT NO.: 6L0001000

SAMPLE NO.: MCG-631
DRILL HOLE LLM-85-02 UNIT 2A
DRILL HOLE DEPTH (FT): 64

PHENOCRYST RATIO (Q/K/P): 1/1.45/0
POROSITY (VOL %): 23

DEGREE OF WELDING: Moderate
OXIDATION STATE OF Fe-Ti OXIDES: C2-C3

ROCK NAME: Rhyolitic Crystal-Vitric Tuff

GENERAL DESCRIPTION IN THIN SECTION: Fine- to medium-grained phenocrysts in a moderately welded groundmass. Pumice fragments are mostly replaced by sanidine and tridymite.

MINERAL COMPONENT	VOL. %		COMMENTS
Groundmass		49	
Glass	(76)		Incipient axiolitic devitrification. Intact bubble walls and Y-shaped shards are present.
Pumice	(24)		Up to 7.26 mm. Replaced/mineralized by sanidine and tridymite. Phenocryst ratio (Q/K) = 1/4.
Phenocrysts		26	
Sanidine	(58)		Fine to medium grained, anhedral to euhedral.
Quartz	(40)		Fine to medium grained, anhedral to euhedral. Some grains are embayed.
Opaques	(1)		Fine grained, anhedral to euhedral. Magnetite-ilmenite intergrowths (exsolution).
Pyroxene	(1)		Fine grained, subhedral to euhedral. Usually associated with opaques.
Plagioclase	(tr)		Fine grained, euhedral.
Amphibole	(tr)		Fine grained, anhedral to euhedral.
Zircon	(tr)		Very fine grained, euhedral.
Pore Space		23	

(continued on next page)

LANL VAPOR TRANSPORT STUDY
REQUEST NO.: 402553
PROJECT NO.: 6L0001000

SAMPLE NO.: MCG-631 (continued)
DRILL HOLE LLM-85-02 UNIT 2A
DRILL HOLE DEPTH (FT): 64

MINERAL COMPONENT	VOL. %	COMMENTS
Lithic Fragments	1	Largest grain was on a corner of the thin section; grain is larger than 5.56 mm. Present are densely welded, partly devitrified vitric tuff; flow-banded rock; andesites; and other lithic types.
Zeolite(?)	1	Very fine grained, subhedral. Occurs in pore space.

LANL VAPOR TRANSPORT STUDY
REQUEST NO.: 402553
PROJECT NO.: 6L0001000

SAMPLE NO.: MCG-632
DRILL HOLE LLM-85-02 UNIT 2A (1B)
DRILL HOLE DEPTH (FT): 74

PHENOCRYST RATIO (Q/K/P): 1/1.07/0
POROSITY (VOL %): 21

DEGREE OF WELDING: Moderate
OXIDATION STATE OF Fe-Ti OXIDES: C3-C4

ROCK NAME: Rhyolitic Lithic-Crystal Tuff

GENERAL DESCRIPTION IN THIN SECTION: Fine- to medium-grained phenocrysts in a moderately welded groundmass. Pumice fragments resemble those in Samples MCG-628 and -629 (Unit 1b).

MINERAL COMPONENT	VOL. %	COMMENTS
Groundmass	38	
Glass	(64)	Incipient axiolitic devitrification. Intact bubble walls and Y-shaped shards are present.
Pumice	(36)	Up to 5.85 mm. Spherulitic devitrification. Phenocryst ratio (Q/K) = 1/3.83. Pyroxene phenocrysts are present. Some mineralization by tridymite or a zeolite.
Phenocrysts	21	
Sanidine	(49)	Fine to medium grained, anhedral to euhedral.
Quartz	(46)	Fine to medium grained, anhedral to euhedral. Some grains are embayed.
Opaques	(5)	Fine grained, anhedral to euhedral. Intergrown magnetite, ilmenite, and hematite.
Plagioclase	(tr)	Fine to medium grained, subhedral to euhedral.
Pyroxene	(tr)	Fine grained, anhedral to euhedral.
Amphibole	(tr)	Fine to medium grained, anhedral to euhedral.
Pore Space	21	

(continued on next page)

LANL VAPOR TRANSPORT STUDY
REQUEST NO.: 402553
PROJECT NO.: 6L0001000

SAMPLE NO.: MCG-632 (continued)
DRILL HOLE LLM-85-02 UNIT 2A (1B)
DRILL HOLE DEPTH (FT): 74

MINERAL COMPONENT	VOL. %	COMMENTS
Lithic Fragments	20	Up to 13.2 mm. Two large lithics fragments are strongly welded, crystal-vitric tuffs. Another large lithic is densely welded with totally devitrified glass. Andesites are also present.
Unknown Component	tr	Euhedral to subhedral grain shape, 0.54 mm, associated with sanidine and opaque grains in a glomerophenocryst. Grain has a thin, discontinuous rim of hematite with flakes of randomly oriented clay (chlorite?) and a grain of magnetite with exsolved ilmenite. Magnetite is altering to hematite. Grain also contains some remnant(?) pyroxene.

LANL VAPOR TRANSPORT STUDY
REQUEST NO.: 402553
PROJECT NO.: 6L0001000

SAMPLE NO.: MCG-633
DRILL HOLE LLM-85-02 UNIT 1B
DRILL HOLE DEPTH (FT): 111

PHENOCRYST RATIO (Q/K/P): 1/0.95/0
POROSITY (VOL %): 16

DEGREE OF WELDING: Moderate
OXIDATION STATE OF Fe-Ti OXIDES: C2-C3

ROCK NAME: Rhyolitic Lithic-Vitric Tuff

GENERAL DESCRIPTION IN THIN SECTION: Fine- to medium-grained phenocrysts in a moderately welded groundmass containing some brown glass. Large lithic fragments are present.

MINERAL COMPONENT	VOL. %		COMMENTS
Groundmass		41	
Glass	(61)		Incipient axiolitic devitrification. Mottled brown glass may indicate alteration to clay. Intact bubble walls and Y-shaped shards are present.
Pumice	(39)		Up to 9.11 mm. Spherulitic devitrification. Mineralization by a fibrous phase (zeolite?). Phenocryst ratio (Q/K) = 3/1.
Lithic Fragments		30	Up to 29.3 mm. Two major types: strongly welded, crystal-vitric tuff partially altered to clay, and a densely welded, vitric-crystal tuff that is totally devitrified.
Pore Space		16	
Phenocrysts		13	
Quartz	(49)		Fine to medium grained, anhedral to euhedral. Resorption features are common.
Sanidine	(46)		Fine to medium grained, anhedral to euhedral. Some embayments are present.
Opaques	(5)		Fine grained, anhedral to euhedral. Magnetite and ilmenite intergrowths.
Plagioclase	(tr)		Fine grained, subhedral to euhedral. Zoned grains are present.
Pyroxene	(tr)		Fine grained, anhedral. Associated with opaques.

LANL VAPOR TRANSPORT STUDY
REQUEST NO.: 402553
PROJECT NO.: 6L0001000

SAMPLE NO.: MCG-634
DRILL HOLE LLM-85-06 UNIT 2B
DRILL HOLE DEPTH (FT): 30

PHENOCRYST RATIO (Q/K/P): 1/1.20/0
POROSITY (VOL %): 25

DEGREE OF WELDING: Moderate
OXIDATION STATE OF Fe-Ti OXIDES: C3

ROCK NAME: Rhyolitic Crystal-Vitric Tuff

GENERAL DESCRIPTION IN THIN SECTION: Fine- to medium-grained phenocrysts in a moderately welded groundmass. Shards show axiolitic devitrification.

MINERAL COMPONENT	VOL. %	COMMENTS
Groundmass	45	
Glass	(84)	Axiolitic devitrification. Intact bubble walls and Y-shaped shards are present.
Pumice	(16)	Up to 8.15 mm. Two types are present: fragments replaced by sanidine and tridymite with quartz phenocrysts (dominant type), and andesitic fragments with plagioclase and amphibole phenocrysts and mineralization by tridymite.
Phenocrysts	26	
Sanidine	(53)	Fine to medium grained, anhedral to euhedral.
Quartz	(44)	Fine to medium grained, anhedral to euhedral. Embayments are present.
Opaques	(3)	Fine grained, anhedral to euhedral. Magnetite and ilmenite intergrowths.
Plagioclase	(tr)	Fine grained, euhedral to subhedral. Zoned grains are present.
Biotite	(tr)	Fine grained, anhedral.
Pyroxene	(tr)	Fine grained, anhedral to subhedral.
Amphibole	(tr)	Fine grained, anhedral.
Pore Space	25	

(continued on next page)

LANL VAPOR TRANSPORT STUDY
REQUEST NO.: 402553
PROJECT NO.: 6L0001000

SAMPLE NO.: MCG-634 (continued)
DRILL HOLE LLM-85-06 UNIT 2B
DRILL HOLE DEPTH (FT): 30

MINERAL COMPONENT	VOL. %	COMMENTS
Lithic Fragments	3	Up to 1.41 mm. Two types are present: densely welded, lithic tuff with spherulitic devitrification (see Samples MCG-550 and -645) and a strongly welded, vitric tuff which is devitrified.
Tridymite	tr	Occurs in pore spaces. Fine grained, euhedral.

LANL VAPOR TRANSPORT STUDY
REQUEST NO.: 402553
PROJECT NO.: 6L0001000

SAMPLE NO.: MCG-635
DRILL HOLE LLM-85-06 UNIT 2A
DRILL HOLE DEPTH (FT): 50

PHENOCRYST RATIO (Q/K/P): 1/1.22/0.07 DEGREE OF WELDING: Slight to Moderate
POROSITY (VOL %): 19 OXIDATION STATE OF Fe-Ti OXIDES: C3

ROCK NAME: Rhyolitic Lithic-Crystal Tuff

GENERAL DESCRIPTION IN THIN SECTION: Fine- to medium-grained phenocrysts in a slightly to moderately welded groundmass.

MINERAL COMPONENT	VOL. %	COMMENTS
Groundmass	36	
Glass	(61)	Incipient axiolitic devitrification. Intact bubble walls and Y-shaped shards are present.
Pumice	(39)	Up to 5.70 mm. Axiolitic devitrification and some replacement by sanidine and tridymite. Only quartz phenocrysts are present.
Phenocrysts	22	
Sanidine	(50)	Fine to medium grained, anhedral to euhedral.
Quartz	(41)	Fine to medium grained, anhedral to euhedral. Resorption features are common.
Opaques	(4.5)	Fine grained, anhedral to euhedral. Magnetite and ilmenite intergrowths.
Plagioclase	(3)	Fine grained, subhedral to euhedral. Zoned grains are present.
Pyroxene	(1.5)	Fine grained, euhedral to subhedral. Associated with opaques.
Lithic Fragments	22	Up to 19.3 mm. Predominant type of lithic is a strongly welded, crystal-vitric tuff containing pumice fragments from Unit 1b. Another type has a spongy lithology consisting of sanidine crystals.
Pore Space	19	

(continued on next page)

LANL VAPOR TRANSPORT STUDY
REQUEST NO.: 402553
PROJECT NO.: 6L0001000

SAMPLE NO.: MCG-635 (continued)
DRILL HOLE LLM-85-06 UNIT 2A
DRILL HOLE DEPTH (FT): 50

MINERAL COMPONENT	VOL. %	COMMENTS
Tridymite	1	Fine grained, euhedral. Occurs in pores.
Unknown Component	tr	Rounded grains, 0.54 and 0.91 mm, consisting of a discontinuous rim of hematite and magnetite with exsolved ilmenite. Some rutile is associated with grains of magnetite; magnetite is altering to hematite. The interiors of these rounded grains contain randomly oriented clay (chlorite?) flakes and epidote or pyroxene.

LANL VAPOR TRANSPORT STUDY
REQUEST NO.: 402553
PROJECT NO.: 6L0001000

SAMPLE NO.: MCG-636
DRILL HOLE LLM-85-06 UNIT 1B
DRILL HOLE DEPTH (FT): 99

PHENOCRYST RATIO (Q/K/P): 1/1.53/0
POROSITY (VOL %): 26

DEGREE OF WELDING: Moderate
OXIDATION STATE OF Fe-Ti OXIDES: C1-C2

ROCK NAME: Rhyolitic Vitric-Crystal Tuff

GENERAL DESCRIPTION IN THIN SECTION: Fine- to medium-grained phenocrysts in a fresh-glass groundmass. Glass in pumice fragments is fresh and not devitrified. Some pumice fragments are flattened.

MINERAL COMPONENT	VOL. %	COMMENTS
Groundmass	57	
Glass	(53)	Moderate welding, brown glass; not devitrified. Intact bubble walls and Y-shaped shards are present.
Pumice	(47)	Up to 5.93 mm. Some of the fragments are flattened. Glass is not devitrified. Phenocryst ratio (Q/K) for flattened pumice is 1/11; for non-flattened pumice, 1/1.25. Overall pumice phenocryst ratio is 1/3.20.
Pore Space	26	
Phenocrysts	17	
Sanidine	(57)	Fine to medium grained, anhedral to euhedral.
Quartz	(37)	Fine to medium grained, anhedral to euhedral.
Opaques	(4)	Fine grained, anhedral to euhedral. Magnetite, and magnetite with exsolved ilmenite.
Pyroxene	(2)	Fine grained, anhedral to euhedral.
Plagioclase	(tr)	Fine grained, anhedral.
Lithic Fragments	tr	Up to 1.42 mm. Hyalopilitic basalt/andesite.

LANL VAPOR TRANSPORT STUDY
REQUEST NO.: 402553
PROJECT NO.: 6L0001000

SAMPLE NO.: MCG-637
DRILL HOLE LLM-85-06 UNIT 1A
DRILL HOLE DEPTH (FT): 113

PHENOCRYST RATIO: Not Determined
DEGREE OF WELDING: Not Welded
POROSITY (VOL %): Not Determined
OXIDATION STATE OF Fe-Ti OXIDES: C3 (Pumice)

ROCK NAME: Rhyolitic Vitric-Crystal(?) Tuff

GENERAL DESCRIPTION IN THIN SECTION: The sample was not welded and the thin-section preparer provided a section of the pumice fragments only. Grain mounts of the fine fraction were prepared in immersion oil and Canada balsam. Each of these mounts contains brown-glass shards and a large proportion of fine, flattened pumice fragments. The glass in the shards and fine pumice fragments is not devitrified. Phenocrysts of sanidine, quartz, zoned plagioclase, opaques, pyroxene, and amphibole are present in the fine fraction. The medium fraction was examined using a binocular microscope. This fraction consisted of quartz and sanidine phenocrysts, pumice fragments, and lithic fragments. The coarse pumice fragments are similar to those in Sample MCG-636; some of these are flattened. Compositions of the coarse pumice fragments (based on phenocrysts) are rhyolitic to andesitic. The largest pumice fragment (26 mm) contains zoned plagioclase, euhedral lamprobolite, and anhedral pyroxene phenocrysts in a partially flattened pumice structure. Other pumice fragments range from not flattened to totally collapsed; glass is not devitrified.

LANL VAPOR TRANSPORT STUDY
REQUEST NO.: 402553
PROJECT NO.: 6L0001000

SAMPLE NO.: MCG-638
DRILL HOLE LLM-85-11 UNIT 2B
DRILL HOLE DEPTH (FT): 5

PHENOCRYST RATIO (Q/K/P): 1/1.82/0
POROSITY (VOL %): 22

DEGREE OF WELDING: Slight to Moderate
OXIDATION STATE OF Fe-Ti OXIDES: C3-C4

ROCK NAME: Rhyolitic Crystal-Vitric Tuff

GENERAL DESCRIPTION IN THIN SECTION: Fine- to medium-grained phenocrysts in a groundmass exhibiting slight to moderate welding and axiolitic devitrification of glass.

MINERAL COMPONENT	VOL. %		COMMENTS
Groundmass		55	
Glass	(65)		Axiolitic devitrification.
Pumice	(35)		Up to 2.52 mm. Replaced/mineralized by sanidine and tridymite. Phenocryst ratio (Q/K) = 1/2.25. Opaque and zircon phenocrysts are also present.
Pore Space		22	
Phenocrysts		21	
Sanidine	(63)		Fine to medium grained, anhedral to euhedral.
Quartz	(34)		Fine to medium grained, anhedral to euhedral. Some embayments are present.
Opaques	(3)		Fine grained, anhedral to euhedral. Magnetite, ilmenite, and hematite intergrowths.
Pyroxene	(tr)		Fine grained, anhedral to euhedral. Associated with opaques.
Plagioclase	(tr)		Fine grained, anhedral to subhedral. Zoned grains are present.
Amphibole	(tr)		Fine grained, anhedral.
Lithic Fragments		2	Up to 3.64 mm. Several types: strongly welded, vitric-crystal tuff, both devitrified and nondevitrified varieties; andesitic tuff, not devitrified; and hyalopilitic basalt.

LANL VAPOR TRANSPORT STUDY
REQUEST NO.: 402553
PROJECT NO.: 6L0001000

SAMPLE NO.: MCG-639
DRILL HOLE LLM-85-11 UNIT 2B
DRILL HOLE DEPTH (FT): 30.5

PHENOCRYST RATIO (Q/K/P): 1/0.77/0
POROSITY (VOL %): 24

DEGREE OF WELDING: Moderate
OXIDATION STATE OF Fe-Ti OXIDES: C4

ROCK NAME: Rhyolitic Crystal-Lithic Tuff

GENERAL DESCRIPTION IN THIN SECTION: Fine- to medium-grained phenocrysts in a moderately welded, devitrified groundmass.

MINERAL COMPONENT	VOL. %		COMMENTS
Groundmass		42	
Glass	(70)		Axiolitic devitrification. Intact bubble walls and Y-shaped shards are present.
Pumice	(30)		Up to 4.89 mm. Replaced/mineralized by sanidine and tridymite. Phenocryst ratio (Q/K) = 1/2.
Pore Space		24	
Phenocrysts		24	
Quartz	(55)		Fine to medium grained, anhedral to euhedral. Some embayments are present.
Sanidine	(42)		Fine to medium grained, anhedral to euhedral.
Opaques	(3)		Fine grained, anhedral to euhedral. Magnetite, ilmenite, and hematite intergrowths.
Pyroxene	(tr)		Fine grained, subhedral to euhedral.
Plagioclase	(tr)		Fine grained, euhedral. Zoned grains.
Amphibole	(tr)		Fine grained, subhedral.
Lithic Fragments		10	Up to 31.9 mm. Lenticular, strongly welded, crystal-vitric tuff with axiolitic devitrification and hyalopilitic basalts.

LANL VAPOR TRANSPORT STUDY
REQUEST NO.: 402553
PROJECT NO.: 6L0001000

SAMPLE NO.: MCG-640
DRILL HOLE LLM-85-11 UNIT 1B
DRILL HOLE DEPTH (FT): 95

PHENOCRYST RATIO (Q/K/P): 1/1.30/0
POROSITY (VOL %): 16

DEGREE OF WELDING: Moderate
OXIDATION STATE OF Fe-Ti OXIDES: C2

ROCK NAME: Rhyolitic Lithic-Vitric Tuff

GENERAL DESCRIPTION IN THIN SECTION: Fine- to medium-grained phenocrysts in a moderately welded groundmass.

MINERAL COMPONENT	VOL. %		COMMENTS
Groundmass		41	
Glass	(58)		Not devitrified; some brown glass is present.
Pumice	(42)		Up to 8.52 mm. Three types of pumice are present: nonflattened pumice with spherulitic devitrification [phenocryst ratio (Q/K) = 1/3]; flattened pumice that is not devitrified; and nonflattened pumice of andesitic composition.
Lithic Fragments		27	Up to 14.8 mm. Three types are present: strongly welded, crystal-vitric tuff; densely welded, vitric-crystal tuff that is totally devitrified; and altered basalt.
Pore Space		16	
Phenocrysts		16	
Sanidine	(54)		Fine to medium grained, anhedral to euhedral.
Quartz	(42)		Fine to medium grained, anhedral to euhedral. Some embayments are present.
Opaques	(2)		Fine grained, anhedral to euhedral. Magnetite with exsolved ilmenite.
Pyroxene	(2)		Fine grained, anhedral to euhedral.
Amphibole	(tr)		Fine grained, subhedral.

LANL VAPOR TRANSPORT STUDY
REQUEST NO.: 402553
PROJECT NO.: 6L0001000

SAMPLE NO.: MCG-641
DRILL HOLE LLM-85-11 UNIT 1A
DRILL HOLE DEPTH (FT): 116

PHENOCRYST RATIO: Not Determined
DEGREE OF WELDING: Not Welded
POROSITY (VOL %): Not Determined
OXIDATION STATE OF Fe-Ti OXIDES: C2 (Pumice)

ROCK NAME: Rhyolitic Vitric-Crystal(?) Tuff

GENERAL DESCRIPTION IN THIN SECTION: The sample was not welded and the thin-section preparer provided a section of the pumice fragments only. A grain mount of the fine fraction was prepared in Canada balsam. The fine fraction consists of glass shards, flattened pumice fragments, phenocrysts of quartz, sanidine, plagioclase, pyroxene, amphibole, and opaques. Goethite and goethite-stained material is present in the fine fraction. Glass is not devitrified in the shards and pumice fragments. The medium fraction was examined using a binocular microscope. This fraction consists of quartz, sanidine, opaque phenocrysts, and pumice (some flattened) and lithic fragments. The coarse pumice fragments have rhyolitic compositions based on the phenocrysts of sanidine, quartz, opaques, and (few) pyroxene. The pumice fragments vary from partially flattened to not flattened. Glass in the pumice fragments is not devitrified.

LANL VAPOR TRANSPORT STUDY
REQUEST NO.: 402553
PROJECT NO.: 6L0001000

SAMPLE NO.: MCG-642
DRILL HOLE LLM-85-14 UNIT 2B (LITHIC)
DRILL HOLE DEPTH (FT): 18

PHENOCRYST RATIO (Pl/Px): 4.57/1
POROSITY (VOL %): 5

DEGREE OF WELDING: Dense
OXIDATION STATE OF Fe-Ti OXIDES: C3-C4

ROCK NAME: Basalt Porphyry

GENERAL DESCRIPTION IN THIN SECTION: Fine- to medium-grained phenocrysts in a hyalopilitic groundmass.

MINERAL COMPONENT	VOL. %		COMMENTS
Groundmass		67	
Glass	(56)		Spherulitic devitrification.
Plagioclase Laths	(41)		Very fine grained, euhedral to subhedral.
Opaques	(3)		Very fine grained, anhedral to euhedral. Magnetite, ilmenite, and hematite.
Phenocrysts		28	
Plagioclase	(77)		Fine to medium grained, euhedral to anhedral. Spongy resorption textures.
Pyroxene	(17)		Fine to medium grained, euhedral to subhedral. Pigeonite.
Opaques	(6)		Fine grained, anhedral to euhedral. Magnetite, ilmenite, and hematite intergrowths.
Pore Space		5	Microporosity (in the groundmass) around and within some plagioclase phenocrysts.
Fracture Filling		tr	Goethite.

LANL VAPOR TRANSPORT STUDY
REQUEST NO.: 402553
PROJECT NO.: 6L0001000

SAMPLE NO.: MCG-643
DRILL HOLE LLM-85-13 UNIT 2B
DRILL HOLE DEPTH (FT): 42

PHENOCRYST RATIO (Q/K/P): 1/3.06/0.17 DEGREE OF WELDING: Moderate
POROSITY (VOL %): 28 OXIDATION STATE OF Fe-Ti OXIDES: C2

ROCK NAME: Rhyolitic Crystal-Lithic Tuff

GENERAL DESCRIPTION IN THIN SECTION: Fine- to medium-grained phenocrysts in a moderately welded groundmass with axiolitic devitrification. Glass has coatings of clay.

MINERAL COMPONENT	VOL. %		COMMENTS
Groundmass		34	
Glass	(81)		Axiolitic devitrification. Intact bubble walls and Y-shaped shards are present. Clay coatings are present.
Pumice	(19)		Up to 2.06 mm. Replaced/mineralized by sanidine and tridymite. No phenocrysts are present.
Pore Space		28	
Phenocrysts		27	
Sanidine	(68)		Fine to medium grained, anhedral to subhedral.
Quartz	(23)		Fine to medium grained, anhedral to euhedral. Embayed grains are present.
Plagioclase	(4)		Fine to medium grained, subhedral to euhedral.
Opaques	(4)		Fine grained, anhedral to euhedral. Magnetite with exsolved ilmenite; one grain contains an inclusion of pyrite.
Amphibole	(1)		Fine to medium grained, subhedral.
Pyroxene	(tr)		Fine grained, subhedral to euhedral.
Lithic Fragments		10	Up to 11.1 mm. Andesitic crystal-vitric tuff.
Tridymite		1	Very fine grained; occurs in pores.

LANL VAPOR TRANSPORT STUDY
REQUEST NO.: 402553
PROJECT NO.: 6L0001000

SAMPLE NO.: MCG-644
DRILL HOLE LLM-85-17 UNIT 2B
DRILL HOLE DEPTH (FT): 11

PHENOCRYST RATIO (Q/K/P): 1/1.75/0
POROSITY (VOL %): 25

DEGREE OF WELDING: Moderate
OXIDATION STATE OF Fe-Ti OXIDES: C3-C4

ROCK NAME: Rhyolitic Crystal-Lithic Tuff

GENERAL DESCRIPTION IN THIN SECTION: Fine- to medium-grained phenocrysts in a moderately welded groundmass. Although this sample has a fracture containing smectite, no clay was observed in thin section.

MINERAL COMPONENT	VOL. %		COMMENTS
Groundmass		41	
Glass	(71)		Axiolitic devitrification is present.
Pumice	(29)		Up to 3.39 mm. Replaced/mineralized by sanidine and tridymite. Phenocryst ratio (Q/K) = 1/1.
Pore Space		25	
Phenocrysts		23	
Sanidine	(61)		Fine to medium grained, anhedral to euhedral.
Quartz	(35)		Fine to medium grained, anhedral to subhedral. Some grains are embayed.
Opaques	(3)		Fine grained, anhedral to euhedral. Ilmenite with exsolved magnetite; grains of rutile are present.
Pyroxene	(1)		Fine grained, subhedral to anhedral.
Plagioclase	(tr)		Fine grained, euhedral. Zoned grains are present.
Lithic Fragments		10	Up to 12.7 mm. Several types: strongly welded, crystal-vitric tuff with fresh glass; densely welded, vitric-crystal tuff with coarse spherulitic devitrification; and a devitrified, andesitic/latitic vitric tuff.
Tridymite		1	Fine grained, euhedral. Occurs in pore spaces.

LANL VAPOR TRANSPORT STUDY
REQUEST NO.: 402553
PROJECT NO.: 6L0001000

SAMPLE NO.: MCG-645
DRILL HOLE LLM-85-17 UNIT 1B (LITHIC)
DRILL HOLE DEPTH (FT): 109

PHENOCRYST RATIO (Q/K/P): 1/4.33/0.67 DEGREE OF WELDING: Dense
POROSITY (VOL %): 9 OXIDATION STATE OF Fe-Ti OXIDES: C3-C4

ROCK NAME: Rhyolitic Vitric Tuff

GENERAL DESCRIPTION IN THIN SECTION: Densely welded glass with lithophysae filled by sanidine, tridymite, opaques, and late-stage alpha quartz. A few fine- to medium-grained phenocrysts are present.

MINERAL COMPONENT		VOL. %	COMMENTS
Groundmass		53	Densely welded glass with well-developed spherulitic devitrification. Glass is brown in part.
Vapor Phase Minerals		33	
Sanidine	(70)		Porous, microcrystalline linings of lithophysae.
Tridymite	(23)		Fine grained, euhedral. Partially fills interiors of lithophysae. Wedge-shaped twins are common.
Alpha Quartz	(4)		Fine grained, anhedral to euhedral. Late-stage lining and filling of lithophysae.
Opaques	(3)		Fine grained, anhedral. Associated with sanidine stage of lithophysae filling. Magnetite/ilmenite altering to hematite.
Pore Space		9	Associated with vapor-phase crystallites.
Phenocrysts		5	
Sanidine	(56)		Fine to medium grained, euhedral to subhedral.
Alpha Quartz	(44)		Fine grained, anhedral to euhedral. Embayed grains are present.
Opaques	(tr)		Fine grained, euhedral. Magnetite intergrown with ilmenite.
Plagioclase	(tr)		Fine grained, euhedral.

LANL VAPOR TRANSPORT STUDY
REQUEST NO.: 402553
PROJECT NO.: 6L0001000

SAMPLE NO.: MCG-646
DRILL HOLE LLM-85-09 UNIT 2B
DRILL HOLE DEPTH (FT): 10

PHENOCRYST RATIO (Q/K/P): 1/1.64/0
POROSITY (VOL %): 21

DEGREE OF WELDING: Moderate
OXIDATION STATE OF Fe-Ti OXIDES: C3-C4

ROCK NAME: Rhyolitic Crystal-Vitric Tuff

GENERAL DESCRIPTION IN THIN SECTION: Fine- to medium-grained phenocrysts in a moderately welded groundmass with axiolitic devitrification.

MINERAL COMPONENT	VOL. %		COMMENTS
Groundmass		55	
Glass	(68)		Axiolitic devitrification.
Pumice	(32)		Up to 9.93 mm. Replaced/mineralized by sanidine and tridymite.
Phenocrysts		22	
Sanidine	(62)		Fine to medium grained, anhedral to euhedral.
Quartz	(38)		Fine to medium grained, anhedral to euhedral. Embayed grains are present.
Pyroxene	(tr)		Fine grained, anhedral to subhedral.
Opaques	(tr)		Fine grained, anhedral to euhedral. Magnetite, ilmenite, hematite, and rutile.
Plagioclase	(tr)		Fine grained, euhedral. Zoned grain.
Allanite(?)	(tr)		Fine grained, euhedral.
Pore Space		21	
Lithic Fragments		2	Up to 1.70 mm. Mostly basalts.
Tridymite		tr	Fine grained, euhedral. Occurs in pore spaces.

LANL VAPOR TRANSPORT STUDY
REQUEST NO.: 402553
PROJECT NO.: 6L0001000

SAMPLE NO.: MCG-647
DRILL HOLE LLM-85-09 UNIT 2B
DRILL HOLE DEPTH (FT): 20

PHENOCRYST RATIO (Q/K/P): 1/2.77/0.04 DEGREE OF WELDING: Moderate
POROSITY (VOL %): 22 OXIDATION STATE OF Fe-Ti OXIDES: C2-C3

ROCK NAME: Rhyolitic Crystal-Vitric Tuff

GENERAL DESCRIPTION IN THIN SECTION: Fine- to medium-grained phenocrysts in a moderately welded groundmass with axiolitic devitrification.

MINERAL COMPONENT	VOL. %		COMMENTS
Groundmass		42	
Glass	(69)		Axiolitic devitrification.
Pumice	(31)		Up to 10.37 mm. Replaced/mineralized by sanidine and tridymite. Phenocryst ratio (Q/K) = 1/1.
Phenocrysts		34	
Sanidine	(71)		Fine to medium grained, anhedral to euhedral.
Quartz	(26)		Fine to medium grained, anhedral to euhedral.
Opaques	(2)		Fine grained, anhedral to euhedral. Magnetite and ilmenite intergrowths.
Plagioclase	(1)		Fine to medium grained, subhedral to euhedral. Some grains are zoned.
Pyroxene	(tr)		Fine grained, anhedral to subhedral.
Pore Space		22	
Lithic Fragments		2	Up to 1.30 mm. Mostly basalts.
Tridymite		tr	Fine grained, euhedral to anhedral. Occurs in pore space.
Unknown Component		tr	Rounded grain, 0.32 mm, consisting of a partial rim of hematite and randomly oriented flakes of clay (chlorite?). A grain of ilmenite with exsolved hematite is present as an inclusion.

LANL VAPOR TRANSPORT STUDY
REQUEST NO.: 402553
PROJECT NO.: 6L0001000

SAMPLE NO.: MCG-648
DRILL HOLE LLM-85-09 UNIT 2A
DRILL HOLE DEPTH (FT): 35

PHENOCRYST RATIO (Q/K/P): 1/2.17/0
POROSITY (VOL %): 26

DEGREE OF WELDING: Moderate
OXIDATION STATE OF Fe-Ti OXIDES: C3-C4

ROCK NAME: Rhyolitic Crystal-Vitric Tuff

GENERAL DESCRIPTION IN THIN SECTION: Fine- to medium-grained phenocrysts in a moderately welded groundmass with axiolitic devitrification. Although this sample has a fracture containing smectite, no clay was observed in thin section.

MINERAL COMPONENT	VOL. %		COMMENTS
Groundmass		48	
Glass	(70)		Axiolitic devitrification.
Pumice	(30)		Up to 4.70 mm. Replaced/mineralized by sanidine and tridymite. Phenocryst ratio (Q/K) = 1/1.
Pore Space		26	
Phenocrysts		25	
Sanidine	(68)		Fine to medium grained, anhedral to euhedral.
Quartz	(32)		Fine to medium grained, anhedral to euhedral. Embayed grains are present.
Pyroxene	(tr)		Fine grained, euhedral to anhedral.
Opaques	(tr)		Fine grained, subhedral to anhedral. Magnetite, ilmenite, and hematite.
Plagioclase	(tr)		Medium grained, euhedral. Zoned grain.
Amphibole	(tr)		Fine grained, anhedral.
Lithic Fragments		tr	Up to 1.67 mm. Mostly basalt/andesite.
Tridymite		tr	Fine grained, euhedral. Occurs in pore space.

(continued on next page)

LANL VAPOR TRANSPORT STUDY
REQUEST NO.: 402553
PROJECT NO.: 6L0001000

SAMPLE NO.: MCG-648 (continued)
DRILL HOLE LLM-85-09 UNIT 2A
DRILL HOLE DEPTH (FT): 35

MINERAL COMPONENT	VOL. %	COMMENTS
Unknown Component	tr	Two grains. One is rounded, 0.80 mm, with a thin rim of hematite and almost totally filled by sheaves of clay (chlorite?); inclusion of magnetite (altering to hematite) with exsolved ilmenite. The other is subhedral, 0.29 mm, with a thin rim of hematite and sparse, randomly oriented flakes of clay (chlorite?).

LANL VAPOR TRANSPORT STUDY
REQUEST NO.: 402553
PROJECT NO.: 6L0001000

SAMPLE NO.: MCG-649
DRILL HOLE LLM-85-09 UNIT 1B
DRILL HOLE DEPTH (FT): 47

PHENOCRYST RATIO (Q/K/P): 1/0.81/0.03 DEGREE OF WELDING: Moderate
POROSITY (VOL %): 21 OXIDATION STATE OF Fe-Ti OXIDES: C2-C3

ROCK NAME: Rhyolitic Crystal-Vitric Tuff

GENERAL DESCRIPTION IN THIN SECTION: Fine- to medium-grained phenocrysts in a groundmass containing glass that is not devitrified. Brown-colored glass is present in the groundmass and some pumice fragments.

MINERAL COMPONENT	VOL. %		COMMENTS
Groundmass		54	
Glass	(66)		Not devitrified. Some brown glass.
Pumice Fragments	(34)		Up to 7.78 mm. Some flattened fragments and andesitic compositions (based on phenocrysts). Phenocryst ratio in rhyolitic fragments (Q/K) = 1/1.83.
Phenocrysts		23	
Quartz	(52)		Fine to medium grained, anhedral to euhedral. Some grains are embayed.
Sanidine	(42)		Fine to medium grained, anhedral to euhedral.
Opaques	(4)		Fine grained, anhedral to euhedral. Magnetite and ilmenite intergrowths.
Plagioclase	(2)		Fine grained, subhedral. Zoned grain.
Pyroxene	(tr)		Fine grained, anhedral to euhedral.
Pore Space		21	
Lithic Fragments		2	Up to 0.97 mm. Several types: altered, flow-banded rock; altered, spherulitically devitrified rock; aphanitic rock; and hyalopilitic basalt.

LANL VAPOR TRANSPORT STUDY
REQUEST NO.: 402553
PROJECT NO.: 6L0001000

SAMPLE NO.: MCG-650
DRILL HOLE LLM-85-09 UNIT 1B
DRILL HOLE DEPTH (FT): 68

PHENOCRYST RATIO (Q/K/P): 1/1.04/0
POROSITY (VOL %): 24

DEGREE OF WELDING: Moderate
OXIDATION STATE OF Fe-Ti OXIDES: C3

ROCK NAME: Rhyolitic Vitric-Crystal Tuff

GENERAL DESCRIPTION IN THIN SECTION: Fine- to medium-grained phenocrysts in a moderately welded groundmass. Shards exhibit incipient axiolitic devitrification. Most pumice fragments have spherulitic devitrification.

MINERAL COMPONENT	VOL. %		COMMENTS
Groundmass		55	
Glass	(54)		Incipient axiolitic devitrification.
Pumice Fragments	(46)		Up to 6.74 mm. Most have spherulitic devitrification. Some are partially flattened. An andesitic composition (based on phenocrysts) is present. Phenocryst ratio (Q/K) in rhyolitic fragments is 1/1.33.
Pore Space		24	
Phenocrysts		18	
Sanidine	(47)		Fine to medium grained, anhedral to euhedral.
Quartz	(45)		Fine to medium grained, anhedral to euhedral. Resorption features are abundant.
Opaques	(6)		Fine grained, anhedral to euhedral. Ilmenite with exsolved magnetite.
Pyroxene	(2)		Fine grained, anhedral to euhedral. Most grains are associated with opaques; some grains are coated with celadonite.
Lithic Fragments		3	Up to 3.41 mm. Several types: altered basalt; hyalopilitic basalt; vitric tuff with spherulitic devitrification; granophyre; and an altered, flow-banded rock.

B.2 FISCAL YEAR 1986 FIELDWORK

A total of 11 drill-core and outcrop samples from the Tshirege Member of the Bandelier Tuff were submitted to the GJPO Petrology Laboratory for petrographic characterization. There were two samples each from Unit 1a, Unit 1b, and Unit 2b; one sample from Unit 2a; and four lithic lapilli and pumice fragments from Unit 1a.

The samples as received consisted of sections of 5-cm-diameter drill core and irregular samples from outcrops. From these samples, portions were removed using a core splitter for polished-thin-section preparation. The samples were impregnated with blue-colored epoxy to emphasize the porosity in the thin sections.* Each thin section was subjected to point-count analysis (300 counts) to determine mineral and component abundance. Tuffaceous rocks were named according to the classification of Cook (1965). As shown in Figure B-2, the rocks from this study plot in the following fields: VII (crystal-vitric tuff) and VIII (vitric-crystal).

The optical identifications of major and minor minerals, especially devitrification products, were confirmed using X-ray diffraction (XRD). The compositional modifiers to tuffaceous rock names are based on bulk XRD data. These modifiers were assigned according to the classification of Streckeisen (1967).

Petrographic descriptions of these samples are presented on the pages following Figure B-2. They are presented in consecutive order by sample number, although the drill-hole number, depth of the sample, and geologic unit are also identified near the top of the page. The volume percent of each mineral component is given, together with the petrographic description. Phenocrysts and groundmass are further subdivided into individual components, and these subcomponents are followed by a number in parentheses which indicates their volume percentage of the main component. The petrographic descriptions were taken from a report entitled Petrography of the Tshirege Member of the Bandelier Tuff, Mesita del Buey, Los Alamos County, New Mexico: Second Report (Fukui, 1986).

*There is considerable discrepancy between porosity measured in thin section and that determined by means of helium injection (see Section 3.1.2). The significantly lower porosity determined in thin section is due to the fact that most of the thin sections were cut parallel to the core axis (parallel to the direction of flattening), resulting in erroneous extrapolation based on the cross section of the gas tubes rather than on their true shape.

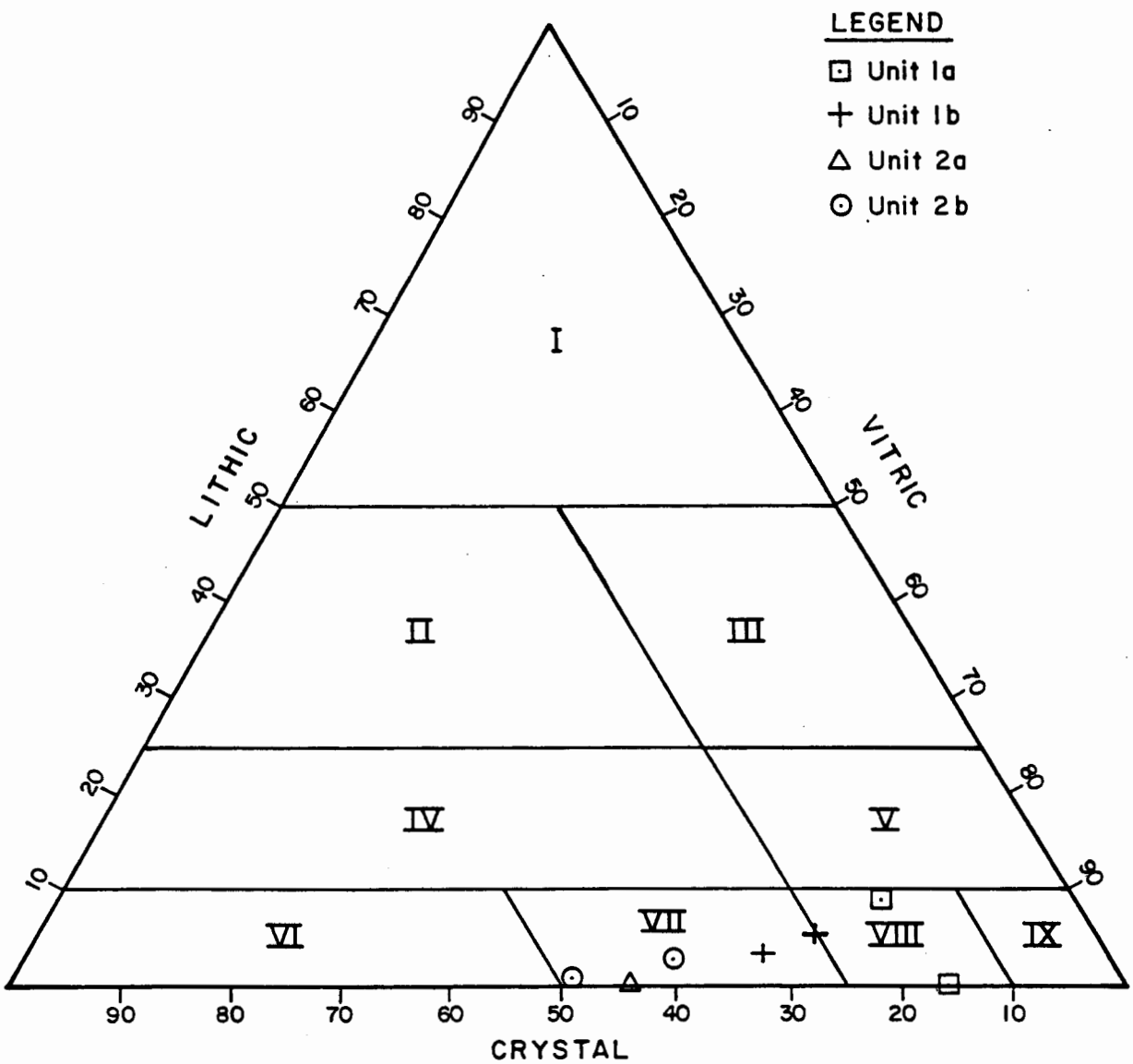

Figure B-2. Classification of Cook (1965) Used to Name Tuffaceous Rocks in This Study on the Basis of the Normalized Vitric (including pumice), Crystal, and Lithic Components Determined From the Modal Analysis.

LANL VAPOR TRANSPORT STUDY
REQUEST NO.: 403353
PROJECT NO.: 6L0001000

SAMPLE NO.: MCG-651
DRILL HOLE LLC-86-19 UNIT 1a (Lithic)
DRILL HOLE DEPTH (FT): 190

BANDELIER TUFF PHENOCRYST-RATIO (Q/K/P): 1/7.3/5.5
DEGREE OF WELDING: Strong
POROSITY (VOL. %): 1
OXIDATION STATE OF Fe-Ti OXIDES: C7

ROCK NAME: Altered Crystal-Vitric Tuff

GENERAL DESCRIPTION IN THIN SECTION: Lithic fragment with feldspar phenocrysts replaced by analcime(?).

MINERAL COMPONENT	VOL. %		COMMENTS
Groundmass		62	
Glass	(93)		Glass appears partially altered to clay that is iron stained. The glass is not devitrified. Shard structure is preserved.
Opaques	(7)		Hematite.
Phenocrysts		35	
Plagioclase	(44)		Pseudomorphic replacement by analcime. Compositional-zoning structure is preserved.
K-feldspar	(33)		Pseudomorphic replacement by analcime.
Biotite	(13)		Totally altered to chlorite and hematite.
Pyroxene(?)	(9)		Altered to serpentine(?) and hematite.
Opaques	(tr)		Altered to pseudobrookite and hematite.
Lithics(?)		3	Altered.
Vug		2	Vugs are lined by opal and filled by chalcedony.
Pore Space		1	

LANL VAPOR TRANSPORT STUDY
REQUEST NO.: 403353
PROJECT NO.: 6L0001000

SAMPLE NO.: MCG-652
DRILL HOLE LLC-86-19 UNIT 1a (Lithic)
DRILL HOLE DEPTH (FT): 175

BANDELIER TUFF PHENOCRYST-RATIO (Q/K/P): Unknown
DEGREE OF WELDING: Strong
POROSITY (VOL. %): 22
OXIDATION STATE OF Fe-Ti OXIDES: C7

ROCK NAME: Altered, Crystal-Vitric Tuff

GENERAL DESCRIPTION IN THIN SECTION: Groundmass is silicified. Phenocrysts are replaced by clay minerals. Vague features in the rock may be pumice and lithic fragments.

MINERAL COMPONENT	VOL. %		COMMENTS
Groundmass		67	
Glass	(91)		Replaced by quartz and clay minerals.
Pumice Fragments	(9)		Up to 5.45 mm. Replaced by silica. Texturally, these resemble the pumice in Units 2a and 2b.
Pore Space		22	
Phenocrysts		6	
Feldspars(?)	(68)		Totally replaced by clay.
Opaques	(32)		Totally replaced by pseudobrookite and hematite.
Lithic Fragments(?)		5	Vague textural features.

LANL VAPOR TRANSPORT STUDY
REQUEST NO.: 403353
PROJECT NO.: 6L0001000

SAMPLE NO.: MCG-653
DRILL HOLE LLC-86-19 UNIT 1a (Lithic)
DRILL HOLE DEPTH (FT): 162

BANDELIER TUFF PHENOCRYST-RATIO (Q/K/P): 1/3.4/0
DEGREE OF WELDING: Strong
POROSITY (VOL. %): 13
OXIDATION STATE OF Fe-Ti OXIDES: C4

ROCK NAME: Rhyolitic Vitric Tuff

GENERAL DESCRIPTION IN THIN SECTION: Fine- to medium-grained phenocrysts in a strongly welded groundmass with axiolitic and spherulitic devitrification and vapor-phase mineralization.

MINERAL COMPONENT		VOL. %	COMMENTS
Groundmass		73	Strongly welded glass with axiolitic and spherulitic devitrification.
Pore Space		13	
Vapor-Phase Minerals		9	Fills vugs.
Sanidine	(53)		
Tridymite	(29)		
Alpha Quartz	(18)		
Phenocrysts		5	
Sanidine	(63)		
Opaques	(31)		Ilmenite, magnetite, and hematite.
Alpha Quartz	(6)		
Pyroxene	(tr)		Augite. Rimmed by goethite.

LANL VAPOR TRANSPORT STUDY
REQUEST NO.: 403353
PROJECT NO.: 6L0001000

SAMPLE NO.: MCG-654
DRILL HOLE LLC-86-20 UNIT 1a
DRILL HOLE DEPTH (FT): 148

BANDELIER TUFF PHENOCRYST-RATIO (Q/K/P): NA
DEGREE OF WELDING: Slight
POROSITY (VOL. %): 46
OXIDATION STATE OF Fe-Ti OXIDES: C2-C3

ROCK NAME: Andesitic Pumice Fragment

GENERAL DESCRIPTION IN THIN SECTION: Sample is a pumice fragment; fine- to medium-grained phenocrysts in fresh glass. The pumice is not flattened.

MINERAL COMPONENT	VOL. %		COMMENTS
Pore Space		46	
Phenocrysts		36	
Plagioclase	(76)		Medium-grained phenocrysts exhibit normal zoning; finer grains do not appear to be zoned. Fresh.
Amphibole	(23)		Basaltic hornblende (lamprobolite).
Opaques	(1)		Magnetite and ilmenite.
Groundmass (Pumice)		18	Fresh, colorless glass.

LANL VAPOR TRANSPORT STUDY
REQUEST NO.: 403353
PROJECT NO.: 6L0001000

SAMPLE NO.: MCG-655
DRILL HOLE LLC-86-20 UNIT 1a
DRILL HOLE DEPTH (FT): 176

BANDELIER TUFF PHENOCRYST-RATIO (Q/K/P): 1/1.4/0.06
DEGREE OF WELDING: Slight
POROSITY (VOL. %): 33
OXIDATION STATE OF Fe-Ti OXIDES: C2-C3

ROCK NAME: Rhyolitic Vitric-Crystal Tuff

GENERAL DESCRIPTION IN THIN SECTION: Fine-to medium-grained phenocrysts in a slightly welded, fresh-glass groundmass. Glass in pumice fragments is also fresh. Some pumice fragments are flattened.

MINERAL COMPONENT	VOL. %		COMMENTS
Groundmass		49	
Pumice Fragments	(59)		Up to 6.73 mm. Fresh glass. Some fragments are totally flattened. The only phenocrysts in the fragments are sanidine, amphibole, and opaques.
Glass	(41)		Fresh. Y-shaped shards are present.
Pore Space		33	
Phenocrysts		12	
Sanidine	(49)		
Quartz	(49)		Embayed grains are common.
Opaques	(2)		Magnetite and ilmenite.
Pyroxene	(tr)		Augite.
Amphibole	(tr)		Lamprobolite.
Lithic Fragments		6	Up 2.56 mm. Mostly basaltic tuffs.

LANL VAPOR TRANSPORT STUDY
REQUEST NO.: 403353
PROJECT NO.: 6L0001000

SAMPLE NO.: MCG-656
DRILL HOLE LLC-86-20 UNIT 1b
DRILL HOLE DEPTH (FT): 126

BANDELIER TUFF PHENOCRYST-RATIO (Q/K/P): 1/2/0.01
DEGREE OF WELDING: Slight
POROSITY (VOL. %): 38
OXIDATION STATE OF Fe-Ti OXIDES: C3-C4

ROCK NAME: Rhyolitic Crystal-Vitric Tuff

GENERAL DESCRIPTION IN THIN SECTION: Fine- to medium-grained phenocrysts in a slightly welded, fresh-glass groundmass. Glass in pumice fragments is also fresh. Some pumice fragments are flattened.

MINERAL COMPONENT	VOL. %		COMMENTS
Groundmass		41	
Glass	(66)		Fresh; brown-colored.
Pumice	(46)		Up to 5.45 mm. Some pumice fragments are totally flattened. Phenocryst ratio in pumice is two sanidine for every quartz.
Pore Space		38	
Phenocrysts		19	
Sanidine	(56)		
Quartz	(40)		Many grains are embayed.
Opaques	(4)		Ilmenite, magnetite, and hematite.
Pyroxene	(tr)		Augite.
Plagioclase	(tr)		
Amphibole	(tr)		Lamprobolite.
Lithic Fragments		2	Up to 3.45 mm. Altered and fresh hyalopilitic basalts; altered lithic-vitric tuff with abundant basaltic material; altered, thoroughly welded, spherulitically devitrified, vitric tuff; and silicified vitric tuff.

LANL VAPOR TRANSPORT STUDY
REQUEST NO.: 403353
PROJECT NO.: 6L0001000

SAMPLE NO.: MCG-657
DRILL HOLE LLC-86-20 UNIT 1a
DRILL HOLE DEPTH (FT): 134

BANDELIER TUFF PHENOCRYST-RATIO (Q/K/P): 1/1.3/0.1 (In Pumice Fragments)
DEGREE OF WELDING: Slight
POROSITY (VOL. %): 53
OXIDATION STATE OF Fe-Ti OXIDES: C3-C4

ROCK NAME: Rhyolitic Vitric-Crystal Tuff

GENERAL DESCRIPTION IN THIN SECTION: Fine- to medium-grained phenocrysts in a groundmass consisting mainly of fresh-glass, pumice fragments. Many pumice fragments are partially flattened.

MINERAL COMPONENT		VOL. %	COMMENTS
Pore Space		53	
Groundmass		40	
Pumice Fragments	(85)		Up to 34 mm. Many pumice fragments are partially flattened. Glass is fresh. Some brown-colored glass.
Glass	(15)		Fresh; brown colored. Y-shaped shards and intact bubble walls indicate slight welding.
Phenocrysts		7	Mainly in pumice fragments.
Sanidine	(50)		
Quartz	(36)		
Opaques	(14)		Ilmenite, magnetite, and hematite.
Pyroxene	(tr)		Augite.

LANL VAPOR TRANSPORT STUDY
REQUEST NO.: 403353
PROJECT NO.: 6L0001000

SAMPLE NO.: MCG-658
DRILL HOLE LLC-86-20 UNIT 1b
DRILL HOLE DEPTH (FT): 119

BANDELIER TUFF PHENOCRYST-RATIO (Q/K/P): 1/1.5/0.01
DEGREE OF WELDING: Slight to Moderate POROSITY (VOL. %): 21
OXIDATION STATE OF Fe-Ti OXIDES: C4

ROCK NAME: Rhyolitic Vitric-Crystal Tuff

GENERAL DESCRIPTION IN THIN SECTION: Fine- to medium-grained phenocrysts in a slightly to moderately welded, fresh-glass groundmass. Some pumice fragments are flattened.

MINERAL COMPONENT	VOL. %		COMMENTS
Groundmass		55	
Glass	(75)		Mostly fresh, incipient alteration to clay. Minor amounts of brown-colored glass are present.
Pumice	(25)		Up to 7.73 mm. Some fragments are flattened. Phenocryst ratio is 1:1 quartz to sanidine.
Pore Space		21	
Phenocrysts		20	
Sanidine	(55)		
Quartz	(40)		
Opaques	(3)		Magnetite, ilmenite, rutile, and hematite.
Plagioclase	(2)		
Pyroxene	(tr)		Augite
Lithic Fragments		4	Up to 2.88 mm. Altered hyalopilitic basalts and vitric tuffs; a vitric tuff with spherulitic devitrification; and a fresh, porous, basaltic crystal-vitric tuff.

LANL VAPOR TRANSPORT STUDY
REQUEST NO.: 403353
PROJECT NO.: 6L0001000

SAMPLE NO.: MCG-659
OUTCROP SAMPLE
UNIT 2b

BANDELIER TUFF PHENOCRYST-RATIO (Q/K/P): 1/2.5/0.01
DEGREE OF WELDING: Slight
POROSITY (VOL. %): 34
OXIDATION STATE OF Fe-Ti OXIDES: C4

ROCK NAME: Rhyolitic Crystal-Vitric Tuff

GENERAL DESCRIPTION IN THIN SECTION: Fine- to medium-grained phenocrysts in a slightly welded groundmass. Shards show axiolitic devitrification. Pumice fragments are replaced by sanidine and tridymite.

MINERAL COMPONENT	VOL. %		COMMENTS
Groundmass		38	
Glass	(67)		Axiolitic devitrification. Y-shaped shards are present.
Pumice Fragments	(33)		Up to 2.58 mm. Replaced/mineralized by sanidine and tridymite. Phenocryst ratio (Q/K) = 1/2.5.
Pore Space		34	
Phenocrysts		26	
Sanidine	(60)		
Quartz	(38)		Some grains are embayed.
Opaques	(2)		Ilmenite, magnetite, rutile, and hematite.
Pyroxene	(tr)		
Plagioclase	(tr)		One zoned grain.
Lithic Fragments		2	Up to 2.61 mm. Basalts.

LANL VAPOR TRANSPORT STUDY
REQUEST NO.: 403353
PROJECT NO.: 6L0001000

SAMPLE NO.: MCG-660
OUTCROP SAMPLE
UNIT 2b

BANDELIER TUFF PHENOCRYST-RATIO (Q/K/P): 1/2.5/0.04
DEGREE OF WELDING: Slight
POROSITY (VOL. %): 43
OXIDATION STATE OF Fe-Ti OXIDES: C4

ROCK NAME: Rhyolitic Crystal-Vitric Tuff

GENERAL DESCRIPTION IN THIN SECTION: Fine- to medium-grained phenocrysts in a slightly welded groundmass. Shards show axiolitic devitrification. Pumice fragments are replaced by sanidine and tridymite.

MINERAL COMPONENT	VOL. %		COMMENTS
Pore Space		43	
Groundmass		29	
Glass	(69)		Axiolitic devitrification.
Pumice	(31)		Up to 6.15 mm. Replaced/mineralized by sanidine and tridymite. Some pumice fragments contain a fibrous zeolite, others have amphibole, pyroxene, and zoned-plagioclase phenocrysts. One pumice fragment had a phenocryst ratio (Q/K) = 1/1.5.
Phenocrysts		28	
Sanidine	(47)		May have oriented overgrowths of sanidine; this may be vapor-phase mineralization.
Quartz	(46)		
Opaques	(5)		Ilmenite, magnetite, rutile, and hematite.
Plagioclase	(1)		
Amphibole	(1)		Lamprobolite.
Pyroxene	(tr)		Augite.
Lithic Fragments		tr	Up to 1.45 mm. Altered tuff and grains consisting of pyroxene and opaques, possibly from a basalt.

LANL VAPOR TRANSPORT STUDY
REQUEST NO.: 403353
PROJECT NO.: 6L0001000

SAMPLE NO.: MCG-661
OUTCROP SAMPLE
UNIT 2a

BANDELIER TUFF PHENOCRYST-RATIO (Q/K/P): 1/3.2/0.05
DEGREE OF WELDING: Slight
POROSITY (VOL. %): 44
OXIDATION STATE OF Fe-Ti OXIDES: C4

ROCK NAME: Rhyolitic Crystal Vitric Tuff

GENERAL DESCRIPTION IN THIN SECTION: Fine- to medium-grained phenocrysts in a slightly welded groundmass. Shards show axiolitic devitrification. Pumice fragments are replaced by sanidine and tridymite.

MINERAL COMPONENT	VOL. %		COMMENTS
Pore Space		44	
Groundmass		31	
Glass	(59)		Axiolitic devitrification. Y-shaped shards and intact bubble-walls.
Pumice Fragments	(41)		Up to 4.03 mm. Replaced/mineralized by sanidine and tridymite. Some pumice fragments are andesitic (plagioclase and amphibole phenocrysts); the other pumice only contain quartz phenocrysts.
Phenocrysts		25	
Sanidine	(41)		Some sanidine phenocrysts have been partially dissolved (intragranular porosity).
Quartz	(28)		
Opaques	(14)		Ilmenite, magnetite, rutile, and hematite.
Plagioclase	(3)		Zoned grains.
Amphibole	(tr)		Lamprobolite.
Biotite	(tr)		
Pyroxene	(tr)		Augite.
Lithic Fragment		tr	The lithic is a silicified tuff and measures 1.82 mm.

Appendix C

MOISTURE CHARACTERISTIC CURVES

Table C-1. Data Used to Plot the Moisture Characteristic Curves (drying curves only)

Hole Number	Sample Number	Depth (ft)	Capillary Pressure (psi)	Wetting Fluid Saturation (percent)
LLM-85-01	MCG-602	30	0.510	91.6
			0.906	86.4
			1.420	81.2
			2.055	76.1
			2.814	70.9
			3.701	65.8
LLM-85-01	MCG-603	52	0.455	90.0
			0.823	84.7
			1.385	79.7
			2.230	74.9
			3.495	70.2
			5.403	65.8
LLM-85-01	MCG-604	101	0.493	88.6
			0.955	82.1
			1.738	76.6
			3.220	71.9
			6.555	67.8
LLM-85-01	MCG-605	124	0.392	83.5
			0.620	76.9
			0.955	70.5
			1.450	64.4
			2.189	58.5
			3.319	52.9
LLM-85-02	MCG-606	7	0.392	88.6
			0.812	81.1
			1.450	73.9
			2.372	66.8
			3.663	60.0
			5.440	53.3
LLM-85-02	MCG-607	36	0.097	92.0
			0.181	87.3
			0.494	79.1
			0.799	75.8
			1.382	73.4
			2.975	71.8
LLM-85-02	MCG-608	67	0.424	90.7
			0.681	86.6
			1.050	82.6
			1.573	78.7
			2.315	75.0
			3.375	71.5

Table C-1 (continued). Data Used to Plot the Moisture Characteristic Curves (drying curves only)

Hole Number	Sample Number	Depth (ft)	Capillary Pressure (psi)	Wetting Fluid Saturation (percent)
LLM-85-02	MCG-609	117	0.252	94.2
			0.626	89.3
			1.135	84.2
			1.757	79.1
			2.474	73.9
			3.268	68.6
LLM-85-05	MCG-610	15	0.174	90.0
			0.328	84.5
			0.563	79.1
			0.913	73.9
			1.429	68.9
			2.188	64.2
LLM-85-05	MCG-611	36	0.259	96.1
			1.014	90.8
			1.879	85.0
			2.715	78.5
			3.482	71.4
			4.171	63.7
LLM-85-05	MCG-612	76	0.072	97.1
			0.344	94.0
			0.800	90.9
			1.424	87.8
			2.198	84.6
			3.109	81.4
LLM-85-05	MCG-613	123	0.166	85.1
			0.243	82.4
			0.382	79.7
			0.671	77.1
			1.426	74.6
			4.598	72.1
LGM-85-06	MCG-614	29	0.446	83.2
			0.679	77.2
			1.020	71.4
			1.526	65.8
			2.295	60.5
			3.500	55.4

Table C-1 (continued). Data Used to Plot the Moisture Characteristic Curves (drying curves only)

Hole Number	Sample Number	Depth (ft)	Capillary Pressure (psi)	Wetting Fluid Saturation (percent)
LGM-85-06	MCG-615	51	0.419	90.8
			0.650	86.9
			0.970	83.1
			1.411	79.5
			2.016	76.0
			2.850	72.6
LGM-85-06	MCG-616	99	0.322	85.6
			0.403	85.4
			0.542	84.5
			0.818	84.3
			1.527	83.4
			4.825	82.2
LGM-85-06	MCG-617	115	0.068	96.9
			0.309	92.3
			0.810	87.8
			1.716	83.6
			2.388	81.6
			3.259	79.6
LGM-85-11	MCG-618	3	0.296	88.7
			0.594	81.9
			1.063	75.3
			1.775	69.0
			2.841	62.9
			4.429	57.1
LGM-85-11	MCG-619	30	0.491	90.5
			1.188	81.6
			2.040	72.3
			2.976	62.6
			3.950	52.5
			4.934	42.0
LGM-85-11	MCG-620	94	0.161	93.3
			0.376	88.7
			0.734	84.2
			1.297	79.9
			2.163	75.8
			3.483	71.9

Table C-1 (continued). Data Used to Plot the Moisture Characteristic Curves (drying curves only)

Hole Number	Sample Number	Depth (ft)	Capillary Pressure (psi)	Wetting Fluid Saturation (percent)
LGM-85-11	MCG-621	115	0.270	92.3
			0.446	89.2
			0.727	86.3
			1.191	83.5
			1.991	80.9
			3.463	78.5

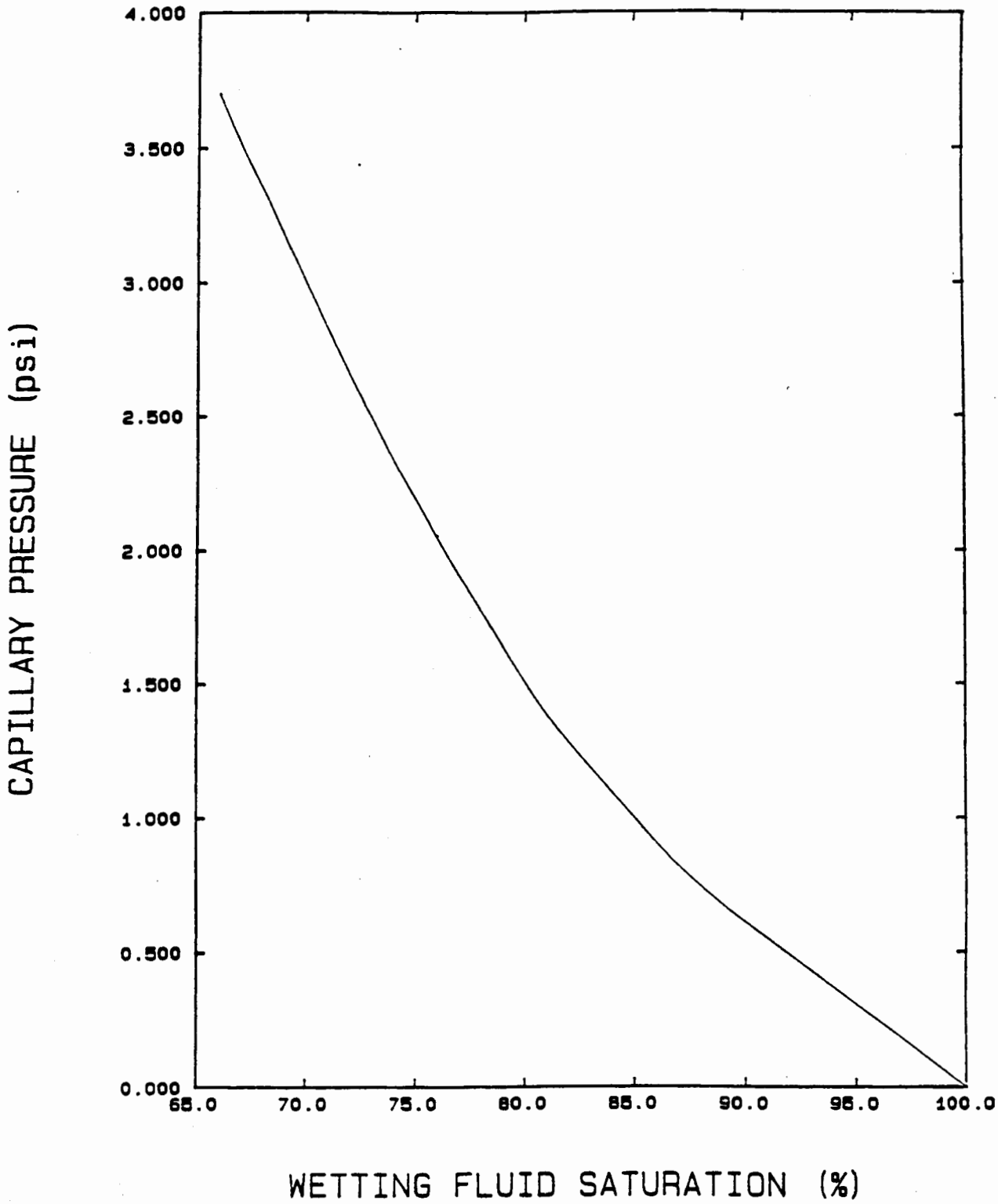

Figure C-1. Moisture Characteristic Curve for Sample MCG-602, Hole LLM-85-01, Depth of 30 Feet

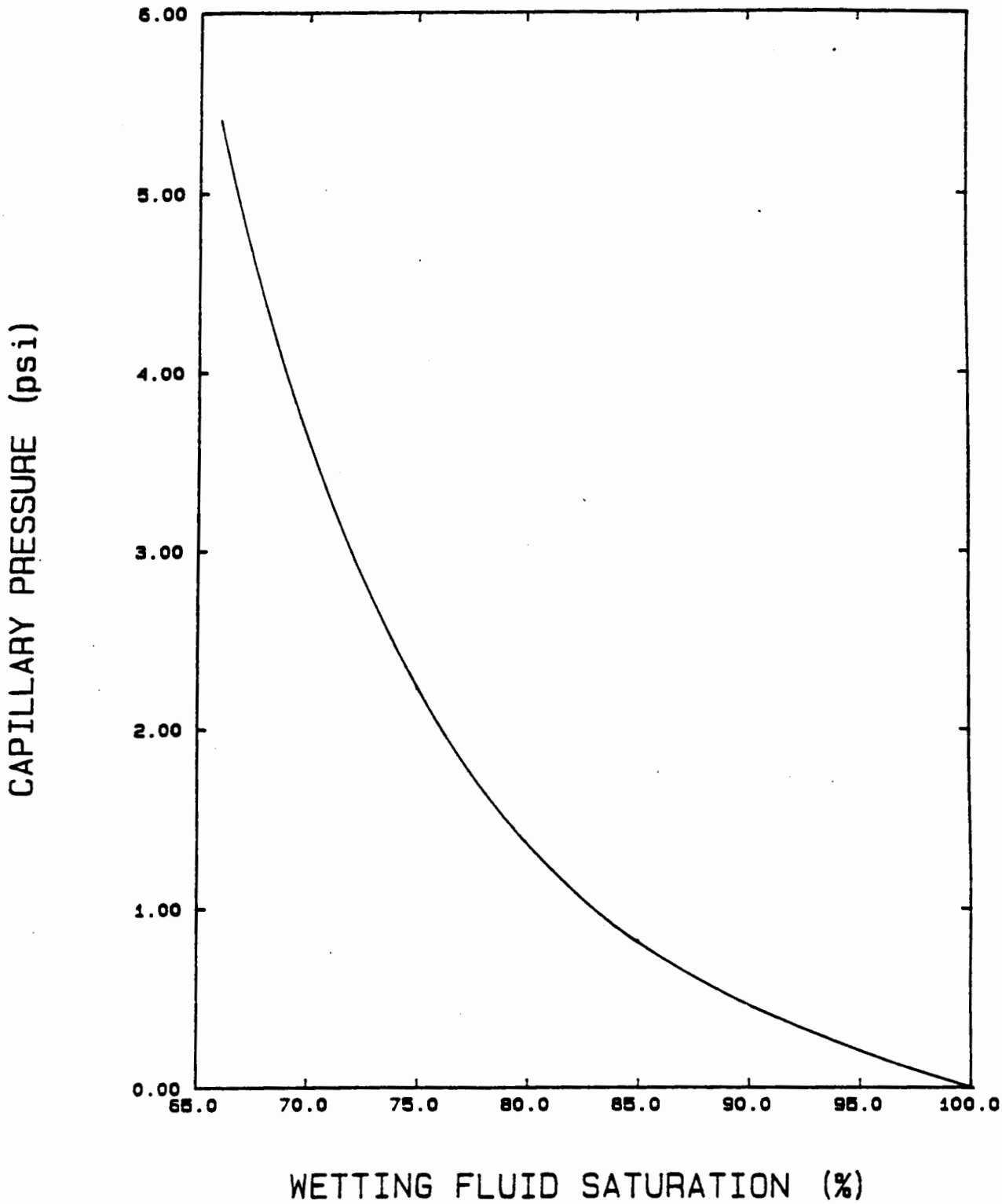

Figure C-2. Moisture Characteristic Curve for Sample MCG-603, Hole LLM-85-01, Depth of 52 Feet

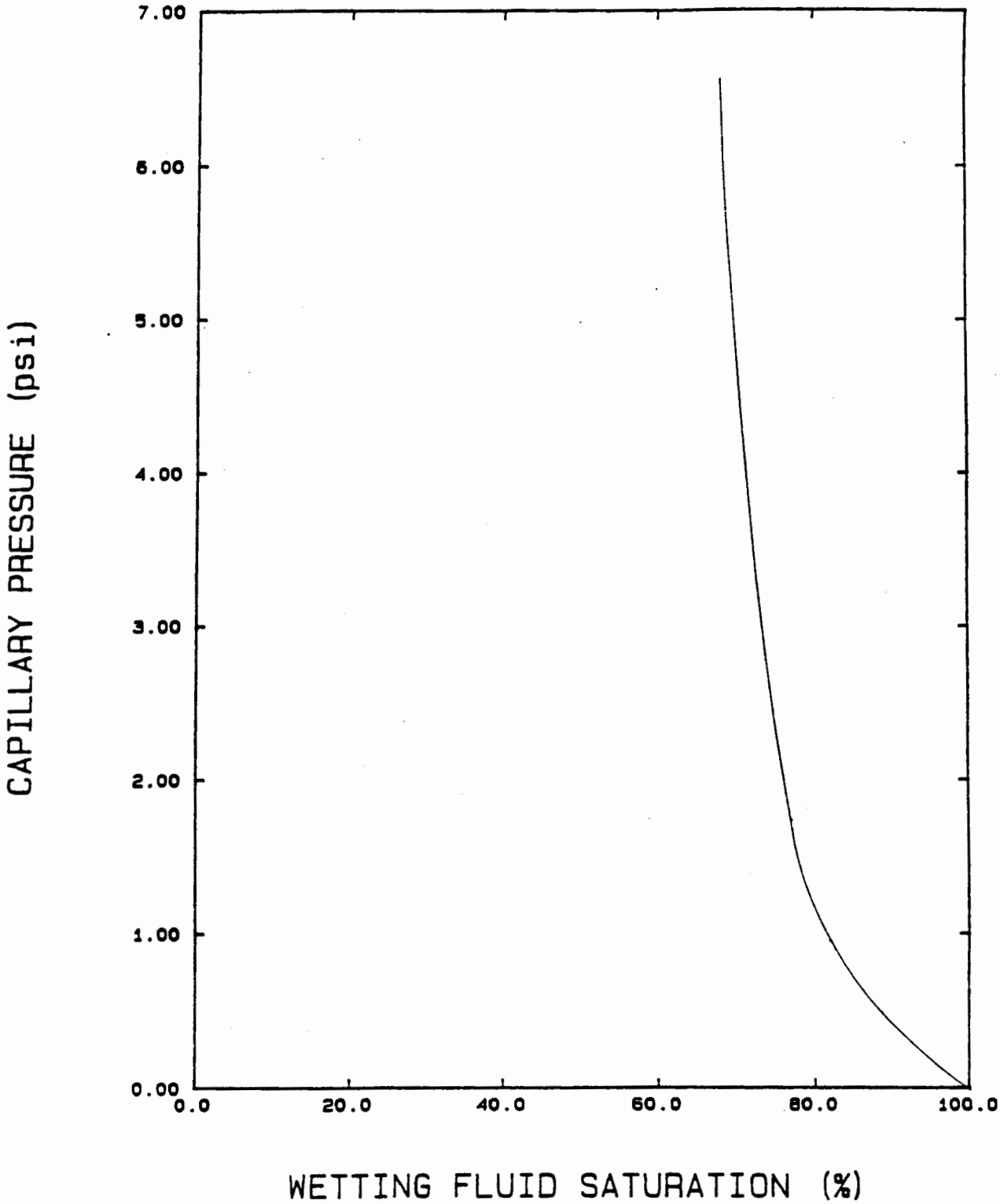

Figure C-3. Moisture Characteristic Curve for Sample MCG-604, Hole LLM-85-01, Depth of 101 Feet

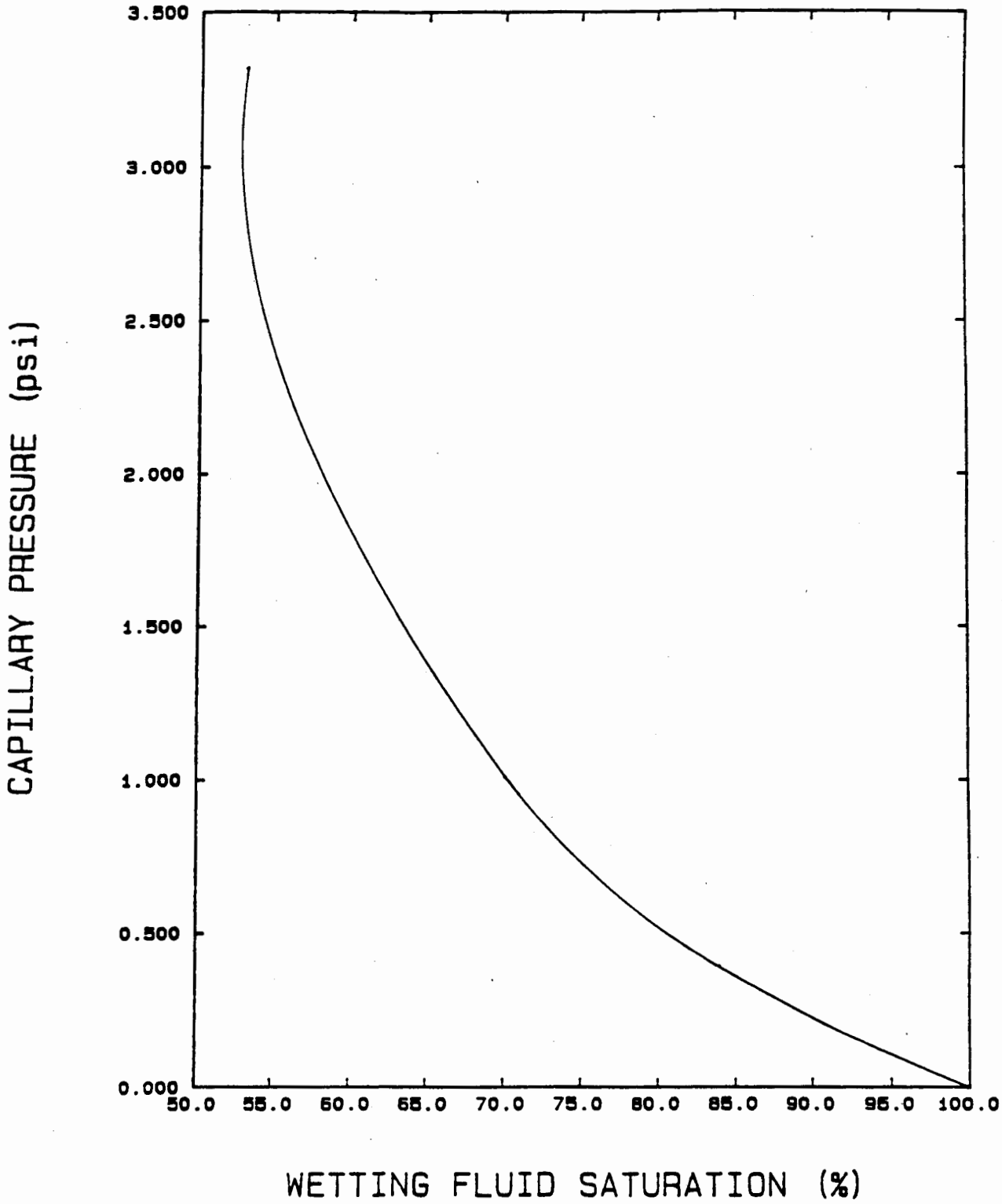

Figure C-4. Moisture Characteristic Curve for Sample MCG-605, Hole LLM-85-01, Depth of 124 Feet

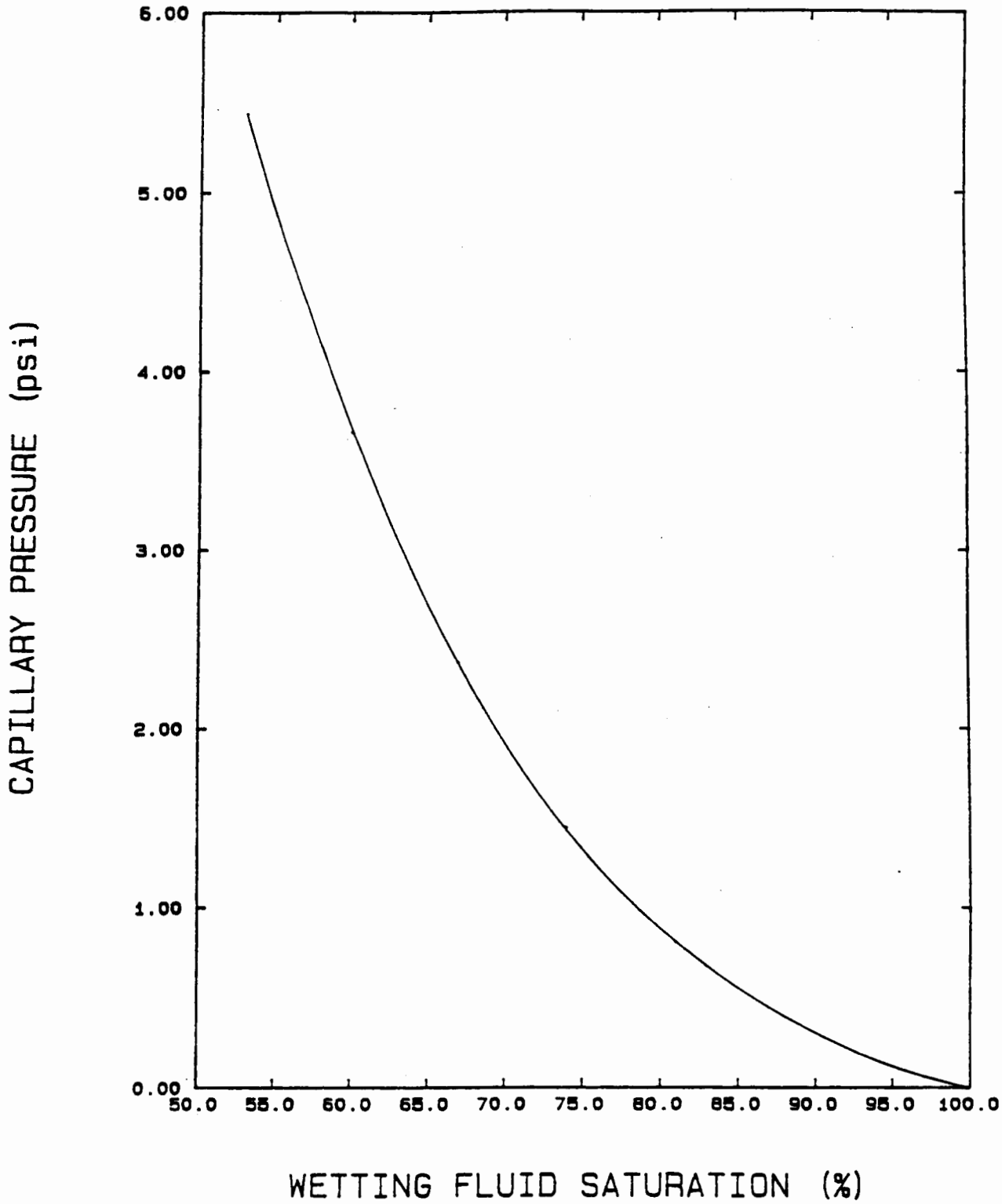

Figure C-5. Moisture Characteristic Curve for Sample MCG-606, Hole LLM-85-02, Depth of 7 Feet

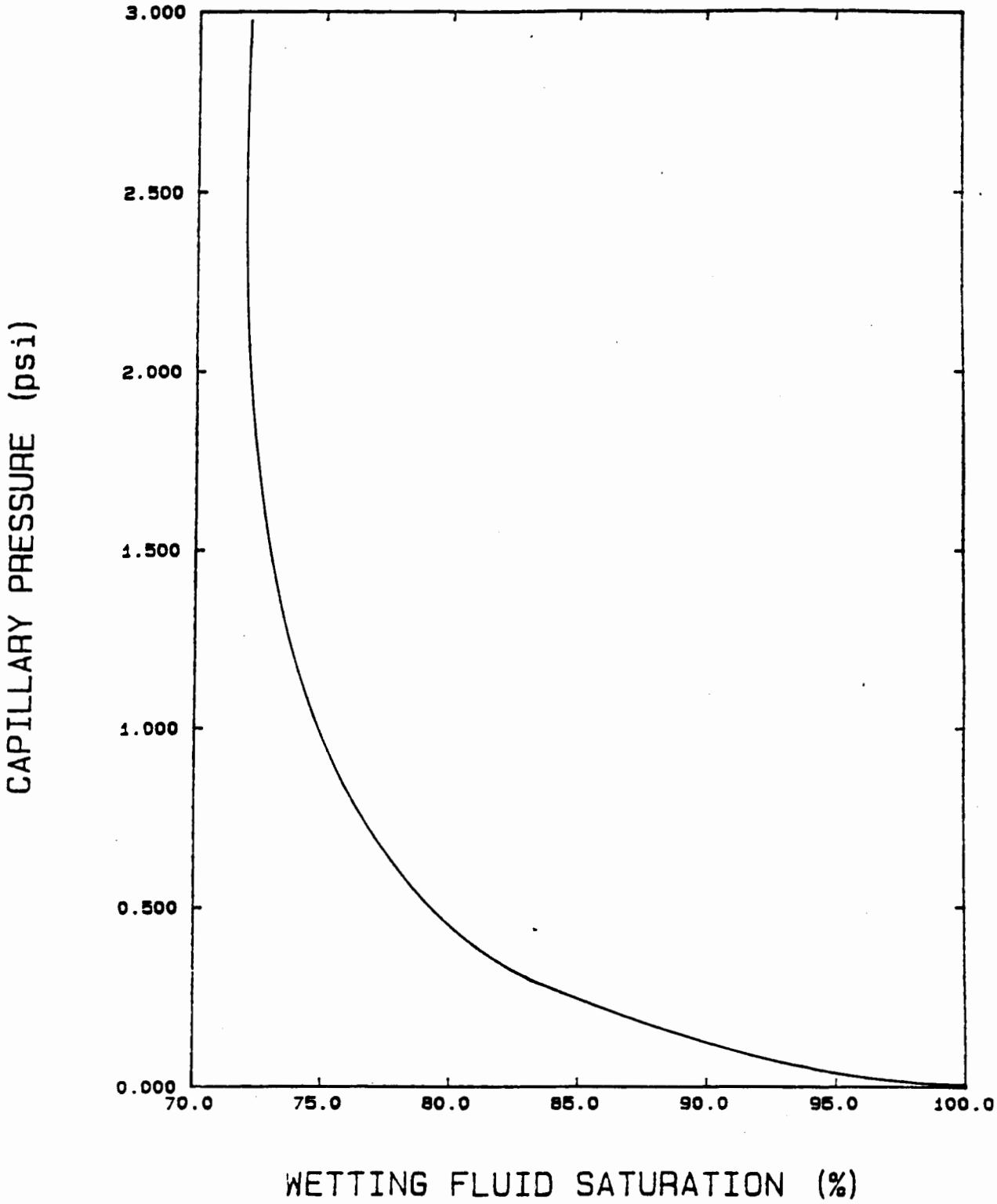

Figure C-6. Moisture Characteristic Curve for Sample MCG-607, Hole LLM-85-02, Depth of 36 Feet

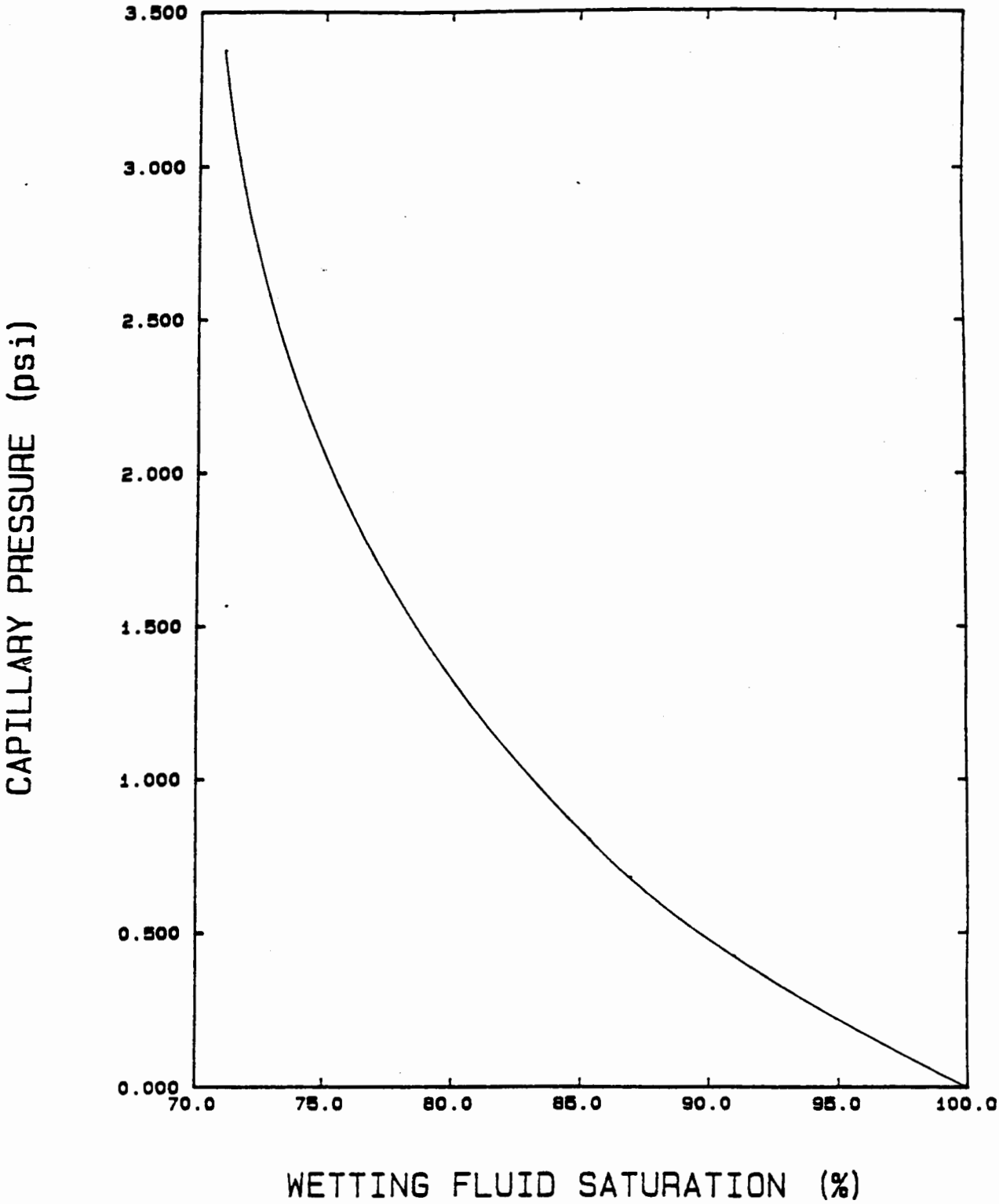

Figure C-7. Moisture Characteristic Curve for Sample MCG-608, Hole LLM-85-02, Depth of 67 Feet

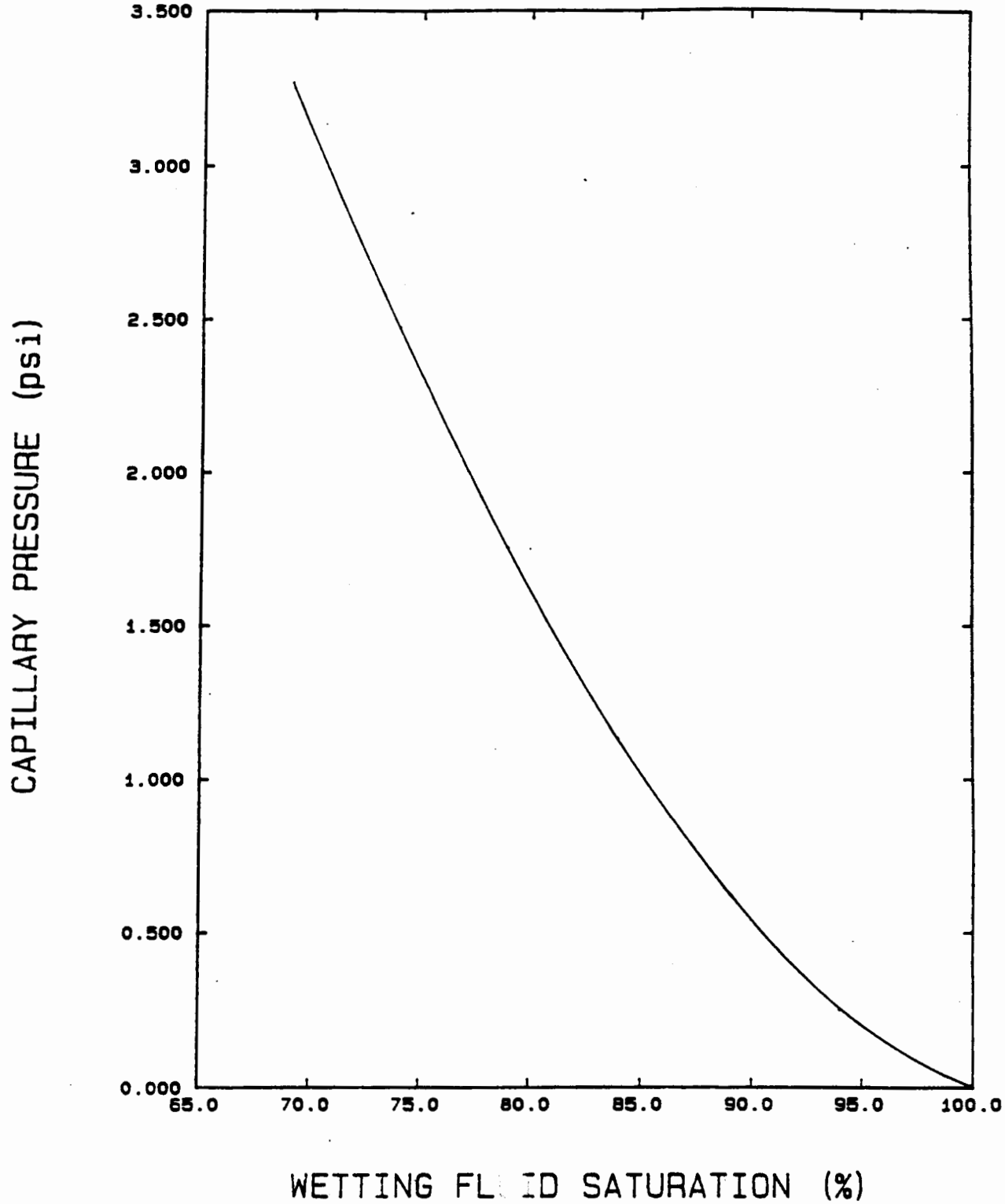

Figure C-8. Moisture Characteristic Curve for Sample MCG-609, Hole LLM-85-02, Depth of 117 Feet

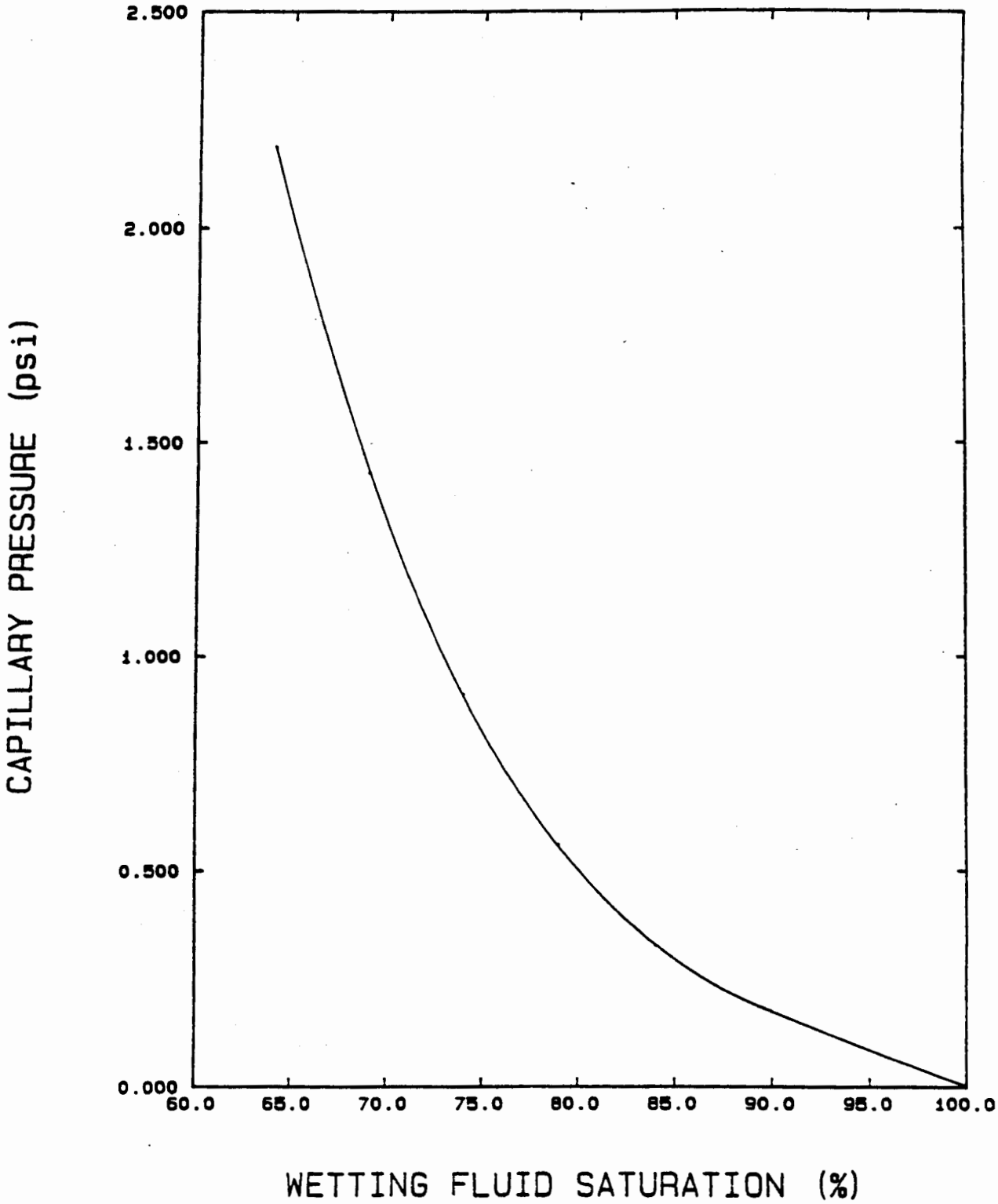

Figure C-9. Moisture Characteristic Curve for Sample MCG-610, Hole LLM-85-05, Depth of 15 Feet

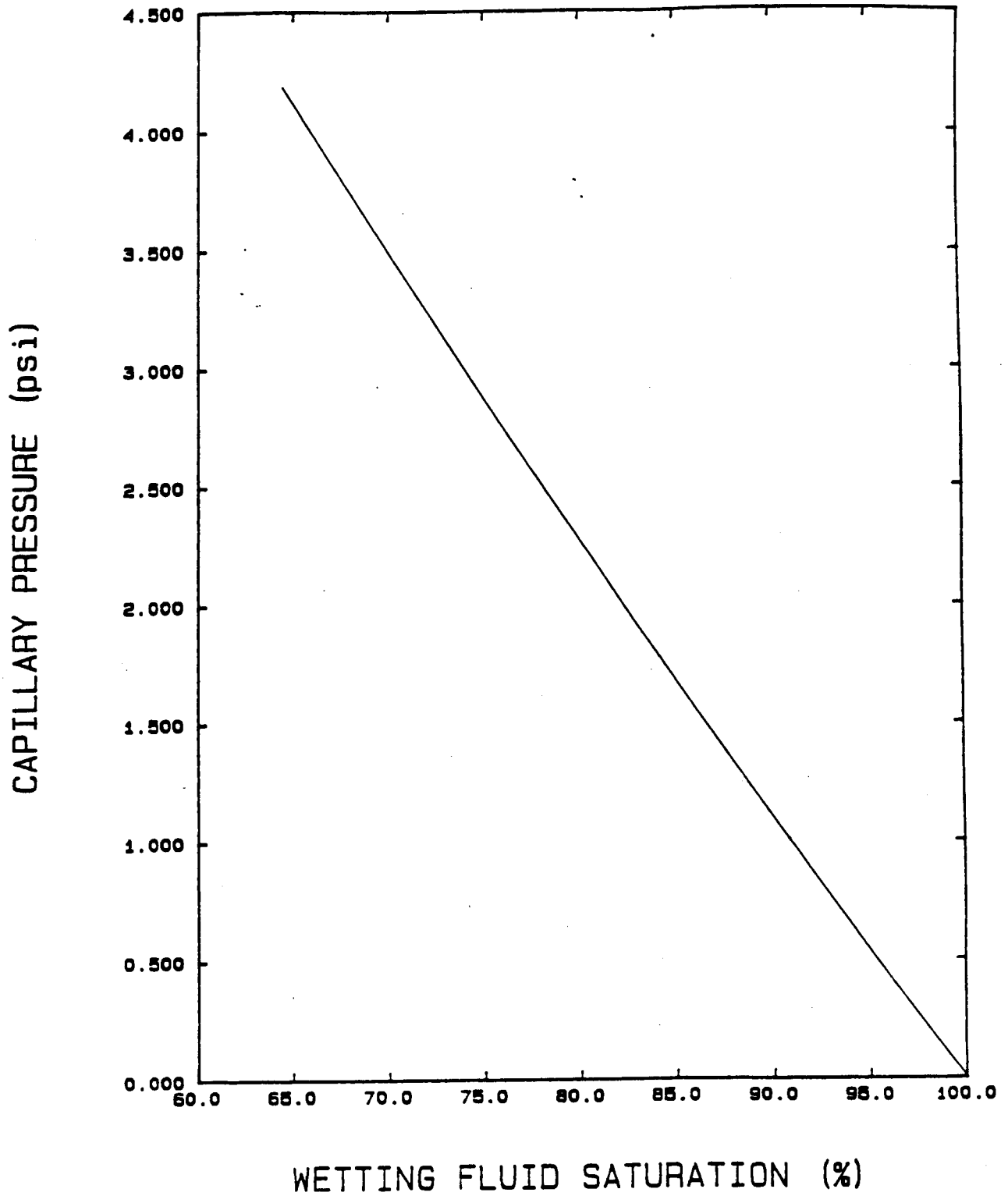

Figure C-10. Moisture Characteristic Curve for Sample MCG-611, Hole LLM-85-05, Depth of 36 Feet

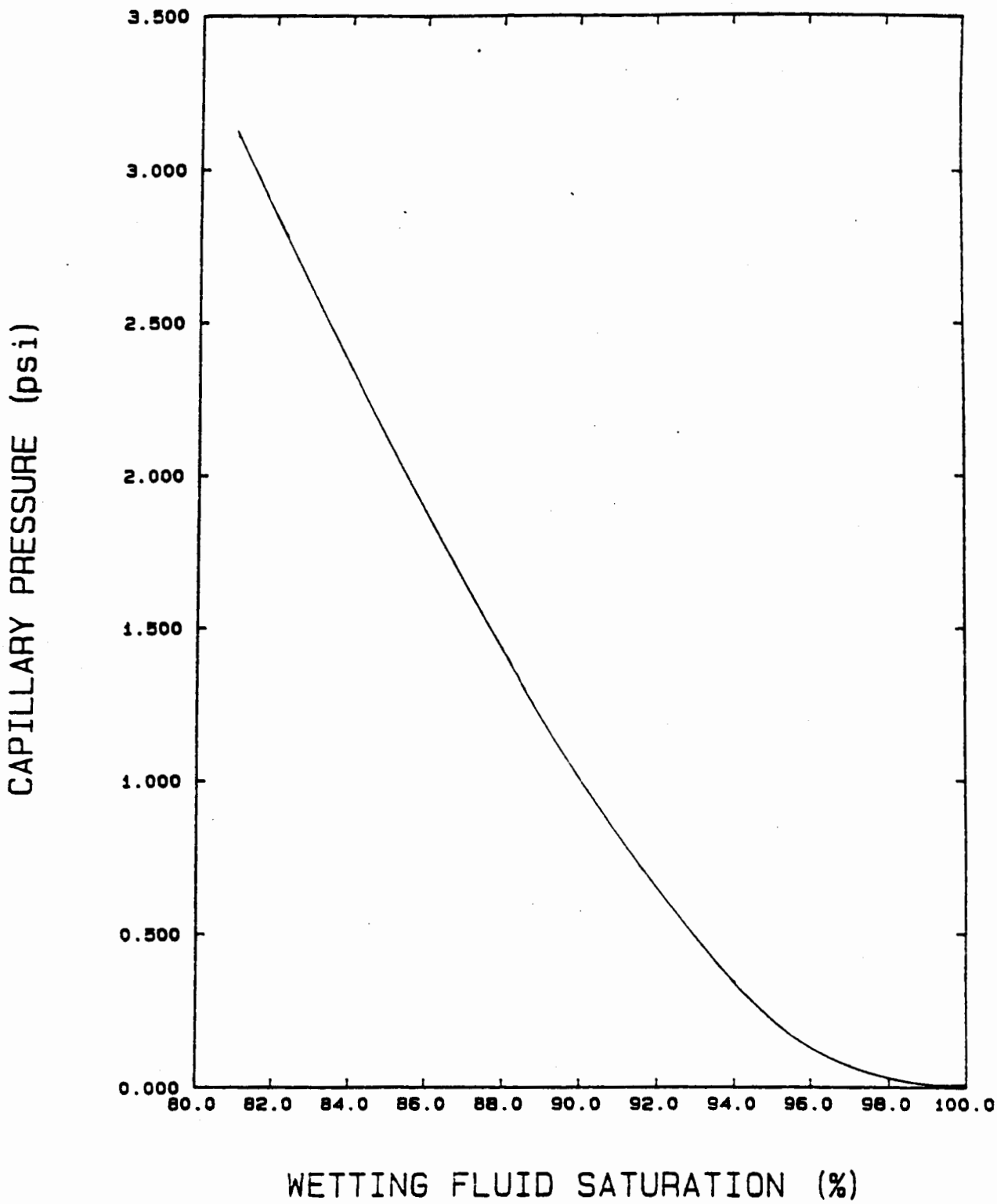

Figure C-11. Moisture Characteristic Curve for Sample MCG-612, Hole LLM-85-05, Depth of 76 Feet

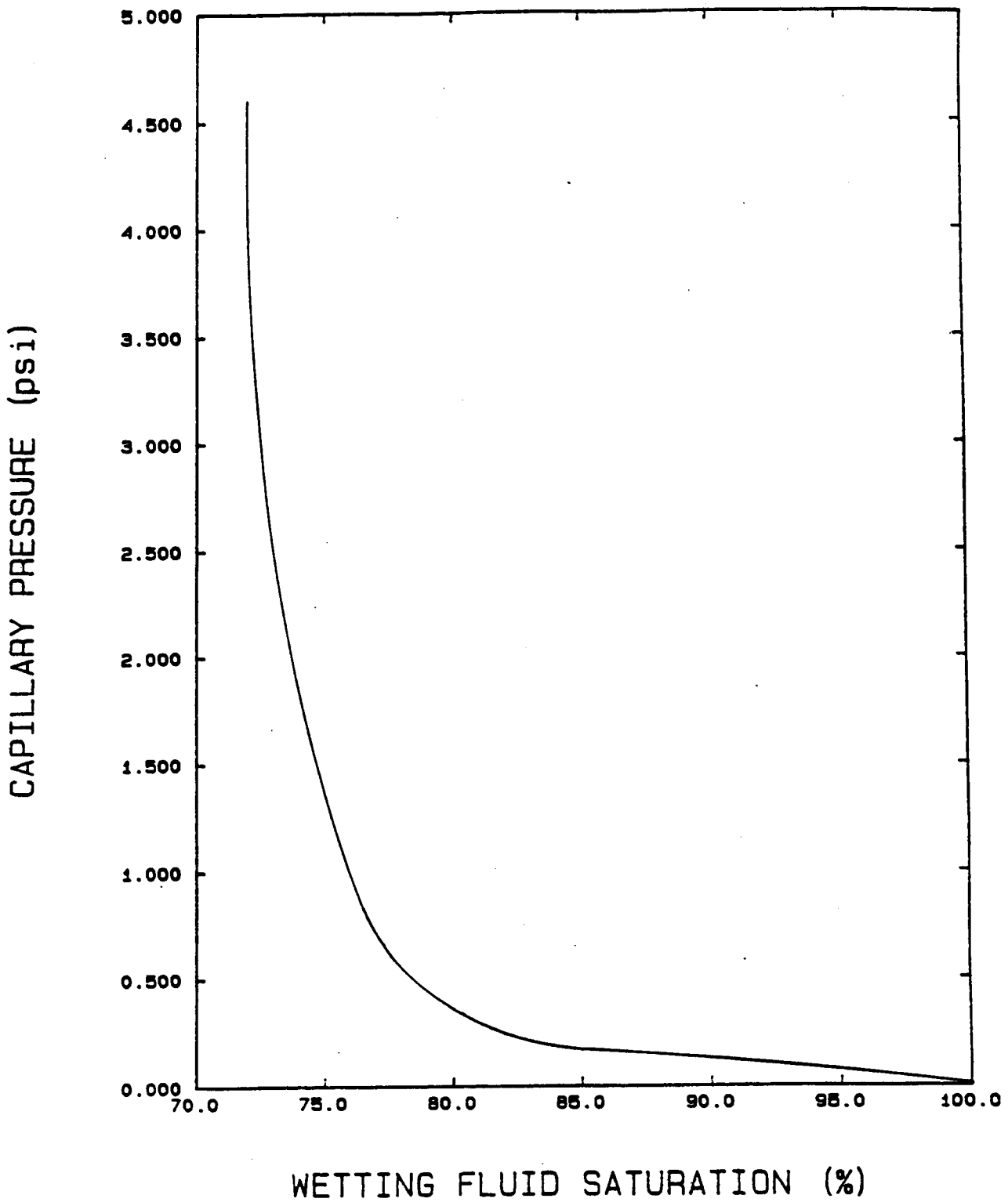

Figure C-12. Moisture Characteristic Curve for Sample MCG-613, Hole LLM-85-05, Depth of 123 Feet

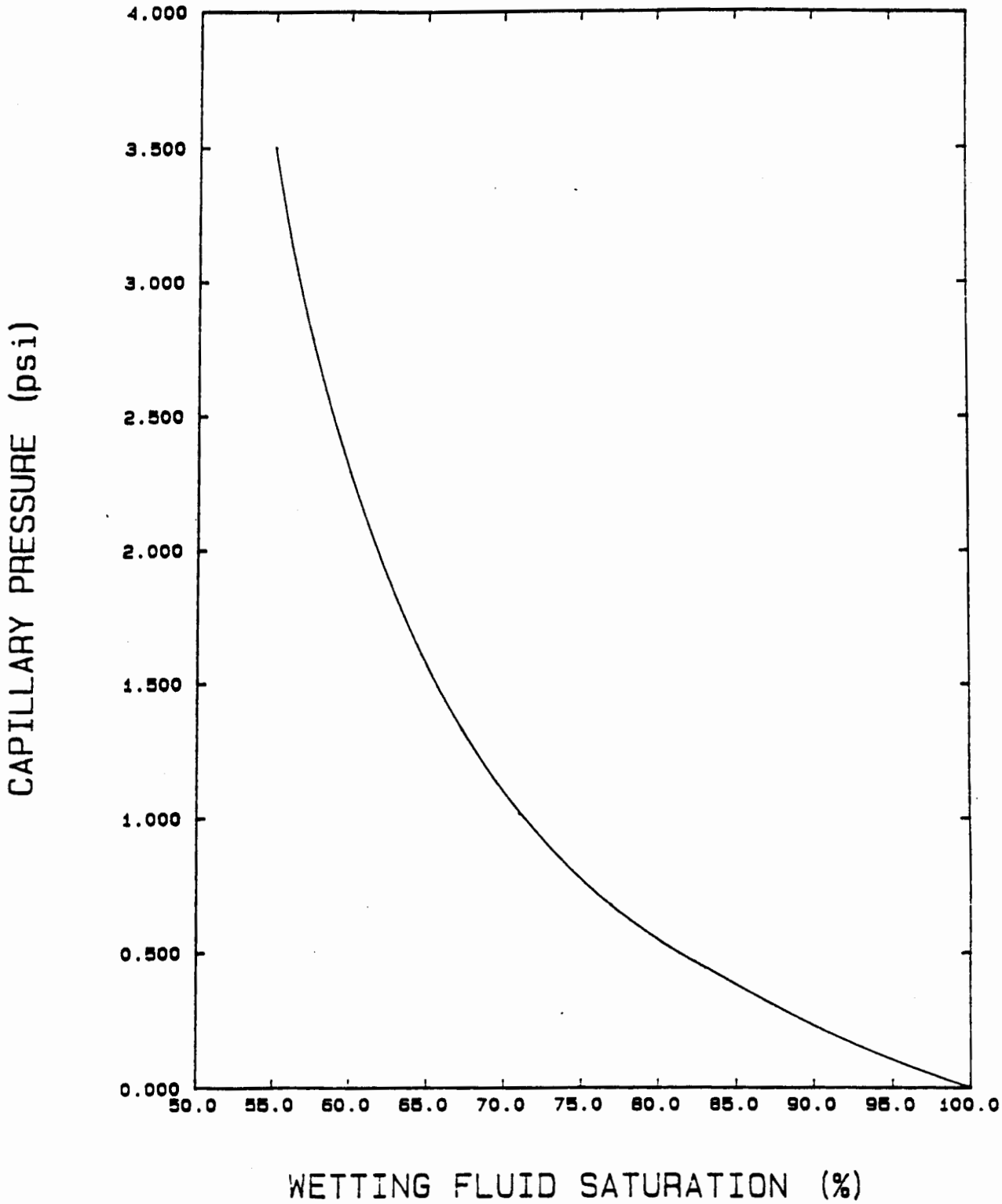

Figure C-13. Moisture Characteristic Curve for Sample MCG-614, Hole LGM-85-06, Depth of 29 Feet

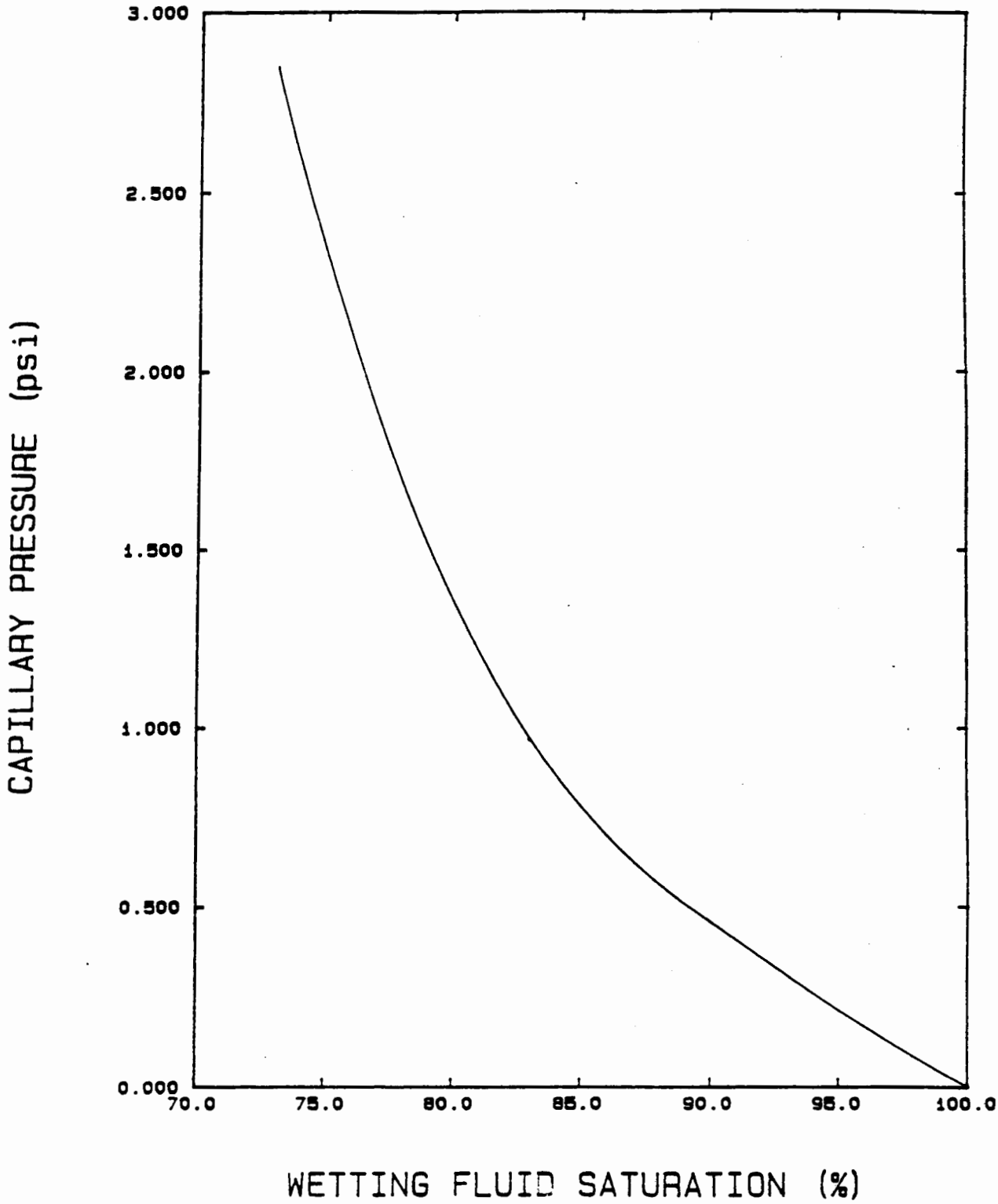

Figure C-14. Moisture Characteristic Curve for Sample MCG-615, Hole LGM-85-06, Depth of 51 Feet

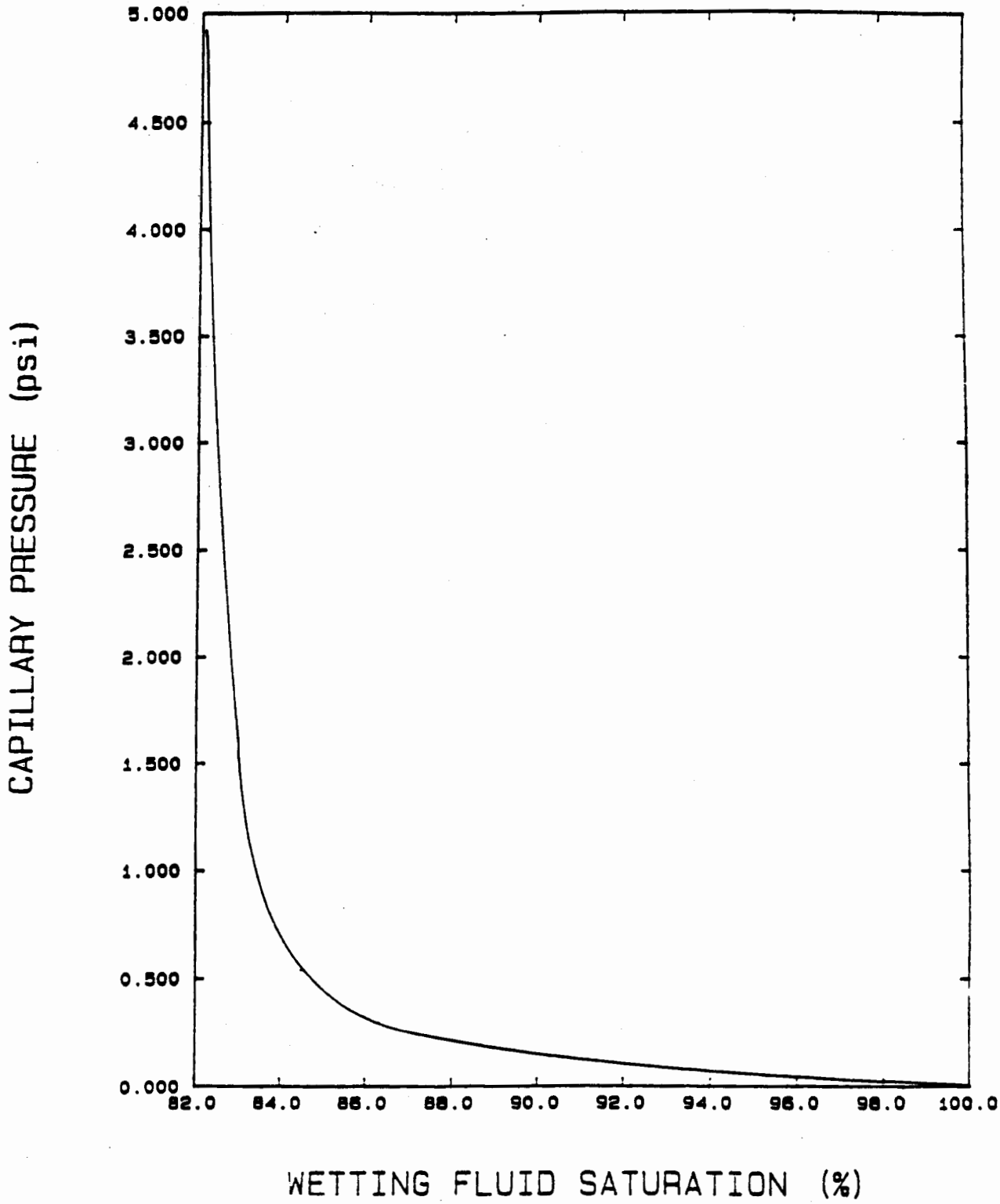

Figure C-15. Moisture Characteristic Curve for Sample MCG-616, Hole LGM-85-06, Depth of 99 Feet

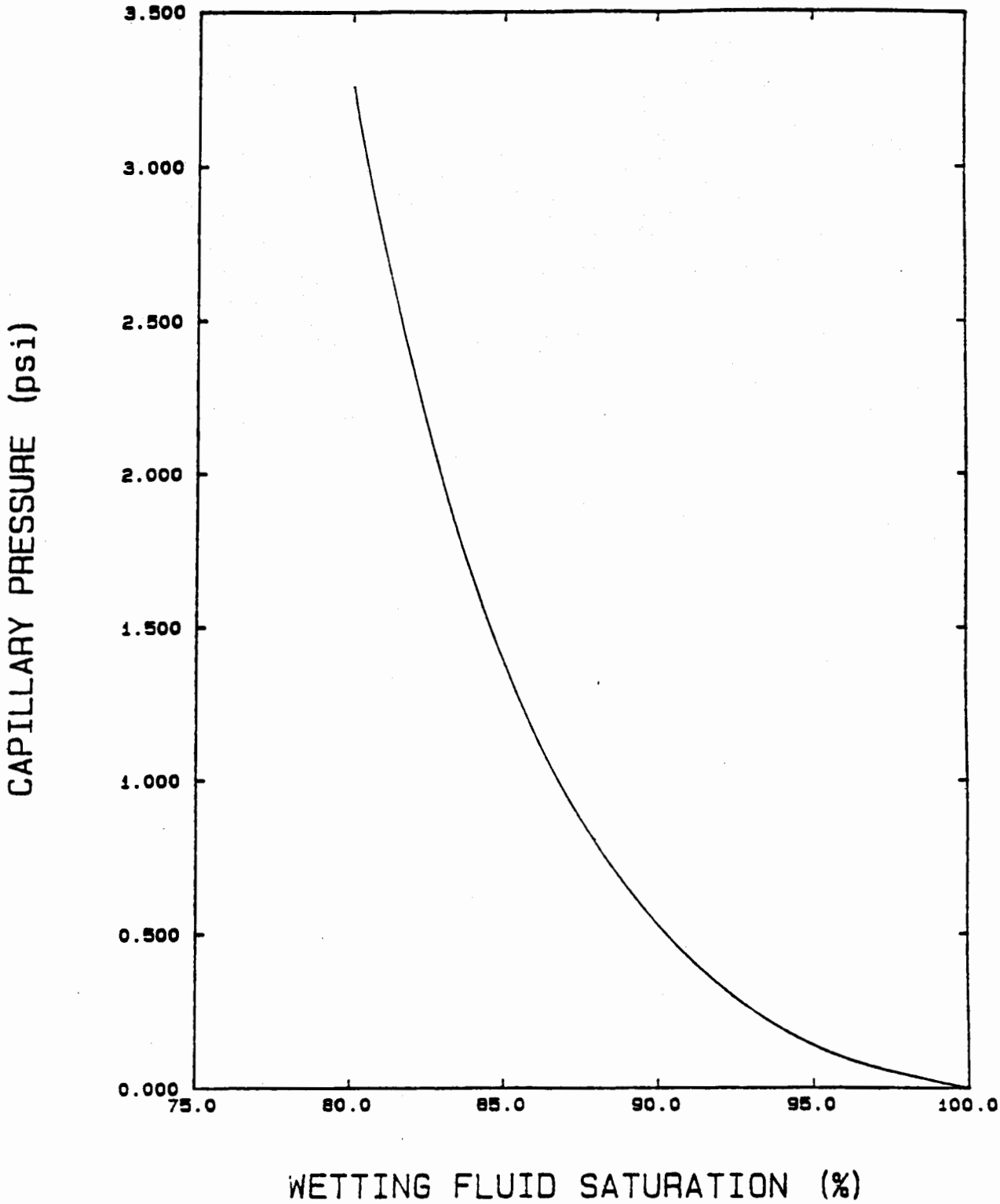

Figure C-16. Moisture Characteristic Curve for Sample MCG-617, Hole LGM-85-06, Depth of 115 Feet

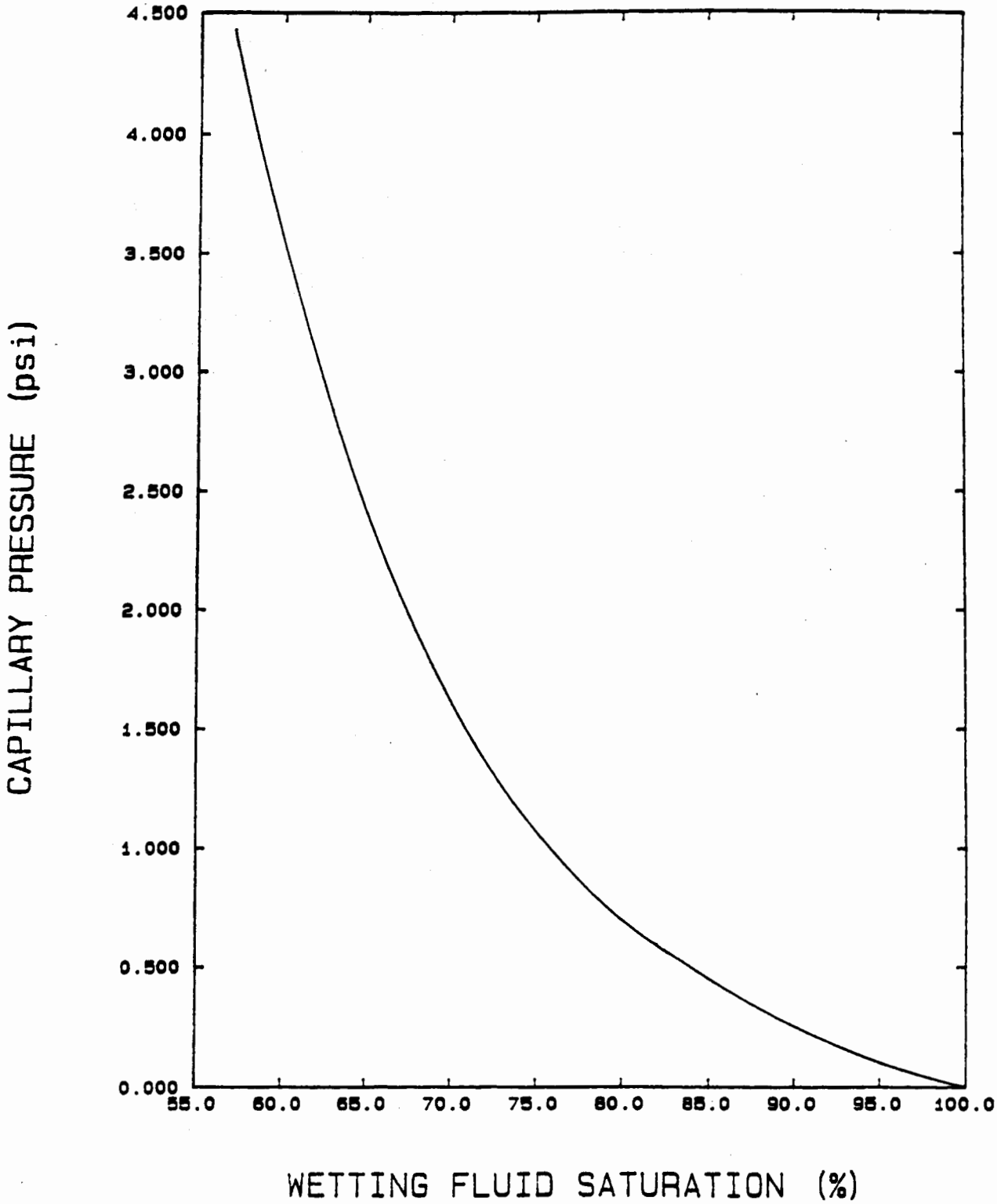

Figure C-17. Moisture Characteristic Curve for Sample MCG-618, Hole LGM-85-11, Depth of 3 Feet

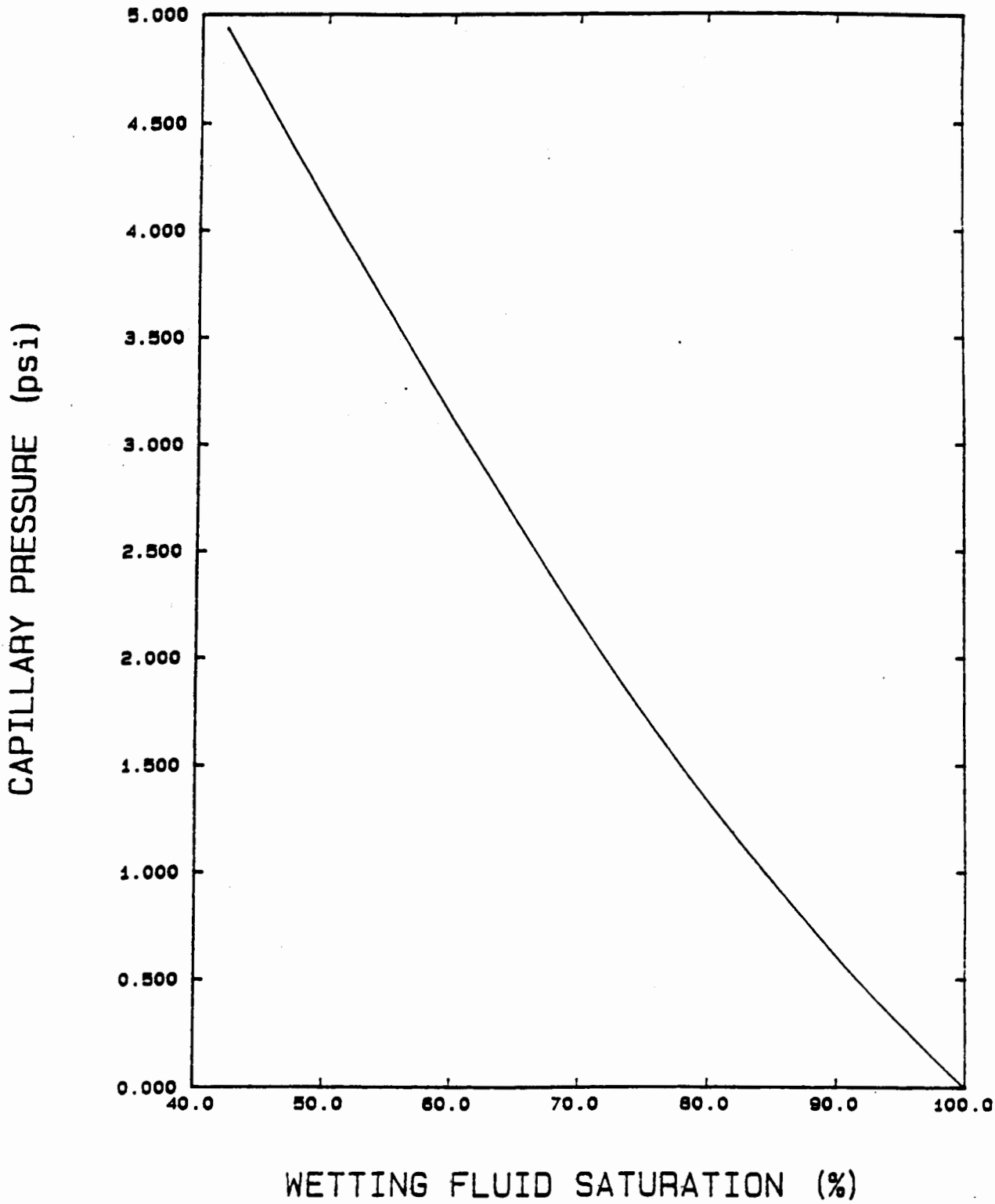

Figure C-18. Moisture Characteristic Curve for Sample MCG-619, Hole LGM-85-11, Depth of 30 Feet

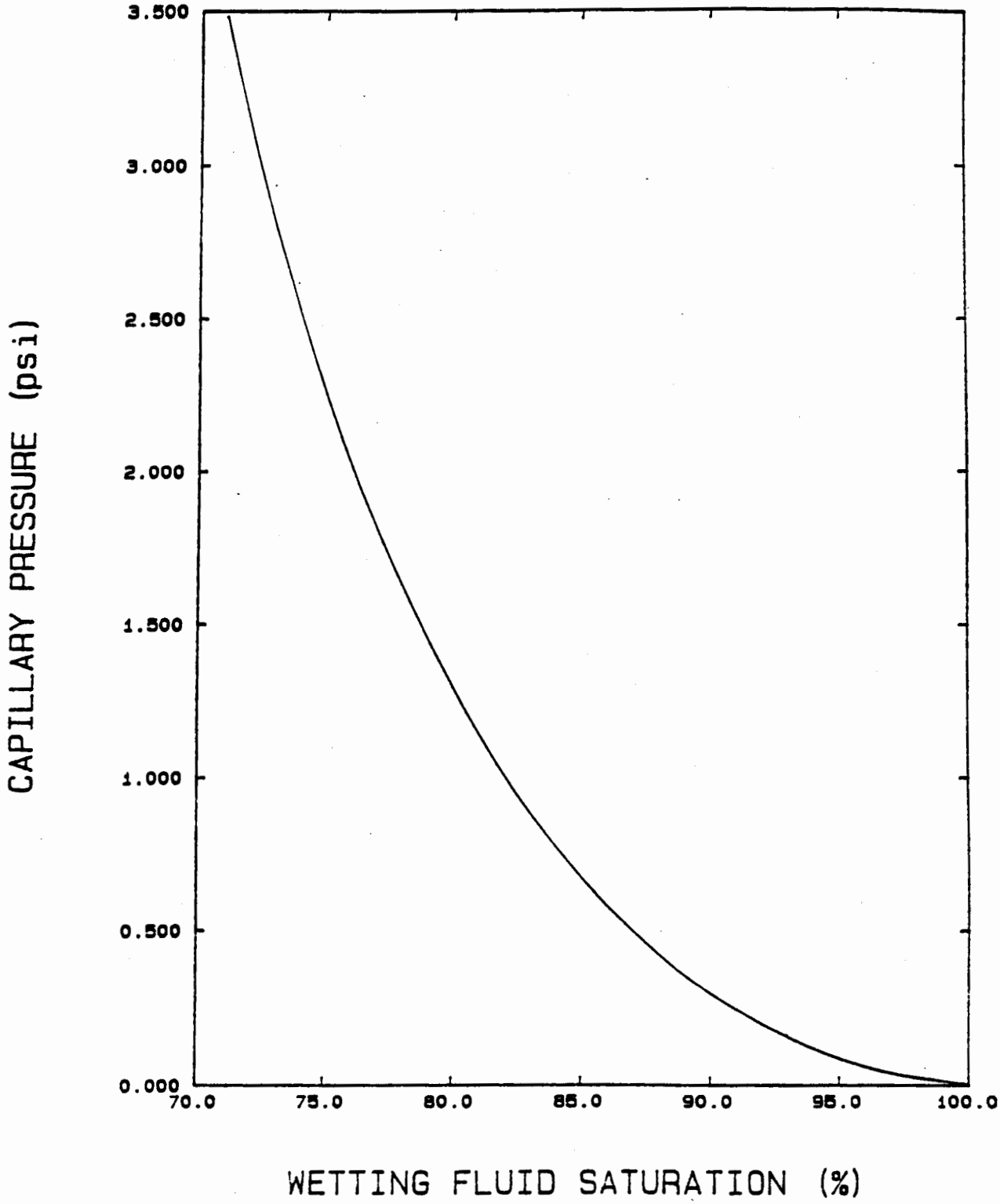

Figure C-19. Moisture Characteristic Curve for Sample MCG-620, Hole LGM-85-11, Depth of 94 Feet

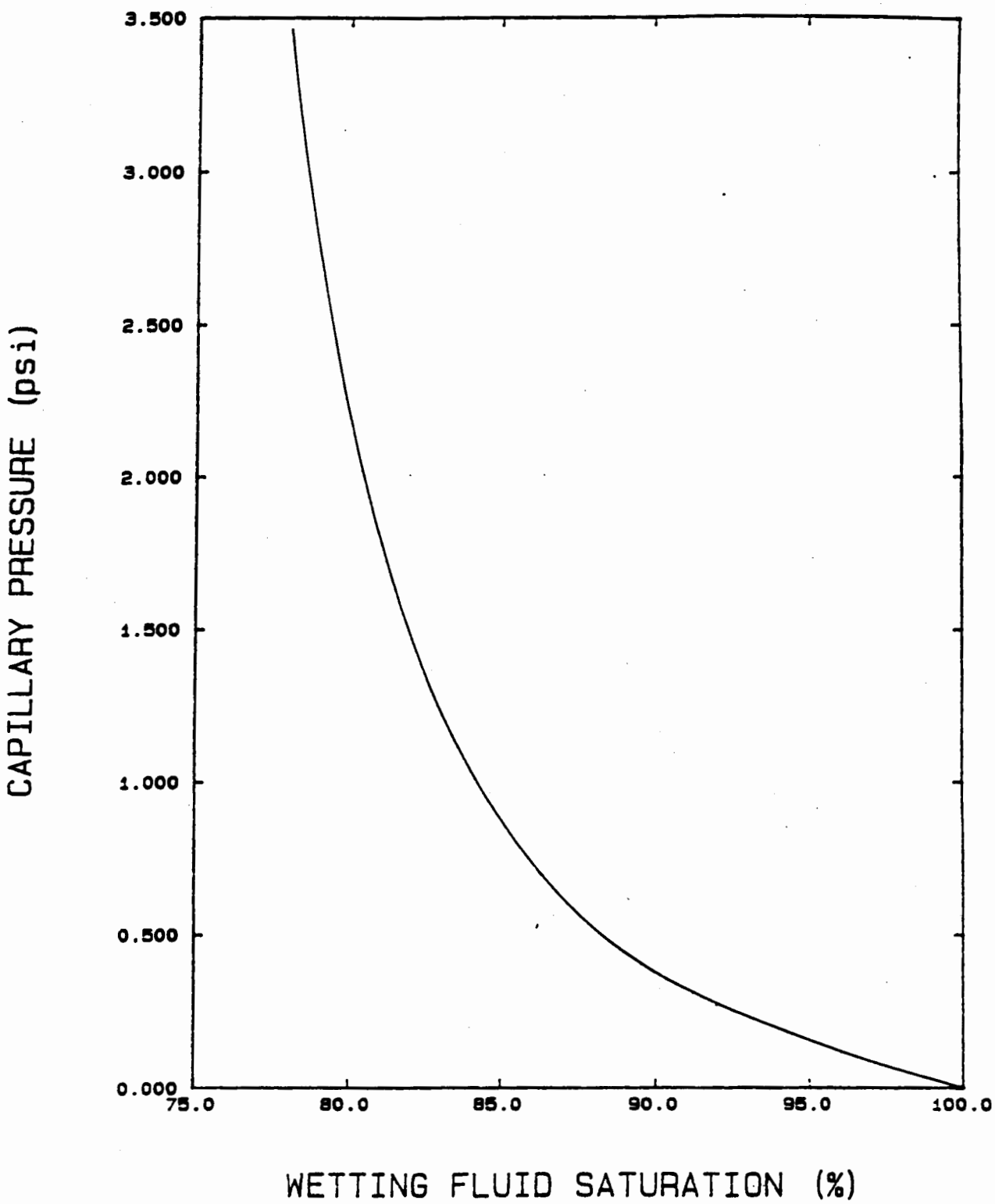

Figure C-20. Moisture Characteristic Curve for Sample MCG-621, Hole LGM-85-11, Depth of 115 Feet

Appendix D

EFFECTIVE PERMEABILITY AS A FUNCTION OF SATURATION

(saturation refers to total air saturation)

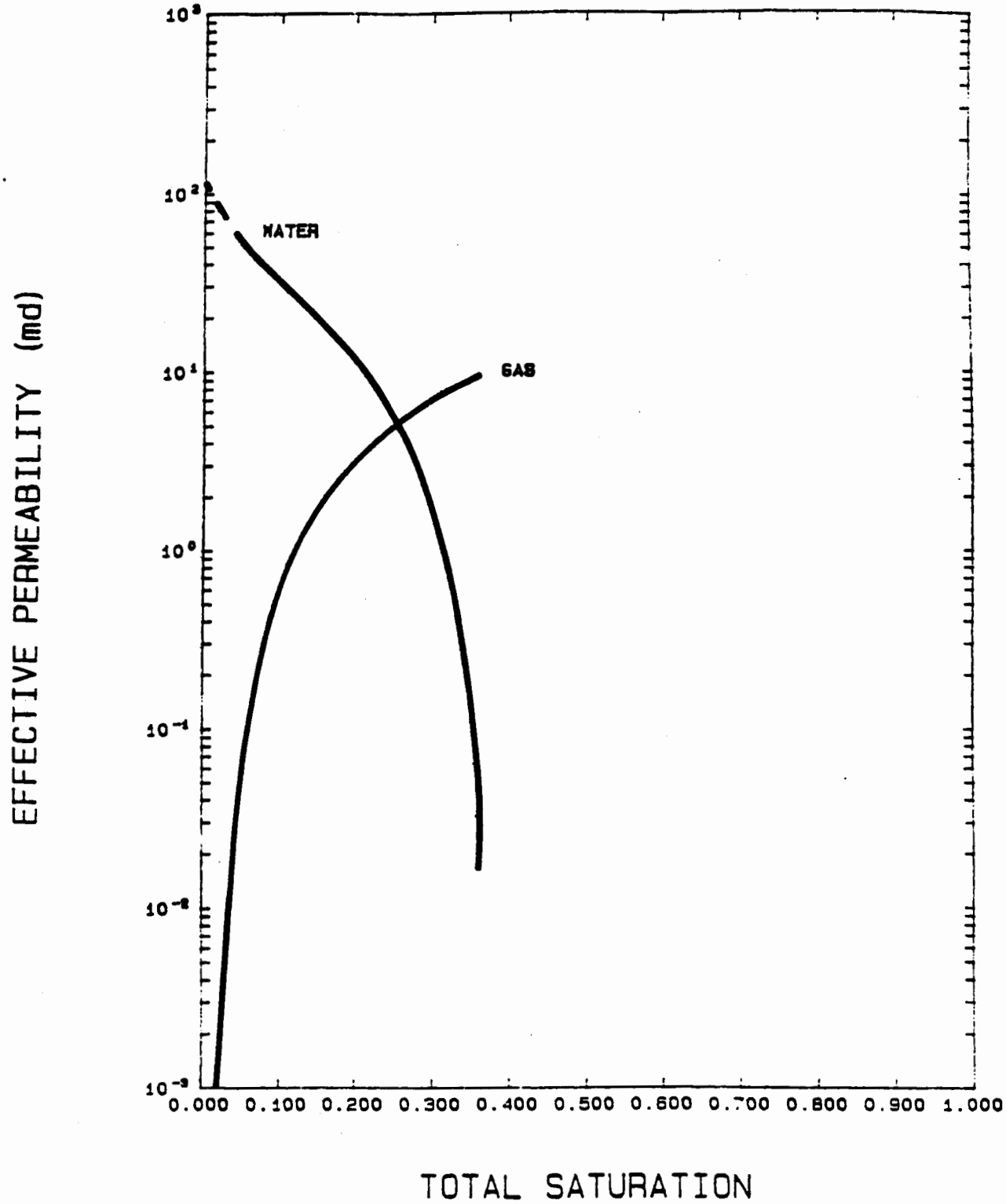

Figure D-1. Effective Permeability as a Function of Saturation for Sample MCG-602, Hole LLM-85-01, Depth of 30 Feet

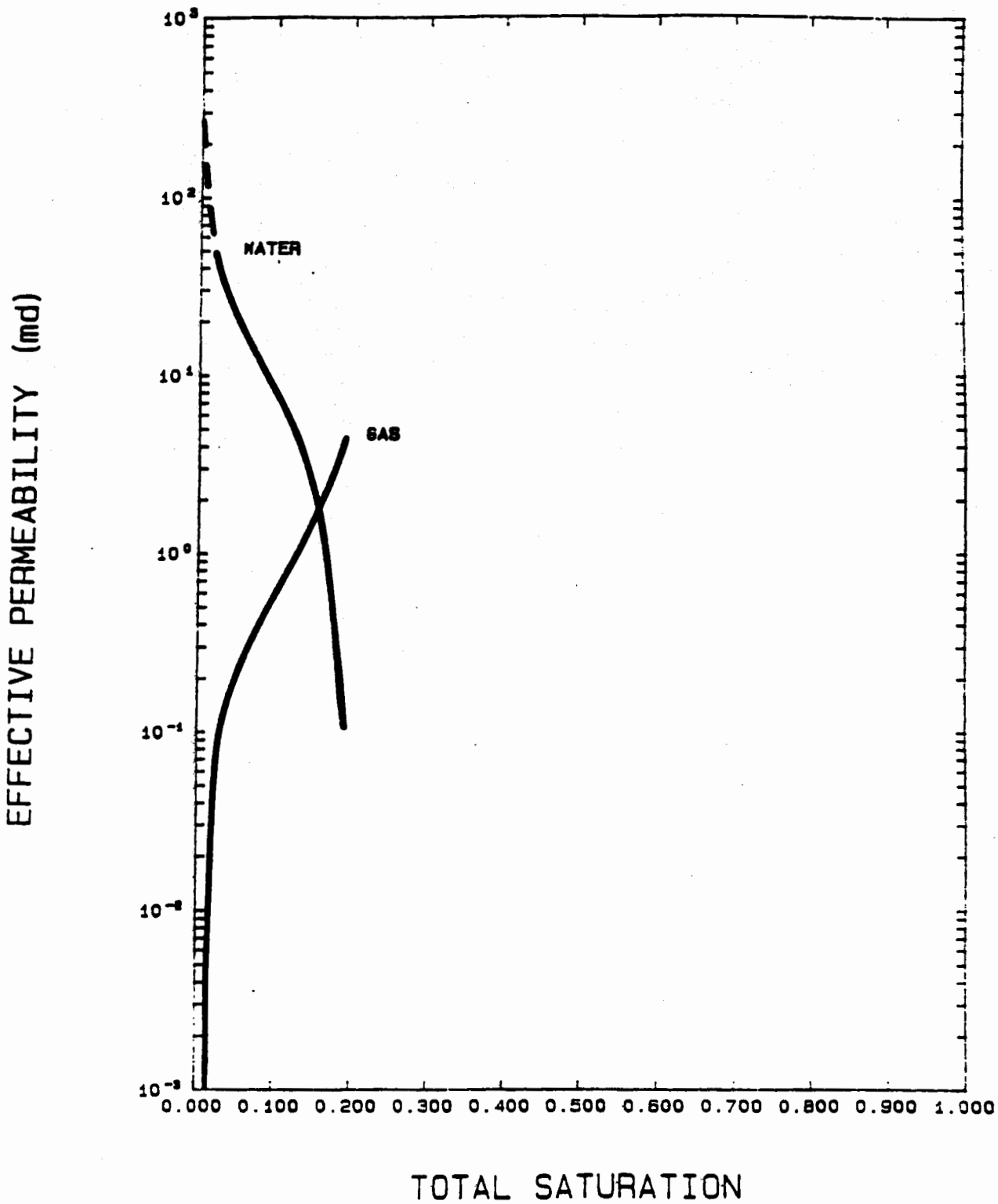

Figure D-2. Effective Permeability as a Function of Saturation for Sample MCG-603, Hole LLM-85-01, Depth of 52 Feet

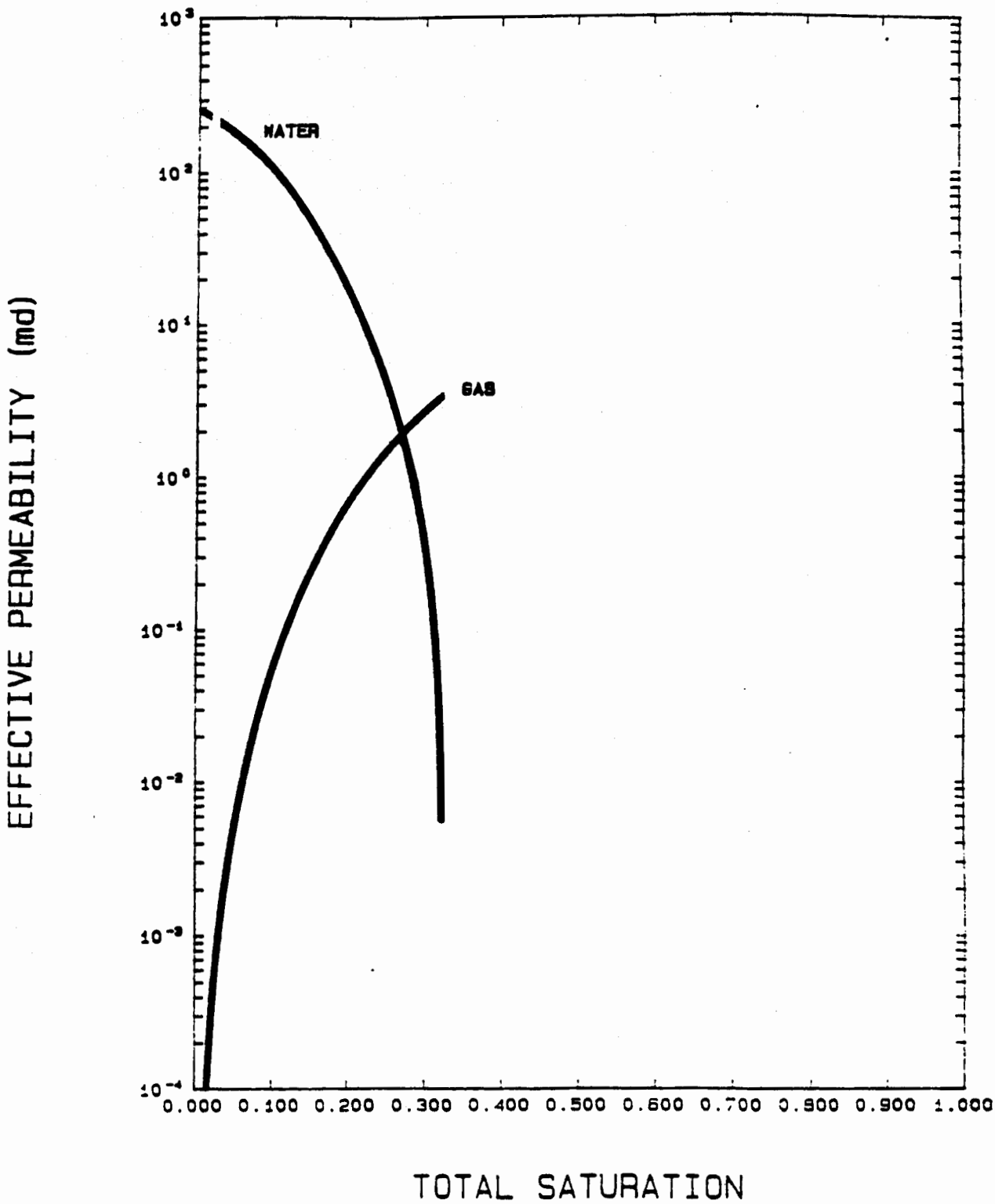

Figure D-3. Effective Permeability as a Function of Saturation for Sample MCG-604, Hole LLM-85-01, Depth of 101 Feet

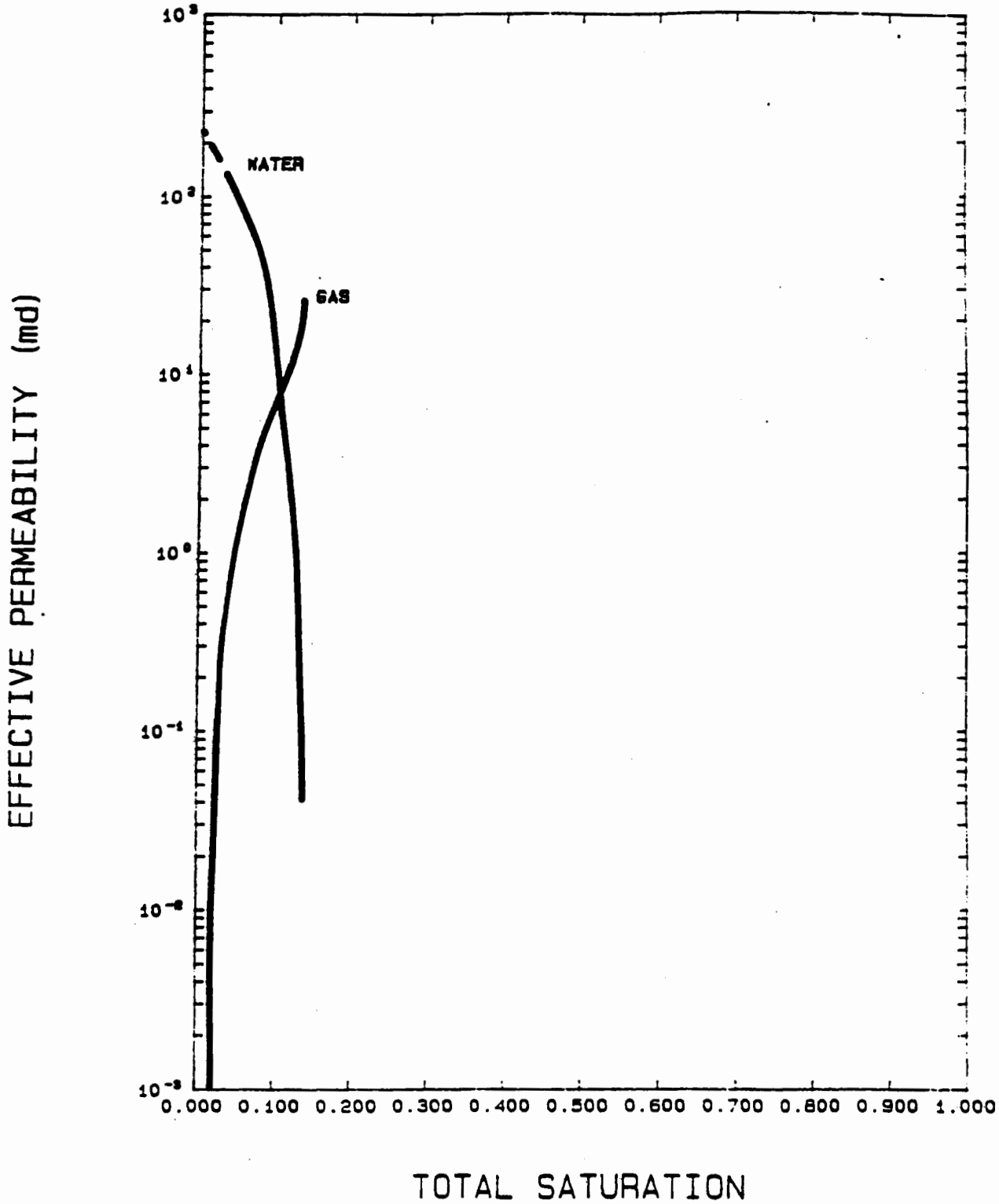

Figure D-4. Effective Permeability as a Function of Saturation for Sample MCG-605, Hole LLM-85-01, Depth of 124 Feet

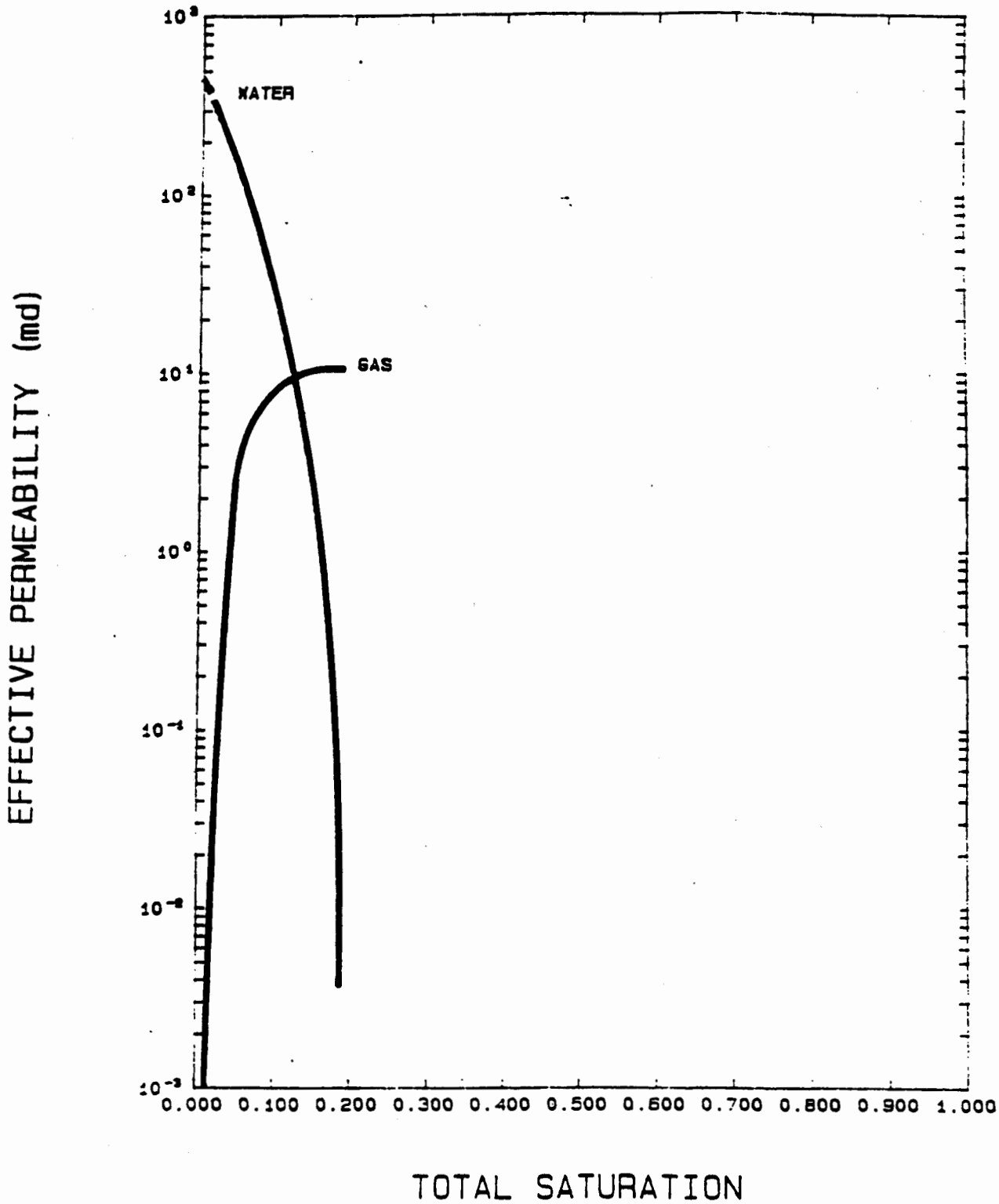

Figure D-5. Effective Permeability as a Function of Saturation for Sample MCG-606, Hole LLM-85-02, Depth of 7 Feet

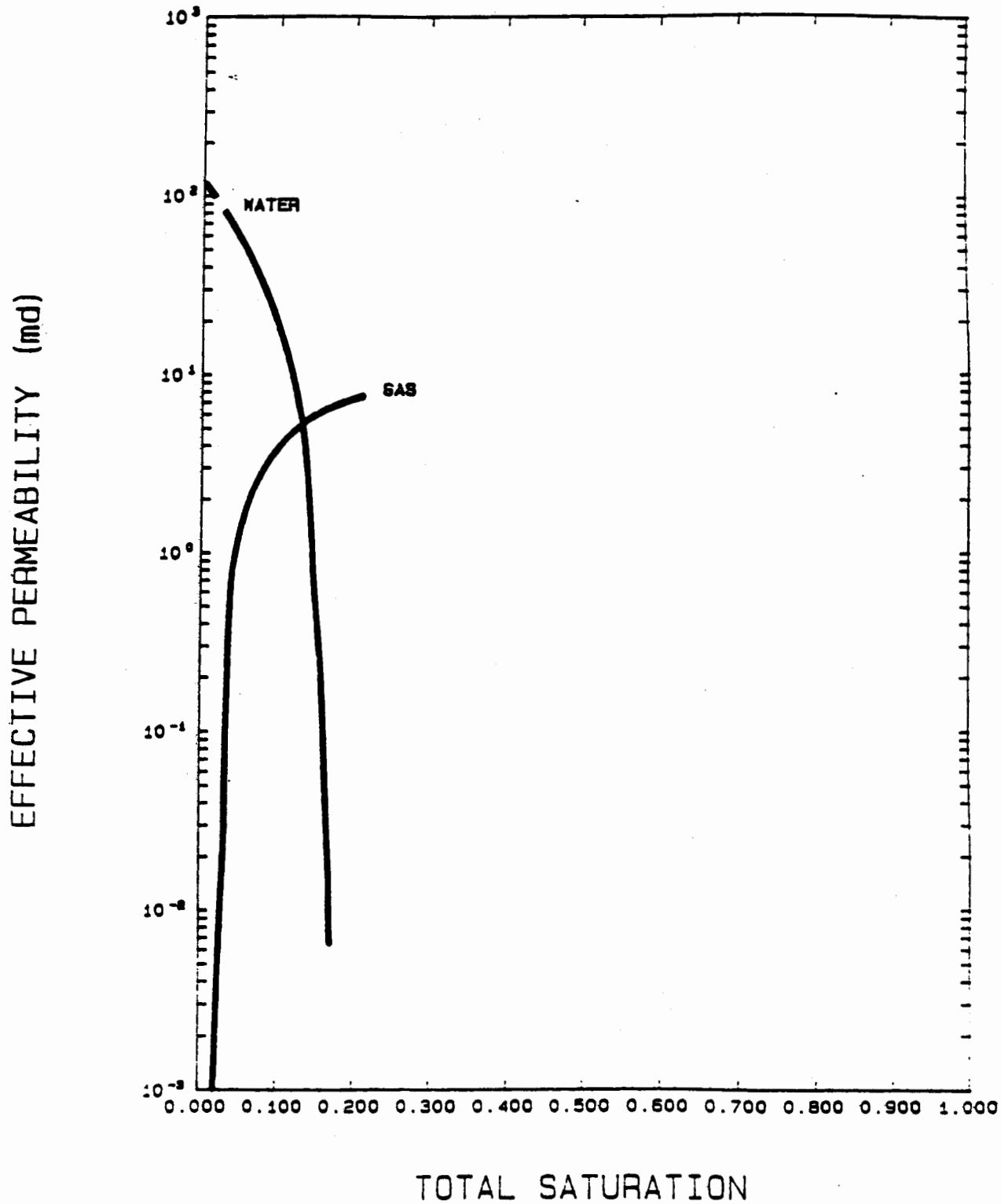

Figure D-6. Effective Permeability as a Function of Saturation for Sample MCG-607, Hole LLM-85-02, Depth of 36 Feet

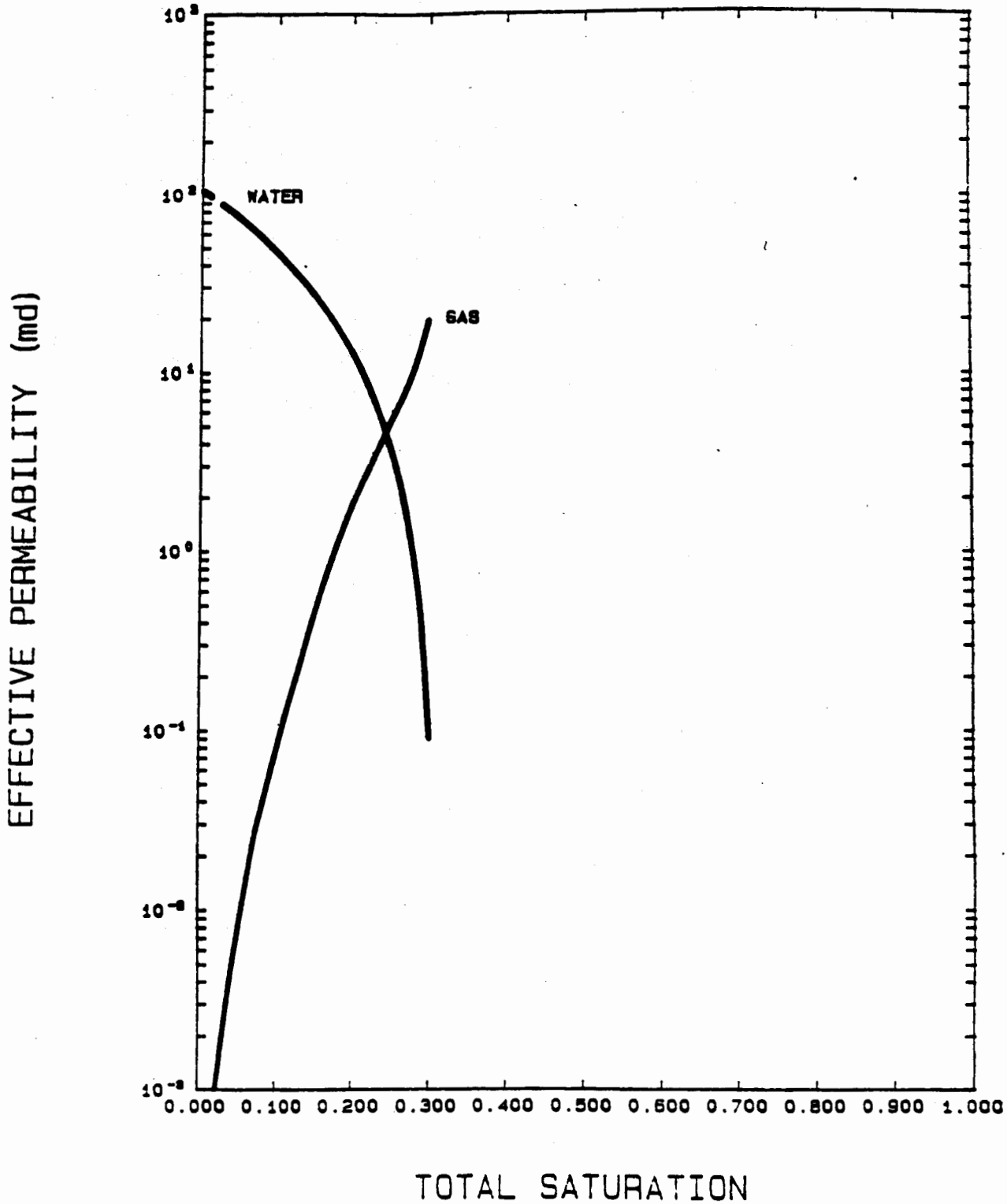

Figure D-7. Effective Permeability as a Function of Saturation for Sample MCG-608, Hole LLM-85-02, Depth of 67 Feet

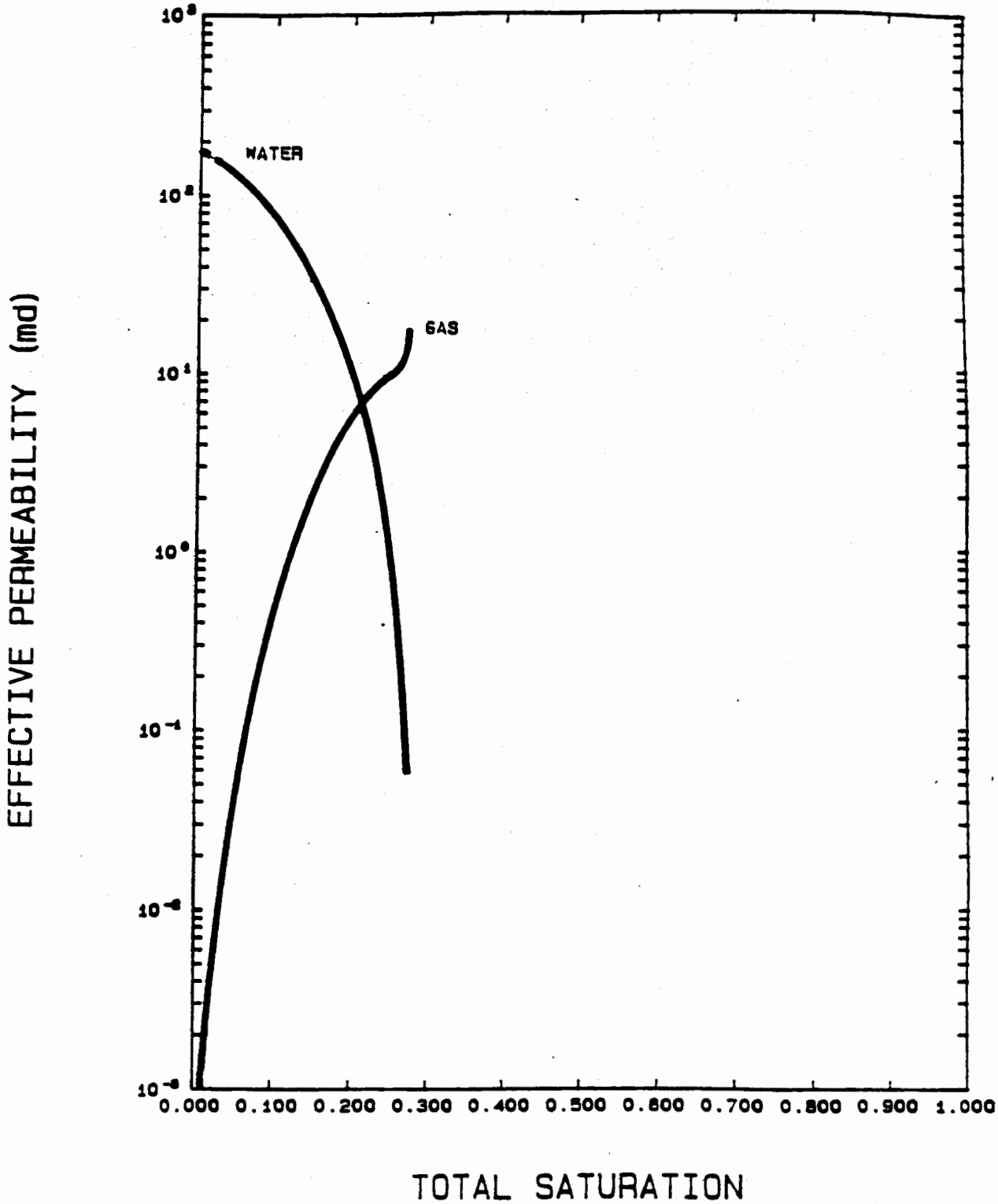

Figure D-8. Effective Permeability as a Function of Saturation for Sample MCG-609, Hole LLM-85-02, Depth of 117 Feet

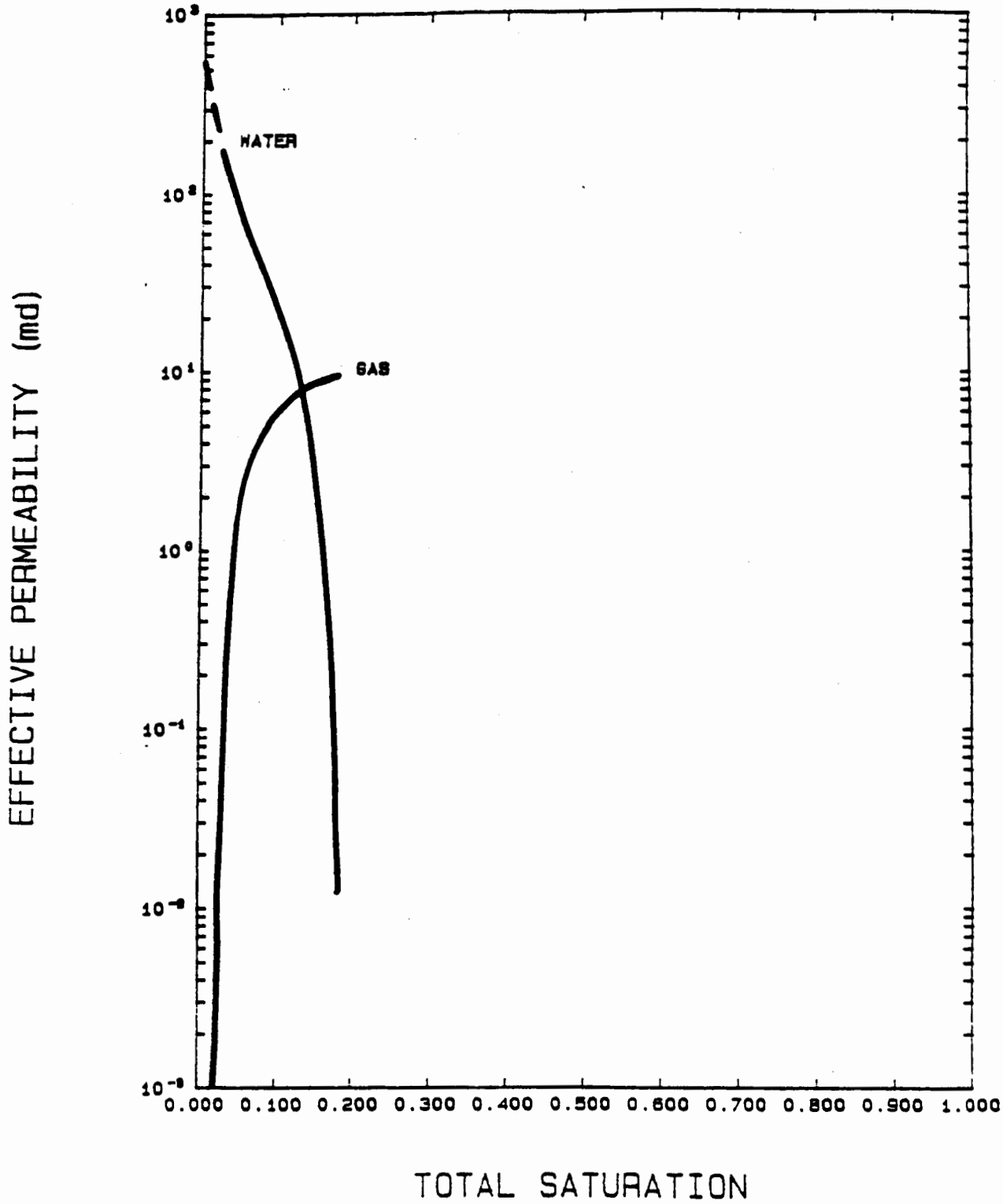

Figure D-9. Effective Permeability as a Function of Saturation for Sample MCG-610, Hole LLM-85-05, Depth of 15 Feet

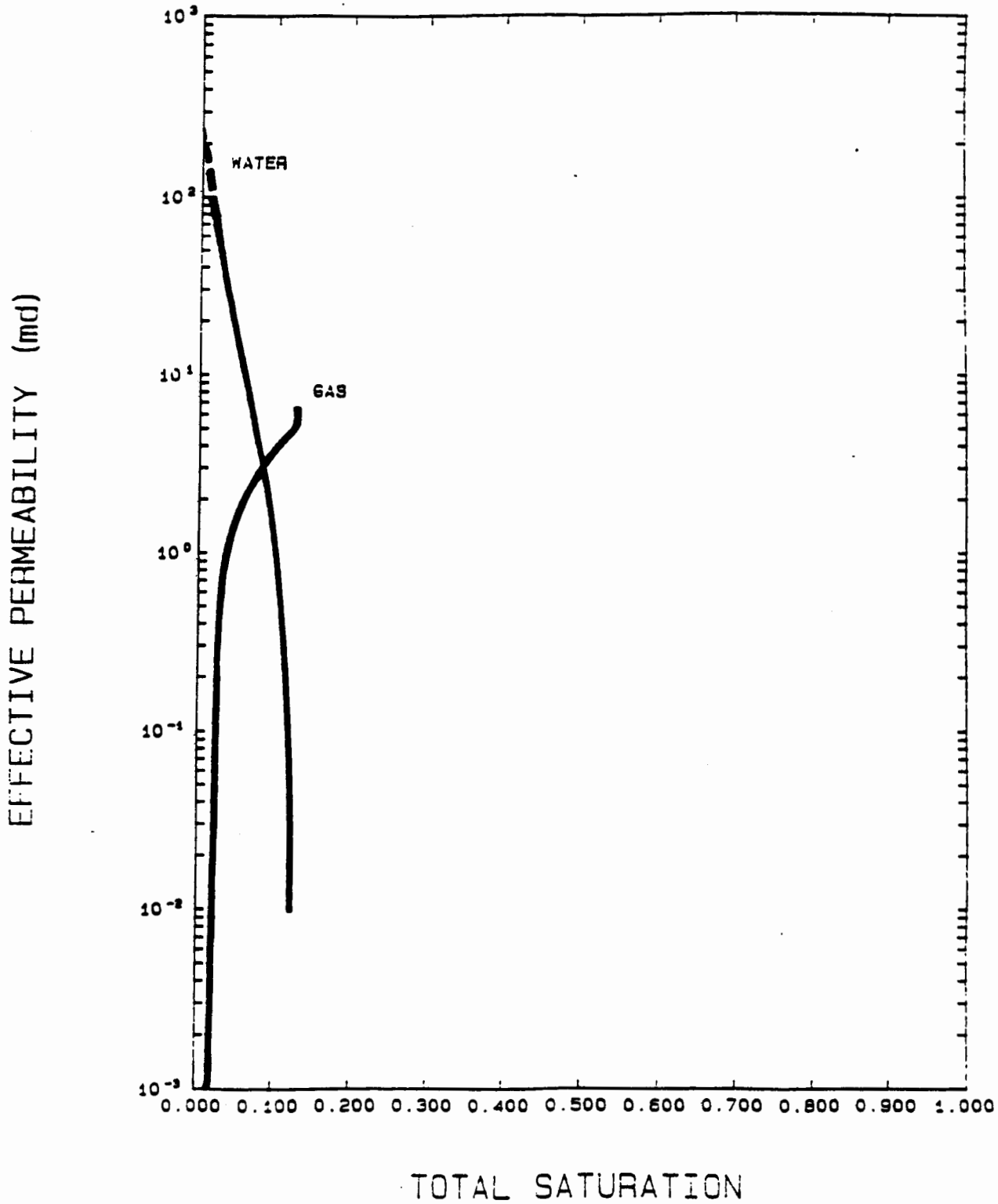

Figure D-10. Effective Permeability as a Function of Saturation for Sample MCG-611, Hole LLM-85-05, Depth of 36 Feet

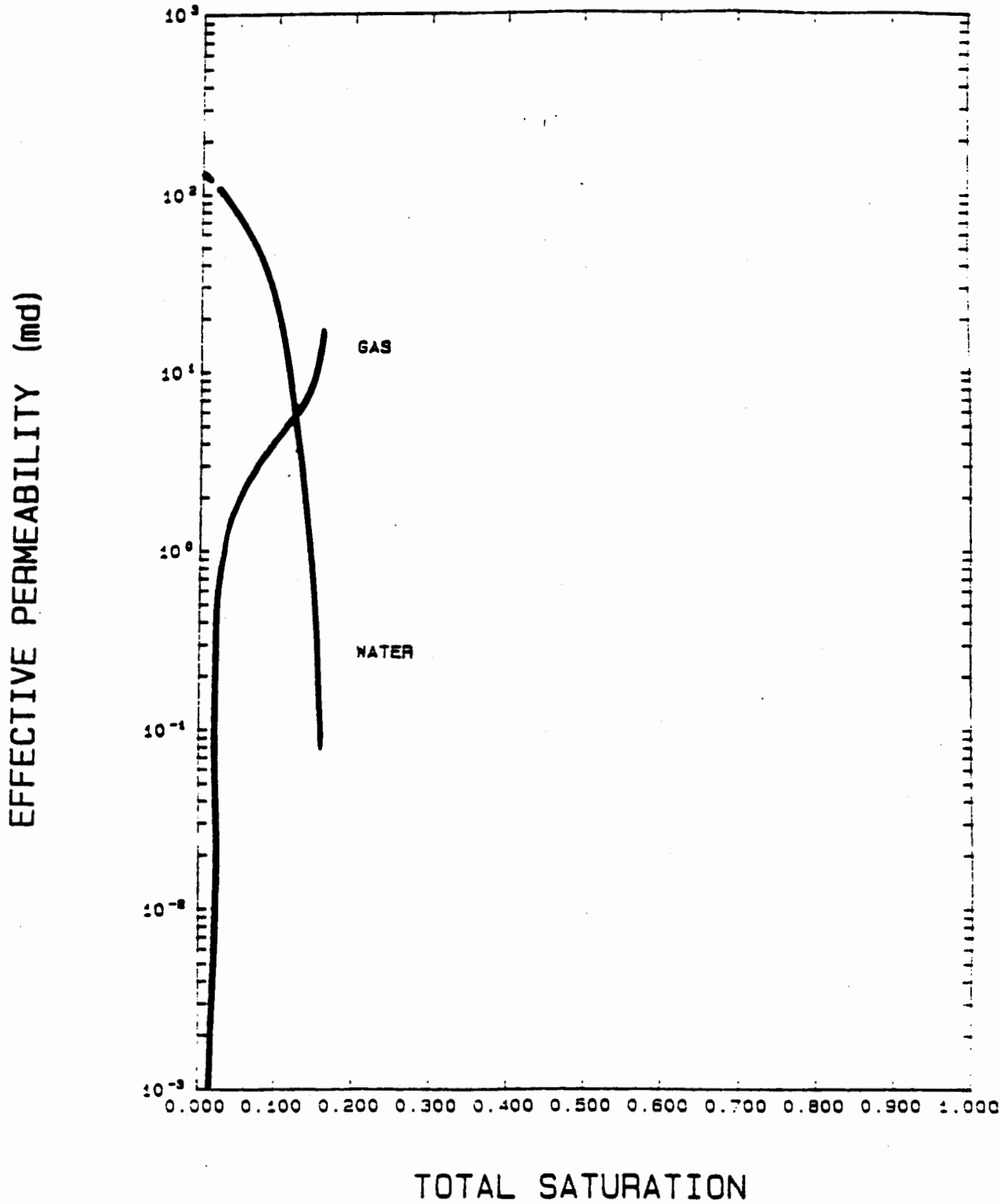

Figure D-11. Effective Permeability as a Function of Saturation for Sample MCG-612, Hole LLM-85-05, Depth of 76 Feet

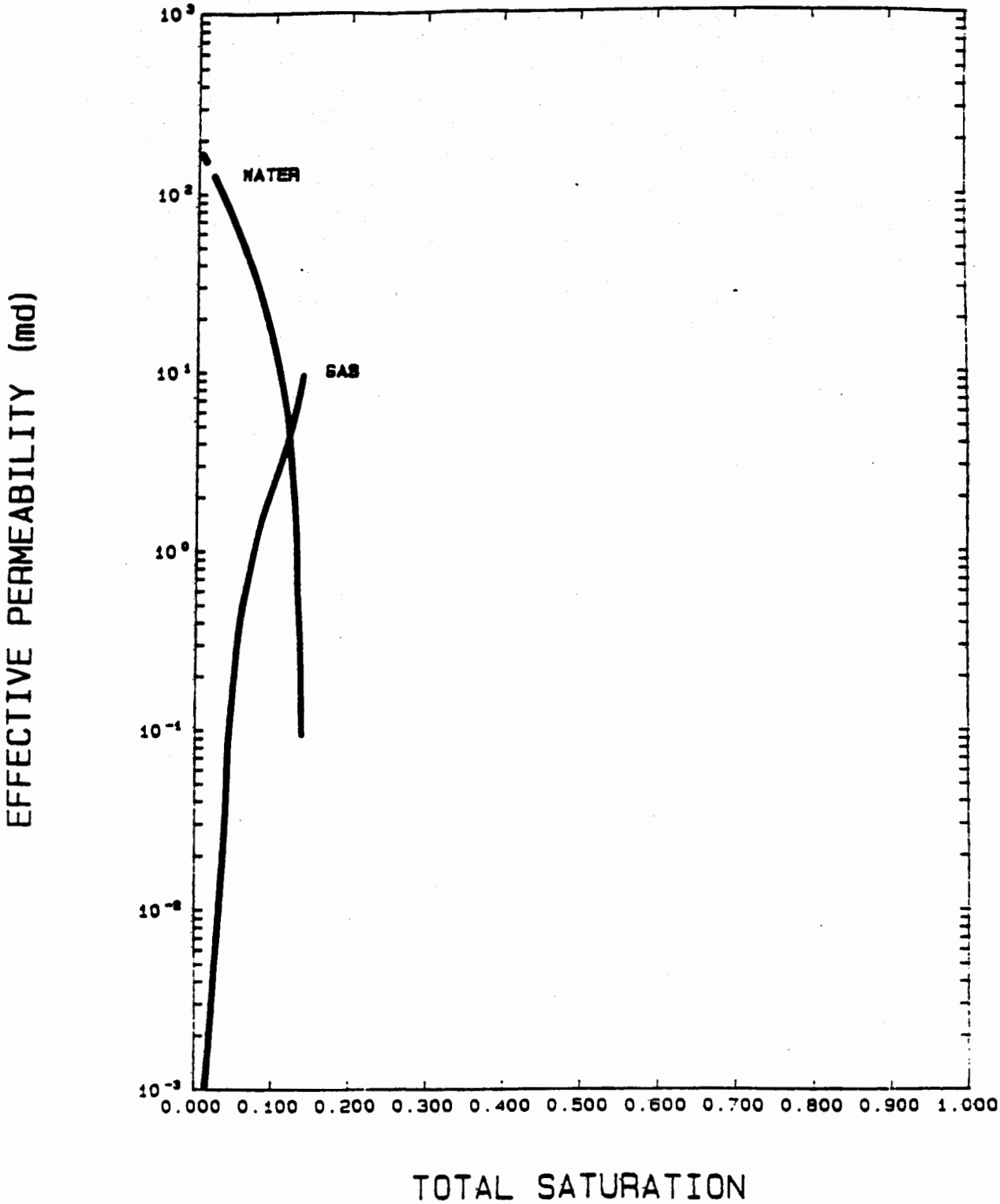

Figure D-12. Effective Permeability as a Function of Saturation for Sample MCG-613, Hole LLM-85-05, Depth of 123 Feet

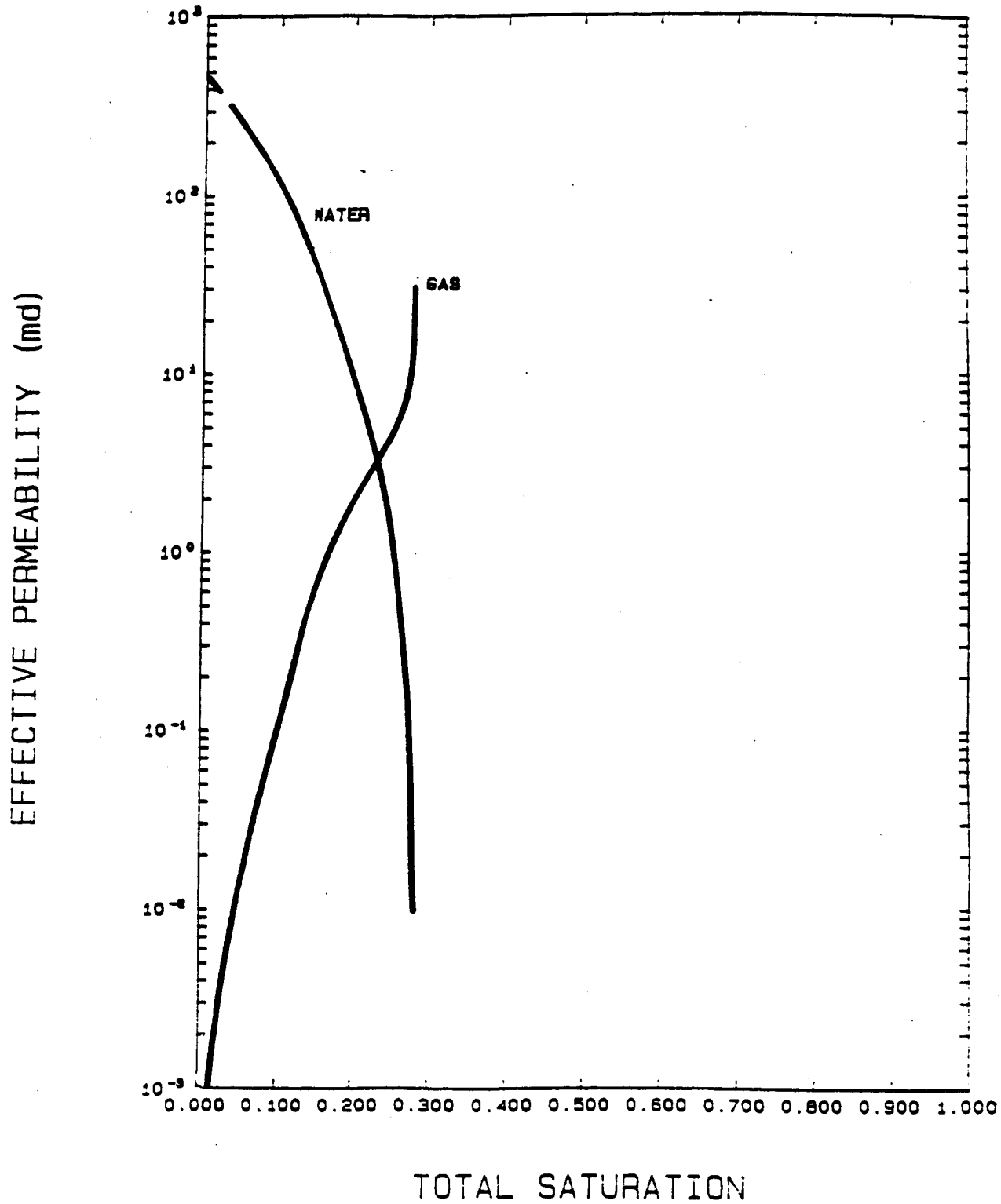

Figure D-13. Effective Permeability as a Function of Saturation for Sample MCG-614, Hole LGM-85-06, Depth of 29 Feet

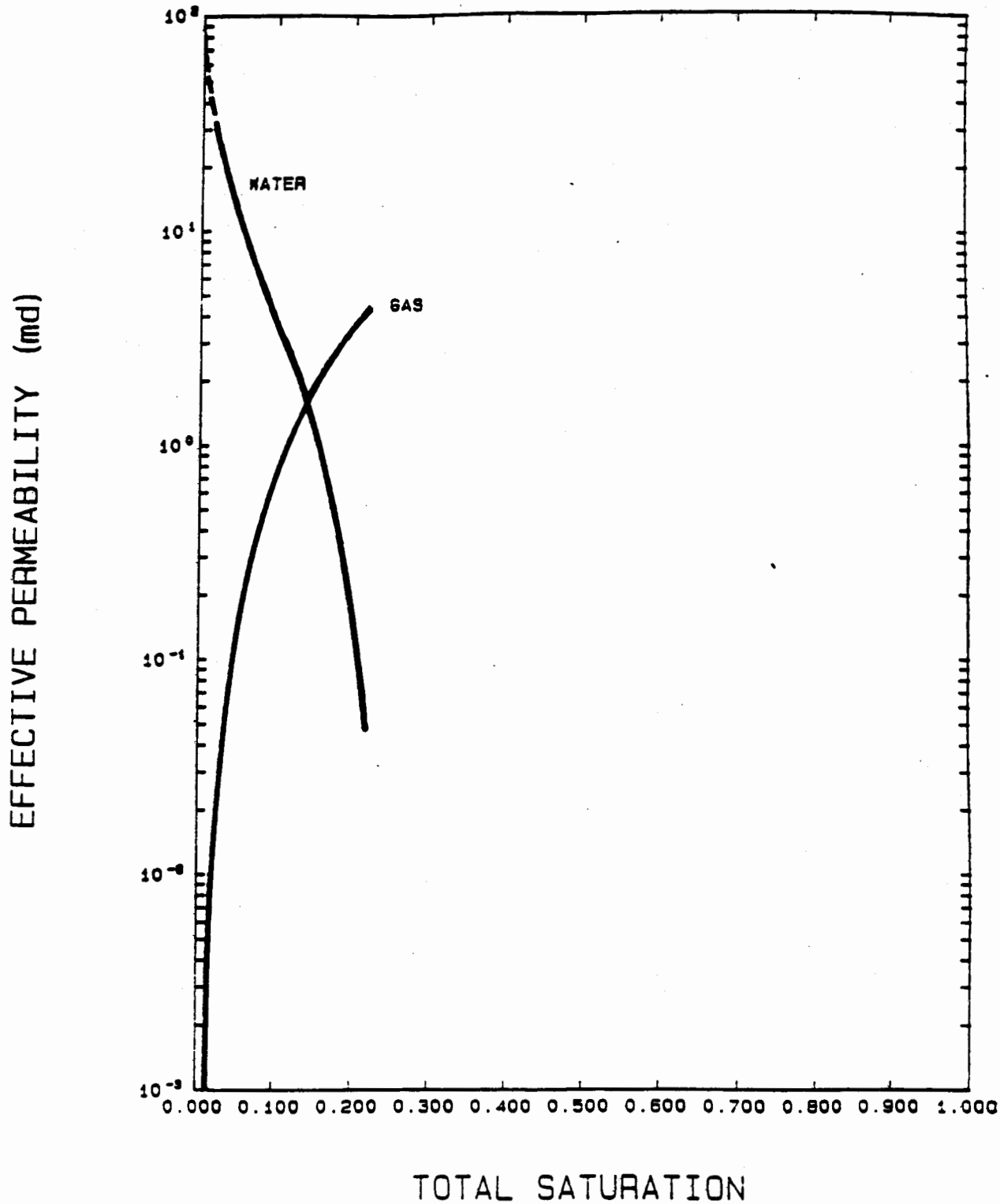

Figure D-14. Effective Permeability as a Function of Saturation for Sample MCG-615, Hole LGM-85-06, Depth of 51 Feet

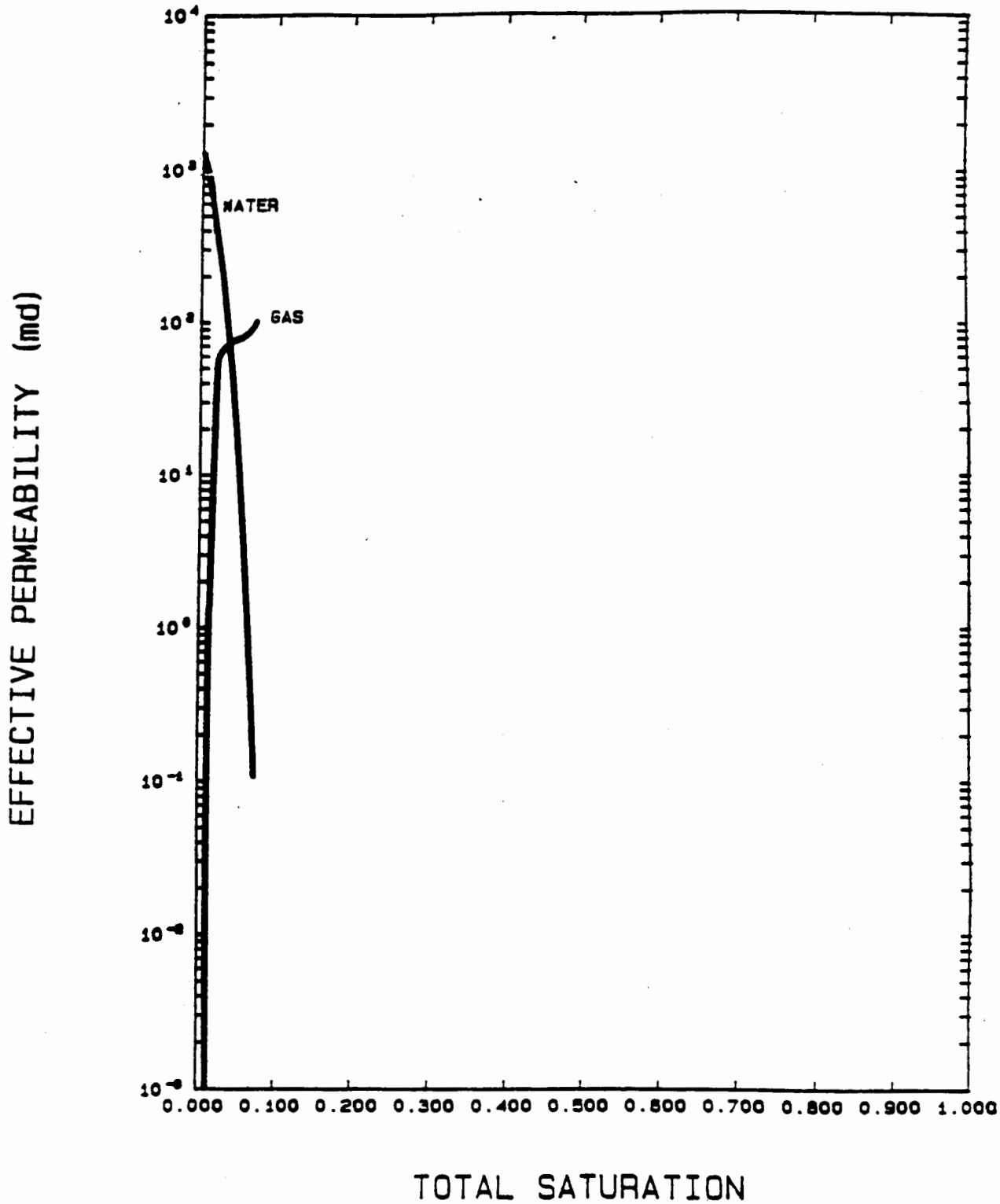

Figure D-15. Effective Permeability as a Function of Saturation for Sample MCG-616, Hole LGM-85-06, Depth of 99 Feet

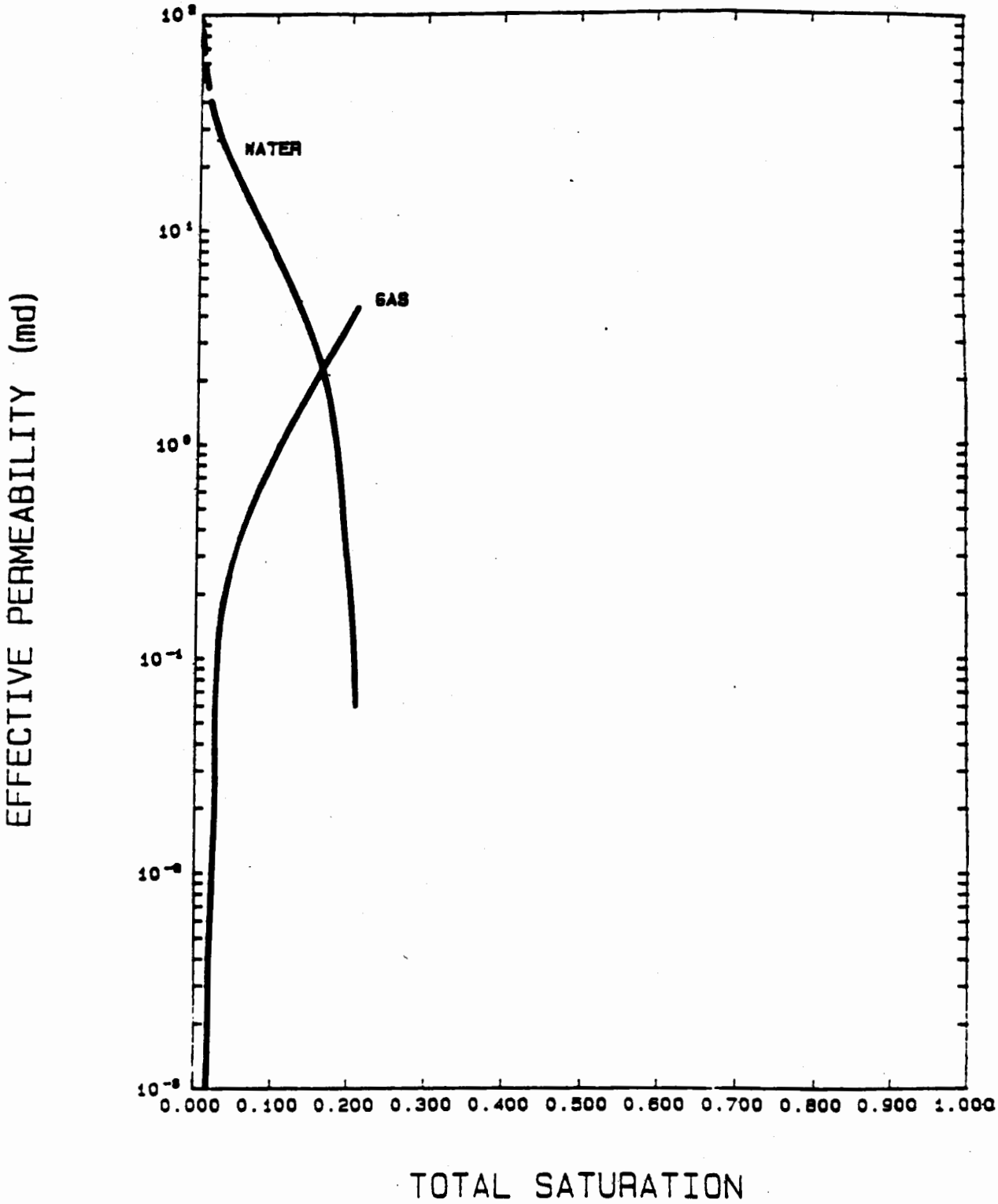

Figure D-16. Effective Permeability as a Function of Saturation for Sample MCG-617, Hole LGM-85-06, Depth of 115 Feet

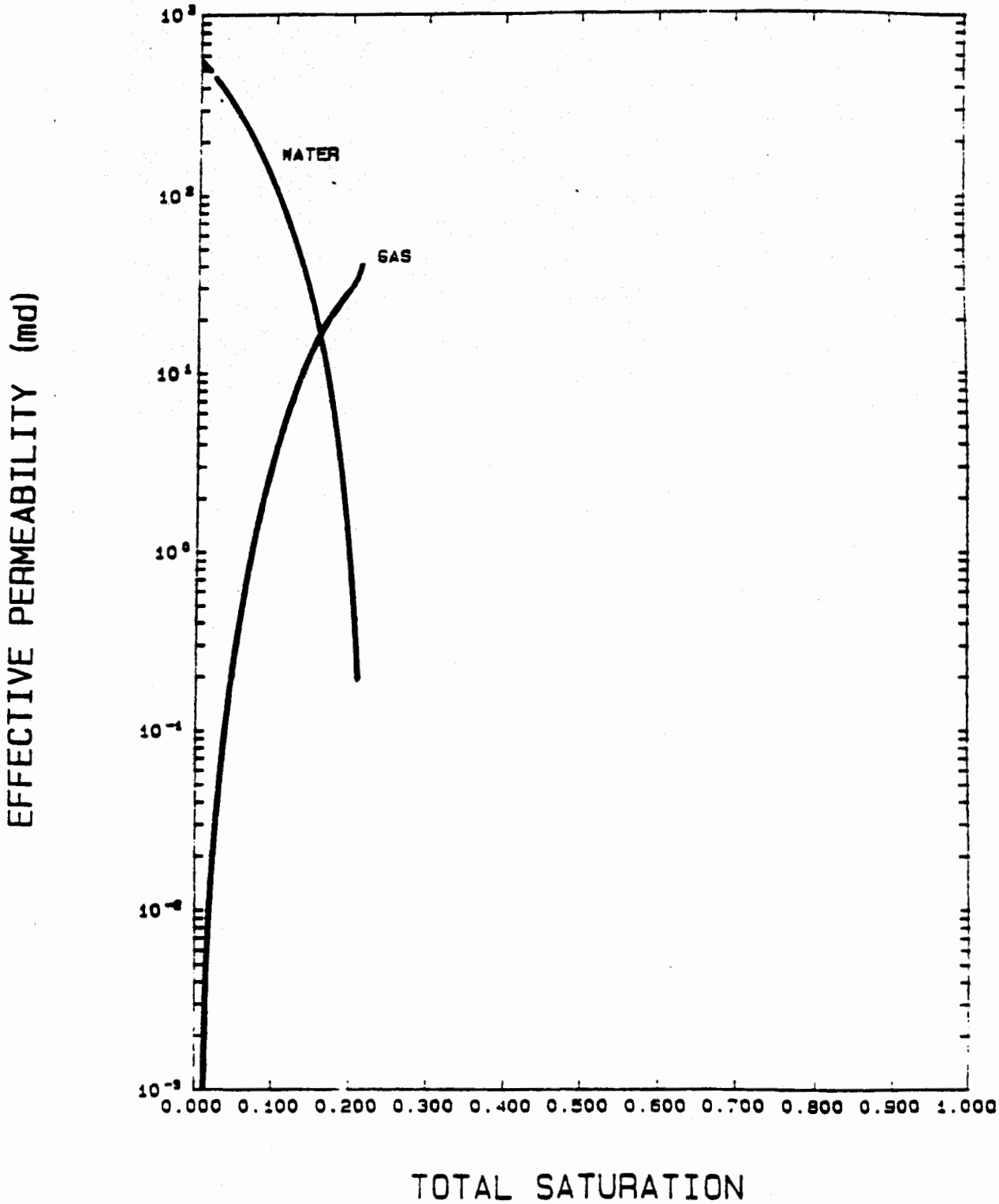

Figure D-17. Effective Permeability as a Function of Saturation for Sample MCG-618, Hole LGM-85-11, Depth of 3 Feet

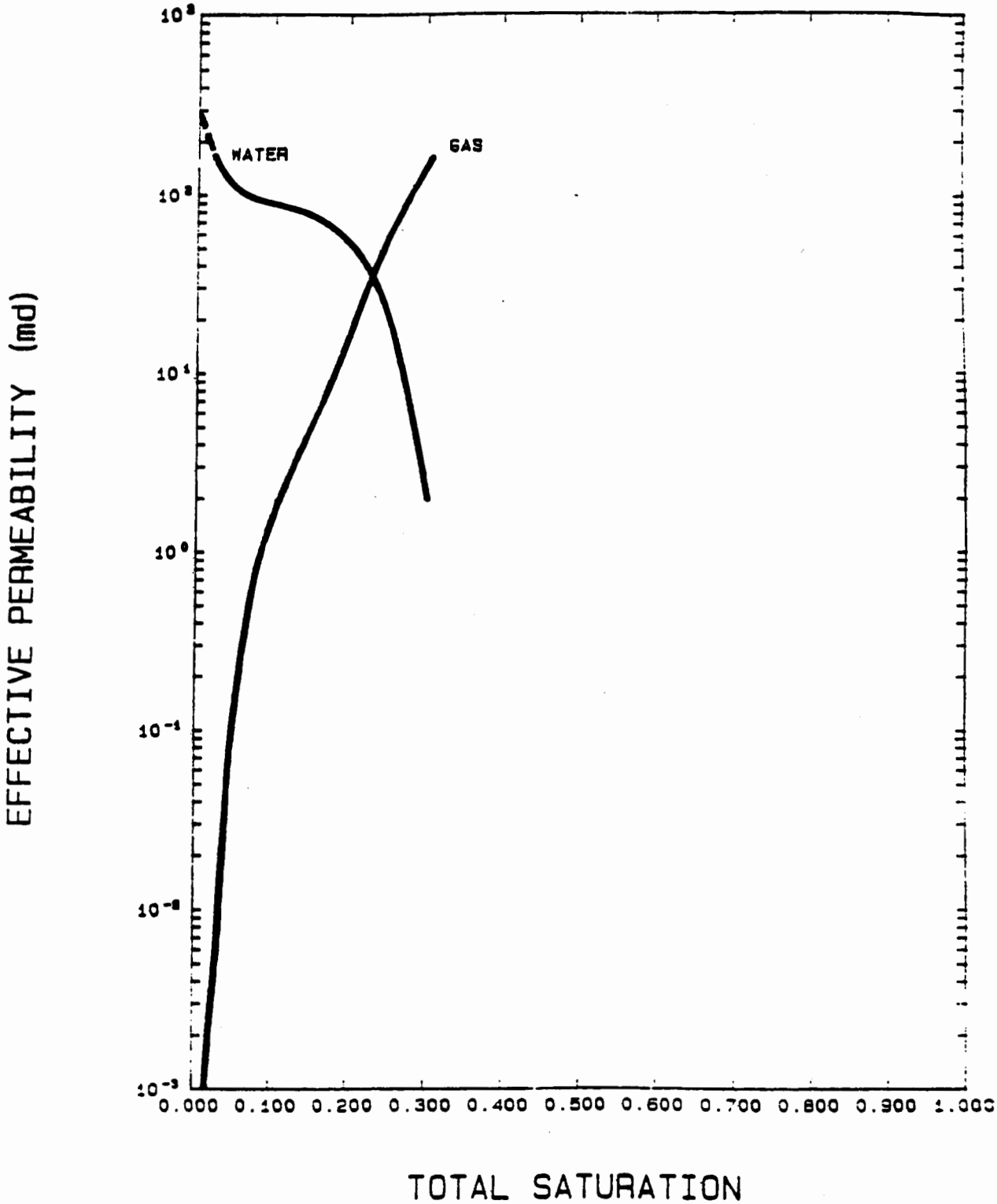

Figure D-18. Effective Permeability as a Function of Saturation for Sample MCG-619, Hole LGM-85-11, Depth of 30 Feet

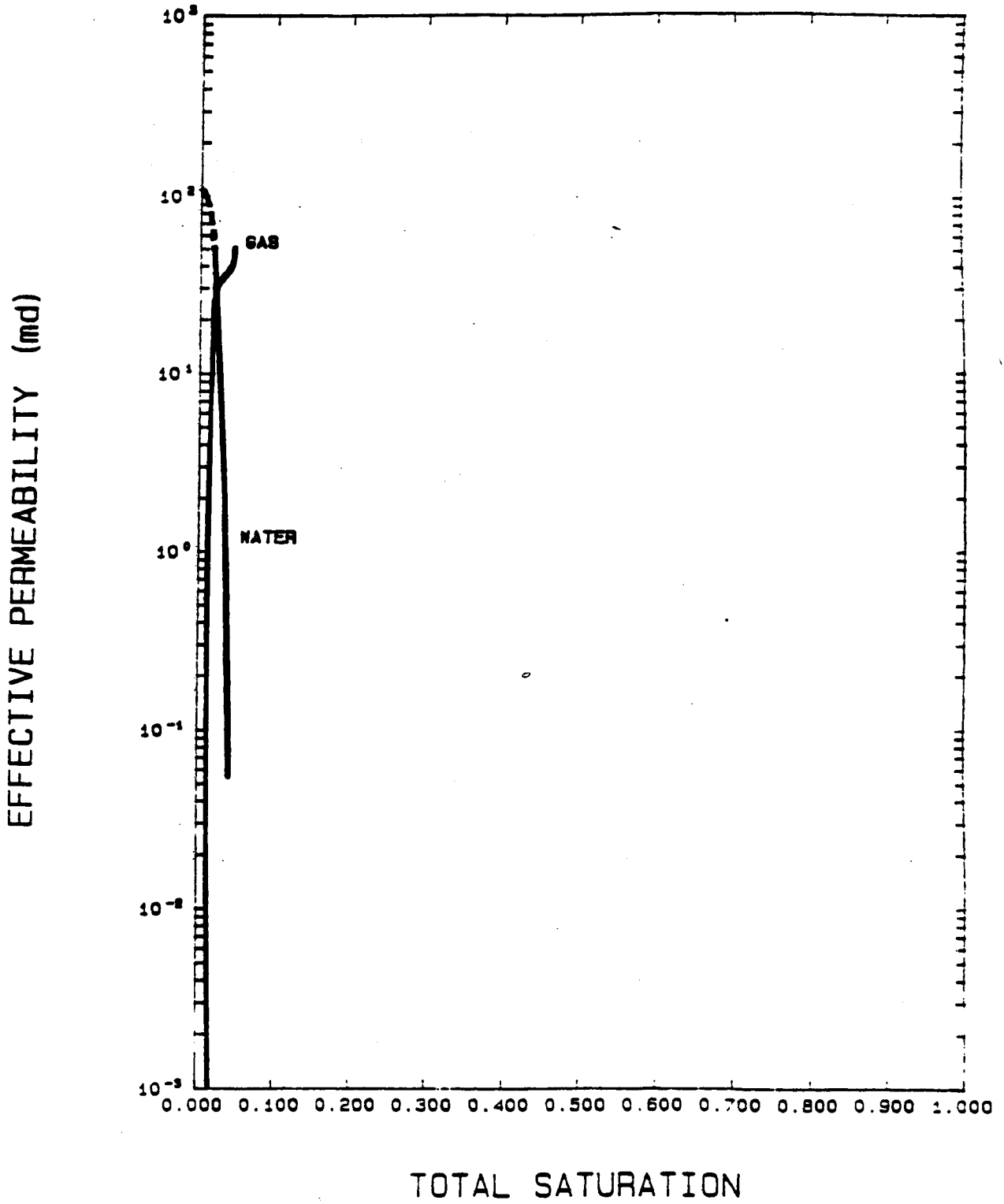

Figure D-19. Effective Permeability as a Function of Saturation for Sample MCG-620, Hole LGM-85-11, Depth of 94 Feet

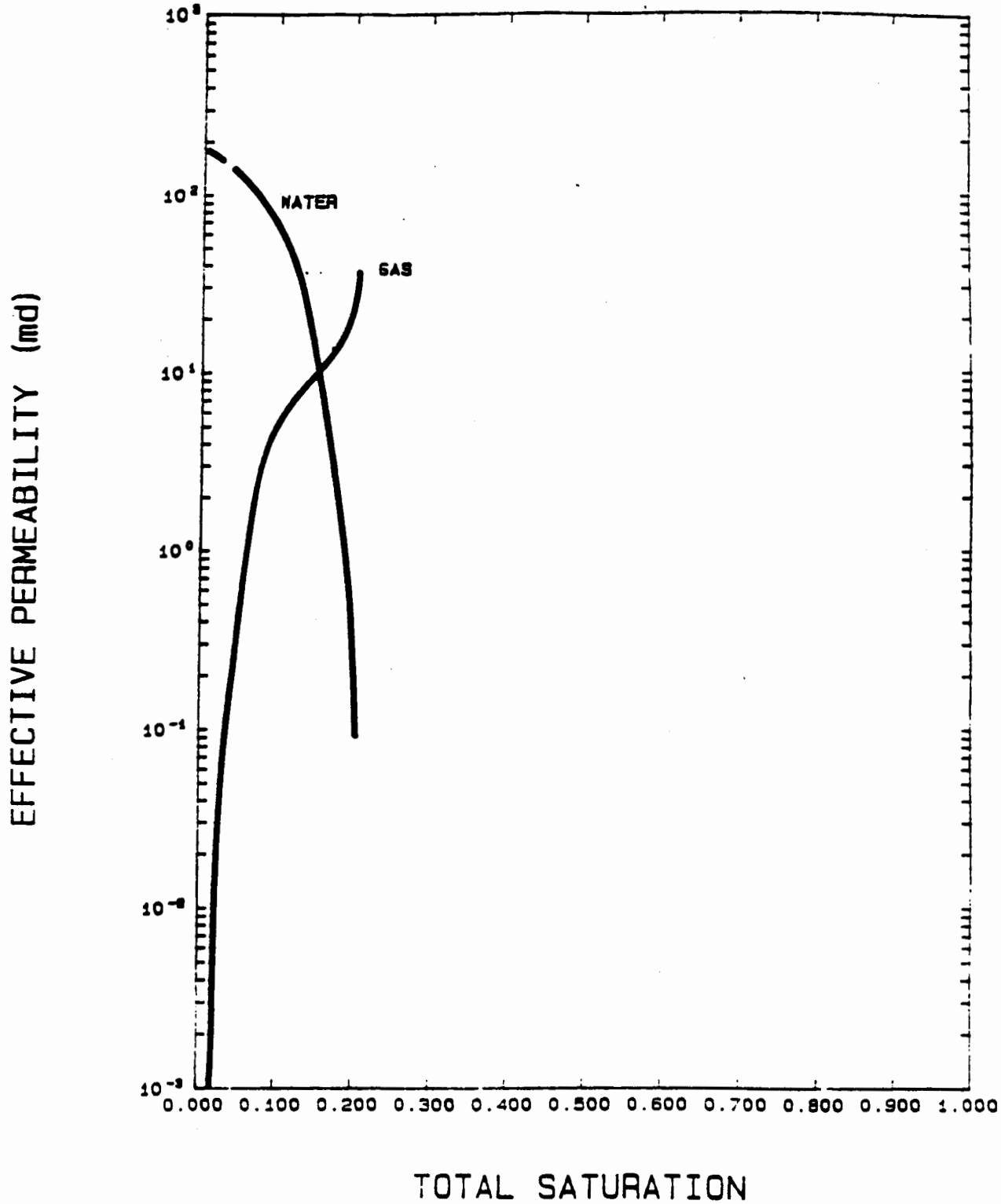

Figure D-20. Effective Permeability as a Function of Saturation for Sample MCG-621, Hole LGM-85-11, Depth of 115 Feet

Appendix E

LISTING OF FORTRAN V PROGRAM FOR CONVERTING PSYCHROMETER MICROVOLTAGE OUTPUTS TO WATER POTENTIAL

(modified from Brown and Bartos, 1982)

```
      PROGRAM H2OPOTU(INPUT,OUTPUT,TAPE5=INPUT,TAPE6=OUTPUT)
C**** LIMITS OF APPLICATION
C**** 14 < SEC < 61
C**** -1 < TEMP, DEGREES CEL < 41
C**** MV <= VIS*B*C
C**** -61 < OMV < 61
      REAL MV,MS,M15,IS,I15,LNS,LN15,NS,N15,MVS,MV15
      DATA SEC/15./
      IF(SEC.GE.14..AND.SEC.LE.61.) GO TO 10
      WRITE(6,5)
    5 FORMAT(' COOLING TIME IS NOT WITHIN MODEL RANGE')
      STOP
C
C**** READ INPUT DATA FOR FILE
   10 READ(22,20,END=100) I,DATE,TIME,B,TEMP,OMV,MV,DEPTH
   20 FORMAT(I4,A9,A7,F6.2,5F6.1)
      IF(TEMP.GE.-1..AND.TEMP.LE.41.) GO TO 30
      WRITE(6,25)
   25 FORMAT(' PSYCHROMETER TEMPERATURE IS NOT WITHIN MODEL RANGE')
      WP=-999.9
      GO TO 70
   30 IF(OMV.GE.-61..AND.OMV.LE.61.) GO TO 40
      WRITE(6,35)
   35 FORMAT(' ZERO OFFSET IS NOT WITHIN MODEL RANGE')
      WP=-999.9
      GO TO 70
   40 IF(MV.GT.0.) GO TO 50
      WRITE(6,45)
   45 FORMAT(' MICROVOLT READING .LE. 0.')
      WP=-999.9
      GO TO 70
C
   50 WPK=-22.5
      MS=2.5+EXP(-(ABS(((60.-SEC)/60.-1.)/.405)**3))
      M15=2.5+EXP(-(ABS(((60.-15.)/60.-1.)/.405)**3))
      IS=.45+.000333*SEC+1.9846E-19*SEC**10
      I15=.45+.000333*15.+1.9846E-19*15.**10
      RNS=EXP(-((1./(1.-IS))**MS))
      RN15=EXP(-((1./(1.-I15))**M15))
      DS=1.-RNS
      D15=1.-RN15
      X1AS=12.1-.003475*(60.-SEC)**1.63
      X1A15=12.1-.003475*(60.-15.)**1.63
      X1YS=39.2-.0004346*(60.-SEC)**2.45
      X1Y15=39.2-.0004346*(60.-15.)**2.45
      X2AS=88.-.0002579*(60.-SEC)**2.7
      X2A15=88.-.0002579*(60.-15.)**2.7
      X2YS=8.4+2.734E-07*(60.-SEC)**3.97
      X2Y15=8.4+2.734E-07*(60.-15.)**3.97
      LNS=EXP(-(ABS(((40.-TEMP)/40.-1.)/(1.-IS))**MS))
      LN15=EXP(-(ABS(((40.-TEMP)/40.-1.)/(1.-I15))**M15))
      NS=((LNS-RNS)/DS)*.185+1.18
      N15=((LN15-RN15)/D15)*.185+1.18
      UIS=X1AS+.017288*X1YS*TEMP**1.1
```

```
      UI15=X1A15+.017288*X1Y15*TEMP**1.1
      SPS=(X2AS-X2YS*.00017185*(40.-TEMP)**2.35)*(-1.)
      SP15=(X2A15-X2Y15*.00017185*(40.-TEMP)**2.35)*(-1.)
      MVS=(UIS-(UIS/(ABS(SPS)**NS))*(ABS(SPS-WPK)**NS))
      MV15=(UI15-(UI15/(ABS(SP15)**N15))*(ABS(SP15-WPK)**N15))
      ZOE=(.015*OMV+.001471*OMV*TEMP)
      C=(MVS+(MVS/MV15)*ZOE)/MVS
      R=UIS*C
      IF(MV.LE.R) GO TO 60
      WRITE(6,55)
   55 FORMAT(' MICROVOLT READING IS NOT WITHIN MODEL RANGE')
      WP=-999.9
      GO TO 70
   60 WP=((((ABS(SPS)**NS)*(UIS*C-MV))/(UIS*C))**(1./NS)+SPS)*B
      WP=-WP
   70 WRITE(23,20) I,DATE,TIME,B,TEMP,OMV,MV,DEPTH,WP
      GO TO 10
C
  100 CONTINUE
      STOP
      END
```

Appendix F

GEOPHYSICAL LOGS
(in attached envelope)